FLEXURAL CAPACITY OF COMPOSITE GIRDERS: DESIGN EQUATION ACCOUNTING FOR BRIDGE HIGH PERFORMANCE STEELS

（合成桁の曲げ強度：橋梁用高性能鋼を考慮した設計式）

2013 年 9 月

埼玉大学大学院理工学研究科（博士後期課程）

理工学専攻（主指導教員　奥井　義昭）

Dang Viet Duc

Flexural Capacity of Composite Girders: Design Equation Accounting for Bridge High Performance Steels

by

Dang Viet Duc

B.E. in Civil Engineering, UTC, Vietnam, 2000

M.E. in Computational Engineering, RUB, Germany, 2008

Dissertation

Submitted to the Faculty of Engineering for the
partial fulfillment of the requirements for the degree of
DOCTOR OF PHILOSOPHY

Department of Civil and Environmental Engineering
Graduate School of Science and Engineering
Saitama University
Saitama, Japan
2013

This dissertation was presented

by

Dang Viet Duc

It was defended on August, 20th 2013

and was approved by

Professor Yoshiaki Okui (Supervisor)

Professor Yasunao Matsumoto

Associate Professor Takeshi Maki

Associate Professor Masato Saitoh

ABSTRACT

The steel-concrete composite girder is one of the most common supper-structural types for highway and railway bridges. In composite girders under un-shored construction method, which is very common for composite girders, first, a steel girder only resists a bending moment due to dead loads of steel and wet concrete. The local buckling of the top flange plate in the steel girder due to the initial bending moment critically dominates the flexural resistance of the composite girders in the construction state. Besides, application of bridge high performance steels SBHS500, SBHS700 and hybrid steel girders is expected to be an economical solution for composite girder bridges. Steels SBHS500 and SBHS700, with yield strengths of 500 and 700 MPa, respectively, have been standardized in 2008 in Japannese Industrial Standards (JIS). They present the advantage of high yield strength, good weldability. However, if compared to conventional (normal) steels they possess different inelastic behavior, such as almost no yield plateau, smaller ductility, and a greater yield-to-tensile strength ratio. The bending moment capacity of a composite girder largely depends on local bucking of compressive components, such as flange plates and web plates. Hence, the local buckling strength of simply supported steel plates and section classifications based on the web slenderness limits of composite girders with SBHS steels for homogeneous as well as hybrid sections are investigated in the current study.

In this dissertation, a probabilistic distribution of buckling strengths for compressive plates with normal and bridge high performance steels was obtained through numerical analyses to propose nominal design strength and a corresponding safety factor. In the numerical analyses, Monte Carlo based simulation, which is combined with the response surface method, was employed to reduce exertion of finite element analyses. For each of 10 width-to-thickness parameter R values ranging from 0.4 to 1.4, a response surface of the normalized compressive strength was identified based on 114 finite element analysis results which include 4 normal and 2 high strength steel grades with different residual stresses and initial defections. The response surface is approximated as a simple algebraic function of the residual stress and the initial deflection. For the Monte Carlo based simulation in the current study, a pair of variables of residual stress and initial deflection is generated randomly in accordance with the probabilistic characteristics reported by Fukumoto and Itoh (1984). The LBS is evaluated deterministically by means of the response surface for the generated random variables. The probabilistic distribution of LBS is obtained from

simulating 10,000 pairs of the random variables. The mean values obtained from results of LBS probabilistic distribution in the current study agree to those from experiments reported by Fukumoto and Itoh (1984). The obtained standard deviations of the current study exhibit about half of experimental results in a range of $0.6<R<1.2$. Regarding each of 6 steel grades, the mean LBS strength of SBHS steel plates is greater than that of the normal steel plate. For $R>0.55$ the standard deviation of LBS regarding SBHS steel plate is lower that that of normal steel plates. Judging this behavior, the design normalized LBS strength of steel plate will attain higher value with application of SBHS steels than normal steels for $R>0.55$. In the range of $0.4\leq R\leq 0.85$, the variance of LBS is more sensitive with initial deflection than residual stress. Whereas in the range of $R>0.9$, the variance of LBS is more sensitive with residual than initial deflection. For the nominal strength set to the mean value and probabilistic distribution of LBS is the normal distribution, the partial safety factors are obtained as 1.11, 1.13, and 1.16 for non-exceedance probability of the probabilistic LBS with respect to the nominal LBS equal to 5.0, 3.0, and 1.0%, respectively.

For investigation of web slenderness limits for section classifications of composite girders, the positive bending moment capacity of composite girders is examined through parametric study employing elasto-plastic finite element analyses. The section classification based on web slenderness limits for composite homogeneous and hybrid steel girders with bridge high performance steel SBHS500 are explored. Besides, the effects of the initial bending moment due to unshored construction method on the web slenderness limit are investigated. For section classification of composite hybrid girders, the yield moment, which is calculated from the yield moment of the corresponding composite homogeneous girders and hybrid factor, is an essential quantity. However, the hybrid factor specified in AASHTO was proposed without considering the initial bending moment. In the current study, the modified hybrid factor is proposed to determine the yield moment of hybrid sections from the corresponding homogeneous sections. Under the effect of different inelastic behavior of SBHS500 steel and the initial bending moment, it is shown that the compact- noncompact web slenderness limits in conventional design standards are over-conservative for both composite SBHS500 homogeneous and SBHS500-SM490Y hybrid steel girders. Many composite sections, which are classified as slender by current specifications, demonstrate sufficient flexural capacity as noncompact. The compact-noncompact web slenderness limit of composite SBHS500-SM490Y steel sections is greater than that of composite SBHS500 homogeneous steel sections. However, the noncompact-slender web slenderness limit for SBHS500-SM490Y hybrid sections is a little lower than that of SBHS500 homogeneous sections. For composite

girders with non-compact sections with the initial bending moment, the proposal hybrid factors are slightly lower than those obtained from FEM analysis results, and the difference is about 5%. With considering a higher level of the initial bending moment, the hybrid factors using in AASHTO shows un-conservativeness. The investigation of section classification based on web slenderness limits of composite girders with SBHS500 steel for both homogeneous and hybrid steel girders shows that the web plate of steel girder can be designed with higher slenderness than requirements of current specifications such as AASHTO and Eurocode.

Keywords*: bridge high performance steels, local bucking strength, residual stress, initial deflection, Monte Carlo based simulation, response surface, partial safety factor, composite I-girder, web slenderness limit, ultimate flexural strength.*

To two women of my life

Mạ Út và em, Hạt mít khô

ACKNOWLEDGEMENTS

After four years of study and research, number of simulations and reports, the work has been finished. It was the most special period that consisted of important changes in both my professional and personal life. This was a period that shaped my mind to research standard, which I had not experienced before. This dissertation is thus only a very small part of a four-year adventure.

I am most grateful to my supervisor, Prof. OKUI Yoshiaki, for his continuous and significant support, guidance and contributions throughout the research work in my doctoral program and especially for making this dissertation possible. I would like to thank him for his advice, flexibility, inspiration and motivation. Prof. Okui has given me valuable research and practical experiences for structural engineering and the motivation to excel in all endeavors. It's my great honor to have conducted this research under his guidance. I will never forget the endless lists of corrections and critical questions. These resulted in discussions that oriented my research. Deeply thank you, Sir.

I would like to express my appreciation to Prof. Hiroki Yamaguchi for giving me difficult but valuable questions at the Lab. Meetings, which helps me master the important contents of my research.

I also owe my research to the members of my dissertation committee for the integral parts they played in this research: Prof. Yasunao Matsumoto, Ass. Prof. Takeshi Maki, Ass. Prof. Masato Saitoh. Their valuable comments, direction, support, guidance and enthusiasm are such contributions throughout the process to complete this research.

My numerous hours at the Structural Mechanics and Dynamics Laboratory were made much more enjoyable by the indispensable aid of all doctoral students in our room. I want to thank them for their support, discussions, cheerful greetings, occasional serenades, kind words and for good times we have had together. I appreciate and would like to thank my co-researchers Miss Zhang, Miss Zhiyan, Mr. Hagiwara and Mr. Wataru, for their numerical analysis, as well as friendliness and logistic support. It was a great pleasure to work with you all.

Finally, I am indebted to my family members for their unending support, which has grown substantially over the past four years. This work is especially dedicated to my wife, for

bearing my temper, comforting my disappointments and for keeping things running while I was at work. I thank for her love, patience, understanding, and the sacrifice she made by not seeing me for four years.

TABLE OF CONTENTS

ABSTRACT ..... **iii**
ACKNOWLEDGEMENTS ..... **vii**
TABLE OF CONTENTS ..... **ix**
LIST OF FIGURES ..... **xi**
LIST OF TABLES ..... **xvii**

CHAPTER 1 ..... **1**
BACKGROUND **1**
1.1 Introduction of composite girder bridge 1
1.2 Design issues for composite girder bridges 5
1.2.1 Thicker steel plates and new steel grades 5
1.2.2 Allowable Stress and Limit State Design Method 8
1.3 Trend of recent design methods 9
1.3.1. Probability-based design 9
1.3.2. Allowable stress of JSHB 11
1.3.3. AASHTO – Load and Resistance Factor Design (LRFD) 11
1.3.4. Eurocode – Format of partial safety factor format 12
1.4 Summary of issues 13

CHAPTER 2 ..... **15**
LITERATURE REVIEW AND OBJECTIVES 15
2.1 Reviews on compressive steel plates 15
2.2 Review on bending composite girder 21
2.2.1. Hybrid factor 21
2.2.2. Current classification of composite sections 23
2.2.3. Study of Gupta et al., (2006) 24
2.3 Objectives 26

CHAPTER 3 ..... **28**
STATISTICAL INFORMATION OF LBS FOR STEEL PLATES **28**
3.1. Introduction 28
3.2. Plates properties 30
3.3. Random inputs 32
3.4. FE steel plate model 37
3.5. Response surface 42
3.6. Results from random simulation and discussion 46
3.6.1. Convergence of the random simulation results 46
3.6.2. Results from random simulation 47
3.6.3. Approximate estimation of mean and variance 55
3.6.4. Proposal of partial safety factor 60

3.7. Conclusions 67

CHAPTER 4 69
WEB SLENDERNESS LIMITS FOR SECTION CLASSIFICATION OF COMPOSITE GIRDERS 69
4.1. Introduction 69
4.2. FEM simulation model of pure flexural composite girder 73
4.3. Proposal of hybrid factor 81
4.4. Web slenderness limits in design of composite girders 86
4.5. Conclusions 95

CHAPTER 5 97
CONCLUSIONS AND RECOMMENDATIONS 97
5.1. Conclusion remarks 97
5.2. Contribution of the current study 100
5.3. Recommendations for future research 100

REFERENCES 102

APPENDIX 1 106
RESPONSE SURFACES 106
A1-1 . Case 1 – regarding all 6 steel grades for each R value 106
A1-2 . Case 2 – regarding each among 6 steel grades for each R value 108

APPENDIX 2 120
PROBABILISTIC INFORMATION OF LBS 120
A2-1 Case 1 – regarding all 6 steel grades for each R value 120
A2-2 Case 2 – regarding each steel grade for each R value 122

APPENDIX 3 132
PROPERTIES OF COMPOSITE SECTION 132
A3-1 . Yield moment 132
A3-2 . Plastic neutral axis and plastic moment capacity of homogeneous and hybrid section 136

LIST OF FIGURES

Fig. 1.1-1 The continuous composite twin I-girder bridges in Europe (Sétra, 2010)..... 1

Fig. 1.1-2 Local buckling mode in compressive flange of I girder under loading of wet concrete and simplified outstanding plate..... 3

Fig. 1.1-3 Local buckling mode in compressive flange of un-stiffened box girder under loading of wet concrete and simplified simply supported plate..... 4

Fig. 1.1-4 Simplified design of composite girder..... 4

Fig. 1.1-5 Simplified composite girder structure under pure bending moment..... 5

Fig. 1.2-1 The actual test stress-strain relations of normal and high strength SBHS steel grades..... 6

Fig. 1.2-2 Nagata Bridge with application of SBH500 steel grade to the space truss system..... 7

Fig. 1.2-3 Tokyo Gate Bridge with application of SBH500 steel grade to the full-welded truss girder..... 7

Fig. 1.3-1 Probability density functions for load and resistance..... 10

Fig. 1.3-2 Definition of safety index for R and Q..... 10

Fig. 2.1-1 Comparison of current design equation..... 15

Fig. 2.1-2 Comparison of M, M-2S curves proposed in Fukumoto and Itoh (1984) to..... 16

Fig. 2.1-3 Comparison of LBS scatterness of steel plates to..... 18

Fig. 2.1-4 Comparison of Usami (1992) results to Elastic buckling and current JSHB curves..... 18

Fig. 2.1-5 Comparison of Kitada (2002) results to Elastic buckling and current JSHB curves..... 20

Fig. 2.2-1 Stress distribution in non-composite hybrid beam section..... 22

Fig. 2.2-2 Stress distribution in composite hybrid beam section..... 22

Fig. 2.2-3 Assumption of full plastic stress distribution in..... 23

Fig. 2.2-4 Assumption of yield stress distribution in..... 23

Fig. 2.2-5 Comparison of compact- noncompact web slenderness limit design curve proposed by Vivek, AASHTO and Eurocode..... 25

Fig. 2.2-6 Comparison of noncompact-slender web slenderness limit design curve proposed by Vivek, AASHTO and Eurocode with M_1=0 25

Fig. 2.2-7 Comparison of noncompact-slender web slenderness limit design curve proposed by Vivek, AASHTO and Eurocode with M_1=0.2M_{ys} 25

Fig. 2.2-8 Comparison of noncompact-slender web slenderness limit design curve proposed by Vivek, AASHTO and Eurocode with M_1=0.4M_{ys} 25

Fig. 3.1-1 The Monte Carlo based simulation applied in the current study 29

Fig. 3.2-1 Slenderness parameter values and yield strength considered in the current study 32

Fig. 3.3-1 Actual residual stress distribution reported in Komatsu (1977) 33

Fig. 3.3-2 Initial measurement on steel plate reported in Soares and Kmiecik (1993) 33

Fig. 3.3-3 Histogram of normalized initial deflection reported in Fukumoto and Itoh (1983) 34

Fig. 3.3-4 Histogram of normalized residual stress reported in Fukumoto and Itoh (1983) 34

Fig. 3.3-5 Normalized residual stress results in Komatsu (1997) 35

Fig. 3.3-6 Generated random input of initial deflection 36

Fig. 3.3-7 Generated random input of residual stress 36

Fig. 3.3-8 The dependence relation function 37

Fig. 3.4-1 Idealized stress-strain relation identified from actual test 37

Fig. 3.4-2 Idealized stress-strain relations of steel grades considered in the current study 38

Fig. 3.4-3 Inelastic characteristic of 6 steel grades 38

Fig. 3.4-4 Idealized residual stress distribution and sinusoidal initial deflection surface 39

Fig. 3.4-5 Plate meshing and constrains of 4 edges 39

Fig. 3.4-6 Actual residual stress distribution in steel plate model 40

Fig. 3.5-1 Experimental points to identify a response surface. 42

Fig. 3.5-2 Response surface plotted along with FEM results for R=0.8 43

Fig. 3.5-3 6 response surfaces obtained at R=0.8 45

Fig. 3.6-1 Convergence of random simulation. μ_N and σ_N are mean value and standard deviation of LBS obtained from N random simulations 46

Fig. 3.6-2 Histogram of normalized LBS results..... 47

Fig. 3.6-3 Comparison between current study, ... 48

Fig. 3.6-4 Normalized LBS of steel plate 48

Fig. 3.6-5 Normalized LBS of steel plate with mean – twice of standard deviation level of normalized residual stress and initial deflection 49

Fig. 3.6-6 Comparison of standard deviation values obtained in the current study with those reported in Fukumoto and Itoh (1984) 49

Fig. 3.6-7 Probabilistic distribution LBS regarding 6 steel grades for R=0.8 52

Fig. 3.6-8 Comparison between mean results of the current study, ... 53

Fig. 3.6-9 Comparison between standard deviation results of the current study 53

Fig. 3.6-10 Comparison between the results of the current study with M-2S levels,..... 54

Fig. 3.6-11 Mean values of LBS obtained by 3 methods..... 56

Fig. 3.6-12 Standard Comparison of standard deviation of LBS obtained from Monte Carlo based simulation, Taylor series finite difference (TSFD) and DRS estimations..... 57

Fig. 3.6-13 Variance values with respect to residual stress and initial deflection obtained from TSFD, DRS and Monte Carlo based methods 57

Fig. 3.6-14 Variance of LBS due to individual input random variables: residual stress $\bar{\sigma}_r$ and initial deflection $\bar{W}_0$; TSDF method 59

Fig. 3.6-15 Variance of LBS due to individual input random variables: residual stress $\bar{\sigma}_r$ and initial deflection $\bar{W}_0$; DRS method 59

Fig. 3.6-16 Variance of LBS due to individual input random variables: residual stress $\bar{\sigma}_r$ and initial deflection $\bar{W}_0$; M.C. method..... 60

Fig. 3.6-17 Proposal of safety factor from assumption of normal distribution function 61

Fig. 3.6-18 Partial safety factors obtained in the range of R 0.4≤R≤1.4 62

Fig. 3.6-19 The exceedance probability corresponding to 100, 1000, 10000 and 100000 random input couples processed..... 63

Fig. 3.6-20 The error value corresponding to random simulation processed with 100, 1000, and 10000 random input couples..... 63

Fig. 3.6-21 Identification of σ_{cr}/σ_y values corresponding to fractile level = 1, 3 and 5 % 63

Fig. 3.6-22 Identification of σ_{cr}/σ_y values corresponding to fractile level = 1, 3 and 5 % 64

Fig. 3.6-23 Identification of σ_{cr}/σ_y values corresponding to fractile level = 1, 3 and 5 % 64

Fig. 3.6-24 Partial safety factors obtained directly from the random simulation and compared to Eurocode and AASHTO safety factors 65

Fig. 3.6-25 Comparison of local buckling design resistance of steel plates 66

Fig. 3.6-26 Proposal standard strength curve for compressive simply supported steel plates 66

Fig. 4.1-1 Consideration of stress stage due to initial bending moment 70

Fig. 4.1-2 The plastic stress distribution for homogeneous and hybrid sections 71

Fig. 4.1-3 Yield bending moment of composite homogeneous and hybrid steel section with considering the initial bending moment 71

Fig. 4.1-4 Section classified as compact 72

Fig. 4.1-5 Section classified as non-compact 73

Fig. 4.1-6 Section classified as slender 73

Fig. 4.2-1 Drucker-Prager and Mohr-Coulomb yield criterions 75

Fig. 4.2-2 Stress – strain relation for concrete material model 75

Fig. 4.2-3 Idealized stress – strain relations for steel material model 76

Fig. 4.2-4 Simplified composite girder structure and its dimensions 77

Fig. 4.2-5 Boundary condition for the simplified structure 77

Fig. 4.2-6 Pure bending moment produced by displacement control method 78

Fig. 4.2-7 Cross-section and type of elements 80

Fig. 4.2-8 Initial deflection for the web of the composite girder models 80

Fig. 4.3-1 Assumption on stress distributions for estimation of hybrid yield moment; (a) Initial bending moment on steel section alone, (b) Bending moment on composite section, (c) Superposed stress distribution 81

Fig. 4.3-2 Comparison of hybrid factors for the case without considering initial bending moment 84

Fig. 4.3-3 Comparison of hybrid factors for the case with initial bending moment M_1 = 0.2 M_{ys} 85

Fig. 4.3-4 Comparison of hybrid factors for the case with initial bending moment M_1 = 0.4 M_{ys} 85

Fig. 4.3-5 Comparison of hybrid factors when with initial bending moment M_1 = 0.6 M_{ys} 86

Fig. 4.4-1 Compact-noncompact limit of homogeneous SBHS500 steel section (M_1=0)..... 87

Fig. 4.4-2 Noncompact-slender limit of homogeneous SBHS500 steel sections (M_1=0) 87

Fig. 4.4-3 Noncompact-slender limit of homogeneous SBHS500 steel sections (M_1=0.2M_{ys}) 88

Fig. 4.4-4 Noncompact-slender limit of homogeneous SBHS500 steel sections (M_1=0.4M_{ys}) 89

Fig. 4.4-5 Noncompact-slender limit of homogeneous SBHS500 steel sections (M_1=0.6M_{ys}) 90

Fig. 4.4-6 Compact-noncompact slenderness limit of hybrid SBHS500-SM490Y steel section (M_1=0)..... 91

Fig. 4.4-7 Noncompact-slender limit of hybrid SBHS500-SM490Y steel section (M_1=0)..... 92

Fig. 4.4-8 Noncompact-slender limit of hybrid SBHS500-SM490Y steel section (M_1=0.2 M_{ys}) 92

Fig. 4.4-9 Noncompact-slender limit of hybrid SBHS500-SM490Y steel section (M_1=0.4 M_{ys}) 93

Fig. 4.4-10 Noncompact-slender limit of hybrid SBHS500-SM490Y steel section (M_1=0.6 M_{ys}) 93

Fig. A 1-1.1 Response surface regarding 6 steel grades for each R value..... 107

Fig. A 1-2.1 Response surface regarding each steel grade for R=0.4 108

Fig. A 1-2.2 Response surface regarding each steel grade for R=0.5 109

Fig. A 1-2.3 Response surface regarding each steel grade for R=0.6 110

Fig. A 1-2.4 Response surface regarding each steel grade for R=0.7 112

Fig. A 1-2.5 Response surface regarding each steel grade for R=0.8 113

Fig. A 1-2.6 Response surface regarding each steel grade for R=0.92..... 113
Fig. A 1-2.7 Response surface regarding each steel grade for R=1.04..... 115
Fig. A 1-2.8 Response surface regarding each steel grade for R=1.16..... 116
Fig. A 1-2.9 Response surface regarding each steel grade for R=1.28..... 117
Fig. A 1-2.10 Response surface regarding each steel grade for R=1.40..... 118
Fig. A 2-1.1 Probabilistic distribution of LBS for R ranging from 0.4 to 1.4..... 121
Fig. A 2-2.1 Probabilistic distribution of LBS for R =0.4 122
Fig. A 2-2.2 Probabilistic distribution of LBS for R =0.5 123
Fig. A 2-2.3 Probabilistic distribution of LBS for R =0.6 124
Fig. A 2-2.4 Probabilistic distribution of LBS for R =0.7 125
Fig. A 2-2.5 Probabilistic distribution of LBS for R =0.8 126
Fig. A 2-2.6 Probabilistic distribution of LBS for R =0.92 127
Fig. A 2-2.7 Probabilistic distribution of LBS for R =1.04 128
Fig. A 2-2.8 Probabilistic distribution of LBS for R =1.16 129
Fig. A 2-2.9 Probabilistic distribution of LBS for R =1.28 130
Fig. A 2-2.10 Probabilistic distribution of LBS for R =1.40 131
Fig. A 3-1.1 Composite section elastic stress distribution under positive bending..... 132
Fig. A 3-1.2 Steel section elastic stress distribution under positive bending..... 133
Fig. A 3-1.3 Flexural stresses at first yield 135
Fig. A 3-2.1 Stress block for a composite homogeneous steel section at the ultimate limit state..... 136

LIST OF TABLES

Table 2.2-1 Definition and web slenderness limits in AASHTO and Eurocode 24

Table 3.2-1 Plate dimensions and related information 30

Table 3.3-1 Steel material properties in Komatsu (1997) 35

Table 3.3-2 Scatterness of normalized residual stress applied for 6 steel grades 37

Table 3.4-1 Inelastic characteristic of 6 steel grades 38

Table 3.5-1 Mean value and standard deviation of input random variables 43

Table 3.5-2 R-square values of response surfaces in the range of $0.4 \leq R \leq 1.4$ 43

Table 3.5-3 Coefficient values of 10 response surface functions 44

Table 3.5-4 Coefficient values of 6 Response surfaces regarding 6 steel grades for R=0.8 44

Table 3.6-1 Mean and standard deviation results in whole range of consideration R 47

Table 3.6-2 Mean values 52

Table 3.6-3 Standard deviation results 52

Table 3.6-4 Obtained results of partial safety factors 61

Table 3.6-5 Obtained results of partial safety factors with normal distribution assumption 62

Table 3.6-6 Partial safety factors directly from random simulation based method 64

Table 4.2-1 Girders with compact composite SBHS500 homogeneous steel sections 78

Table 4.2-2 Girders with noncompact and 78

Table 4.2-3 Girders with noncompact and 79

Table 4.3-1 Investigation girders for proposal hybrid factor 84

Table A 3-2.1 Results regarding girders with compact SBHS500 homogeneous steel section 138

Table A 3-2.2 Results regarding girders with noncompact and slender SBHS500 homogeneous steel section for M_1=0 138

Table A 3-2.3 Results regarding girders with noncompact and slender SBHS500 homogeneous steel section for M_1=0.2 M_{ys} 139

Table A 3-2.4 Results regarding girders with noncompact and slender SBHS500 homogeneous steel section for M_1=0.4 M_{ys} 139

Table A 3-2.5 Results regarding girders with noncompact and slender SBHS500 homogeneous steel section for M_1=0.6 M_{ys} 140

Table A 3-2.6 Results of hybrid factor obtained from FEM analysis and proposal of the current study for M_1=0.0 M_{ys} 141
Table A 3-2.7 Results of hybrid factor obtained from FEM analysis and proposal of the current study for M_1=0.2 M_{ys} 141
Table A 3-2.8 Results of hybrid factor obtained from FEM analysis and proposal of the current study for M_1=0.4 M_{ys} 141
Table A 3-2.9 Results of hybrid factor obtained from FEM analysis and proposal of the current study for M_1=0.9 M_{ys} 142
Table A 3-2.10 Results regarding girders with noncompact and slender SBHS500-SM490Y hybrid steel section for M_1=0.0 M_{ys} 143
Table A 3-2.11 Results regarding girders with noncompact and slender SBHS500-SM490Y hybrid steel section for M_1=0.2 M_{ys} 143
Table A 3-2.12 Results regarding girders with noncompact and slender SBHS500-SM490Y hybrid steel section for M_1=0.4 M_{ys} 144
Table A 3-2.13 Results regarding girders with noncompact and slender SBHS500-SM490Y hybrid steel section for M_1=0.6 M_{ys} 144

CHAPTER 1

BACKGROUND

1.1 Introduction of composite girder bridge

Steel-Concrete composite girder is one of the best structural options for short and medium Railway and Highway bridge superstructures. This structural type can employ steel and concrete materials in ultimate strength by assigning a concrete slab part under total compression and a steel girder under in-plane bending or under tension. Regarding the service characteristics, the concrete slab works well with asphalt surface layer eliminating the fatigue problem as in the case of orthotropic deck. The composite superstructure is lighter and more slender as compared to a concrete bridge with the same span length and width, this characteristic reduces the mass effect on supports under seismic loads. In Japan, an industrialized country with priority in environment protection, the employment of steel material in bridge constructions has been a reasonable trend

Like in Germany and some European countries, in Japan just after the World War II, the total cost of composite girder bridges was governed by the cost of construction materials, i.e steel. Saving steel material was prioritized in structural design. However, with the industrial development, steel production increased rapidly and hence resulted in the lower steel material cost. Recently the increase of labor cost has changed the total cost of composite construction. The influence of labor cost increase on total construction cost outweighs the influence of steel material saving . Thus to reduce the labor work, composite girder bridges have been designed with the trend of simpler structures such as thicker web plates with minimum amount of stiffeners.

Fig. 1.1-1 The continuous composite twin I-girder bridges in Europe (Sétra, 2010)

From 1995 to 2000 in Japan, with the aim of reducing the bridge construction cost, many research projects, which develop new economical solutions, have started under the leadership of Japan Highway Public Corporation (JH). Among the study results, a continuous composite twin I-girder bridge (presented in Fig.1.1-1) has been proposed as a competitive structural option to conventional multi I-girder with "dense" transverse stiffening members. This structural bridge type was found to be good structural solution for medium span bridge with span length within the range from 30m to 60m. The cross-beams are designed with standard structural steel sections. However, cross-beams at bearing locations bracing 2 main longitudinal girders against horizontal loads (wind and earthquake) are deeper and fabricated by shop-welding. The cross-beams could be designed without contact or with contact with the concrete slab. The design process will be more convenient with non-contact cross-beams.

In 1995, Chidorinosawagawa Bridge was built as a typical composite girder bridge structure as an economical solution for medium span bridges. The superstructure was designed with twin steel I-shape girders, continuously over piers. The smaller-sized I steel cross beams are arranged at the distance from 5 to 10 m without lateral bracing members. For the construction, the complete steel girder system was launched forward into the design location and then the concrete slab was *casted-in-situ* in sequence segments without un-shored system. For segments at pier location, the steel girders were jacked up in advance and when concrete material hardened, the girder was jacked down on bearing level and consequently, the compression was induced in concrete segments on pier location. With only 2 main longitudinal girders, simple I cross beams, and without shore system the work of fabrication and the number of labor was reduced significantly. Since then the application of this bridges superstructure type has become a popular trend in Japan. Although some design assignments of this bridge violated several provisions of Japanese Specification for Highway Bridge (JSHB) the validity has been verified by analytical and experimental studies.

Besides the steel-concrete composite twin I-shape girder structures, recently the composite box and multi-box girders have been employed popularly in Japan for the range of medium spans. When subject to bending, steel box and plate girders behave similarly but they are under a torsional moment due to either eccentric loading or horizontal curvature of the structure, the box girders present a greater stiffness. The composite box girders also have a more aesthetical appearance than that of composite I-shape plate girders. Moreover, the composite box or multi box girders can be placed at small areas available for supports and this is a common problem in Tokyo and other big Cities in Japan. With these advantages the

composite box and multi-box superstructure types have been applied commonly for viaducts, curved bridges, and interchanges in urban areas in Japan.

The construction method for concrete slab is an important issue for designing composite girders. The unshored construction method with movable formwork system is applied commonly for casting the concrete slab of composite superstructure. This method is stated in AASHTO "The unshored construction generally is expected more economical" and preferred over shored construction. For unshored construction, in the period of casting concrete, only the steel girder resists acting loads from wet concrete, the self-weight of the steel girder, the formwork system and construction equipments. Those acting loads induce an initial bending moment M_1 (as shown in Fig.1.1-2 and Fig.1.1-3) in the steel girder. In this stage, under a pure bending moment, the local buckling resistance at the mid-span zone of compressive flange (Fig.1.1-2 and 1.1-3) is considered as critical strength of the steel girder. Referring famous assumption for studying local bucking in steel structures, the local buckling strength of I-shaped and un-stiffened box girders can be determined by corresponding simplified outstanding plate (simply supported plate with 1 free edge) and 4 edge simply supported plate respectively as described in Fig.1.1-2 and Fig.1.1-3.

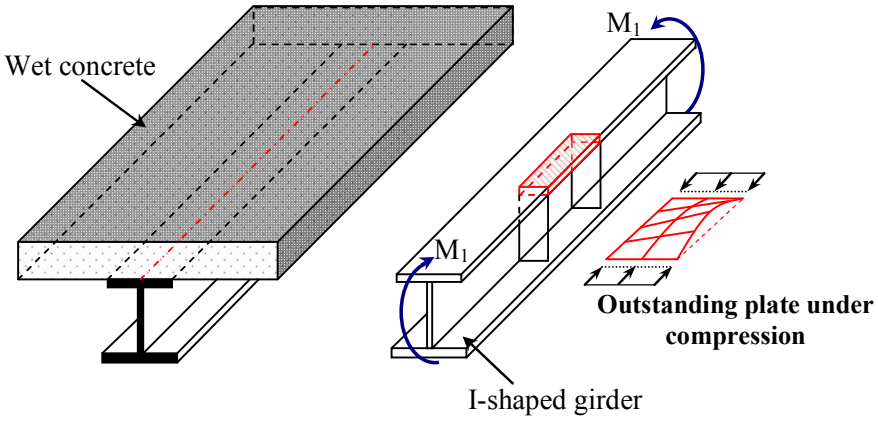

Fig. 1.1-2 Local buckling mode in compressive flange of I-girder under loading of wet concrete and simplified outstanding plate

When concrete becomes sufficiently hardened, the girder section starts acting compositely with secondary dead loads, live loads and other service loads. Based on the internal load distribution, the composite girder can be simply divided into 3 zones as presented in Fig.1-4.

Under the self-weight of the girder and secondary dead loads, zone 1 is dominated by shear force induced from bearings reaction, zone 3 is mainly affected by pure bending moment and

zone 2 is the combination of shear force and bending moment. For acting of vehicle loads zone 1 is also under the domination of shear force, the internal force in zone 2 and 3 is combination of shear force and bending moment but magnitude of bending moment in zone 3 is more significant than that of zone 2. However, Nagai (2009), based on experiments, concluded that the moment-shear interaction effect is negligible in designing composite girder, hence bending and shear strength of composite girders can be studied separately. For typical composite girders, the span-to-depth ratio is within the range from 18 to 20 (Collings, 2005), with this dimension scale, the composite girder is classified as flexural structure therefore the bending moment capacity can be considered as the critical strength of the girder.

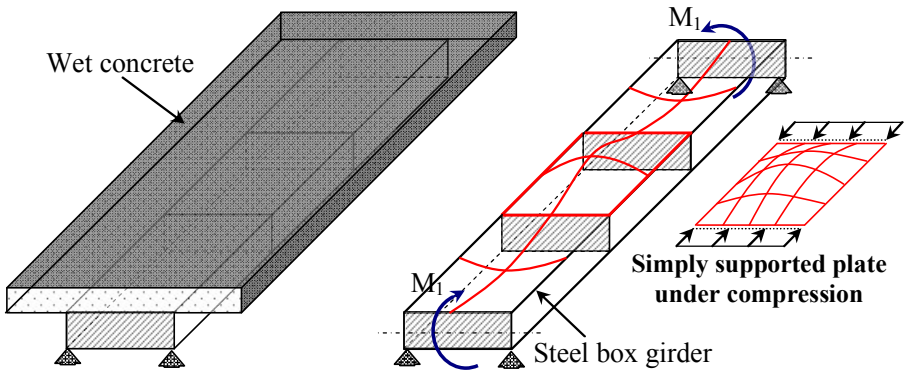

Fig. 1.1-3 Local buckling mode in compressive flange of un-stiffened box girder under loading of wet concrete and simplified simply supported plate

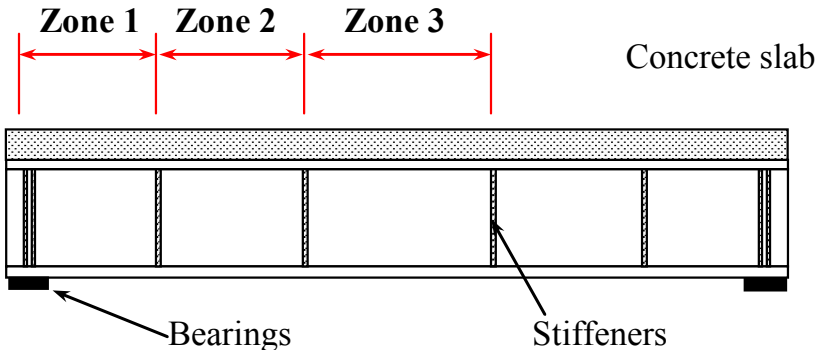

Fig. 1.1-4 Simplified design of composite girder

Under positive bending moment, the compressive flange is restrained by hardened concrete hence the local buckling at that flange no longer affects flexural strength of the composite girder. The bending capacity of composite girder section is mainly affected by local buckling in compressive zone of web plate, lateral buckling of the girder and the crushing in concrete slab. With sufficient distance of web stiffeners or transverse bracing, the lateral bucking can

be avoided. Ignoring the lateral buckling effect, the interaction of local buckling in the web plate and crushing in concrete slab of composite twin I and box girders can be studied with the simplified composite unsymmetrical I-shape girder and concrete slab above as shown in Fig.1.1-5.

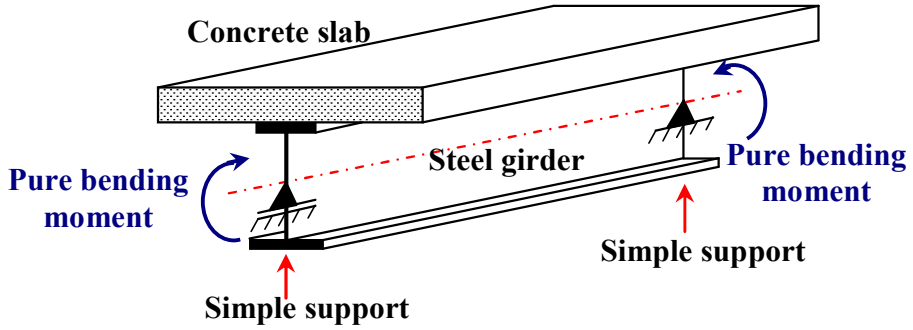

Fig. 1.1-5 Simplified composite girder structure under pure bending moment

The current study concentrates on studying the local buckling (compressive) strength of simply support steel plates and bending capacity of composite girders. The study of outstanding steel plates is implemented simultaneously by another research group.

1.2 Design issues for composite girder bridges

1.2.1 Thicker steel plates and new steel grades

The current design equation of Japanese Specification for Highway Bridge (JSHB, 2002) on load-carrying capacity of 4-edge simply supported steel plates has been originally proposed in version 1980 (JSHB, 1980). This design equation is applied for steel grades with $\sigma_y \leq 450$ MPa. For new requirements of bridge construction practice and by advanced technologies in Japan, the thicker steel plate with thickness up to 100 m has been produced. Consequently, since 1996, JSHB allowed to apply the steel plates with the maximum thickness = 100 mm in steel bridge structures. However for thicker steel plates with thickness > 50 mm, the reduction of yield values appears if compared to thinner steel plates of the same grade. Hence it is necessary to study further on steel plate with thickness > 50 mm.

Application of high strength steel plate in steel structures has been always a desire of consultants and contractors. The high strength steels up to 690 MPa have been produced and employed in bridge constructions since the early 1940's in America but with disadvantages as low ductility and poor weldability due to high carbon content. To fabricate, these steels required the pre-heating treatment but pre-heating work has significantly influence on the

fabrication cost of steel bridges. Recently in Japan, new high strength steels for bridge structures (Bridge High-Performance Steels) have been developed. The carbon content in steel is about 0.05 – 0.25 %, some alloying elements are included such as about 2% manganese and small quantities of copper, nickel, niobium, nitrogen, vanadium, chromium, molybdenum, titanium, calcium, or zirconium, rare earth elements, . . . In 2008 these steels have been standardized by Japanese Industrial Standars (JIS, 2008) under the name SBHS500, SBHS700 with design yield strength = 500 MPa and 700 MPa, respectively. The fabrication of SBHS500 steel doesn't require pre-heating treatment and minimum preheating temperature for SBHS700 steel is at 50^{o}C. SBHS steels pose the advantages of high yield strength and good weldability but their inelastic behavior is different from that of ordinary steels as almost no yield plateau and greater yield-to-tensile strength ratio (as shown in Fig.1.2.-1). The design yield strength of these steel grades doesn't change with the change of the thickness.

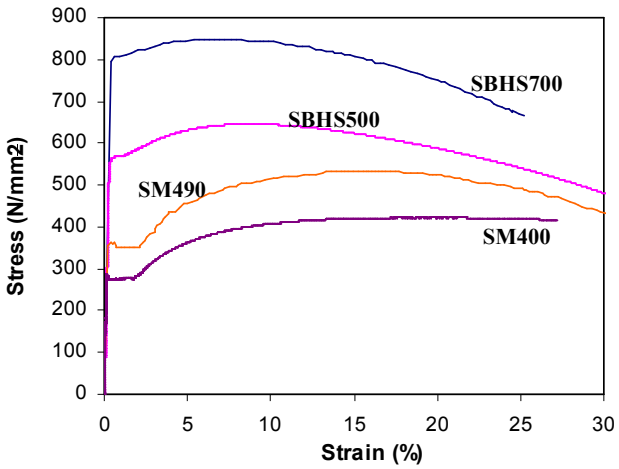

Fig. 1.2-1 The actual test stress-strain relations of normal and high strength SBHS steel grades

By now, the SBHS500 steel has been employed in several steel bridge projects such as Nagata Bridge and Tokyo Gate Bridge. Nagata Bride is on the highway connecting Fussa and Akiruno cities in Tokyo over Tama River. The bridge structure comprises 4 continuous spans with entirely bridge length of about 250 m. The structural type of Nagata Bride could be classified as steel-concrete composite girder bridge but the space steel pipe truss system is employed instead of the conventional I-shape or box girder system (shown in Fig.1.2-2). Thickness of steel pipes employed in this Bridge Project is up to 67 mm. The pipe truss system was fabricated with cold formability and on-site welding.

The Tokyo Gate Bridge can be seen as a Mega Structure and World's largest-scale fully welded continuous truss bridge with 4 traffic lanes, entire length of 2933 m, main span of 440

m, and marine area of 1,618 m, the ship tolerance of 300m x 54.6m, the maximum height from water level of 87.8 m. The bridge connects the central breakwater landfill and Koto-City Wakasu, straddling the Tokyo Port Third Seaway. The general view of Tokyo Gate Bridge is shown in Fig.1.2-3.

Fig. 1.2-2 Nagata Bridge with application of SBH500 steel grade to the space truss system

Fig. 1.2-3 Tokyo Gate Bridge with application of SBH500 steel grade to the full-welded truss girder

As presented above, the SBHS500 steel was employed in a few steel bridge projects and SBHS700 has not been applied in any bridge structure yet. Moreover, most these bridges are considered as steel truss system and steel members are mainly under tension or compression. Besides, just a few studies on application of SBHS steels on steel bridge structures, specifically on local buckling resistance of compressive steel plates and flexural girder structures. To apply the SBHS steel in composite girder bridges, it is necessary to have more compact studies concerning this issue.

So far, only a few studies (Tonegawa et al., 2005; Okada and Kato, 2009) have ever tried to investigate the bending moment capacity of SBHS500 composite girders. Hence, more intensive studies on designing composite girder bridges with application of SBHS500 and SBHS700 steels are required.

1.2.2 Allowable Stress and Limit State Design Method

Beside the issue of applying new steel grade to composite girder bridges, the design method must be considered as well. The current design equations of JSHB were proposed based on the method of Allowable Stress Design (ASD). For this method, the design resistance of the structure are specified as allowable stress values. The allowable stresses are usually taken as yield value of relevant structural materials. The advantage of this method is simplicity because the calculation bases on the assumption of elastic behavior of material and linear relation of stress-strain in the structural sections. Because of applying the linear and elastic assumptions, ASD method can be reasonable for designing steel structures, which behave linearly once stress states are under yield point, which ensures safely below the ultimate tensile strength of steel material. Besides, the local buckling stress of compressive steel plate, one of the most critical design strengths of steel structures, could be dealt by the elastic buckling theory (Timoshenko and Gere, 1961).

The linear – elastic analysis applied in ASD method might not give the proper assessment of structures at inelastic or failure states. When the critical structural components attain sufficient ductility, the plastic hint assumption can be applied for these components and there is the internal forces redistribution, hence the less critical component must be reconsidered. The ASD method, based on structural stress evaluation, is impossible to assess the structural deflection level, sections with yielding or cracking occurrence. In the current study, authors desire to investigate the bending resistance of composite girders considering the interaction of yielding in flange, local buckling in web part and crushing in concrete slab, however, it is too simplified and rough if just based on stress evaluation with assumptions of elastic material and linear stress-strain relation. For design of steel plates under compression, to identify the compressive strength of steel plates with considering inelastic range of steel material, existence of imperfections (residual stress and initial deflection for example) in steel plate, the non-linear behavior of stress redistribution under the step-by-step compression, the application of elastic buckling theory is not the best solution.

On other hand, the Limit State Design (LSD) method evaluates the probability of occurrence for the state which related to the collapse of the whole or substantial part of structure (Ultimate Limit State) or disruption of normal use of structure (Serviceability Limit State). Ultimate limit states are specified by very low probability of failure occurrence.

The common ultimate limit states:

- Loss of static equilibrium of entire structure or part of structure (e.g. overturning, uplift, sliding)
- Loss of load-resistance capacity of a member due to fatigue, or loading beyond material strength, or due to buckling instability, or a combination of these two phenomena.
- Overall instability, inducing very large deformation or collapse, caused by, for example, aerodynamic or elastic critical behavior or transformation into a mechanism

Regarding ULS design, the design resistance can be stress, bending capacity, shear strength, interaction strength of bending-shear, structural deflection, crack opening level, fatigue … And hence, steel plate under compression and flexural composite girder should be designed according to assessment point of view of Ultimate Limit States.

The LSD method has become the orientation design method as applied in current design codes such as Eurocode (1996) and AASHTO (2005). Therefore, it is necessary to shift from ASD method to LSD method to follow the global trend and update the existing Japanese Design Code.

1.3 Trend of recent design methods

1.3.1. Probability-based design

The resistance and load factors are generally designed to ensure that the acting load reaching design resistance just with reasonable small probability of failure. The design based on the probability of failure can be considered as reliability-based design. Considering Load Q and Resistance R as random variables, the reliability of design Resistance is presented in Fig.1.3-1

The shaded region represents the small probability of failure and quantified by Eq.1.3.1-1.

$$p_f = 1 - p_s = P(Q > R) \tag{1.3.1-1}$$

where $p_s = P(R > Q)$ is probability of survival

The probability of failure can also be understood as

$$p_f = 1 - p_s = P(g(R,Q) = Q - R > 0) \tag{1.3.1-2}$$

and presented as a random density distribution shown in Fig.1.3-2

The determination procedure of probability failure p_f can be classified base on 3 levels of approximation.

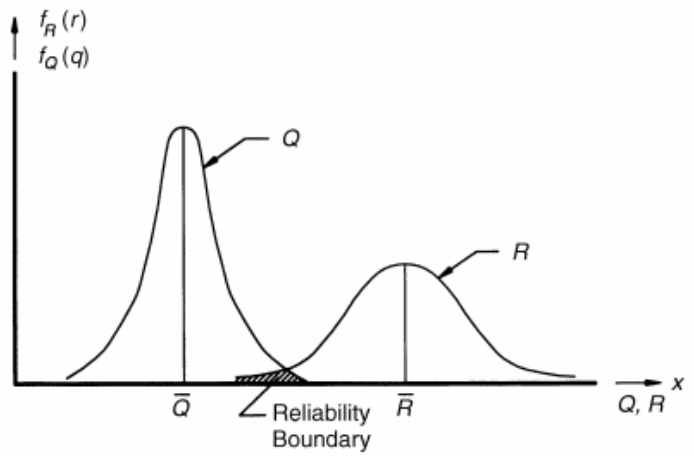

Fig. 1.3-1 Probability density functions for load and resistance

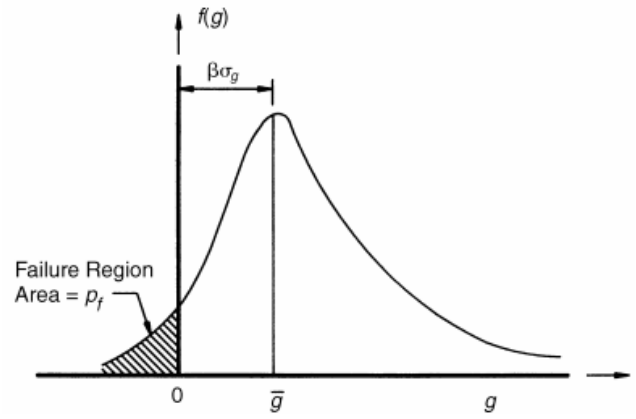

Fig. 1.3-2 Definition of safety index for R and Q

Level 3: The correct answer is obtained by applying full probability methods. This level method is usually difficult to employ due to the frequent lack of statistical data. It is just used for some special structures or extreme loads.

Level 2: To reduce the numerical difficulty and overcome the lack of data, idealizations and reasonable approximations are applied to achieve sufficiently accurate results for most

structural application. The failure boundary of each failure mode is determined by structural theories with respect to random variables of load and resistance.

Level 1: This is a semi-probablistic method in which proper levels of reliability are achieved for each structural element by applying a number of partial safety factors to a pre-defined set of characteristic values of the variables. The characteristic value of each variable has a pre-defined low probability of occurrence and is determined from statistical information of the variable obtained by test or measurements. If the statistical information is not available, the data based on past practice can be applied. The partial safety factors could be determined by a Level II (or III) method depending on the degree of safety.

1.3.2. Allowable stress of JSHB

The format of design equation is presented in Equation

$$\frac{\boldsymbol{R_n}}{\boldsymbol{FS}}\boldsymbol{IC} \geq \sum_{i=1}^{m} \boldsymbol{Q_i} \tag{1.3.2-1}$$

Where: R_n and FS stand for standard ultimate strength (stress) and factor of safety respectively, IC stands for the increase coefficient, which depends on the load combination. The format of design equation applied in JSHB is the improvement from ASD format by employing the increase coefficient IC. The purpose of employing IC is to consider the different variabilities of different loads.

For the design equation of compressive steel plates, FS ≈ 1.7 depends on each steel grade and thickness of the steel plates.

1.3.3. AASHTO – Load and Resistance Factor Design (LRFD)

The format of design equation applied in AASHTO is described in Equation (1.3.3-1)

$$\Phi \boldsymbol{R_n} = \boldsymbol{R_d} \geq \sum_{i} \eta_i \gamma_i \boldsymbol{Q_i} \tag{1.3.3-1}$$

Where Φ and R_n are the resistance factor and nominal design resistance respectively; η_i, γ_i are load modification factor and statistically based load factor, respectively; Q_i is force effect.

The Load and Resistance Factor Design (LRFD) applied in AASHTO is classified as level 2 of probabilistic approximation. In AASHTO-LRFD the probability of failure is expressed by the use of safety index β which shown in Fig.1.3.1-2, the distance from the origin to the mean value in Fig. 1.3.1-2 becomes the level of safety and the number of standard deviation β in this level is the safety index.

The format of design equation applied in AASHTO deals with the different variabilities of different loads by partial load factor γ_i to attempt to achieve uniform safety over the range of the proper loads. However, because of applying only one resistance factor this method does not deal with all the limit states (Chatterjee, 2003).

For the case of designing a steel structure in which its design strength much concerns compressive simply supported steel plate, the resistance factor Φ is equal to 0.9.

1.3.4. Eurocode – Format of partial safety factor format

The format of design equation using in Eurocode is presented in Equation 1.3.4-1

$$R_d = \frac{1}{\gamma_{Rd}} R\left\{\eta_i \frac{X_{k,i}}{\gamma_{m,i}}\right\} \geq Q_d = \sum_{j\geq 1} \gamma_{G,j} G_{k,j} + \gamma_P P + \gamma_{Q,1} Q_{k,1} + \sum_{j\geq 1} \gamma_{Q,i} \psi_{0,i} Q_{k,i} \qquad (1.3.4\text{-}1)$$

$i \geq 1$

The design resistance R_d is defined as a function of partial safety factors: γ_{Rd} covering resistance model and geometric deviation, characteristic material strength $X_{k,i}$, conversion factor ηi, partial safety factor for material $\gamma_{m,i}$. For steel and reinforcement the conversion factor η_i is specified =1 and =0.85 for steel and concrete material, respectively.

The design load Q_d is defined by the combination presented on the right hand side of Eq.(1.3.4-1) in which $G_{k,j}$ and $\gamma_{G,j}$ represent permanent actions and corresponding partial safety factor for unfavorable permanent actions G. P represents prestressing; $Q_{k,1}$ and $\gamma_{Q,1}$ represent leading variable action and corresponding partial safety factor; $Q_{k,i}$, $\gamma_{Q,i}$, and $\Psi_{0,i}$ represent characteristic value of the variable action i, partial factor for unfavourable variable actions i and reduction factor for combination value of load effect, respectively.

The partial safety factor design applied in design equation of Eurocode is classified as level 1 of probabilistic approximation. The design resistance regarding this format is based on combination of separated reliability level of material and prediction model considering the geometrical information or imperfections of design member. For the design of local buckling strength of steel plates regarding steel bridges, Eurocode combined 2 partial safety factors regarding material and geometrical information as $\gamma_{Rd}\,\gamma_{m1} = \gamma_{M1} = 1.1$

The format of partial safety factor applied in Eurocode can help balance the requirements of safety level and saving of construction cost and the improvements of JSHB have tended forward this format. The current study aims to obtain the statistical information of local buckling strength of simply supported steel plates with consideration of geometrical data, imperfections of the plates, current steel grades employing for steel bridges in Japan and new SBHS steel grades. Based on these results the relevant partial safety factor γ_{Rd} will be proposed.

1.4 Summary of issues

As mentioned and discussed in the above section, the issues are summarized and necessary to be considered

First, the thickness of steel plates tends to increase in recent steel bridge construction. In fact, the regulation for the maximum plate thickness in JSHB has been changed from 50mm to 100mm since 1996. However, the LBS design equation in JSHB has not been revised yet to account for thicker plate effects.

Secondly, the Steels for Bridge High Performance Structures (SBHS) have been standardized by Japanese Industrial Standards (JIS) in 2008 (JIS, 2008). SBHS steels possess the advantages of high yield strength and good weldability, but their inelastic behavior is different from that of ordinary steels, for example, almost no yield plateau and greater yield-to-tensile strength ratio. It is therefore necessary to investigate the applicability of current LBS design equation in JSHB to SBHS steel plates.

Thirdly, recent design specifications, such as AASHTO LRFD specifications and Eurocode, employ the partial factor format, in which safety factors consider separately the influence of

uncertainties and variabilities originating from different causes. Currently, JSHB has trended to shift from ASD to LSD method with the format of partial safety factors.

CHAPTER 2

LITERATURE REVIEW AND OBJECTIVES

2.1 Reviews on compressive steel plates

This section reviews important studies on compressive simply supported steel plates, especially with considering the influence of initial imperfections (residual stress and initial deflection) on normalized local buckling strength (LBS) σ_{cr}/σ_y, in which σ_{cr} and σ_y are the critical (local buckling) strength and relevant yield strength of steel plate, respectively.

The literature review in this section is summarized through Fig.2.1-1. The results and proposals of these studies were plotted as format shown in this figure, in which the normalized LBS to the yield strength is presented as function of slenderness parameter R.

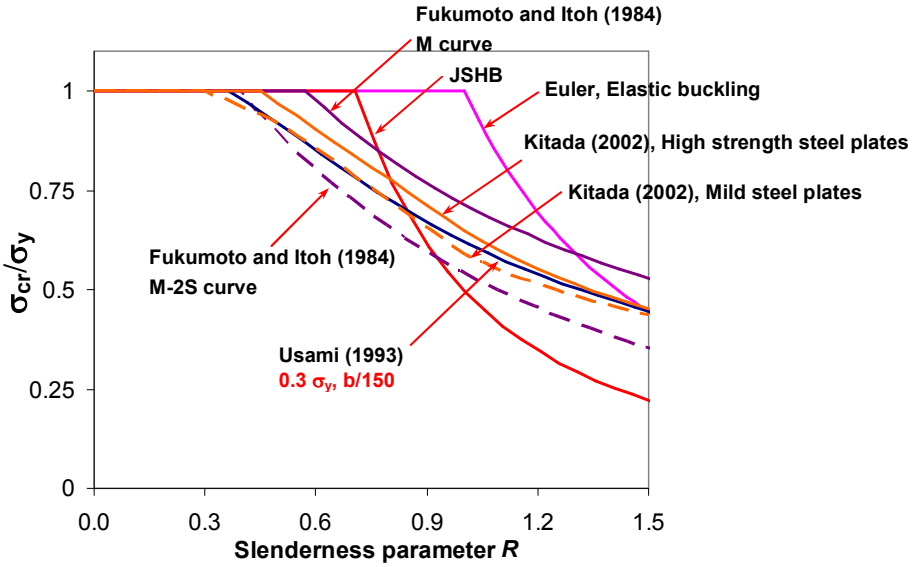

Fig. 2.1-1 Comparison of current design equation for compressive steel plate to results of other studies

$$R = \frac{b}{t}\sqrt{\frac{\sigma_y}{E}\frac{12(1-\nu^2)}{\pi^2 k}} \tag{2.1-1}$$

in which b, t, σ_y, E, μ, k stand for the plate width, thickness, yield strength, elastic modulus, poison ratio, and buckling coefficient, respectively.

The LBS of steel plate can be determined by compressive experiment of single plate or welded box with sufficient short length or by analyzing the FEM models. For compressive

experiment the measurement of imperfections as residual stress and initial deflection should be obtained even it is costly, especially for measurement of residual stress. On other hand with FEM models, imperfections can be assigned without the difficulty. These are two main methods, which applied in these studies to obtained LBS of steel plates.

Fukumoto and Itoh (1984) implemented an extensive investigation on LBS of steel plates based on a large collection test data of single plates, welded square box, square tube, welded rectangular box and rectangular tube, which conducted in Europe, Japan and America. For this test data, significant percentages of tests were targeted on single plates, about 13% of tests was conducted with high tensile strength steels (σ_y>430MPa). The measurement data of residual stress and initial deflection were recorded and reported as histogram form. There were 383 plate tests having record of residual stress, and 172 tests without residual stress. Considering the test with residual stress, the results of LBS were normalized to the relevant yield values and plotted with corresponding slenderness parameter values. Based on the nonlinear regression analysis with these results the authors proposed the mean curve and the mean minus twice of standard deviation (will be presented in following sections). These curves are presented in Fig.2.1-2.

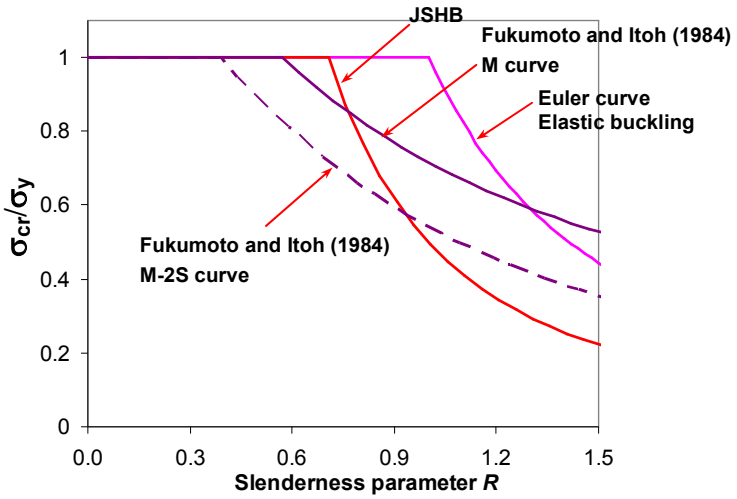

Fig. 2.1-2 Comparison of M, M-2S curves proposed in Fukumoto and Itoh (1984) to Elastic Buckling curve and current design curve of JSHB

Mean (M) curve

$$\frac{\sigma_{cr}}{\sigma_y}=\begin{cases}\dfrac{0.968}{R}-\dfrac{0.286}{R^2}+\dfrac{0.0338}{R^3} & for \quad R\geq R_0=0.571\\ 1 & for \quad R<R_0=0.571\end{cases} \tag{2.1-2}$$

Mean minus twice of standard deviation (M-2S) curve

$$\frac{\sigma_{cr}}{\sigma_y} = \begin{cases} -0.174 + \dfrac{0.968}{R} - \dfrac{0.286}{R^2} + \dfrac{0.0338}{R^3} & for \quad R \geq R_0 = 0.389 \\ 1 & for \quad R < R_0 = 0.389 \end{cases} \tag{2.1-3}$$

In Fig.2.1-2 the M-2S curve showed that the current JSHB design equation is un-conservative within the range 0.4<R<0.9 and over-conservative in the range R>0.9.

However, to propose the M and M-2S curves of compressive strength, the study considered the tests with initial deflection level $W_0/b > 1/150$ which is upper limit specified by the current JSHB. The histogram of residual stress concluded all steel grades and there were not any discussion on the difference of normalized LBS between normal (ordinary) steel and high strength steel. One of conclusions in the study states that further experimental investigations should be implemented for high strength steel plates with slenderness parameter R near limiting value R_0

To obtain the LBS scaterness of simply supported steel plates, collecting test data as implemented in Fukumototo and Itoh (1984) is not the only way. It can be the combination of measurement data and numerical analyses. The numerical analyses of steel plates under compression are processed with considering scaterness of geometrical imperfections obtained from test data, and consequently the LBS scatterness can be obtained. Komatsu and Nara (1983) collected a large data of initial deflection of steel bridge girders. The measurement was implemented for members with aspect ratio (a/b) = 0.5; 1.0; and 2.0. The study concluded that probability density distribution function of the initial deflection W_0/b (W_0 and b are maximum initial deflection and plate width, respectively) can be well described by Weibull distribution. Considering scatterness of initial deflection as a random input for numerical simulation, authors obtained the scatterness of LBS of compression members and proposed the strength curves corresponding to 90%, 95%, 99% fractile values. The proposal function corresponding to 95% fractile of LBS is presented in Fig.2.1-3 and Eq.2.1-4.

$$\frac{\sigma_{cr}}{\sigma_y} = \begin{cases} 1.217 - 0.108R - 0.742R^2 + 0.410R^3 & for \quad R \geq R_0 = 0.5 \\ 1 & for \quad R < R_0 = 0.5 \end{cases} \tag{2.1-4}$$

These results show that the current JSHB design equation un-conservative within the range 0.5<R<0.75 and over-conservative in the range R> 0.75. The study also states that the Weibull distribution is good approximation for the probability density distribution function of LBS scatterness of steel plates.

The scatterness of LBS results was obtained in (Komatsu and Nara, 1983) based on scatterness of initial deflection and the constant conservative level of residual stress σ_{rc}/σ_y = -0.4. However, the residual stress level responses stochastically due to welding condition.

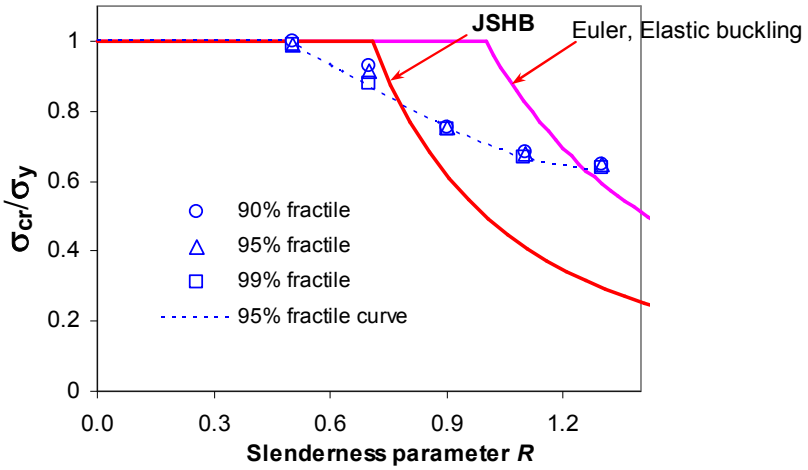

Fig. 2.1-3 Comparison of LBS scatterness of steel plates to Elastic buckling and current JSHB curves

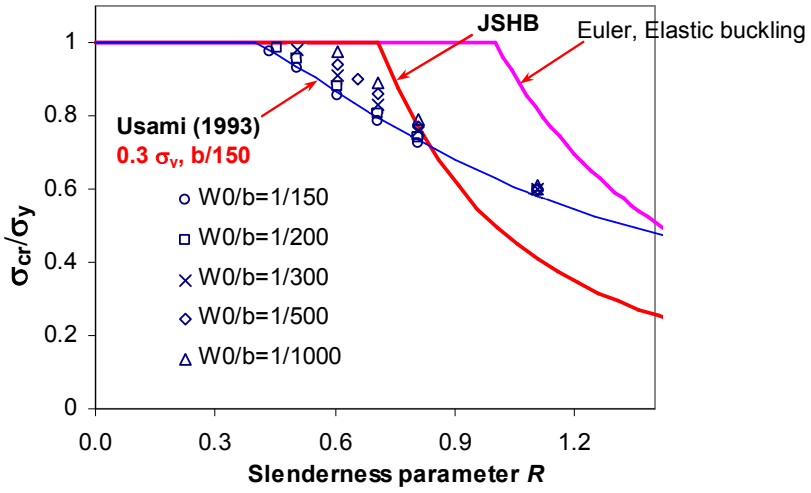

Fig. 2.1-4 Comparison of Usami (1992) results to Elastic buckling and current JSHB curves

With the effort of presenting LBS of steel plates not only as the function of slenderness parameter R, but also explicitly effects of normalized residual stress and initial deflection, Usami (1992) processed a significant number of FEM steel plate model analyses. The normalized initial deflection W_0/b = 1/150, 1/200, 1/250, 1/300, 1/500, 1/1000 and normalized residual stress level σ_{rc}/σ_y = 0.0, 0.1, 0.2, 0.3, 0.4, 0.5 were considered. From the obtained results, the author proposed the equation of steel plate LBS as presented in Fig.2.1-4 and Eq.2.1-5.

$$\frac{\sigma_{cr}}{\sigma_y} = \frac{1}{2\lambda}\left[\beta - \sqrt{\beta^2 - 4\lambda}\right] \tag{2.1-5}$$

$$\beta = 1 + C(\lambda - \lambda_0) + \lambda$$

$$\lambda_0 = A - B\ln\left(\frac{W_0}{b}\right) \le 1.0$$

where:

$$A = -0.05 - 0.542\exp\left(-11.9\frac{\sigma_{rc}}{\sigma_y}\right)$$

$$B = 0.09 + 0.107\exp\left(-12.4\frac{\sigma_{rc}}{\sigma_y}\right)$$

$$C = -157\left(\frac{W_0}{b}\right)\left(\frac{\sigma_{rc}}{\sigma_y}\right) + 43\left(\frac{W_0}{b}\right) + 1.2\left(\frac{\sigma_{rc}}{\sigma_y}\right) + 0.03$$

By plugging values of W_0/b = 1/150 and σ_{rc}/σ_y = 0.3, considered as conservative normalized initial deflection and residual stress, into Eq.2.1-5, the result curve of Usami study represents the un-conservativeness within the range 0.4<R<0.85 and over-conservative in the range R>0.85

Targeting only steel grade SM490Y with σ_y=350 MPa and assumption of elastic-perfectly plastic, the simulation steel plate tests in Usami study did not consider the hardening behavior and hence it is unreasonable to employ these results for considering high strength steel plates with small range of yield plateau strain and steel plates with higher yield values. The assumption of elastic-perfectly plastic for steel material is also unreasonable for considering the LBS of steel plates with low level of slenderness parameter (R<0.5) because within this range of R compressive strain of the plates can attain the hardening strain point. Besides, the assumption of aspect ratio a/b = 0.5 together with conservative level of initial deflection

W_0/b=1/150 for steel plates induced the more conservative results. According to measurement data on compression plates of actual steel bridges reported in Komatsu and Nara (1983), the mean and standard deviation values of initial deflection level for the case of α=0.5 is much lower than for the case α=1, specifically mean $(W_0/b)_{\alpha=0.5}$ = 1/2069, standard deviation $(W_0/b)_{\alpha=0.5}$ = 1/3132, $(W_0/b)_{\alpha=1}$ = 1/591, standard deviation $(W_0/b)_{\alpha=1}$ = 1/981. Based on these actual data of initial deflection level, the LBS of steel plate with α=1 is more reasonable.

Kitada et. al. (2002), by applying FEM models, investigated the difference of steel plate LBS made by normal steel (SM400) and high strength steel (HT685 and HT785). By referring Komatsu (1977), authors assigned the residual stress level σ_{rc}/σ_y = -0.15 to high strength steel plates and σ_{rc}/σ_y = -0.3 to normal steel plates. All steel plate models applied the initial deflection level W0/b = 1/150. From obtained results authors proposed the design strength curves to normal and high strength steel plates as presented in Eq.2.1-6 and Eq. 2.1-7.

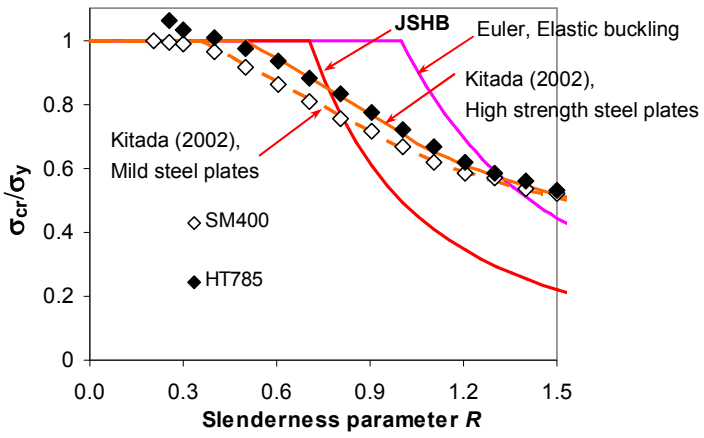

Fig. 2.1-5 Comparison of Kitada (2002) results to Elastic buckling and current JSHB curves

For normal steel plates

$$\frac{\sigma_{cr}}{\sigma_y} = \begin{cases} 1.0 & R \le 0.35 \\ -0.52R + 1.182 & 0.35 < R \le 1.0 \\ \dfrac{0.662}{R^{0.65}} & 1.0 < R \le 2.0 \end{cases} \qquad (2.1\text{-}6)$$

For high strength steel plates

$$\frac{\sigma_{cr}}{\sigma_y} = \begin{cases} 1.0 & R \le 0.5 \\ -0.58R + 1.29 & 0.5 < R \le 1.0 \\ \dfrac{0.7}{R^{0.75}} & 1.0 < R \le 2.0 \end{cases} \tag{2.1-7}$$

As shown in Fig.2.1-5 the current JSHB design equation appears to be un-conservative within the range 0.35<R<0.8 for SM400 steel grade and 0.5<R<0.75 for HT785 steel grade

The studies of Usami (1992) and Kitada el al., (2002) were based on the deterministic method in which obtains conservative results by considering a specific conservative degree of normalized residual stress and initial deflection, hence the application of this method can not result in the statistical information of LBS.

2.2 Review on bending composite girder

2.2.1. Hybrid factor

Yield moment is an important quantity in designing composite girders. To determine the yield moment of composite hybrid steel girders, the hybrid factor as proposed in current AASHTO design code can be applied.

Based on elastic assumption of stress-strain distribution in beam section as shown in Fig.2.2-1 and Fig. 2.2-2, Schilling (1968) and Subcommittee on Hybrid Beams and Girders (1968) derived and proposed the hybrid factors for symmetrical I-shaped non-composite beam and composite hybrid girders as presented Eq.2.2-1, Eq. 2.2-2.

Hybrid factor for non-composite steel section

$$R_h = \frac{M_{yf}}{M_y} = \frac{12 + \beta(3\alpha - \alpha^3)}{(12 + 2\beta)} \tag{2.2-1}$$

where

$$\alpha = \frac{f_{yw}}{f_{yf}} \qquad \beta = \frac{2A_w}{A_f}$$

M_y, M_{yf} stand for yield moment of homogeneous and hybrid beams of flange steel respectively, f_{yf}, f_{yw} stand for flange and web yield point respectively

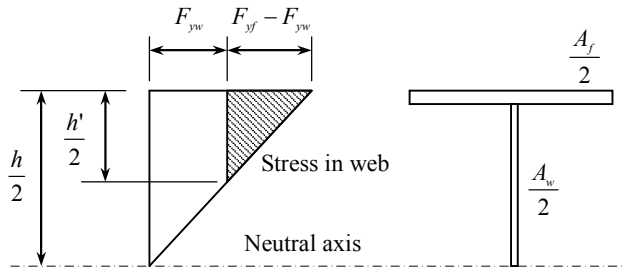

Fig. 2.2-1 Stress distribution in non-composite hybrid beam section

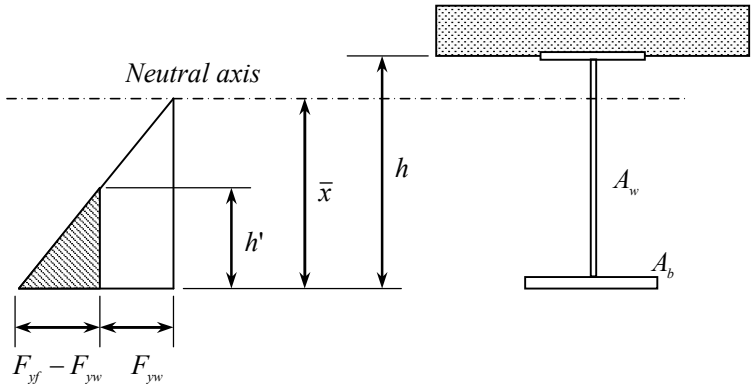

Fig. 2.2-2 Stress distribution in composite hybrid beam section

Hybrid factor for composite hybrid beams

$$R_h = \frac{M_{yf}}{M_y} = \frac{f_{af}}{f_f} = 1 - \frac{\beta\psi(1-\alpha)^2(3-\psi+\psi\alpha)}{6+\beta\psi(3-\psi)} \tag{2.2-2}$$

where: $\psi = \frac{\bar{x}}{h}$

f_{af} stands for allowable bottom – or top-flange stress for hybrid beam ; f_f stands for basic allowable stress for bottom or top flange.

Because of the slightly difference (lower than 5%) and more convenient application AASHTO (2005) has been employing the hybrid factor steel section only for both case of non-composite and composite girder. However the hybrid factor for both steel steel non-

composite and composite beam section in Schilling studies did not consider the effect of initial bending moment due to un-shored construction method.

2.2.2. Current classification of composite sections

As introduced in Background Chapter, for steel concrete composite girders under positive bending moment, the influence of local buckling in compressive flange on flexural strength is eliminated. Web slenderness become an important influence on flexural strength of composite girder and section classification based on web slenderness limits in current AASHTO and Eurocode are discussed in this section.

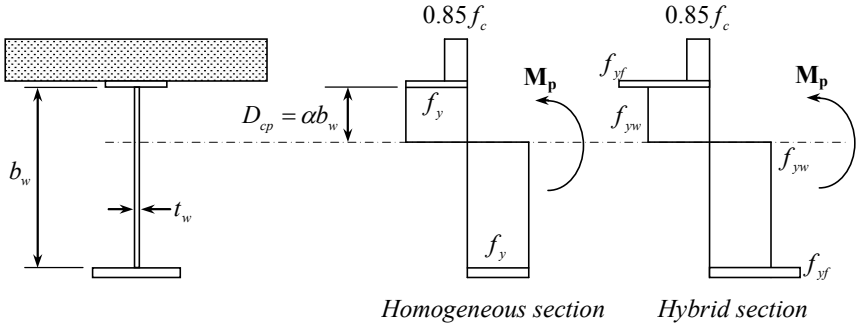

Fig. 2.2-3 Assumption of full plastic stress distribution in composite homogeneous and hybrid steel section

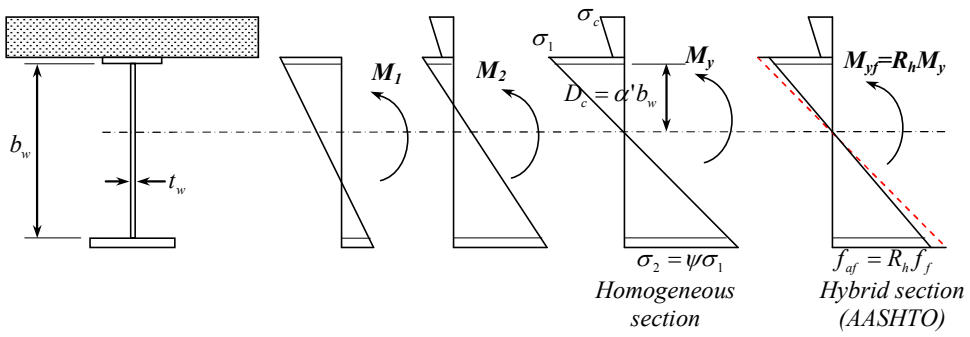

Fig. 2.2-4 Assumption of yield stress distribution in composite homogeneous and hybrid steel section refered by AASHTO

Both AASHTO and Eurocode based on the quantities of plastic moment M_p and yield moment M_y to define section class. The plastic moment M_p is identified with assumption that section can develop full plastic stress distribution as shown in Fig.2.2-3 The yield moment M_y obtained when yield stress attaining at extreme fibre of either top or bottom flange (as shown in Fig.2.2-4). The definition of web slenderness employing in AASHTO specification is

different from that of Eurocode. AASHTO specification considers web slenderness as ratio of twice the compression depth of web to web thickness $2D_{cp}/t_w$ or $2D_c/t_w$ where D_{cp} and D_c, described in Fig.2.2-3 and Fig. 2.2-4, are compression depths corresponding to plastic and yield moment stress distributions, respectively. On the other hand, Eurocode defines web slenderness as width-thickness ratio b_w/t_w. The comparison of web slenderness limits proposed by 2 design codes is presented in Table 2.2-1.

Table 2.2-1 Definition and web slenderness limits in AASHTO and Eurocode

Design code	Section Class	Definition	Web slenderness limits
AASHTO	Compact	$M_u \geq M_p$	$\frac{2D_{cp}}{t_w} \leq 3.76\sqrt{\frac{E_s}{f_y}}$
	Non-compact	$M_p > M_u \geq M_y$	$\frac{2D_c}{t_w} < 5.7\sqrt{\frac{E_s}{f_y}}$
	Slender	$M_u < M_y$	Other than those above
Eurocode	Class 1	$M_u \geq M_p$ *sufficient rotation capacity*	$\frac{b_w}{t_w} \leq \begin{cases} \frac{36\varepsilon}{\alpha} & \alpha \leq 0.5 \\ \frac{396\varepsilon}{13\alpha - 1} & \alpha > 0.5 \end{cases}$
	Class 2	$M_u \geq M_p$ *limited rotation capacity*	$\frac{b_w}{t_w} \leq \begin{cases} \frac{41.5\varepsilon}{\alpha} & \alpha \leq 0.5 \\ \frac{456\varepsilon}{13\alpha - 1} & \alpha > 0.5 \end{cases}$
	Class 3	$M_u \geq M_y$	$\frac{b_w}{t_w} \leq \begin{cases} \frac{42\varepsilon}{0.67 + 0.33\psi} & \psi > -1 \\ 62\varepsilon(1-\psi)\sqrt{-(\psi)} & \psi \leq -1 \end{cases}$
	Class 4	$M_u < M_y$	Other than those above

where $\varepsilon = \sqrt{235/f_y}$, Ψ stands for stress distribution gradient and is shown in Fig.2.2-4.

2.2.3. Study of Gupta et al., (2006)

With effort of investigating the effect of initial bending moment on composite girder sections based on web slenderness limits proposed in AASHTO and Eurocode, Gupta et al., (2006) processed hundreds of non-linear FEM numerical models. The isotropic elasto-plastic hardening assumption for steel material model and geometrical imperfection were assigned for web part to deal with local bucking behavior. A special boundary condition was applied for the end of composite girder model to produce pure bending moment and obtain the

reaction moment due to the flexural stiffness of the girder. Gupta's study did not consider the crushing behavior in concrete slab but the non-linear stress-strain relation is prior crushing by the assumption of linear-elastic, plastic hardening material. The initial bending moment level M_1 = 0, 0.1, 0.2, 0.4 M_{ys}, in which M_{ys} is yield moment of steel girder section only, were considered by phase analysis. The study of Gupta investigated various levels compression depth in web part corresponding to assumption of plastic and yield stress distribution.

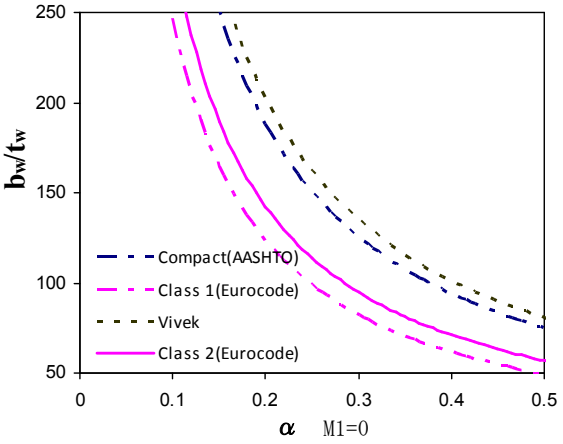

Fig. 2.2-5 Comparison of compact- noncompact web slenderness limit design curve proposed by Vivek, AASHTO and Eurocode

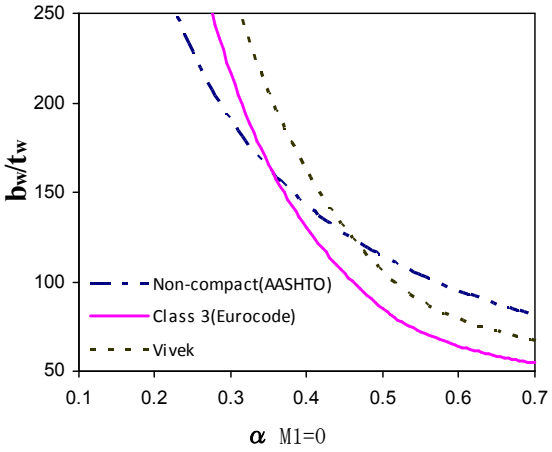

Fig. 2.2-6 Comparison of noncompact-slender web slenderness limit design curve proposed by Vivek, AASHTO and Eurocode with M_1=0

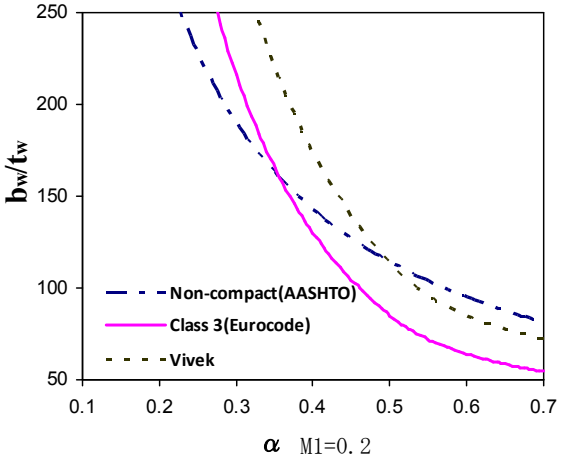

Fig. 2.2-7 Comparison of noncompact-slender web slenderness limit design curve proposed by Vivek, AASHTO and Eurocode with M_1=0.2M_{ys}

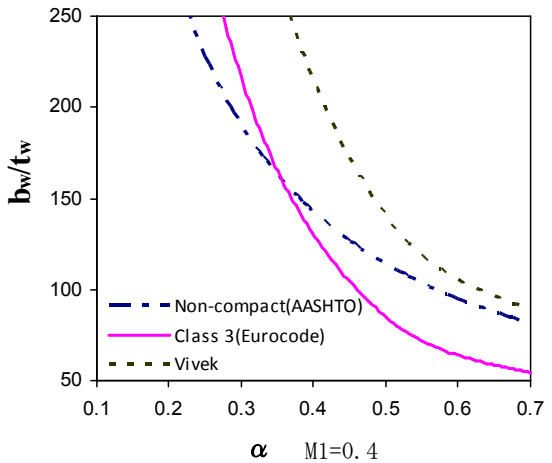

Fig. 2.2-8 Comparison of noncompact-slender web slenderness limit design curve proposed by Vivek, AASHTO and Eurocode with M_1=0.4M_{ys}

In Fig.2.2-5, 2.2-6, 2.2-7 and 2.2-8 , the web slenderness limit equations proposed by Gupta are plotted along with those specified by AASHTO and Eurocode. As shown in these figures the compact-noncompact web slenderness limit proposed in Gupta, 2006 has almost no difference from that specified by AASHTO because, according the study, the initial bending moment has almost no effect on compact-nonconpact slenderness limit. However the initial bending moment significantly influences on noncompact-slender slenderness limit. With the base of numerical results, Gupta proposed the improved noncompact-slender web slenderness limit regarding the form of Eurocode limit equation and also consider the variable of initial bending moment. The web slenderness noncompact – slender limit equation is presented in Eq.2.2-3.

$$\begin{aligned} \frac{b_w}{t_w} &\le \frac{52\varepsilon\Lambda}{(0.67+0.33\psi)} \quad for \quad \psi > -1.0 \\ \frac{b_w}{t_w} &\le 77\varepsilon\Lambda(1-\psi)\sqrt{-\psi} \quad for \quad \psi \le -1.0 \end{aligned} \tag{2.3-3}$$

where $$\Lambda = 1.0 - 0.1\left(\frac{M_1}{M_{ys}}\right) + 2.3\left(\frac{M_1}{M_{ys}}\right)^2$$

However, the study of Gupta targeted only on the most popular steel grade SM490Y and homogeneous steel section.

2.3 Objectives

LBS of steel plates

Rationalization of design for composite girder with considering the new SBHS steel grades and thicker steel plates targeting the format of Partial Safety Factor.

- To obtain the statistical information of LBS of steel plates as a base to propose the standard LBS design equation and corresponding partial safety factor regarding geometrical data and imperfections.
- To investigate the influence of inelastic behavior of Bridge High Performance steels on LBS of simply supported steel plates

Section classification based on web slenderness limits

- To develop the hybrid factor with considering initial bending moment and compared to numerical results.

- To investigate the influence of inelastic behavior of Bridge High Performance Steels on flexural resistance of composite girders by comparing web slenderness limit of composite section classifications proposed in AASHTO and EC to the ones seen in simulation models applying new steel grade in the case of homogeneous and hybrid steel girder sections.

CHAPTER 3

STATISTICAL INFORMATION OF LBS FOR STEEL PLATES

3.1. Introduction

As introduced in the Background chapter, the statistical information of local buckling strength (LBS) for steel plates, such as mean value and standard deviation, is used as a base to propose the partial safety factor and standard designed compressive resistance of steel plates. The statistical information of steel plate LBS can be obtained by conducting or collecting a large number of experiments or applying the Monte Carlo simulation.

For the method based on experiment data, to obtain reliable mean value and standard deviation, it is necessary to conduct or collect a sufficiently large number of tests. Besides, it is also very important to measure all the information, which affects the LBS such as initial deflection, residual stress, and steel plate dimensions for every test. Among these, the measurement of residual stress is particularly costly due to special equipments and extremely scrupulous techniques with highly accuracy requirement. Geometrical information can be measured on actual structures but residual stress distribution. The reliable measurement techniques based on destructive methods such as cutting or drilling the target members are impossible to be applied to actual constructions. Besides, the residual stress level depends on many factors such as the structure's condition, technique, temperature of welding, thickness of steel plate, yielding value of steel material. Consequently, it is very difficult to control the residual stress level. Therefore, the experimental based method to obtain statistical information of steel plate LBS is an expensive method.

The other method to obtain statistical information of the steel plate LBS is the Monte Carlo simulation. The procedure based on this method can be totally programmed and processed by computer and hence it has been seen as a much less expensive method. This method can be summarized as following.

- The random causes, which affect LBS of steel plates such as initial deflection, residual stress, material properties, aspect ratio, boundary condition, plate thickness are considered as random inputs (variables) and probabilistic characteristics of random inputs are based on available experimental data.
- From the probabilistic characteristics of random inputs, a large number of random inputs are generated numerically.

- In the deterministic step the LBS of steel plates is determined by FEM analyses with consideration of all generated inputs.
- The statistical information of LBS is obtained from data collection in the deterministic step

In the current study, the probabilistic distribution is determined by a random simulation, which is based on the Monte Carlo simulation. This Monte Carlo based simulation involves the steps illustrated by flowchart in Fig.3.1-1

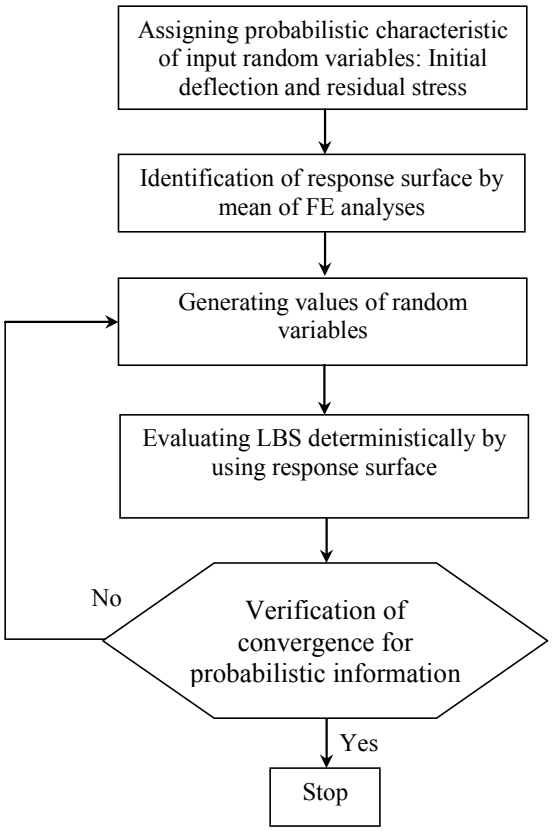

Fig. 3.1-1 The Monte Carlo based simulation applied in the current study

Step 1

Only initial deflection and residual stress are assumed to be two statistically independent random variables, which affect variability of LBS. The probabilistic density functions and their parameters of these random variables are assigned in this step on the basis of previous works. The variation of yield strength is not considered in this simulation so that probabilistic distribution of LBS and the associated safety factor can be considered excluding the effects of the yield strength variation. The variation of steel plate thickness is neglected as well, because

the effect of thickness variation on LBS is considered less than 0.2% judging from the statistical report on steel plate thickness (Murakoshi et al., 2008).

Step 2

In this step, a response surface is identified for each steel grade and several specific values of width thickness ratio parameter. The response surface is an approximate function of normalized LBS with respect to two variables: the residual stress and initial deflection. In standard Monte Carlo simulation, a large number of deterministic FEM analyses are required, and thus it consumes significant amount of time for input data preparation and computation. To avoid this problem, the response surface method is applied to evaluate the LBS for corresponding input data of residual stress and initial deflection. The response surface is identified from a sufficient number of FEM analysis results based on the least squared method. The FEM simulation model and identification of the response surface will be presented more details in the 2 subsection 3.3 and 3.4, respectively.

Step 3

A pair of values for the residual stress and initial deflection is generated in accordance with the probabilistic characteristics assigned in Step 1.

Step 4

The LBS is evaluated by means of the response surface for the generated values.

Step 5

The termination of the random simulation process is decided based on verifying the convergence of LBS probabilistic information such as a mean value and standard deviation. The details of the convergence verification process will be presented in subsection 3.6.2.

3.2. Plates properties

In the current study, the structural plates are considered with various quantities of thickness, edge size and yield strength corresponding to 6 steel grades, SM400; SM490; SM490Y; SM570; SBHS500; and SBHS700, to consider various values of plate slenderness parameter R in the range $0.4 \leq R \leq 1.4$. The range of plate slenderness parameter R and yield strength of different steel grades are shown in Fig.3.2-1. Dimension information of all steel plates considered in the current study is presented in Table.3.2-1.

Table 3.2-1 Plate dimensions and related information

	thickness	width	length	material	yield stress	aspect ratio	width-thickness ratio	bucking coefficient	plate slenderness parameter
	t [mm]	b [mm]	a [mm]		σ_y [N/mm^2]	a/b	b/t	k	R
S40 - 1 - 78 - 10	10	776.5	776.5	SM400	235	1	77.65	4.00	1.400
S40 - 1 - 71 - 20	20	1420	1420	SM400	235	1	71.00	4.00	1.280
S40 - 1 - 64 - 30	30	1930	1930	SM400	235	1	64.33	4.00	1.160
S40 - 1 - 58 - 40	40	2308	2308	SM400	235	1	57.70	4.00	1.040
S40 - 1 - 53 - 50	50	2668	2668	SM400	215	1	53.36	4.00	0.920
S40 - 1 - 46 - 60	60	2784	2784	SM400	215	1	46.40	4.00	0.800
S40 - 1 - 41 - 70	70	2840	2840	SM400	215	1	40.57	4.00	0.700
S40 - 1 - 35 - 80	80	2784	2784	SM400	215	1	34.80	4.00	0.600
S40 - 1 - 29 - 90	90	2610	2610	SM400	215	1	29.00	4.00	0.500
S40 - 1 - 23 - 100	100	2320	2320	SM400	215	1	23.20	4.00	0.400
S49 - 1 - 67 - 10	10	670.7	670.7	SM490	315	1	67.07	4.00	1.400
S49 - 1 - 61 - 20	20	1226.5	1226.5	SM490	315	1	61.33	4.00	1.280
S49 - 1 - 56 - 30	30	1667	1667	SM490	315	1	55.57	4.00	1.160
S49 - 1 - 50 - 40	40	1993	1993	SM490	315	1	49.83	4.00	1.040
S49 - 1 - 46 - 50	50	2277	2277	SM490	295	1	45.54	4.00	0.920
S49 - 1 - 40 - 60	60	2376	2376	SM490	295	1	39.60	4.00	0.800
S49 - 1 - 35 - 70	70	2425	2425	SM490	295	1	34.64	4.00	0.700
S49 - 1 - 30 - 80	80	2376	2376	SM490	295	1	29.70	4.00	0.600
S49 - 1 - 25 - 90	90	2228	2228	SM490	295	1	24.76	4.00	0.500
S49 - 1 - 20 - 100	100	1980	1980	SM490	295	1	19.80	4.00	0.400
S49Y - 1 - 63 - 10	10	632	632	SM490Y	355	1	63.20	4.00	1.400
S49Y - 1 - 58 - 20	20	1155	1155	SM490Y	355	1	57.75	4.00	1.280
S49Y - 1 - 52 - 30	30	1571	1571	SM490Y	355	1	52.37	4.00	1.160
S49Y - 1 - 47 - 40	40	1877	1877	SM490Y	355	1	46.93	4.00	1.040
S49Y - 1 - 43 - 50	50	2137	2137	SM490Y	335	1	42.74	4.00	0.920
S49Y - 1 - 37 - 60	60	2230	2230	SM490Y	335	1	37.17	4.00	0.800
S49Y - 1 - 33 - 70	70	2275	2275	SM490Y	335	1	32.50	4.00	0.700
S49Y - 1 - 28 - 80	80	2264	2264	SM490Y	325	1	28.30	4.00	0.600
S49Y - 1 - 24 - 90	90	2122	2122	SM490Y	325	1	23.58	4.00	0.500
S49Y - 1 - 19 - 100	100	1886	1886	SM490Y	325	1	18.86	4.00	0.400
S57 - 1 - 56 - 10	10	561	561	SM570	450	1	56.10	4.00	1.400
S57 - 1 - 51 - 20	20	1026	1026	SM570	450	1	51.30	4.00	1.280
S57 - 1 - 47 - 30	30	1395	1395	SM570	450	1	46.50	4.00	1.160
S57 - 1 - 42 - 40	40	1668	1668	SM570	450	1	41.70	4.00	1.040
S57 - 1 - 38 - 50	50	1886	1886	SM570	430	1	37.72	4.00	0.920
S57 - 1 - 33 - 60	60	1968	1968	SM570	430	1	32.80	4.00	0.800
S57 - 1 - 29 - 70	70	2010	2010	SM570	430	1	28.71	4.00	0.700
S57 - 1 - 25 - 80	80	1992	1992	SM570	420	1	24.90	4.00	0.600
S57 - 1 - 21 - 90	90	1867	1867	SM570	420	1	20.74	4.00	0.500
S57 - 1 - 17 - 100	100	1660	1660	SM570	420	1	16.60	4.00	0.400
H50 - 1 - 53 - 10	10	532.4	532.4	SBHS500	500	1	53.24	4.00	1.400
H50 - 1 - 49 - 20	20	973.5	973.5	SBHS500	500	1	48.68	4.00	1.280
H50 - 1 - 44 - 30	30	1323	1323	SBHS500	500	1	44.10	4.00	1.160
H50 - 1 - 40 - 40	40	1582	1582	SBHS500	500	1	39.55	4.00	1.040
H50 - 1 - 35 - 50	50	1749	1749	SBHS500	500	1	34.98	4.00	0.920
H50 - 1 - 30 - 60	60	1825	1825	SBHS500	500	1	30.42	4.00	0.800
H50 - 1 - 27 - 70	70	1864	1864	SBHS500	500	1	26.63	4.00	0.700
H50 - 1 - 23 - 80	80	1825	1825	SBHS500	500	1	22.81	4.00	0.600
H50 - 1 - 19 - 90	90	1712	1712	SBHS500	500	1	19.02	4.00	0.500

	thickness	width	length	material	yield stress	aspect ratio	width-thickness ratio	bucking coefficient	plate slenderness parameter
	t [mm]	b [mm]	a [mm]		σ_y [N/mm^2]	a/b	b/t	k	R
H50 - 1 - 15 - 100	100	1521	1521	SBHS500	500	1	15.21	4.00	0.400
H70 - 1 - 45 - 10	10	450	450	SBHS700	700	1	45.00	4.00	1.400
H70 - 1 - 41 - 20	20	823	823	SBHS700	700	1	41.15	4.00	1.280
H70 - 1 - 37 - 30	30	1118	1118	SBHS700	700	1	37.27	4.00	1.160
H70 - 1 - 33 - 40	40	1337	1337	SBHS700	700	1	33.43	4.00	1.040
H70 - 1 - 30 - 50	50	1478	1478	SBHS700	700	1	29.56	4.00	0.920
H70 - 1 - 26 - 60	60	1543	1543	SBHS700	700	1	25.72	4.00	0.800
H70 - 1 - 23 - 70	70	1575	1575	SBHS700	700	1	22.50	4.00	0.700
H70 - 1 - 19 - 80	80	1543	1543	SBHS700	700	1	19.29	4.00	0.600
H70 - 1 - 16 - 90	90	1446	1446	SBHS700	700	1	16.07	4.00	0.500
H70 - 1 - 13 - 100	100	1286	1286	SBHS700	700	1	12.86	4.00	0.400

Regarding Fig. 3.2-1, for all steel plate models, 10 thickness values t= 100, 90, 80, 70, 60, 50, 40, 30, 20, 10 (mm) are corresponding to 10 slenderness parameter values R = 0.4, 0.5, 0.6, 0.7, 0.8, 0.92, 1.04, 1.16, 1.28, 1.4, respectively.

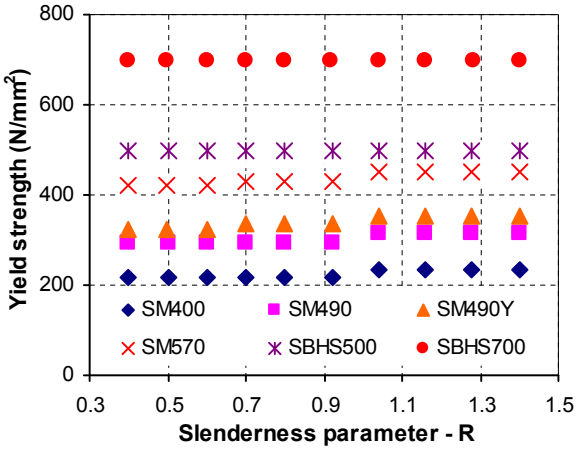

Fig. 3.2-1 Slenderness parameter values and yield strength considered in the current study

3.3. Random inputs

This subsection introduces residual stress and initial deflection in steel plates and the consideration in the current study. Residual stress is always available in welded steel structures. Referring Dwight and Moxham (1969) the un-resisted thermal expansion of steel per 100^{o}C is approximately equal to 0.001 of strain level for mild steel at yield. In welding process, the welding temperature is over 1200 ^{o}C and induces the steel in welding vicinity stressing up to the yield level. For welded structures with longitudinal welding lines, the middle zone is considered as locking area. For the sections at locking area, because of welded vicinity zone stressed up to yield level, the rest of section is in compression for equilibrium condition. An example of residual stress distribution measurement reported in Komatsu *et al.*

(1977) is presented in Fig.3.3-1. For initial deflection, it exists when steel plates are supplied from factories. Furthermore, when welding members together, the initial deflection is induced by angular distortion of the welded potion. The example of initial deflection measurement on a steel plate reported in Soares and Kmiecik (1993) is presented in Fig.3.3-2.

The residual stress and initial deflection are considered under normalized quantity $\overline{W}_0 = W_0 / b$ and $\overline{\sigma}_r = \sigma_{rc} / \sigma_y$ where W_0, b, σ_{rc} and σ_y stand for the maximum deflection (out-of-flatness), plate width, average compressive residual stress and yield strength of steel, respectively. The bases for generating large random variables of $\overline{W}_0$ and $\overline{\sigma}_r$ are mean value, standard deviation and density distribution function. In the current study, these values are identified by reviewing the following studies.

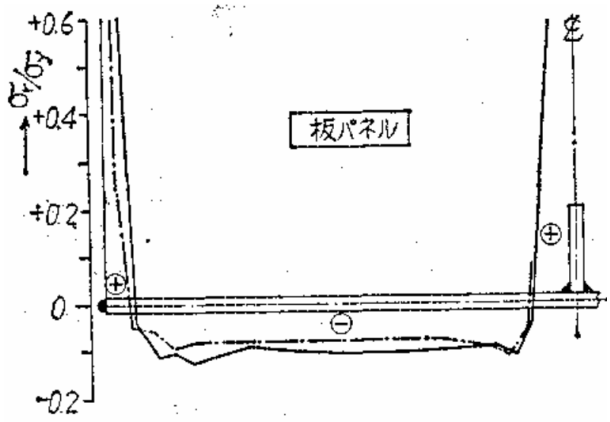

Fig. 3.3-1 Actual residual stress distribution reported in Komatsu (1977)

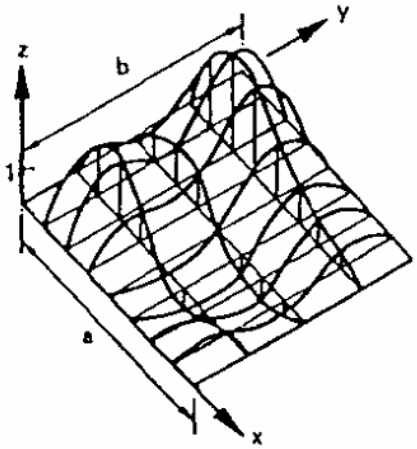

Fig. 3.3-2 Initial measurement on steel plate reported in Soares and Kmiecik (1993)

As mentioned in Introduction section, a large number of random inputs are generated based on the probabilistic characteristics of inputs, which can be obtained from available

experimental data. Practically, not much measurement information of residual stress and initial deflection of un-stiffened steel plate members has been reported. Among published data, the test collection reported in Fukumoto and Itoh (1983) shows the greatest number of initial imperfection (residual stress and initial displacement) measurement. In addition, Fukumoto and Itoh (1983) collected single plates and box column tests, which agree to research target of the current study - un-stiffened steel plate. For these reasons, the current study employs the measurement data of plate initial imperfections reported in Fukumoto and Itoh (1983) as the base of probabilistic characteristics of random inputs.

The histogram of $\overline{W}_0$ and $\overline{\sigma}_r$ reported in Fukumoto and Itoh (1983) is presented in Fig.3.3-3 and Fig.3.3-4, respectively. From these data, without considering tests with $\overline{W}_0$ >1/150, the values of mean ($\overline{W}_0$) = 1/400, standard deviation ($\overline{W}_0$) = 1/520, mean ($\overline{\sigma}_r$) = 0.23 and standard deviation ($\overline{\sigma}_r$) = 0.145 were obtained. The histogram of $\overline{W}_0$ and $\overline{\sigma}_r$ can be well described with Weibull and Lognormal distributions as shown in Fig.3.3-3 and Fig.3.3-4 respectively.

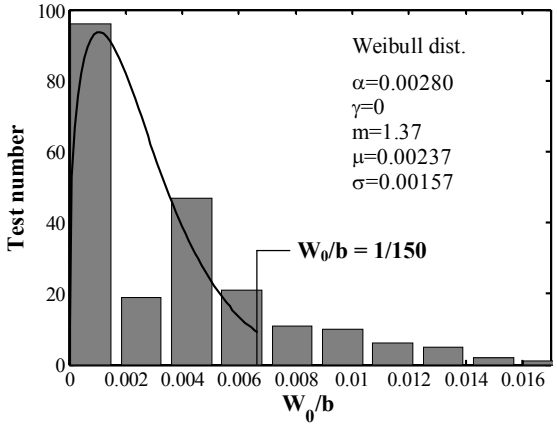

Fig. 3.3-3 Histogram of normalized initial deflection reported in Fukumoto and Itoh (1983)

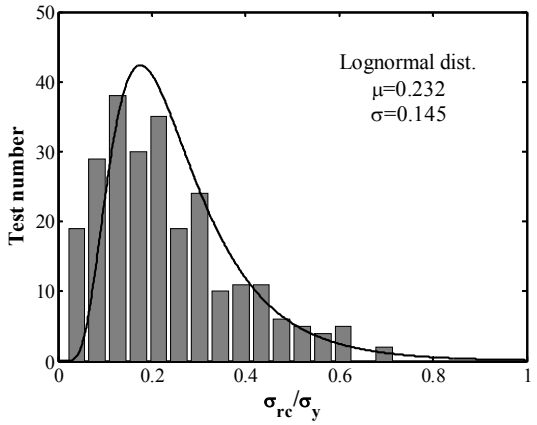

Fig. 3.3-4 Histogram of normalized residual stress reported in Fukumoto and Itoh (1983)

Komatsu et al., (1977) conducted a series of welding experiments to investigate the dependence of $\overline{\sigma}_r$ level on yield strength of steel plates. Komatsu's study considered steel grades SS 41, SM 58, HT 60, and HT 80. The material properties of these steel grades are presented in Table 3.3-1. The dependence of $\overline{\sigma}_r$ level on relevant yield strength is presented in Fig.3.3-5.

The relation curve was proposed based on the upper bound of test results. According to this relation curve, the $\overline{\sigma}_r$ level reduces for steel plates with higher yield strength. From this curve,

the author proposed the $\overline{\sigma}_r$ level for steel plates with grade SM 41, SM 50, SM 53, SM58 and HT 80 with value 0.3, 0.25, 0.23, 0.20 and 0.15, respectively. Practically, SM 41, SM 50, SM 53, and SM 58 are the old steel grade name of current steel grade SM400, SM490, SM490Y and SM570. The mean value of $\overline{\sigma}_r$ level of SM490Y steel plate obtained from Komatsu (1977) = 0.23 is coincident with the mean level obtained in Fukumoto and Itoh (1984), it represents consistency of $\overline{\sigma}_r$ levels proposed in Komatsu *et al.* (1977).

Table 3.3-1 Steel material properties in Komatsu (1997)

供試体	材　質	t	σ_y	σ_s	E	ν
I	SS 41	4.4 ～8.3	2760 ～3990	4410 ～5110	2.1 ～2.3	0.24 ～0.30
II	HT 60 (WEL-TEN 60)	8.0 ～12.4	5700 ～6050	6780 ～6830	2.1	0.26
III	HT 80 (NANKO-HT-80)	9.8 ～13.0	7760 ～7920	8360 ～8410	2.1	0.26 ～0.27
IV	SS 41	15.5	2690	4480	2.1	0.31
	SM58	16.1	5240	6320	2.1	0.27

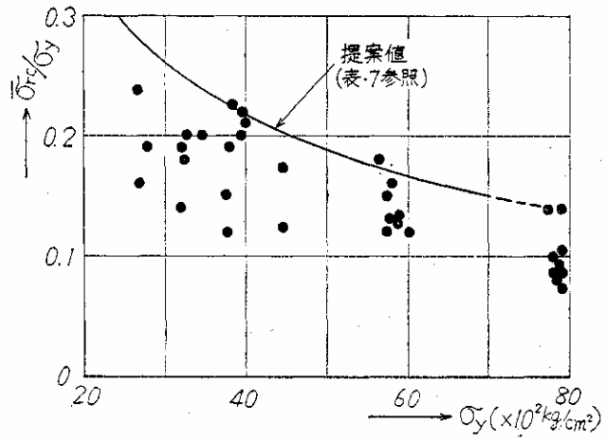

Fig. 3.3-5 Normalized residual stress results in Komatsu (1997)

By reviewing the above studies for generating random variable of $\overline{W}_0$, the current study employs the data reported in Fukumoto and Itoh (1984) without considering plates with $\overline{W}_0 >$ 1/150 hence it results in mean ($\overline{W}_0$) = 1/400; standard deviation ($\overline{W}_0$) = 1/520; Weilbull distribution is assumed for probability density function. 2 cases of generating random variable of $\overline{\sigma}_r$ were considered in the current study.

Case 1 of generating random residual stress

The random variable of $\overline{\sigma}_r$ regarding 6 different steel grades is generated by considering the same mean ($\overline{\sigma}_r$) = 0.232, standard deviation ($\overline{\sigma}_r$) = 0.145, which are obtained in Fukumoto and Itoh (1984), and Lognormal distribution is assumed for probability density function. As for this case, a large number of $\overline{W}_0$ and $\overline{\sigma}_r$ variables are generated as presented in Fig.3.3-6 and Fig.3.3-7.

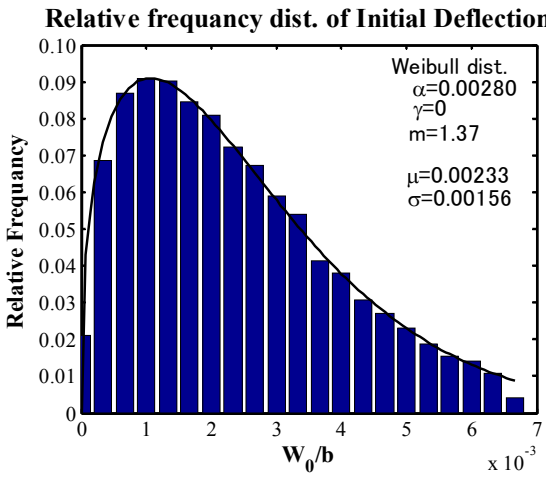

Fig. 3.3-6 Generated random input of initial deflection

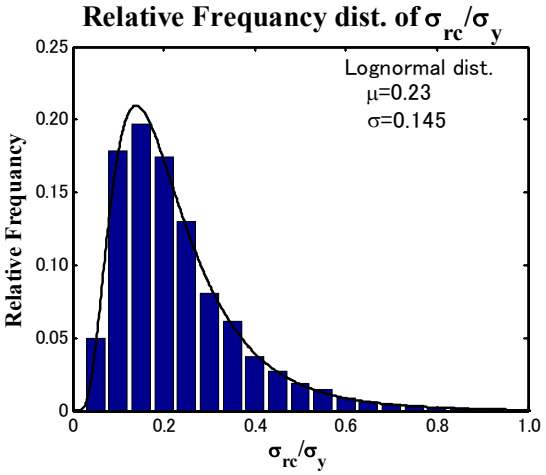

Fig. 3.3-7 Generated random input of residual stress

Case 2 of generating random residual stress

The random variable of $\overline{\sigma}_r$ regarding 6 different steel grades is generated by considering the different mean and standard deviation levels of ($\overline{\sigma}_r$). For plates regarding SM400, SM490, SM490Y and SM570, the mean ($\overline{\sigma}_r$) is the same as that of SM 41, SM 50, SM 53, SM58 reported in Fukumoto *et al.* (1977). For identifying mean ($\overline{\sigma}_r$) regarding SBHS500 and SBHS700 steels, an approximate curve, which is best fit with data of grade SM 41, SM 50, SM 53, SM58 and HT 80 reported in in Fukumoto *et al.* (1977), is employed. This curve is presented in Fig.3.3-8, the mean ($\overline{\sigma}_r$) levels regarding SBHS500 and SBHS700 steels are identified corresponding to yield levels equal to 500 and 700 (MPa), respectively.

The standard deviation ($\overline{\sigma}_r$) regarding different steel grades is identified based on the assumption that Coefficient of Variation (VOC) regarding all 6 steel grades are the same and equal to 0.145/0.232 - the value obtained in Fukumoto and Itoh (1984). The mean($\overline{\sigma}_r$) and standard deviation ($\overline{\sigma}_r$) regarding 6 different steel grades are obtained and presented in table 3.3-2.

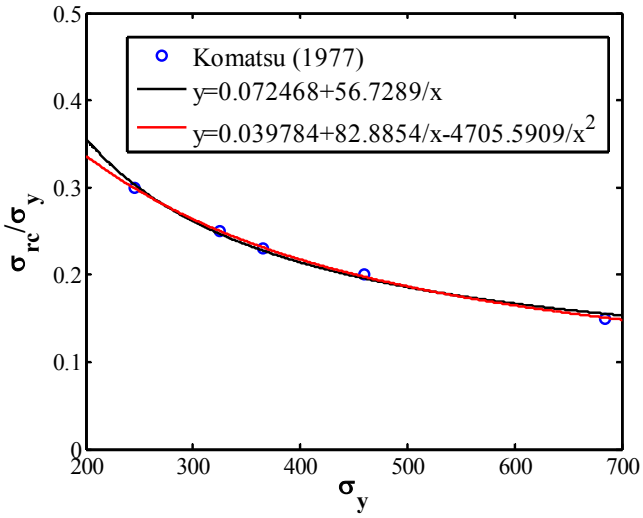

Fig. 3.3-8 The dependence relation function of normalized residual stress on yield strength of steel plate

Table 3.3-2 Scatterness of normalized residual stress applied for 6 steel grades

Steel grade	SM400	SM490	SM490Y	SM570	SBHS500	SBHS700
Mean ($\bar{\sigma}_r$)	0.300	0.250	0.230	0.200	0.185	0.150
Sta.dev.($\bar{\sigma}_r$)	0.189	0.158	0.145	0.126	0.117	0.095

3.4. FE steel plate model

3.4.1. Plate model

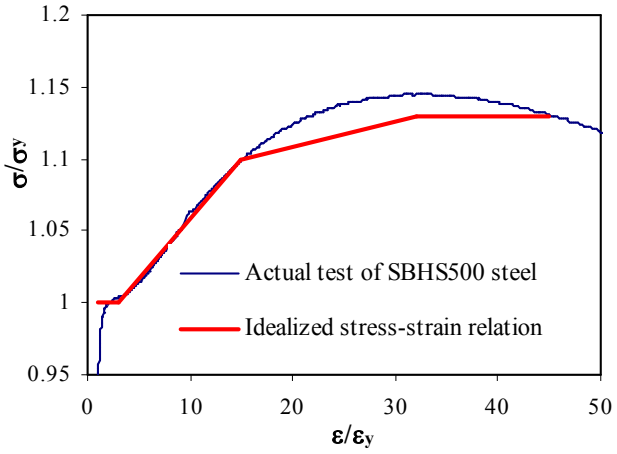

Fig. 3.4-1 Idealized stress-strain relation identified from actual test

For FE simulation model in the current study, both material and geometric nonlinearity are considered. Prandtl-Reuss equation is employed to model the plasticity of steel material. Von Mises yield theory, the most suitable one for ductile material as structural steel, is employed as yield surface criterion. The assumption of strain hardening hypothesis is applied for

hardening rule. The uni-axial stress-strain relation of different steel grades is idealized from actual test as shown in Fig.3.4-1 and all idealized stress-strain relations of 6 steel grades employed in current study are presented in Fig.3.4-1. The inelastic characteristics of these steel grades are shown in Table 3.4-1 and Fig.3.4-2, Fig.3.4-3.

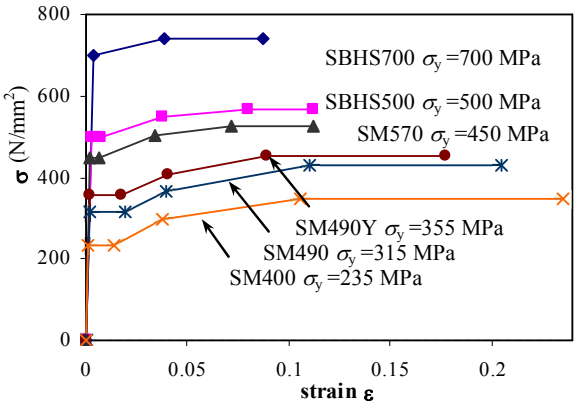

Fig. 3.4-2 Idealized stress-strain relations of steel grades considered in the current study

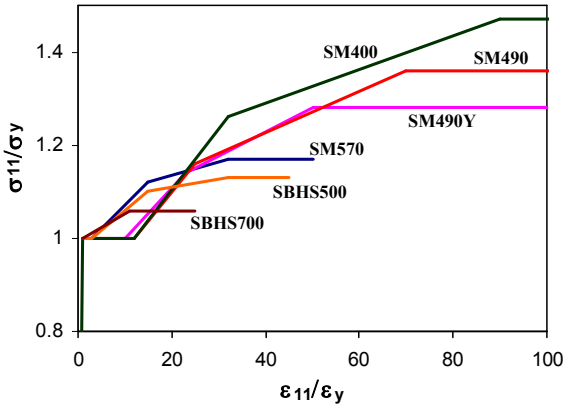

Fig. 3.4-3 Inelastic characteristic of 6 steel grades

Table 3.4-1 Inelastic characteristic of 6 steel grades

	SHBS700		SHBS500		SM570		SM490Y		SM490		SM400	
	ε/εy	σ/σy	ε/εy	σ/σy	ε/εy	σ/σy	ε/εy	σ/σy	ε/εy	σ/σy	ε/εy	σ/σy
1	1	1	1	1	1	1	1	1	1	1	1	1
2	11	1.06	3	1	3	1	10	1	12	1	12	1
3	25	1.06	15	1.1	15	1.12	23	1.14	25	1.16	32	1.26
4			32	1.13	32	1.17	50	1.28	70	1.36	90	1.47
5			45	1.13	50	1.17	100	1.28	130	1.36	200	1.47
E/Est	164		120		100		90.3		81.3		76.9	

For the convenient of simulating residual stress distribution and initial deflection in steel plate models, the idealized residual stress distribution and sinusoidal initial deflection surface is applied as presented in Fig.3.4-4. The assumption of sinusoidal surface function is applied popularly in numerical studies on local buckling problem of steel structures. It is also similar to first elastic buckling mode of square plate. The maximum tensile stress level σ_{rt} is usually assigned equal to yield strength of relevant steel grade. These assumptions ensure the conservative and similar influence on LBS of steel plates.

The simply supported boundary condition is applied for 4 edges of the plate model by assigning the proper constraints for all nodes on 4 edges of plate model; the constraint assignment is described in Fig.3.4-5.

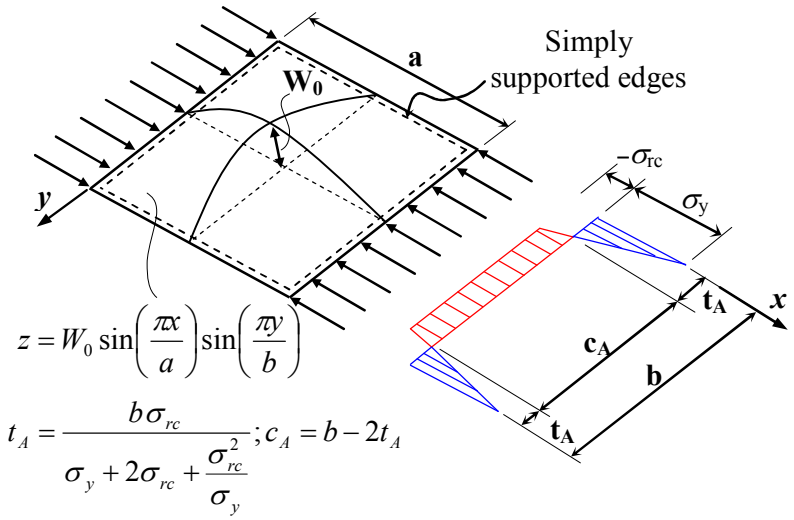

Fig. 3.4-4 Idealized residual stress distribution and sinusoidal initial deflection surface

The compression in plate model is produced by the displacement control method applied in 1 loading edge as presented in Fig.3.4-5. All nodes on loading edge are assigned to displace with sufficiently small distance in the necessary direction. This is the famous method for studying the local buckling behavior on steel structures, it helps stabilizing the solution, especially in considering buckling problems, nonlinear geometrical effects, which are invoked with elasto-plastic material models.

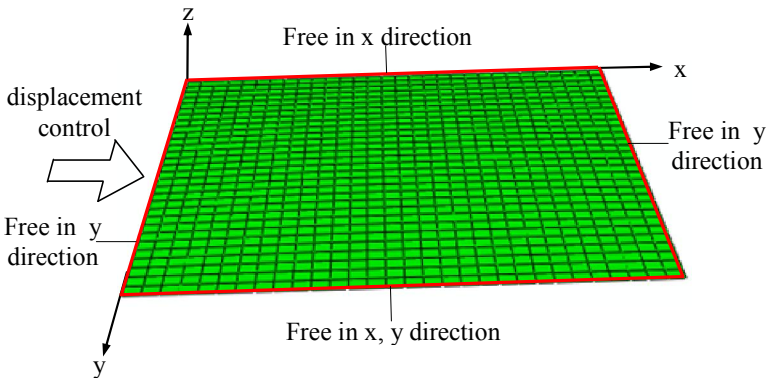

Fig. 3.4-5 Plate meshing and constrains of 4 edges

The plate FE simulation is modeled by the S4R nonlinear, finite strain, shell elements in ABAQUS element library. The S4R shell element is shear deformable, both reduced integration and the strain method assumption are applied to improve the thin-shell behavior of this element. The particular S4R shell element has been developed based on single integration point. In the current study, 11 integration points through the plate thickness are assigned for all steel plate models to produce the finer stress – strain distribution within the element.

Because of single integration point shell element, the residual stress is volume distribution within an element. The actual residual stress distribution assigned for FEM steel plate models is shown in Fig.3.4-6.

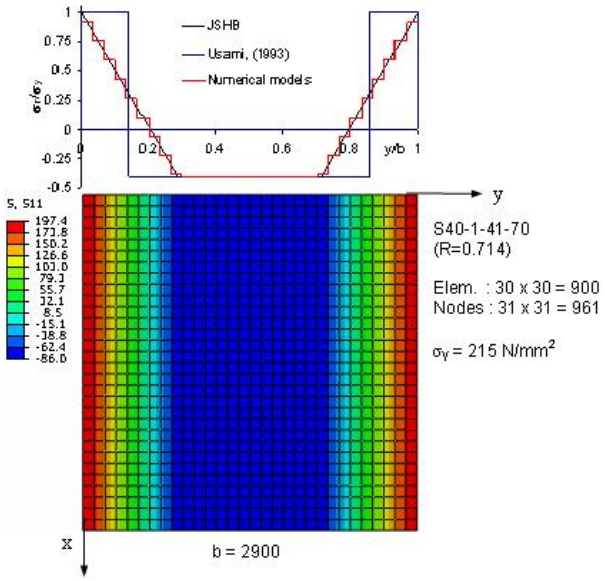

Fig. 3.4-6 Actual residual stress distribution in steel plate model

In the current study the LBS of a steel plate is identified from the ultimate value on relation curve of average compressive stress vs displacement of loading edge as presented in Fig.3.4-7, in which average compressive stress is determined by ratio of total in-plane reaction forces on loading edge to the cross section area of steel plates.

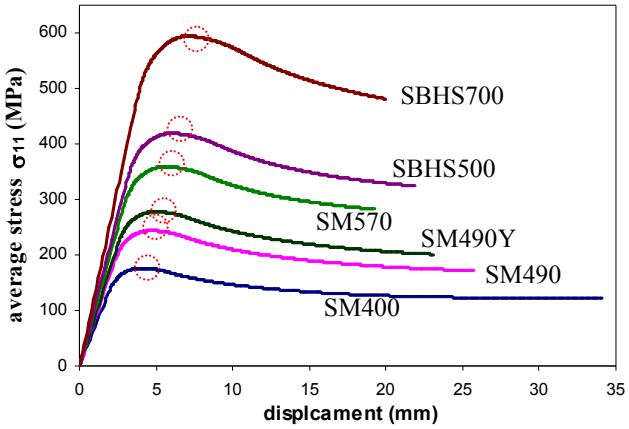

Fig. 3.4-7 The stress – displacement relation curve of steel plates for R = 0.8 with mean level of $\overline{\sigma}_r$ and $\overline{W}_0$

A small study on result convergence regarding the mesh size of the plate model is implemented to identify the application mesh size for the plate model in the current study. Regarding the dependence of LBS result on the mesh size of the plate simulation, Kiymaz (2003) reported that the convergent LBS result of square plate model can be obtained with mesh size 12x12 elements. In the current study the convergent study was implemented on 530x530 (mm) plate model with 10x10, 25x25, 30x30 meshes and the results are presented as average compression stress vs displacement relation in Fig.3.4-8. The mesh size 30x30 element applied in the current study ensures to obtain the convergent results of LBS.

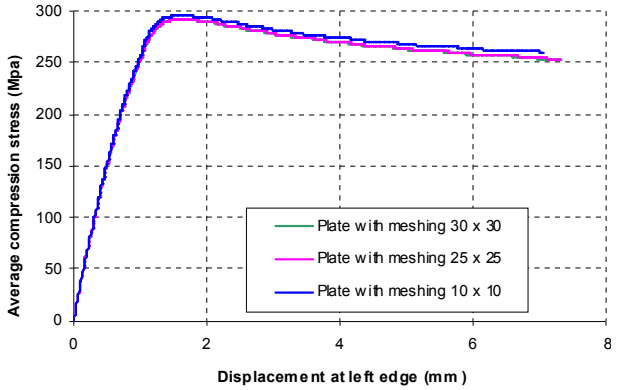

Fig. 3.4-8 Convergent investigation for the steel plate FE simulation mesh

3.4.2. Comparison of FE results to experimental results

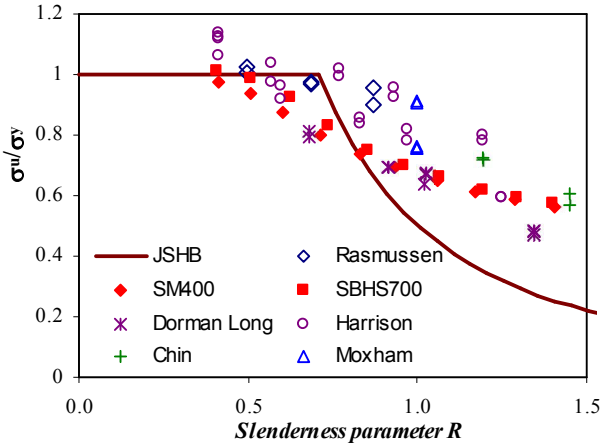

Fig. 3.4-9 FEM results with conservative level of imperfection plotted along with test results and current JSHB standard design strength equation

Before showing the stochastic simulation, deterministic FE analyses results are compared with reported experimental data in this section. The normalized residual stress and initial deflection are assigned to $\overline{\sigma}_r$ = 0.4 and $\overline{W}_0$ =1/150, respectively. The normalized initial defection of 1/150 is the maximum tolerance for steel bridges in Specifications of Highway

Bridges (Japan Road Association, 2012). On the other hand, $\bar{\sigma}_r$ = 0.4 corresponds approximately to the 90th percentile value for the lognormal distribution of the normalized residual stress shown in Fig.3.3-4, because the exceedance probability of $\bar{\sigma}_r$ = 0.4 is 10.8%.

3.5. Response surface

Response surface method (Guan and Melchers, 2001; Gasper et al., 2012) is employed to reduce the excessive computational time for Monte Carlo simulation of LBS. A cubic response function is used to approximate the dependency of normalized LBS on the normalized initial defection and residual stress,

The response surface is presented as a simple algebraic function

$$\bar{\sigma}_{cr} = \bar{\sigma}_{cr}(x_1, x_2) \approx \sum_{\substack{i,j=0 \\ i+j\le 3}}^{3} p_{ij} x_1^i x_2^j \tag{3.5-1}$$

where $x_1 \equiv \bar{\sigma}_r$ and $x_2 \equiv \bar{W}_0$ are the input random variables, and p_{ij} (i, j=0 to 3) are coefficients of the polynomial to be determined through regression analysis using finite element analyses results.

Case 1 of generating random residual stress

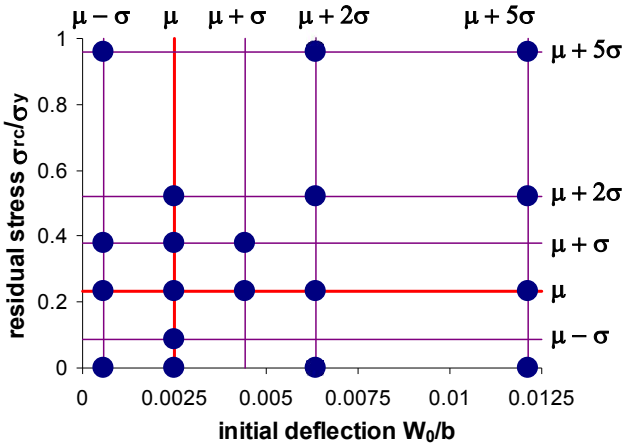

Fig. 3.5-1 Experimental points to identify a response surface.
FEM results at experimental points are used to identified a response surface

To obtain the unknown coefficients, the experimental points for the input variables should be chosen. The experimental points are selected as shown in Fig.3.5-1 according to the mean values and the standard deviations of the input random variables listed in Table 3.5-1. In

Fig.3.5-1, the labels μ and σ stand for the mean value and standard deviation, respectively, for the corresponding input random variables.

The coefficients p_{ij} in Eq.(3.5-1) were determined from a set of 114 deterministic FE results for a specific R value with considering all 6 steel grades based on the least square method. For 10 slenderness parameter values, 10 response surfaces were obtained employing 1140 FE analysis results. The obtained response surfaces are plotted along with FEM LBS based results in Fig.3.5-2 for R=0.8 and appendix A1-1 for R ranging from 0.4 to 1.4.

Table 3.5-1 Mean value and standard deviation of input random variables

	σ_{rc}/σ_y	W_0/b
Mean μ	0.23	0.0025
Std. Dev. σ	0.145	0.0019

Table 3.5-2 R-square values of response surfaces in the range of $0.4 \le R \le 1.4$

R	0.4	0.5	0.6	0.7	0.8	0.92	1.04	1.16	1.28	1.4
R-squared	0.702	0.837	0.920	0.945	0.964	0.964	0.959	0.956	0.961	0.964

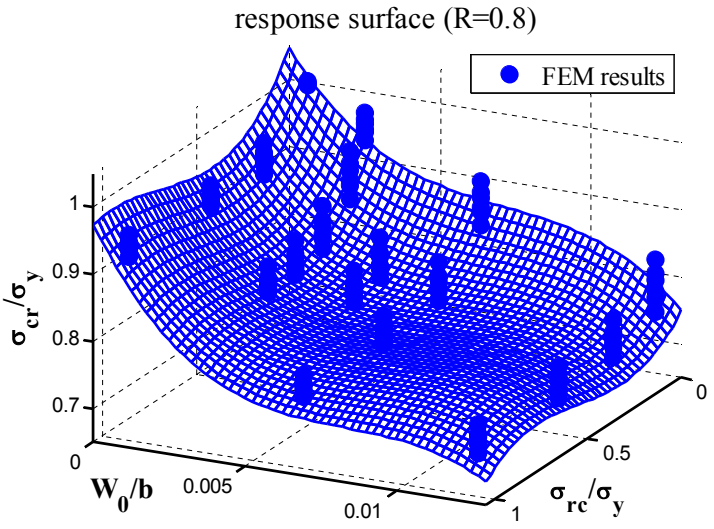

Fig. 3.5-2 Response surface plotted along with FEM results for R=0.8

The goodness of fitting of the obtained response surfaces is evaluated on the basis of R-square values, called the coefficient of determination, presented in Table 3.5-2. For R >0.7, the response surfaces show very good fitting with R-square >95%. For R≤ 0.5, the goodness of fitting seems poor, and it can be explained that the difference of normalized LBSs among different steel grades is significantly affected by different inelastic behavior of individual steel

grades. The constant values of 10 response surface obtained in the current study for this case are illustrated in Table.3.5-3.

Table 3.5-3 Coefficient values of 10 response surface functions

R value	p_{00}	p_{01}	p_{02}	p_{03}	p_{10}	p_{11}	p_{12}	p_{20}	p_{21}	p_{30}
0.40	1.098	-40.22	5442.0	-248100	0.007	-2.320	-48.4	-0.007	2.25	0.000
0.50	1.034	-15.15	1683.0	-90660	-0.012	-8.400	-42.4	0.069	6.72	-0.057
0.60	1.012	-1.72	-1894.0	100500	-0.087	-21.150	507.9	0.284	11.01	-0.198
0.70	1.037	-34.54	3169.0	-135000	-0.234	-32.100	1465.0	0.568	9.74	-0.342
0.80	1.047	-65.98	8382.0	-389100	-0.584	-0.520	1309.0	1.006	-15.13	-0.492
0.92	0.963	-40.44	3081.0	-112100	-0.937	57.210	-891.1	1.368	-35.91	-0.632
1.04	0.850	-23.31	1188.0	-34700	-0.788	47.270	-769.2	1.169	-29.12	-0.556
1.16	0.757	-12.66	377.6	-11430	-0.567	25.720	46.8	0.856	-20.27	-0.419
1.28	0.697	-10.08	367.4	-12430	-0.435	23.330	-269.2	0.617	-15.11	-0.288
1.40	0.650	-7.44	229.3	-8387	-0.343	18.580	-208.5	0.462	-11.63	-0.211

Case 2 of generating random residual stress

At a specific R value, 6 response surfaces are identified for corresponding 6 steel grades. Each response surface is determined from a set of 19 FEM results, hence with 10 R values 60 response surfaces are identified and 1140 FEM LSB results are employed. The constant p_{ij} of 60 response surfaces are present in Table 3.5-3 and Table A2-1 (appendix A2)

Table 3.5-4 Coefficient values of 6 Response surfaces regarding 6 steel grades for R=0.8

R	Grade	p_{00}	p_{01}	p_{02}	p_{03}	p_{10}	p_{11}	p_{12}	p_{20}	p_{21}	p_{30}
0.8	SM400	1.05	-77.08	10010	-469800	-0.517	9.601	985	0.747	-17.74	-0.317
	SM490	1.05	-73.09	9625	-453800	-0.549	2.271	1223	0.877	-14.66	-0.408
	SM490Y	1.05	-67.49	8520	-394700	-0.586	2.445	1255	0.987	-16.88	-0.474
	SM580	1.05	-65.63	8606	-407600	-0.624	-5.952	1782	1.197	-17.36	-0.663
	SBHS500	1.05	-62.26	8111	-384600	-0.641	-10.520	2059	1.296	-17.85	-0.757
	SBHS700	1.05	-55.92	7343	-352600	-0.665	-24.480	2861	1.586	-18.00	-1.095

In Fig.3.5-3 the 6 response surfaces in the case R= 0.8 are plotted along with FEM result-based. The coefficients of all the response surfaces of this case are presented in appendix A2

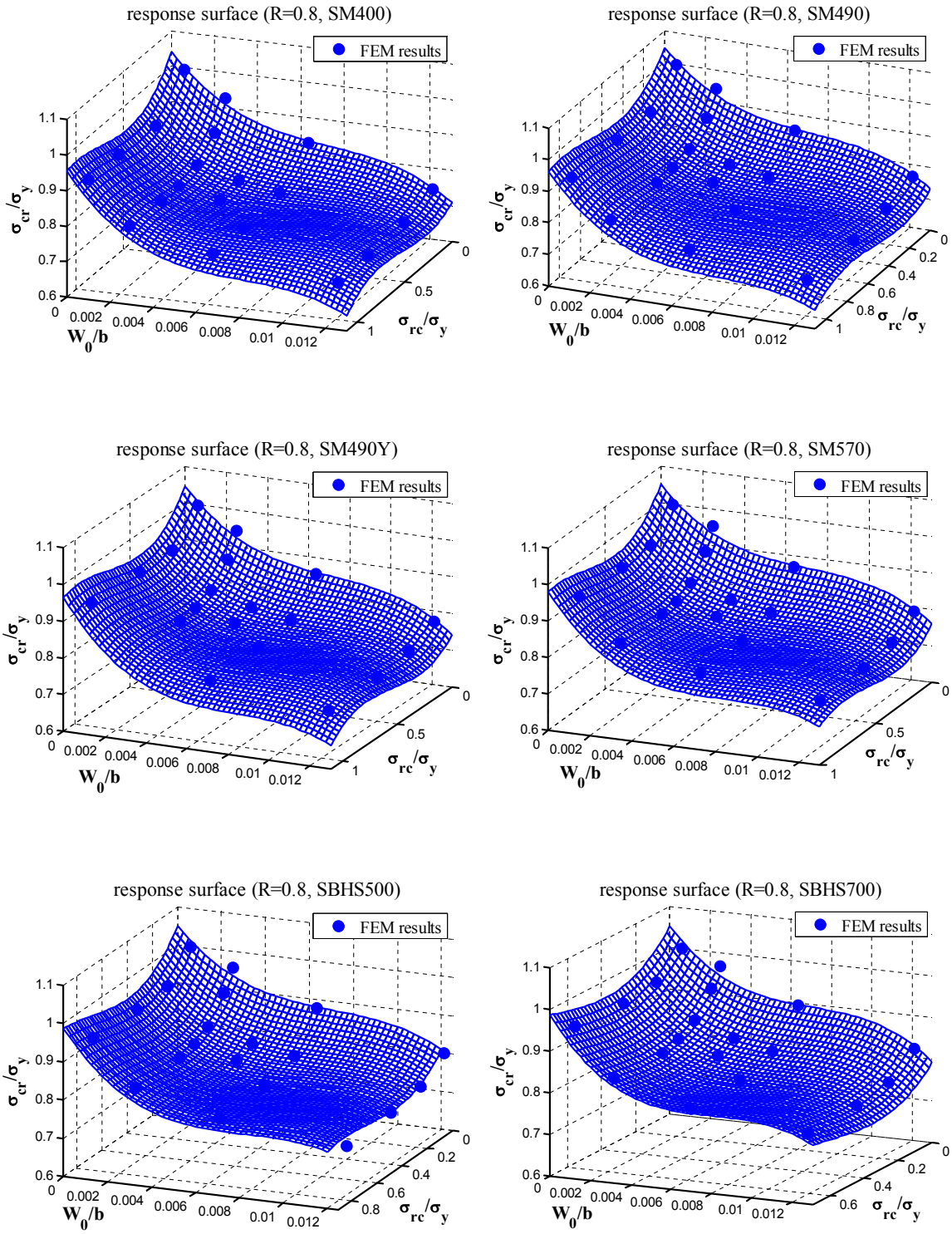

Fig. 3.5-3 6 response surfaces obtained at R=0.8

The obtained functions show very good fit to FEM results. For all 60 response surfaces the quantity R-square is greater than 95%.

3.6. Results from random simulation and discussion

3.6.1. Convergence of the random simulation results

The random simulation is implemented with 100, 1000, 10 000, and 100 000 random input couples of residual stress and initial deflection to check the convergence of random simulation. Fig.3.6-1 (a) and (b) shows the mean value and standard deviation of LBS as a function of the number of random input couples *N*. The mean value and standard deviation converge, as the simulation cycles are increased. The variation of mean values for all range of R values is less than 0.2%, while that of standard deviation is less than about 2%. In the subsequent section, the simulation results with *N*=100,000 will be adopted for discussion.

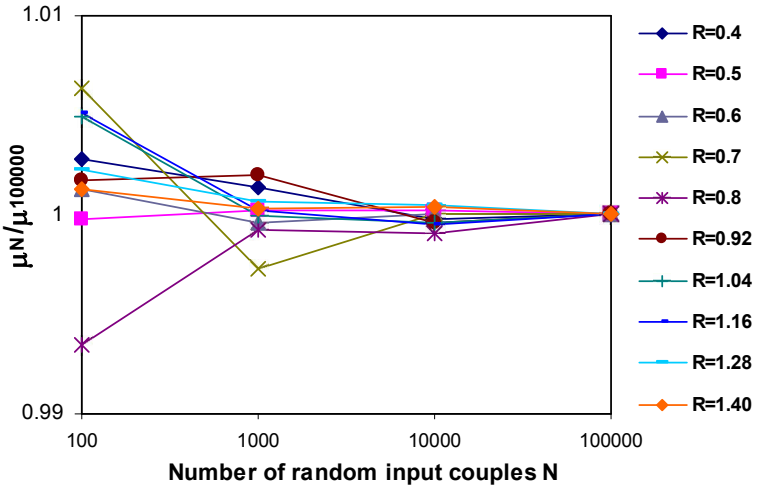

(a) Mean value of normalized LBS

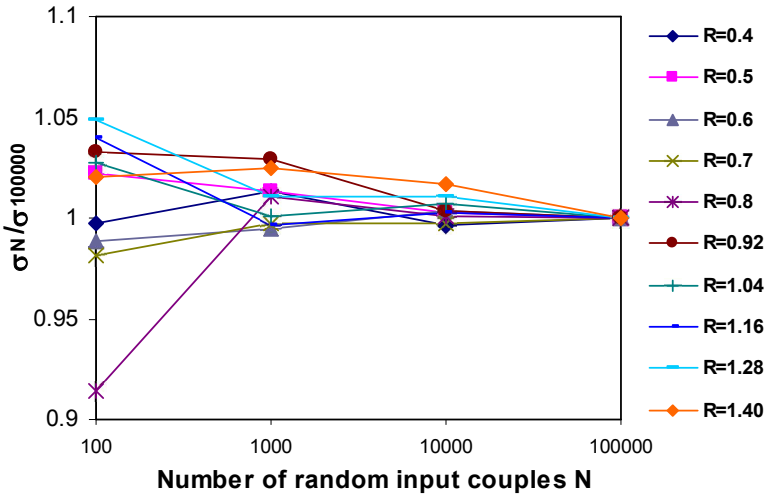

(b) Standard deviation of normalized LBS

Fig. 3.6-1 Convergence of random simulation. μ_N and σ_N are mean value and standard deviation of LBS obtained from N random simulations

3.6.2. Results from random simulation

As investigated in the previous sub-section, the statistical information will be obtained by the random simulation with 10000 random input couples. The direct statistical information results are histograms of LBS for 10 slenderness parameter R values. From these histograms, the mean values and standard deviation levels can be determined and the type of probabilistic distribution functions can be proposed.

Case 1 of generating random residual stress

In this case 10 LBS probabilistic distributions were obtained from Monte Carlo simulation (MC) with processing 10,000 random couples of residual stress and initial deflection variables, (shown in Fig.3.6-2 – as an example) . All results are presented in appendix A2 (Fig.A2-1).

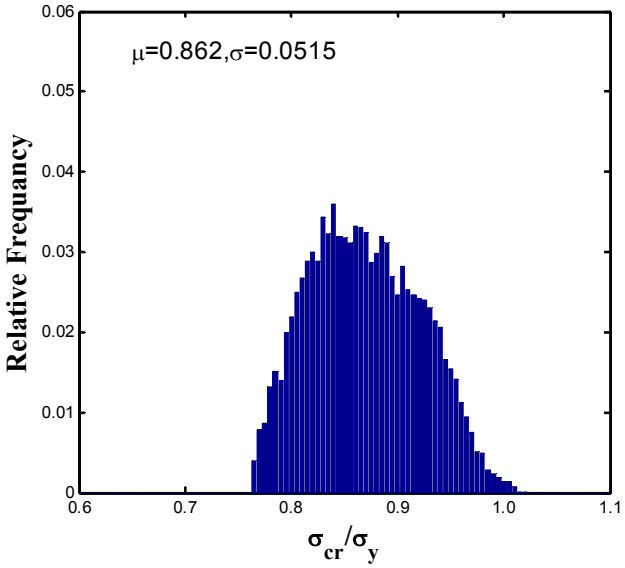

Fig. 3.6-2 Histogram of normalized LBS results corresponding to slenderness parameter R = 0.8

Table 3.6-1 Mean and standard deviation results in whole range of consideration R

R value	0.4	0.5	0.6	0.7	0.8	0.92	1.04	1.16	1.28	1.4
M value	1.039	1.006	0.982	0.938	0.862	0.766	0.701	0.653	0.617	0.586
S value	0.0277	0.0157	0.0212	0.0413	0.0515	0.0399	0.0294	0.0216	0.0171	0.0145

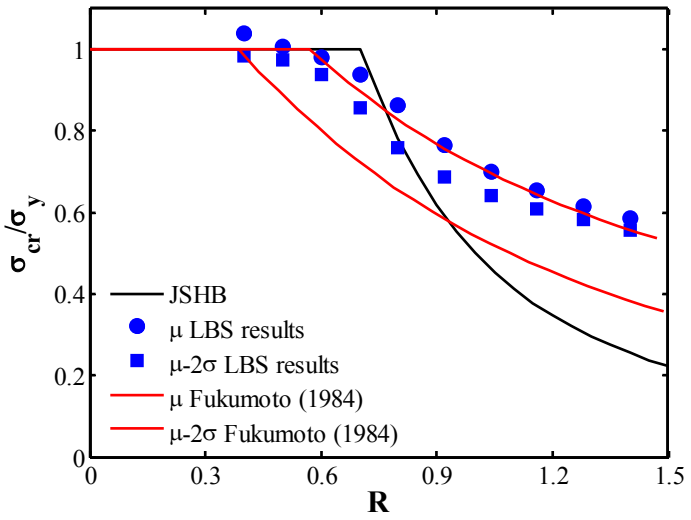

Fig. 3.6-3 Comparison between current study, JSHB (2002), and Fukumoto and Itoh (1984) results

The mean and standard deviation results obtained from 10 LBS probabilistic distributions are shown in Table 3.6-1 and plotted in Fig.3.6-3 along with the current JSHB design equation (JSHB, 2002), Mean and Mean minus twice Standard Deviation curves proposed in Fukumoto and Itoh (1984) (M and M-2S curves).

As seen in Fig.3.6-3, for the similar scatterness of random initial imperfection inputs, the mean (M) results of the current study are close to the Mean (M) curve proposed in Fukumoto and Itoh (1984), it represents that the results obtained from the approximate random simulation agree with the nature of experimental results.

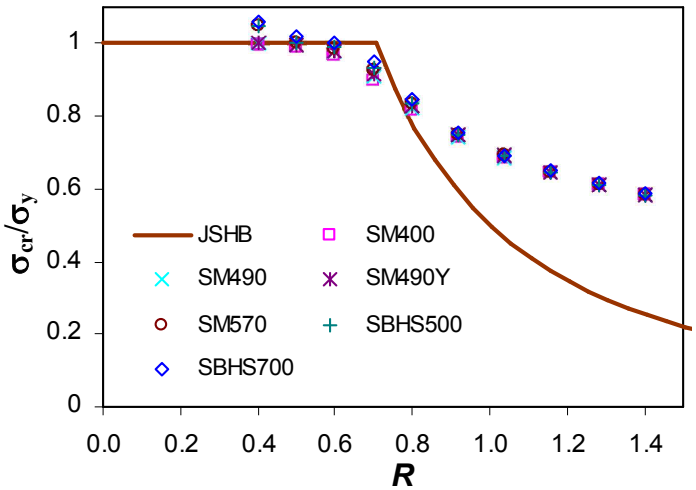

Fig. 3.6-4 Normalized LBS of steel plate with mean level of normalized residual stress and initial deflection

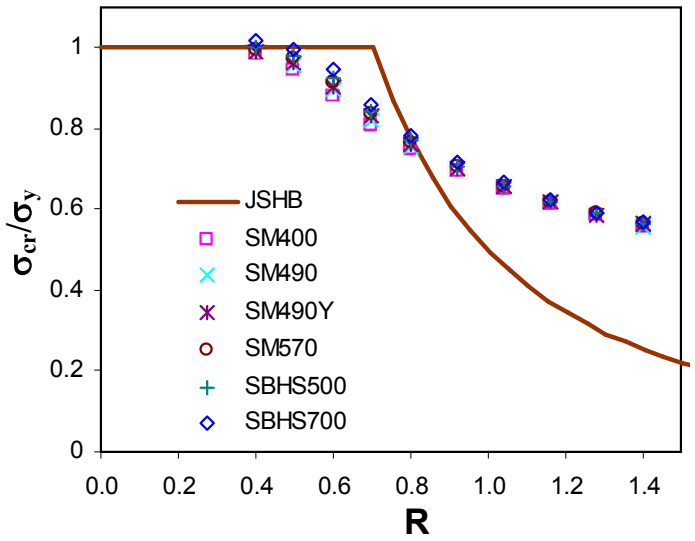

Fig. 3.6-5 Normalized LBS of steel plate with mean – twice of standard deviation level of normalized residual stress and initial deflection

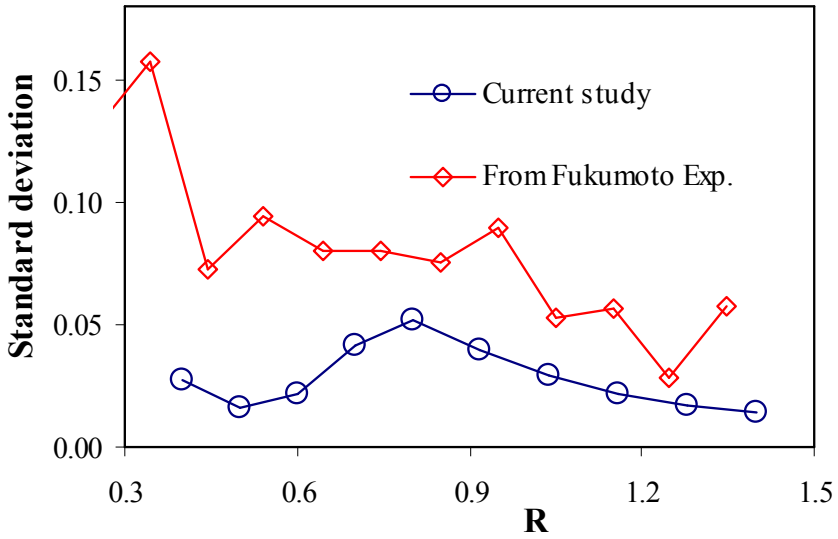

Fig. 3.6-6 Comparison of standard deviation values obtained in the current study with those reported in Fukumoto and Itoh (1984)

In this paragraph the following labels will employed: $\overline{W}_0$, $\overline{\sigma}_r$, $\overline{\sigma}_{cr}$ where $\overline{W}_0 = W_0 / b$; $\overline{\sigma}_r = \sigma_{rc} / \sigma_y$; $\overline{\sigma}_{cr} = \sigma_{cr} / \sigma_y$ Within the range 0.65<R<0.85, the mean values of the current study are slightly greater than the M curve proposed in Fukumoto and Itoh (1984). The possible reasons are that the current study just considers the plates with $\overline{W}_0 \leq 1/150$. Besides, according to FE analysis results, within the range of 0.6<R<0.85, the different of steel plate LBS regarding different steel grades induced by influence of inelastic behavior of different steel is more significant than that in the range R> 0.85 (slender range). For R=0.7 and mean

($\overline{W}_0, \overline{\sigma}_r$) levels, $\overline{\sigma}_{cr}$(SBHS700) is greater than $\overline{\sigma}_{cr}$(SM400) about 5.5% (Fig.3.6-4) and about 7% with mean-twice of standard deviation level ($\overline{W}_0, \overline{\sigma}_r$) for R =0.6 (Fig. 3.6-5).

As shown in Fig.3.6-6, the standard deviation results of the current study are significantly lower than corresponding results which were reported in Fukumoto and Itoh (1984). Within the practical range of 0.6<R<1.2, the current study results are about half values reported in Fukumoto and Itoh (1984). The differences between the current simulation condition and Fukumoto and Itoh's experimental data are as follows:

(a) Boundary condition

Fukumoto and Itoh's experimental data contain LBS of welded boxes as well as single plates with weld beads, while the present simulation contains only simply supported plates. Flanges of welded boxes are assumed as simply supported plates in design practice. However, there is some extent of rotational fixity effect at flange-web junctures, which affects variation of LBS.

(b) Inelastic material property

In the random simulation, variation of yield stresses is not considered, and only 7 deterministic stress-strain curves for different steel grades are employed to account for material property differences in the inelastic regime. The effect of inelastic behavior on LBS is considered to be more significant for plates with smaller R vales, which is consistent with the result show in Fig.3.6-6.

(c) Initial deflection

In the present study, the initial deflection more than the maximum limit specified in a design specification is omitted from the random simulation as explained before, while Fukumoto and Itoh's experimental data contain LBS of plates with initial deflection more than the specification. This results in larger variation in experimental LBS.

The tendency of standard deviation values can be further explained in subsection 3.6.4

Case 2 of generating random residual stress

In this case, 60 probabilistic distributions of normalized LBS of steel plates, regarding 6 steel grades separately at 10 specific slenderness parameter R values, are obtained. Consequently, from these 60 probabilistic distributions, 60 mean values and standard deviation levels are obtained. The range of 0.7≤R≤0.92 shows the most sensitive for steel plate LBS; hence,

following normalized LBS probabilistic distribution for the case of 0.8 are presented in Fig.3.6-7 as an example. All other probabilistic information results of LBS are presented in appendix A2-2, from Fig. A2-2.1 to Fig. A2-2.10

The mean LBS results are plotted along with M and M-2S curves proposed in Fukumoto and Itoh (1984) in Fig.3.6-8. The difference is significant at R=0.4 and within the range 0.55<R<0.95, and almost similar for R>1.0. It shows that the difference of normalized residual stress scatterness applied to difference steel grades does not induce the significant difference of normalized LBS of steel plates. The figure also shows that the normalized LBS of steel plates regarding all 6 steel grades < 1 at R = 0.7 while JSHB specify standard normalized LBS = 1 at R =0.7.

For R=0.8

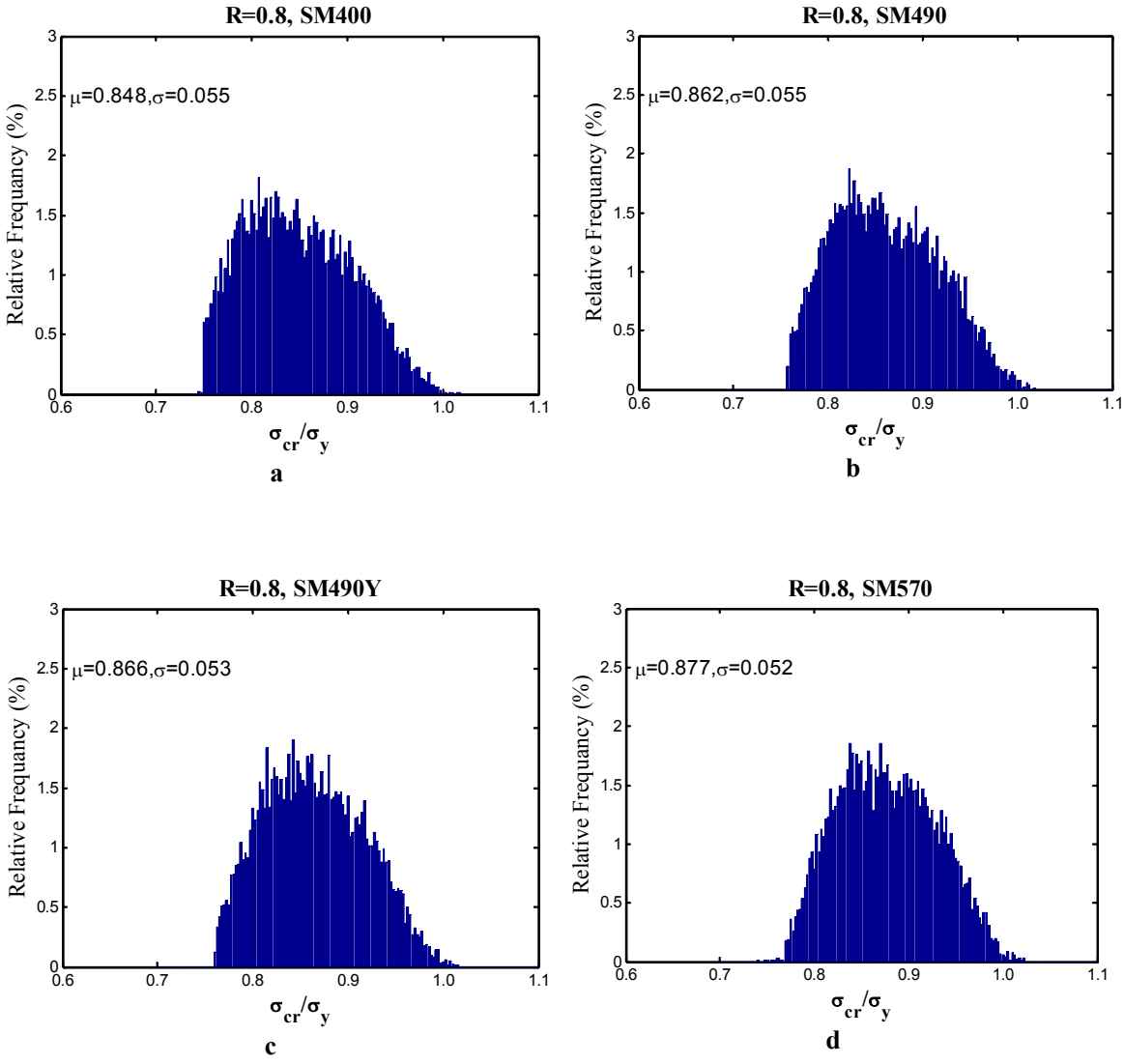

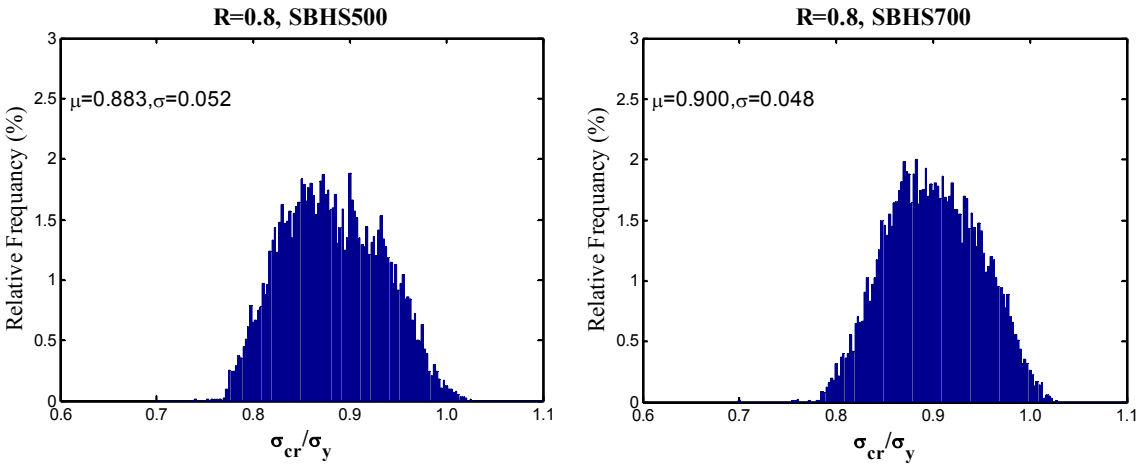

Fig. 3.6-7 Probabilistic distribution LBS regarding 6 steel grades for R=0.8

The obtained mean values and standard deviation level are illustrated in Table 3.6-2 and 3.6-3

Table 3.6-2 Mean values

Grade	0.4	0.5	0.6	0.7	0.8	0.92	1.04	1.16	1.28	1.4
SM400	1.006	0.990	0.968	0.919	0.848	0.759	0.698	0.651	0.614	0.583
SM490	1.011	0.995	0.976	0.931	0.862	0.770	0.706	0.656	0.619	0.588
SM490Y	1.018	0.996	0.978	0.937	0.866	0.775	0.708	0.657	0.621	0.589
SM570	1.069	1.012	0.985	0.944	0.877	0.783	0.715	0.664	0.625	0.593
SBHS500	1.065	1.013	0.988	0.948	0.883	0.790	0.719	0.666	0.626	0.595
SBHS700	1.068	1.027	1.002	0.963	0.900	0.807	0.729	0.674	0.633	0.601

Table 3.6-3 Standard deviation results

Grade	0.4	0.5	0.6	0.7	0.8	0.92	1.04	1.16	1.28	1.4
SM400	0.014	0.012	0.027	0.050	0.055	0.043	0.033	0.025	0.019	0.017
SM490	0.016	0.010	0.022	0.044	0.055	0.044	0.033	0.024	0.019	0.016
SM490Y	0.024	0.009	0.021	0.042	0.053	0.044	0.033	0.024	0.019	0.016
SM570	0.045	0.023	0.019	0.038	0.052	0.045	0.033	0.024	0.019	0.015
SBHS500	0.040	0.021	0.017	0.036	0.052	0.046	0.033	0.024	0.018	0.015
SBHS700	0.026	0.020	0.017	0.032	0.048	0.047	0.033	0.023	0.017	0.014

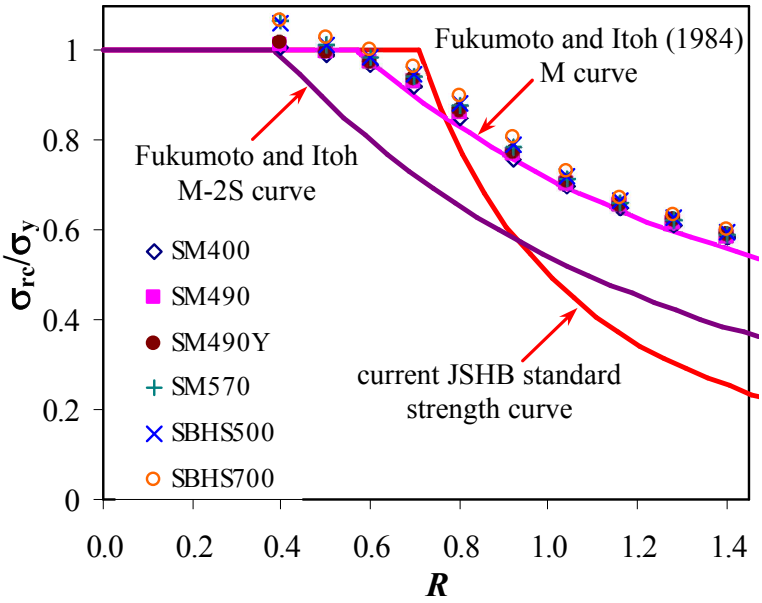

Fig. 3.6-8 Comparison between mean results of the current study, JSHB (2002) design curve, and Fukumoto and Itoh (1984) results

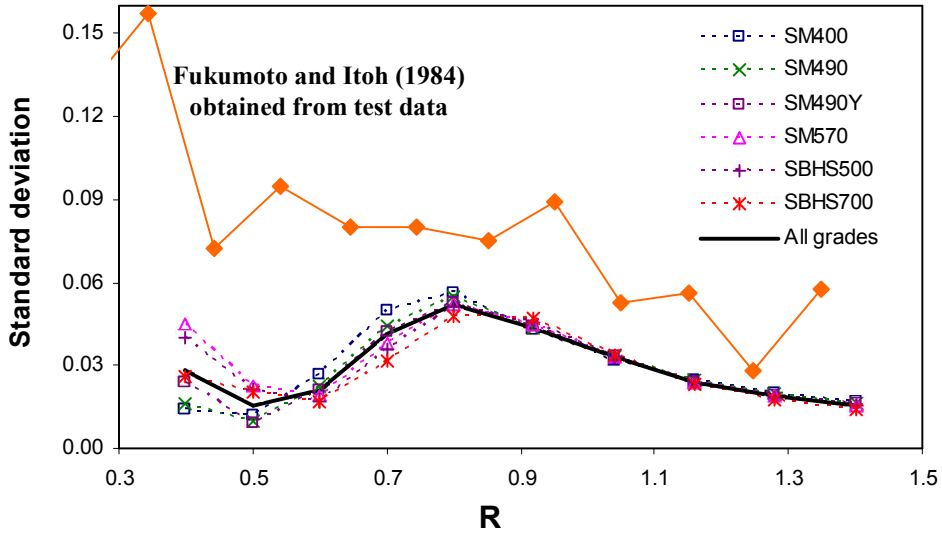

Fig. 3.6-9 Comparison between standard deviation results of the current study and Fukumoto and Itoh (1984) results

As illustrated in Fig.3.6-9, LBS standard deviation results of steel plates regarding each of all 6 steel grades are almost similar for R>0.9. The difference is more significant for R < 0.8, within the range of 0.6≤R≤0.8; the standard deviation results of high strength steel plates are lower than those of normal steel plates but for R < 0.55 the standard deviation results of high strength steel plates are greater than those of normal steel plates. Standard deviation of steel plate LBSs regarding all 6 steel grades attains maximum levels at R = 0.8.

Compared to LBS standard deviation values reported in Fukumoto and Itoh (1984), the corresponding results with all 6 steel grades of the current study are significantly lower, within the practical range of 0.6<R<1.2 the results are about half the results from Fukumoto and Itoh (1984) and have very clear tendency.

In Fig.3.6-10 for the M-2S level of normalized LBSs of steel plates, results regarding all 6 steel grades obtained in the current study are compared to the M and M-2S curves proposed in Fukumoto and Itoh (1984) and JSHB current design equation. The difference of the normalized steel plate LBS regarding different steel grades is more significant, especially within the range 0.6<R<0.85. The maximum difference is around value R=0.7 and about 8% for comparing $\overline{\sigma}_{cr}$ (SM400) and $\overline{\sigma}_{cr}$ (SBHS700), it represents the better design LBS value of SBHS steel plates regarding both absolute and normalized strengths .

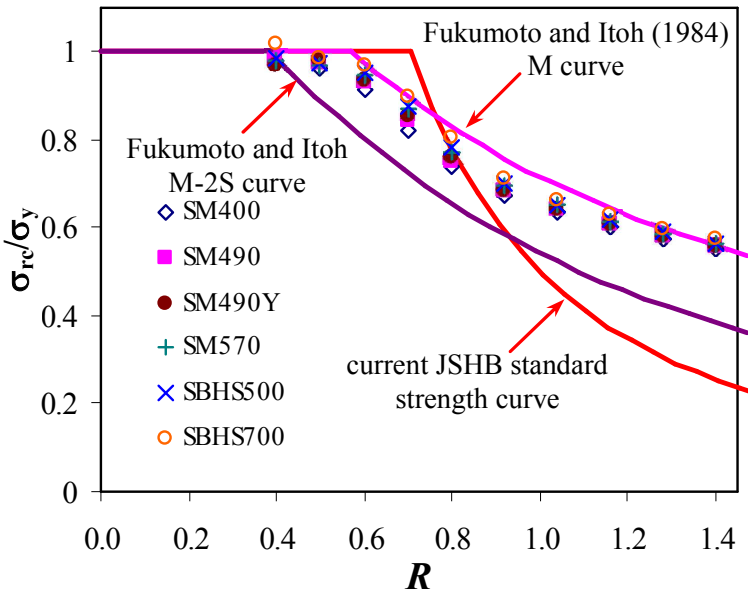

Fig. 3.6-10 Comparison between the results of the current study with M-2S levels, JSHB (2002) design curve, and Fukumoto and Itoh (1984) results

Also for M-2S level the results of the current study are significantly greater than the curve proposed in Fukumoto and Itoh (1984) and the tendency is different from that of JSHB standard design equation. At R = 0.8 the normalized high strength steel plate LBS are greater than standard design value of JSHB but that of normal steel plates. Within the range 0.5<R<0.75, all the M-2S results of current study are lower than standard design values specified by JSHB.

3.6.3. Approximate estimation of mean and variance

To obtain the probabilistic distribution of LBS, it is necessary to use a numerical simulation, such as Monte Carlo method as show in the previous section, because the explicit functional relationship between LBS and the input variables is not known in the current problem. However, an approximate mean and variance of LBS can be extract from the mean and variance of input variables and certain deterministic analysis. In this section, an approximate mean and variance of LBS will be calculated by using Taylor series finite difference (TSFD) estimation procedure (Haldarand and Mahadevan, 1999); and method of Response as General Function of Multiple Random Variables, labeled as D.R.S. (derivative of response surface);

For the first method, the first-order approximation of mean $E(\bar{\sigma}_{cr})$ and variance $Var(\bar{\sigma}_{cr})$ of LBS can be obtained from Eq.3.6-1 and 3.6-2, respectively

$$E(\bar{\sigma}_{cr}) \approx \bar{\sigma}_{cr}(\mu_{x_1}, \mu_{x_2}) \tag{3.6-1}$$

$$Var(\bar{\sigma}_{cr}) \approx \sum_{i=1}^{2}\left(\frac{\partial \bar{\sigma}_{cr}}{\partial x_i}\right)^2 Var(x_i) \approx \sum_{i=1}^{2}\left(\frac{\bar{\sigma}_{cr,i}^{+} - \bar{\sigma}_{cr,i}^{-}}{2}\right)^2 \tag{3.6-2}$$

where μ_{x_i} (i=1,2) is the mean of two input random variables: $\mu_{x_1} \equiv \mu_{\bar{\sigma}_r}$ and $\mu_{x_2} \equiv \mu_{\bar{W}_0}$; and

$$\begin{aligned} \bar{\sigma}_{cr,1}^{\pm} &\equiv \bar{\sigma}_{cr}(\mu_{x_1} \pm \sigma_{x_1}, \mu_{x_2}) \\ \bar{\sigma}_{cr,2}^{\pm} &\equiv \bar{\sigma}_{cr}(\mu_{x_1}, \mu_{x_2} \pm \sigma_{x_2}) \end{aligned} \tag{3.6-3}$$

σ_{x_i}(i=1,2) is the standard deviation of two input variables: $\sigma_{x_1} \equiv \sigma_{\bar{\sigma}_r}$ and $\sigma_{x_2} \equiv \sigma_{\bar{W}_0}$. In Eq. (3.6-1) and (3.6-2), $\bar{\sigma}_{cr}(\mu_{x_1}, \mu_{x_2})$ and $\bar{\sigma}_{cr,1}^{\pm}$can be evaluated with deterministic FEM analyses. Fig.3.6-11 shows a comparison of the mean values of LBS obtained from the random simulation and those from TSFD. The mean values obtained from the random simulation are slightly greater than those from TSFD.

In the second method, the second-order mean values

$$E(\overline{\sigma}_{cr}) \approx \overline{\sigma}_{cr}(\mu_{x1}, \mu_{x2}) + \frac{1}{2}\sum_{i=1}^{2}\left(\frac{\partial^2(\overline{\sigma}_{cr})}{x_i^2}\right)Var(x_i) \tag{3.6-4}$$

and first-order variances

$$Var(\overline{\sigma}_{cr}) \approx \sum_{i=1}^{2} E_i^2 Var(x_i) \tag{3.6-5}$$

are determined by means of partial derivatives at mean values of input variables in which second-order mean and first-order variance levels are reasonable for practical engineering requirement. μ_{X1}, μ_{X2} stand for the mean levels of normalized residual stress and initial deflection respectively, g is corresponding response surface.

The results will be presented according to 2 cases of probabilistic characteristic of normalized residual stress applied to steel plate as in the previous sub sections.

Case 1 of generating random residual stress

The mean values of the steel plate LBS obtained from 3 methods are presented together in Fig. 3.6-11. The difference of results is insignificant. The second-order mean values are slightly greater than the first-order mean values and mean values obtained from approximate random simulation are between the others.

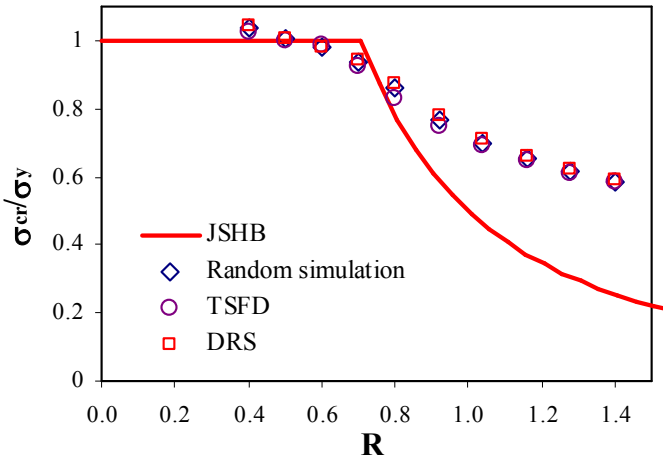

Fig. 3.6-11 Mean values of LBS obtained by 3 methods

In Fig. 3.6-12 the standard deviation values obtained from 3 methods are presented together. As shown in the figure, 3 results have the same tendency but different levels. The standard deviation results from method DRS and TSFD, the approximate methods, are based on gradient level in vicinity of Mean ($\overline{W}_0, \overline{\sigma}_r$) levels while the random simulation considers the whole range of residual stress and initial deflection levels. At R≈0.8 the standard deviation results obtained from 3 methods all yield the maximum level.

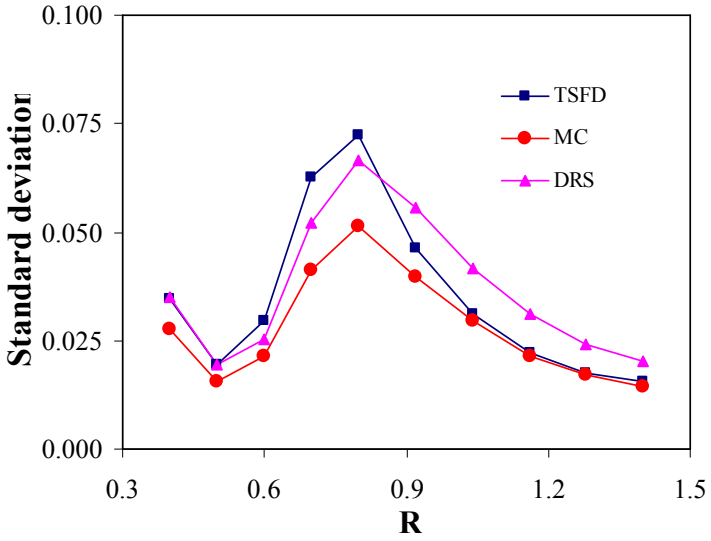

Fig. 3.6-12 Standard Comparison of standard deviation of LBS obtained from Monte Carlo based simulation, Taylor series finite difference (TSFD) and DRS estimations

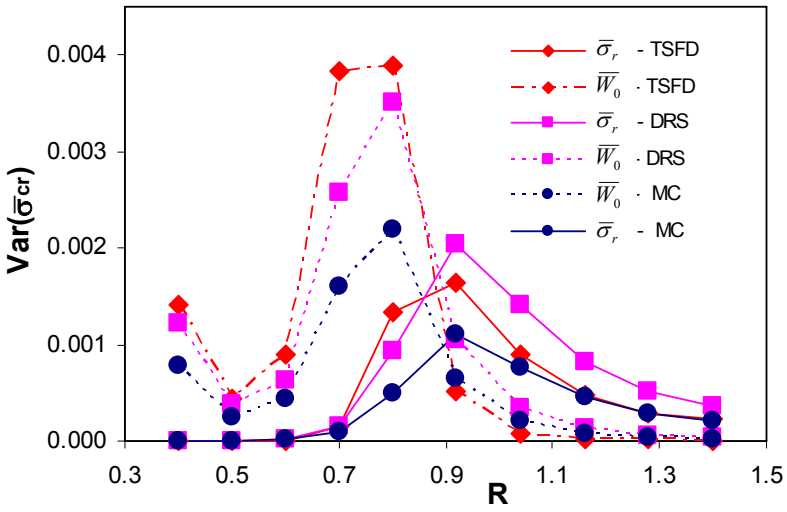

Fig. 3.6-13 Variance values with respect to residual stress and initial deflection obtained from TSFD, DRS and Monte Carlo based methods

Fig.3.6-13 presents the obtained results of normalized LBS variance with respect to normalized residual stress and initial deflection individually by employing DRS, RSFD and

MC methods. At R=0.8 and R=0.92 the results obtained by 3 methods attained maximum level of variance with respect to normalized residual stress and initial deflection, respectively. With these R values the results obtained by MC method are the lowest among those obtained by the 3 methods. The results yielded from 3 methods have the similar tendency.

Fig.3.6-13 also shows that for R<0.8, LBS variances are more sensitive with initial deflection than with residual stress. For R>0.9 the opposite tendency is observed, the influence of residual stress on the LBS variances is more sensitive than that of initial deflection. Within the range $0.8 \leq R \leq 0.9$, both variance values with respect to initial deflection and residual stress attain significant levels but based on the maximum levels it can be concluded that the LBS variances of steel plates are more sensitive with initial deflection than with residual stress.

Case 2 of generating random residual stress

Fig.3.6-14, Fig 3.6-15 and Fig 3.6-16 present the LBS variances accounting 6 steel grades with respect to normalized residual stress and initial deflection separately, which was obtained by D.R.S. (Fig. 3.6-14), TSDF (Fig. 3.6-15) and M.C. (Fig. 3.6-16) methods. All 3 figure showed that the difference of the LBS standard deviations regarding different steel grades is significant for $R < 0.8$. The investigation of the LBS variance with respect to normalized initial deflection and residual will explain the reason of this difference. As shown from results of the 3 methods, for R<0.85 the difference of the LBS variances regarding different steel grades with respect to initial deflection is significant while LBS variances with respect to normalized residual stress are almost similar. Therefore it can be stated that the difference of the LBS standard deviations regarding different steel grades is due to influence of initial deflection, which is much concerned with the different inelastic behaviors of different grades.

All the 3 methods represent the same tendency that the LBS variances with respect to residual stress regarding high strength steels are greater than those regarding normal steels, especially within the range of 0.8<R<1.04. This behavior indicates that the influence of residual stress on high strength steel plates is more sensitive than that on LBS of normal steel plates. With respect to initial deflection within the range of 0.55<R<0.85 the LBS variances regarding normal steels are greater than those regarding high strength steel. Hence within this range of R, the effect of initial deflection on LBS of normal steel plates is more sensitive than that on LBS of high strength steel plates. However, for the range of 0.40<R<0.55 the LBS variances with respect to initial deflection regarding high strength steels are greater than those regarding normal steels. The reason for the change of this tendency might be due to the small range of

plastic strain of high strength steels. And among the high strength steels, because of the steepest first strain hardening slope the LBS variances regarding SM570 steel are greater than those regarding SBHS500 and SBHS700 steels.

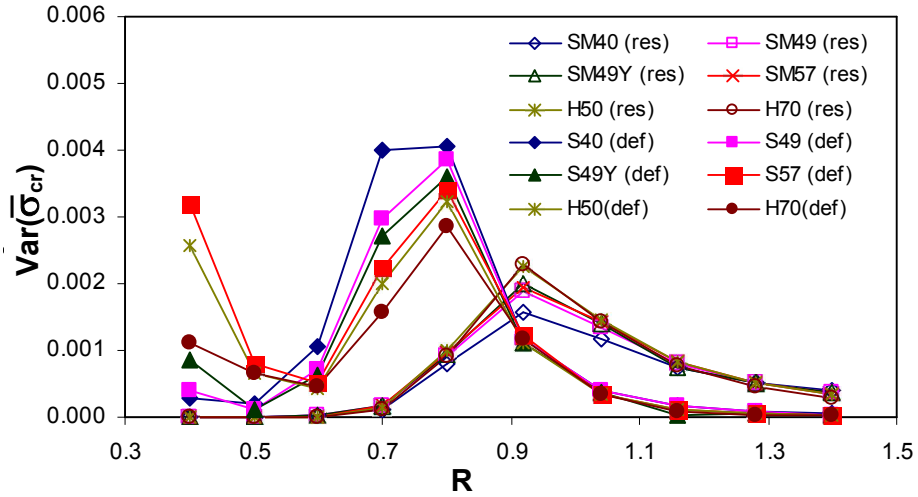

Fig. 3.6-14 Variance of LBS due to individual input random variables: residual stress $\bar{\sigma}_r$ and initial deflection $\bar{W}_0$; TSDF method

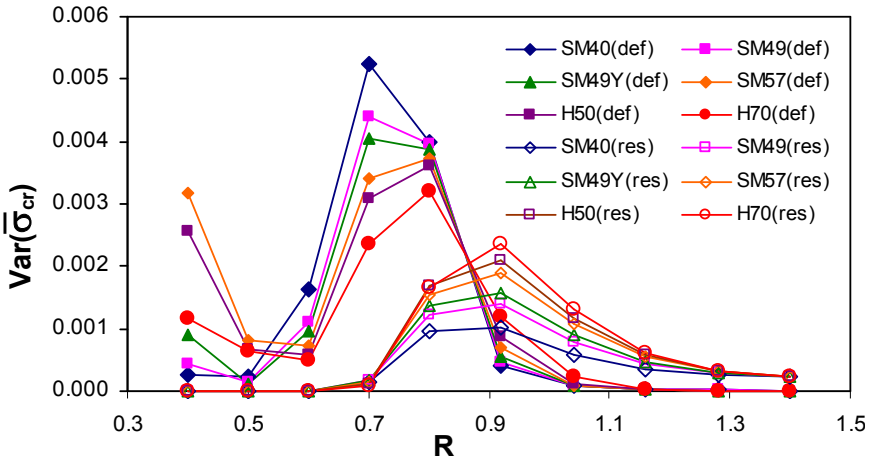

Fig. 3.6-15 Variance of LBS due to individual input random variables: residual stress $\bar{\sigma}_r$ and initial deflection $\bar{W}_0$; DRS method

Similar to the case in which the response surface considering all 6 steel grades, for R > 1.0, the steel plate LBS variances with respect to residual stress regarding all 6 steel grades separately are greater than those with respect to initial deflection. It represents that for this range of R LBS variances are more sensitive with residual stress with respect to any steel grade. In contras for R< 0.8 initial deflection mainly effects on LBS variances of steel plates regarding any steel grade. Within the range of 0.8<R<0.95 LBS variances are sensitive with both residual stress and initial deflection but the sensitivity of initial deflection is dominant.

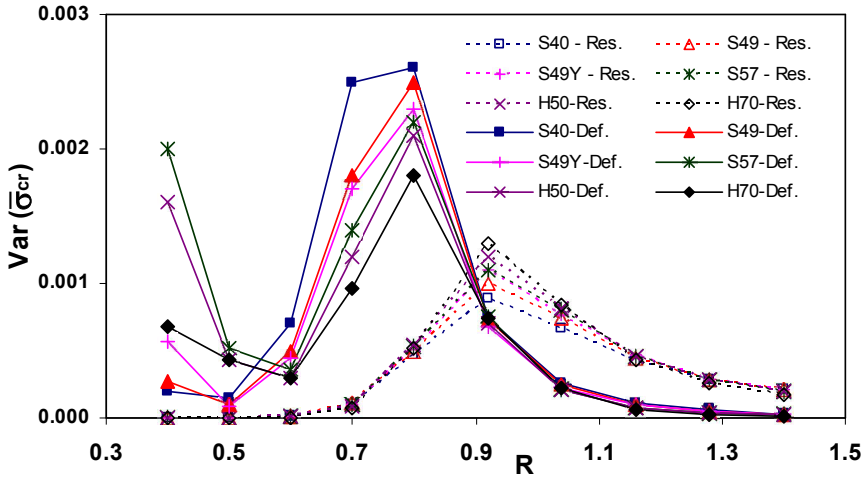

Fig. 3.6-16 Variance of LBS due to individual input random variables: residual stress $\bar{\sigma}_r$ and initial deflection $\bar{W}_0$; M.C. method

As discussed in the previous paragraph, for R≥1 (slender range) the LBS variances are mainly influenced by scaterness of residual stress, however, with the different mean levels of applied normalized residual stress from 0.15 to 0.3 the LBSs variances regarding 6 steel grades obtained from TSDF and MC methods are almost similar. The reason for this similarity is that for this range of R the LBS of steel plates is dominant by elastic local buckling behavior and the influence of residual stress on LBS might be almost the same for different steel grades.

3.6.4. Proposal of partial safety factor

Proposal of partial safety factor employs the results of case 1 of generating random residual stress, in which all steel plates apply the same probabilistic characteristics of random normalized residual stress level. The current study presents the proposal of partial safety factor based on 2 methods: employing the target safety index (assumption of normal probability density distribution function) and exceedance probability obtained directly from statistical results.

Assumption of normal distribution

Assumption of normal distribution is applied to describe the probabilistic distribution of normalized LBS of steel plates and nominal design strength is set to be equal to mean normalized LBS, partial safety factor γ is identifed by solving the Eq.3.6-5, which is explained in Fig.3.6-17 (for the example case R=0.8).

$$\mu - \beta_T \sigma = \frac{1}{\gamma} f_N \tag{3.6-5}$$

The results yield

$$\gamma = \frac{1}{1 - \beta_T \left(\frac{\sigma}{\mu} \right)} \tag{3.6-6}$$

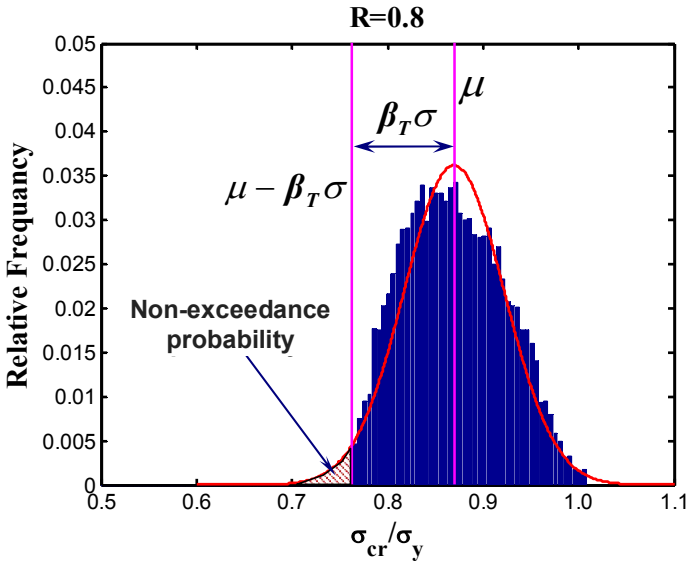

Fig. 3.6-17 Proposal of safety factor from assumption of normal distribution function

where σ and μ are the mean and standard deviation of normalized LBS, respectively; β_T stands for the target reliability index; γ and f_N are the safety factor and the corresponding nominal strength, see Fig.3.6-17 for the probability density function and the approximated normal distribution at R=0.8. Once the target reliability index and the nominal strength are specified, the corresponding safety factor is calculated from Eq.(3.6-6) with mean and standard deviation obtained from the Monte Carlo simulation. The target safety indexes and corresponding non-exceedance probabilities are presented in Table 3.6-4.

Table 3.6-4 Obtained results of partial safety factors

β_T	1.64	1.88	2.33
$P_f = \Phi(-\beta_T)$	5%	3%	1%

Assuming that the probability density of LBS is described by a normal distribution, and assigning non-exceedance probabilities of LBS to 5.0, 3.0, and 1.0%, then the corresponding target reliability incises become 1.64, 1.88, and 2.33. Furthermore, setting the nominal LBS

equal to the mean of LBS as an example, the partial safety factor can be obtained as shown in Table 3.6-5.

Table 3.6-5 Obtained results of partial safety factors with normal distribution assumption

R	0.4	0.5	0.6	0.7	0.8	0.92	1.04	1.16	1.28	1.4
μ	1.039	1.006	0.982	0.938	0.862	0.766	0.701	0.653	0.617	0.586
γ(5%)	1.05	1.03	1.04	1.08	1.11	1.09	1.07	1.06	1.05	1.04
γ(3%)	1.05	1.03	1.04	1.09	1.13	1.11	1.09	1.07	1.06	1.05
γ(1%)	1.07	1.04	1.05	1.11	1.16	1.14	1.11	1.08	1.07	1.06

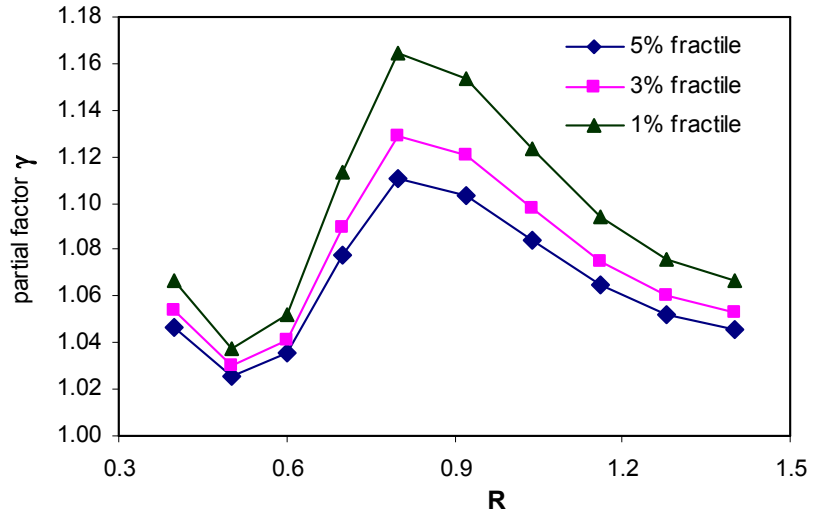

Fig. 3.6-18 Partial safety factors obtained in the range of R 0.4≤R≤1.4

As shown in Fig.3.6-18, the maximum partial safety factor values regarding exceedance probability of 5%, 3%, and 1% are equal to 1.11, 1.13, and 1.16, respectively.

Direct application of exceedance probability

The exceedance probability of a specific normalized compressive value $\overline{\sigma}_{cr}$ can be identified directly by the numerical random simulation employed in the current study. Because of the random simulation based method, the results varied for each analysis process. Hence in the current study the exceedance probability for a specific $\overline{\sigma}_{cr}$ value is obtained by taking the average value from 10 random analyses.

In the current study the mean result and standard deviation are obtained from the random simulation with processing 10.000 random variable couples of residual stress and initial displacement, hence the convergence of statistical results with this number of random input couple should be investigated. The convergent investigation is processed similarly as

presented in section 3.6.2. Fig.3.6-19 and 3.3-20 present the investigation for the case R=0.8 with value $\overline{\sigma}_{cr}$ =0.789

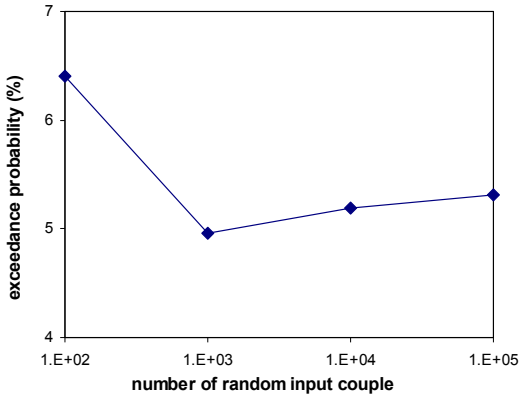

Fig. 3.6-19 The exceedance probability corresponding to 100, 1000, 10000 and 100000 random input couples processed

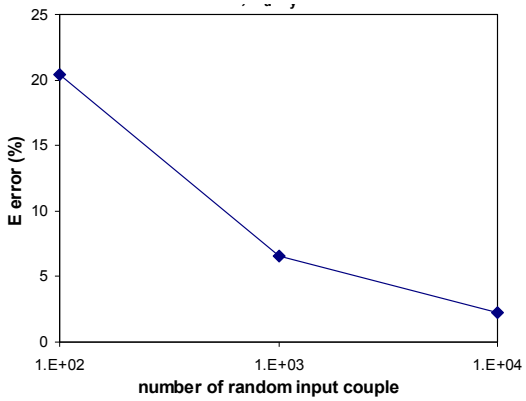

Fig. 3.6-20 The error value corresponding to random simulation processed with 100, 1000, and 10000 random input couples

As shown in Fig.3.6-20 the error values (E) decrease with increasing of the random input number. Corresponding to the simulation with 10000 random input couples, the E value is equal to 2.24%, this error level is sufficiently small and hence the fractile results can be employed to the investigation.

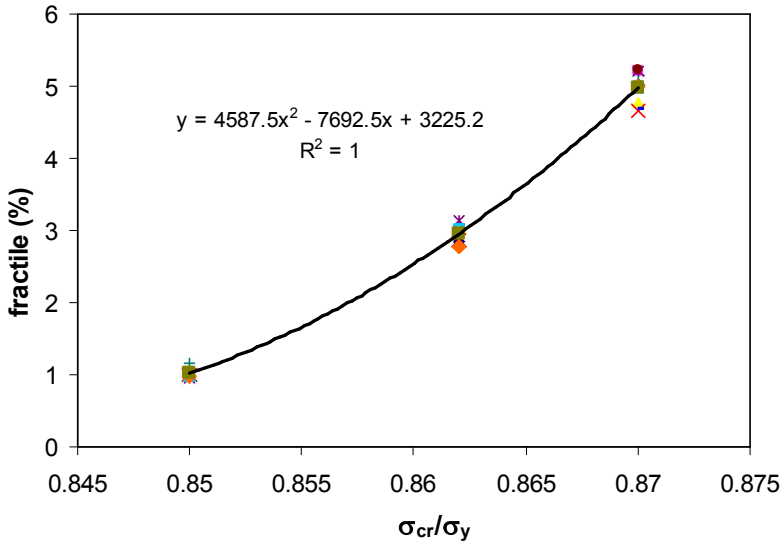

Fig. 3.6-21 Identification of σ_{cr}/σ_y values corresponding to fractile level = 1, 3 and 5 % for the case R =0.7

To identify the $\overline{\sigma}_{cr}$ values corresponding to 5%, 3%, 1% fractile, 3 average fractile values within the range from 1% to 5% were plotted with corresponding $\overline{\sigma}_{cr}$ values. Based on these

values the approximate second order algebraic function is defined as shown in Fig.3.6-21, 3.6-22 and 3.6-23 hence the $\overline{\sigma}_{cr}$ values corresponding 5%, 3%, 1% fractile levels can be obtained.

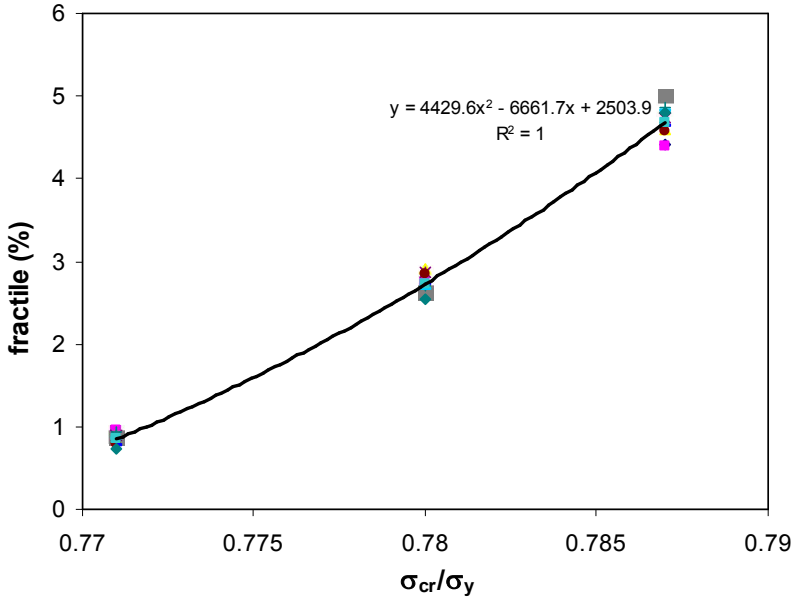

Fig. 3.6-22 Identification of σ_{cr}/σ_y values corresponding to fractile level = 1, 3 and 5 % for the case R =0.8

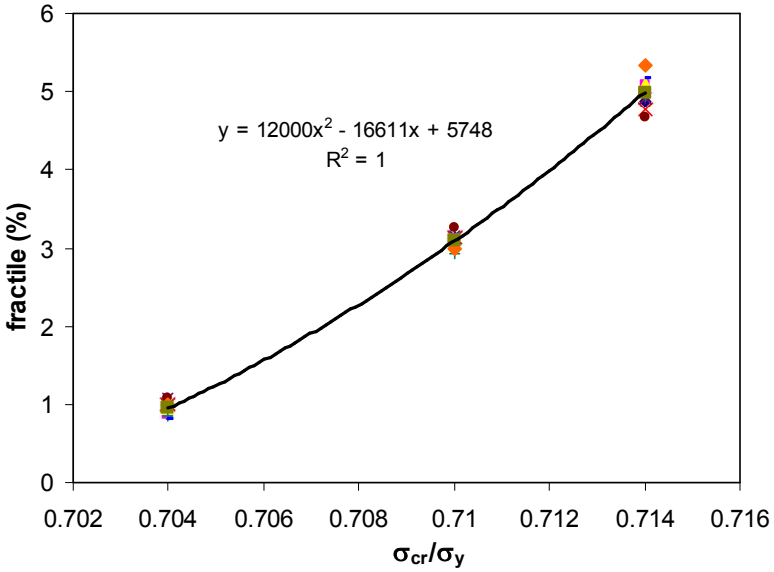

Fig. 3.6-23 Identification of σ_{cr}/σ_y values corresponding to fractile level = 1, 3 and 5 % for the case R =0.92

All results of partial safety factor obtained directly from the random simulation based method are presented in Table 3.3-6 and Fig.3.6-24

Table 3.6-6 Partial safety factors directly from random simulation based method

R	0.4	0.5	0.6	0.7	0.8	0.92	1.04	1.16	1.28	1.4
μ	1.039	1.006	0.982	0.938	0.862	0.766	0.701	0.653	0.617	0.586
γ(5%)	1.04	1.03	1.05	1.08	1.09	1.07	1.06	1.04	1.04	1.04
γ(3%)	1.04	1.03	1.05	1.09	1.10	1.08	1.06	1.05	1.04	1.04
γ(1%)	1.04	1.03	1.07	1.10	1.12	1.09	1.07	1.05	1.04	1.04

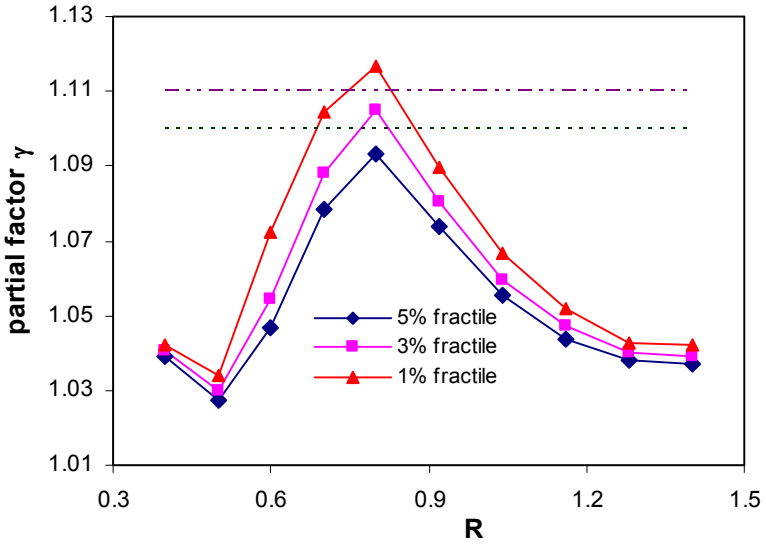

Fig. 3.6-24 Partial safety factors obtained directly from the random simulation and compared to Eurocode and AASHTO safety factors

The results of partial safety factor obtained directly from the random simulation based method are lower than those obtained by applying the assumption of normal.

Comparison to AASHTO and JSHB design strengths

It is a most rigorous way to determine the safety factor and nominal strength based on probability of failure calculated from probability density of LBS. However, the probability of failure largely depends on a shape of the foot of a probability density function, and accordingly its high accuracy is not expected. Therefore, the reliability index is used to specify a safety margin as presented in Eq.3.6-5, the partial safety factor results obtained by assumption of normal distribution should be employed. The mean $\overline{\sigma}_r$ results can be applied as standard strengths but should be $\leq$1.

Fig.3.6-25 plots the nominal and design LBS of steel plates with assumption of mean results as nominal (characteristic) strength and safety factor = 1.11, 1.13 and 1.16 along with the corresponding strength curves specified by AASHTO. The results of the current study represent the different curvature tendency comparing to that of AASHTO nominal strength equation, which is based on elastic buckling curve. The design LBSs resulted from the current

study are significantly lower than those of design strength specified in AASHTO in practical R ranging from 0,7 to 1.2.

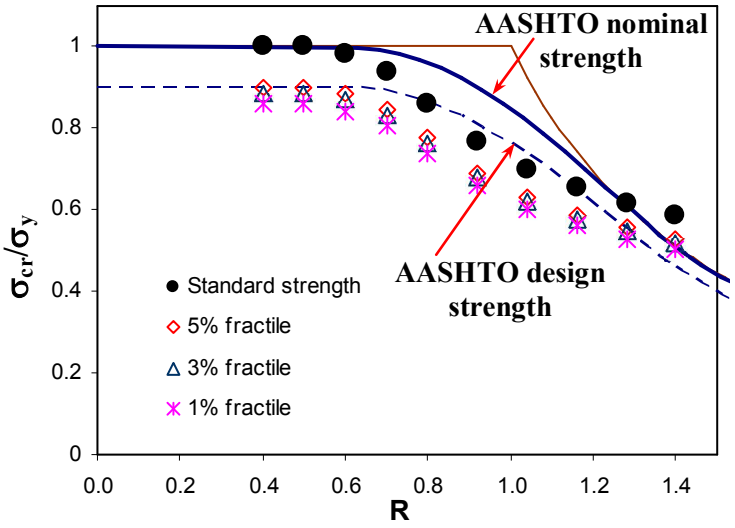

Fig. 3.6-25 Comparison of local buckling design resistance of steel plates specified by AASHTO, JSHB and current study results

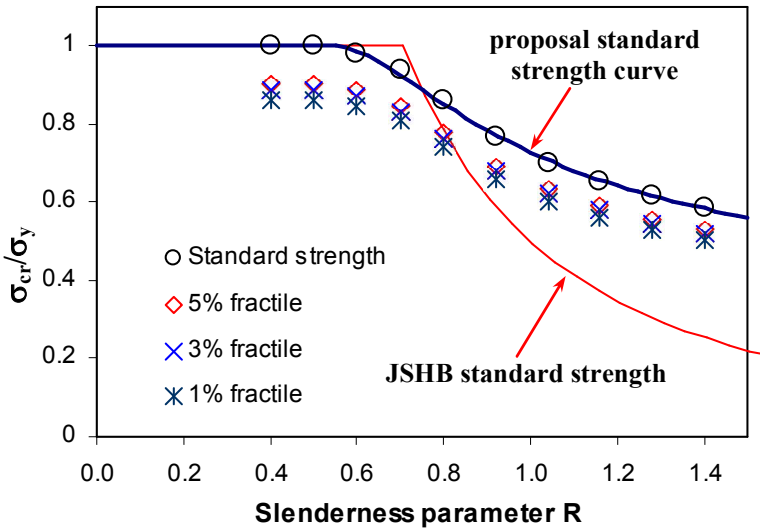

Fig. 3.6-26 Proposal standard strength curve for compressive simply supported steel plates

As the current study only considers the scatterness of initial imperfection and without considering scatterness of steel material yield strength, the Eq.3.6-7, the standard LBS equation for compressive simply supported steel plates is proposed based on LBS mean values. The comparison to JSHB standard strength curve is presented in Fig.3.6-26

$$\frac{\sigma_{cr}}{\sigma_y} = \begin{cases} 1 & R \le 0.55 \\ 0.399 - \dfrac{0.0775}{R} + \dfrac{0.630}{R^2} - \dfrac{0.223}{R^3} & R > 0.55 \end{cases} \tag{3.6-7}$$

The R-squared value (coefficient of variation) of fitting equation (Eq.3.6-7) is equal to 0.997 and hence shows the very good fitness of the approximation.

The general curvature tendency of proposal standard LBS equation is less steep than that of JSHB. This behavior represents the difference of the steel plate LBS which is obtained by considering inelastic material behavior and nonlinear geometrical analysis and the ones which results from the elastic local buckling theory.

3.7. Conclusions

Probabilistic distribution of the steel plate LBS

- The mean results obtained in the current study are similar to the mean (M) curve proposed in Fukumoto and Itoh (1984), which was based on the experimental data. Compared to experimental-based curve the mean results of the current study are slightly greater within the range 0.65<R<0.85 because the current study consider SBHS steel plates and normalized initial deflection levels $\overline{W}_0 \le 1/150$.
- Compared to the standard deviation obtained from experimental results reported in Fukumoto and Itoh (1984), the corresponding results of the current study exhibits about half of that within a range of 0.6<R<1.2 .
- The high strength steel SBHS500 and SBHS700 represent better performance than normal steels in LBS of steel plates.
- In the range of 0.4≤R≤0.85 the influence on the steel plate LBS of initial deflection is more sensitive than that of residual stress. However, in the range of R>0.9 the influence on the steel plate LBS of residual stress is more sensitive than that of initial deflection.
- For 0.8<R<1.04 the influence of residual stress on the plate LBS regarding high strength steels is more sensitive than that regarding normal steels.
- For 0.55<R<0.85 the influence of initial deflection on the plate LBS regarding normal steels is more sensitive than that regarding high strength steels.
- In the range of 0.4≤R≤0.55 under the effect of much smaller plastic strain range of high strength steels compared to normal steels, the influence of initial deflection on the plate LBS regarding high strength steels is more sensitive than that regarding normal steels.

Considering among high strength steels (SBHS500, SBHS700 and SM570) because of the different 1st hardening strain slope, the influence of initial deflection on steel plate LBS regarding SM570 steel is the most sensitive followed by SBHS500 and SBHS700.

- The difference of normalized residual stress within the range $0.15 \leq \bar{\sigma}_r \leq 0.3$ does not induce the significant difference of steel plate LBS.
- (M-2S) results obtained in the current study are significantly greater than (M-2S) curve proposed in Fukumoto and Itoh (1984). However, the compact limits, R value for $\sigma_u/\sigma_y \geq 1$, of both results are pretty similar and ≈ 0.4
- By applying the same mean levels of initial imperfections $\overline{W}_0$ =1/400 and $\bar{\sigma}_r$ =0.23, the LBS of high strength steel plates is slightly greater than that of normal steel plates at R≈0.4 and R≈0.8. At R≈0.4 the difference is induced by hardening behavior of high strength steel plates and the difference at R≈0.8 is due to the difference of elastic-plastic local buckling behavior.
- For R ≤0.5, the difference of plastic strain range and 1st hardening strain slope between high strength steels (SBHS steels and SM570) and normal steels (SM400, SM490 and SM490Y) induces the difference of LBS levels. With mean levels of initial imperfections $\overline{W}_0$ =1/400 and $\bar{\sigma}_r$ =0.23, $\bar{\sigma}_{cr}$ (high strength steels) is greater than 1 while $\bar{\sigma}_{cr}$ (normal steel) is about 1, the difference according to R=0.4 is about 6%.
- The difference of LBS corresponding to level M-2S regarding different steel grades is more significant, it is about 7% between $\bar{\sigma}_{cr}$ (SM400) and $\bar{\sigma}_{cr}$ (SBHS700) within the range of 0.65<R<0.95.

Proposal of LBS standard strengths and their partial safety factor

- With assumption of normal distribution function applying to probabilistic distribution of steel plate LBS and the LBS mean values considered as standard strengths , the partial safety factors obtained are equal to 1.11, 1.13 and 1.16 corresponding to 5%, 3% and 1% fractile, respectively.
- Applying the obtained partial safety factors considering the mean results as characteristic design resistance, the obtained designed LBS values are lower than those specified by AASHTO in the range of 0.6<R<1.3 and greater than those specified by JSHB in whole range of R.
- The tendency of designed LBS results plotted with respect to corresponding R value in the current study are much less steep compared to those specified by AASHTO and JSHB, which are based on result of elastic local buckling theory.

CHAPTER 4

WEB SLENDERNESS LIMITS FOR SECTION CLASSIFICATION OF COMPOSITE GIRDERS

4.1. Introduction

Application of SBHS500 to hybrid girders is expected to be an economical solution for composite girder bridges. For I-shape and composite girders the high strength steel plates are usually applied to the flanges with purpose to improve the bending resistance. The composite girder with flanges and web made from SBHS500 and SM90Y steels, respectively, is targeted in current study. AASHTO Load Resistance Factor Design (LRFD) bridge specifications (AASHTO, 2005) employs the hybrid factor R_h to calculate the yield moment M_{yf} of a hybrid section from the yield moment M_y of the relevant homogeneous section. This hybrid factor formula can be applied to both noncomposite and composite hybrid sections. In previous AASHTO Specifications, separate formulas of the hybrid factor had been specified for noncomposite and composite hybrid sections on the basis of studies by Subcommittee on Hybrid Beams and Girders (1968) and Schilling (1968). However, since the calculated hybrid factor values by both formulas are close to 1.0 for typical cross sections, in current AASHTO Specifications the hybrid factor formulas have been condensed to a single equation (Eq.4.1-1) originally proposed for noncomposite sections to apply to composite sections as well. In this study, the applicability of the current hybrid factor formula in AASHTO specifications to composite hybrid sections with SBHS500 will be examined, and a new hybrid factor formula will be developed.

$$R_h = \frac{M_{yf}}{M_y} = \frac{12 + \beta(3\alpha - \alpha^3)}{(12 + 2\beta)} \tag{4.1-1}$$

As mentioned in Literature Review Chapter, the un-shored construction method has been applied commonly in building composite girder bridges. For this construction method, first, a steel girder only resists a bending moment due to dead loads of steel and wet concrete. Then, after hardening concrete, the corresponding composite girder supports the live load. Hence, the initial bending moment in the construction stage has to be considered. The Eq.4.1-1 is developed based on the assumption of elastic stress distribution on I-shaped steel section and doesn't consider the effect of initial bending moment. Hence, to identify the yield moment value, the current study will derive a formula, which bases on stress distribution on composite section and considers the effect of initial bending moment.

The consideration of the initial bending moment in the stress state of a composite girder is represented as following. The stress state in the service state is the combination of stress state due to initial bending moment in steel section only and stress state of composite section. The combination based on elastic assumptions of stress distribution on steel and composite sections is presented in Fig.4.4-1. The figure shows that with considering the initial bending moment, the neutral axis of the girder section regarding service stage is located lower than that of origin composite section hence the composite section resistance might be changed and it is more favorable for local buckling occurring. Therefore, it is necessary to consider initial bending moment in designing of composite girder.

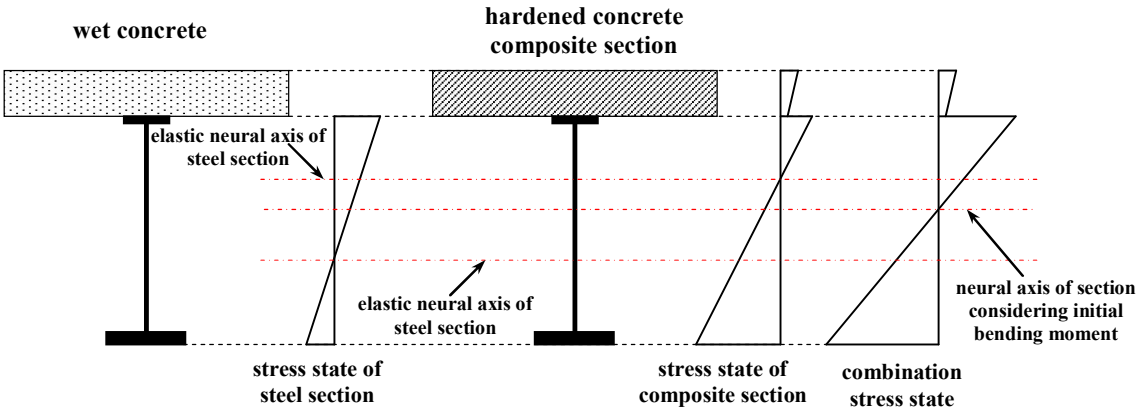

Fig. 4.1-1 Consideration of stress stage due to initial bending moment

The bending moment capacity of a composite section largely depends on a section class and local bucking of components of steel sections. Since the possibility of local buckling is restricted only for the upper part of web plates for composite sections under a positive bending moment, the section classification is governed by a width thickness ratio of web plates under compression. Summary of the section classification criteria in AASHTO Specifications and Eurocode is represented in Table 2-1 chapter 2, where M_u is the bending moment capacity of a composite section; M_p and M_y are the plastic moment and the yield moment, respectively. In the current study, the initial bending moment will be considered in FEM composite girder models and the identification of yield bending moment $\boldsymbol{M_y}$. Regarding the $\boldsymbol{M_p}$ value, Roik el al. (1993) reported that the ultimate loads acting on composite girder constructed by shored and un-shored method are similar for compact sections, the effect of initial bending moment can be neglected.

The plastic moment M_p is identified based on the assumption that the entire cross section has reached its relevant yield stress and inelastic behavior of the steel material obeys the perfectly plastic assumption. The plastic stress distribution for homogeneous and hybrid section is presented in Fig.4.1-2.

σ_y is the yield strength of relevant steel grade in homogeneous section, σ_{yw} and σ_{yf} stand for the yield strength of relevant steel grades in web plate and flanges, respectively. D_{cp} is the compression depth in web plate. f_c is design compressive strength of concrete material.

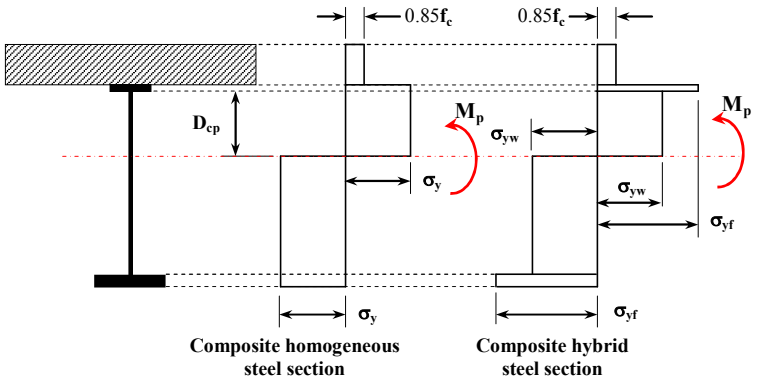

Fig. 4.1-2 The plastic stress distribution for homogeneous and hybrid sections

Yield bending moment M_y is determined once yield stress attained at either extreme fibre of flange, however, the current study just considers the case of yielding stress attaining first at bottom extreme fibre. As mentioned above the determination of yield bending moment in the current study takes into account of the effect of initial bending moment and bases on stress distributions presented in Fig.4.1-3

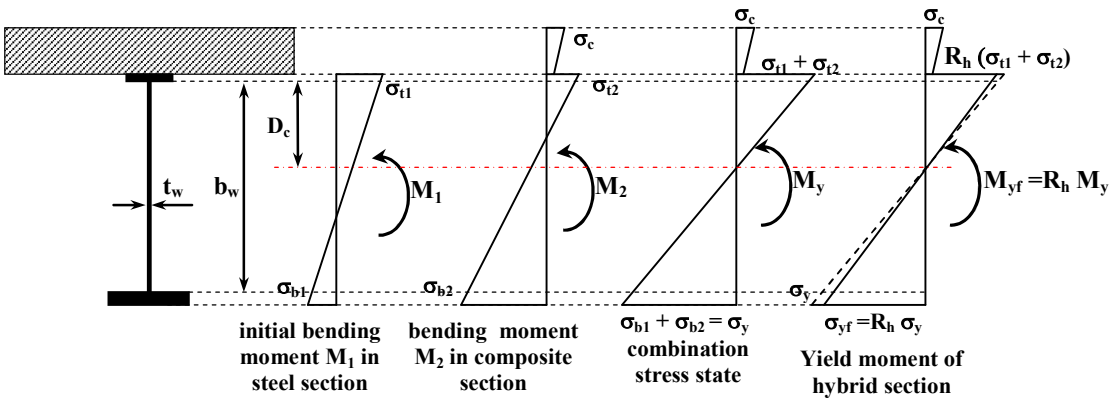

Fig. 4.1-3 Yield bending moment of composite homogeneous and hybrid steel section with considering the initial bending moment

σ_{t1}, σ_{b1} are the label of stress values resulted by initial bending moment M_1 in extreme fibre of top and bottom flange, respectively. σ_{t2}, σ_{b2} are stress value for composite section. In practical design, the yield stress is intended to attain at extreme fibre of bottom flange hence the figure illustrates $\sigma_{b1} + \sigma_{b2} = \sigma_y$. D_c is compressive depth of the web plate, b_w and t_w stand for the thickness and depth of the web plate. The hybrid factor R_h represents the reduction of stress value in prior yielding flange compared to σ_y value due to the partly plasticity in the web plate and results in the value σ_{yf}. As represented above the yield bending moment values are effected by the level of initial bending moment due to unshored construction method and hence the R_h value should also consider the effect of initial bending moment. According to this purpose, the improved hybrid factor will be developed and checked with the values obtained from FEM analysis results. This content will be presented in the following section.

To investigate the web slenderness limit of the composite girder with application of new steel SBHS500, the information of ultimate bending moment M_u, compression parameter α and α', width-to-thickness ratio b_w/t_w from sufficient large number of composite girders are required. This data obtained by experiment must be costly, so application of FEM simulation method is used in the current study as well.

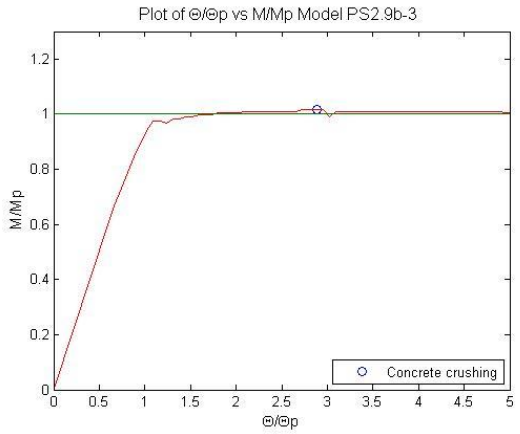

Fig. 4.1-4 Section classified as compact

In the current study, the plastic moment M_p and yield moment M_y are considered as the base of composite girder section classification. For a composite girder, the ultimate bending moment M_u obtained from FEM simulation is compared to the quantities of M_p and M_y. M_u is obtained from ultimate point at the relation curve of bending moment vs rotation at support (shown in Fig.4.1-4, 4.1-5 and 4.1-6). The quantities of M_p and M_y are identified according to the calculation steps presented in appendix A3.

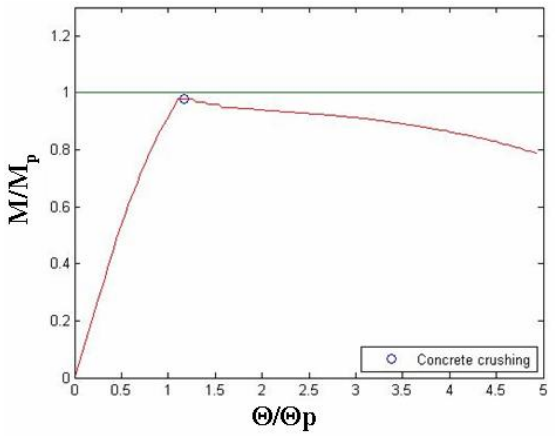

Fig. 4.1-5 Section classified as non-compact

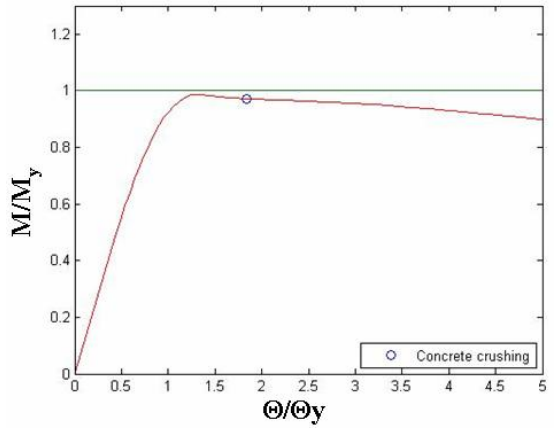

Fig. 4.1-6 Section classified as slender

- If $M_p \leq M_u$, the section is classified as compact
- If $M_p > M_u \geq M_y$, the section is classified as non-compact
- If $M_u < M_y$, the section is classified as slender

In the figures Θp and Θy stand for theoretical rotation corresponding to plastic and yield moment, respectively, with considering elastic behavior. Fig.4.1-4, Fig.4.1-5, Fig.4.1-6 represent the compact, noncompact and slender class respectively.

4.2. FEM simulation model of pure flexural composite girder

Material models

Concrete material model

For the concrete material model, it is necessary to consider the cracking mechanism with tensile cracking strain much lower than ultimate compression strain or also other words the tensile strength of concrete is much less than the compression strength. For numerical

simulation for cracking in concrete, the discrete crack and smeared crack models can be employed. The discrete crack model simulates the initiation and development of the dominant crack. In contrast, the smeared crack model doesn't simulate every single crack, it capture all cracks in a finite member through institutive relation, hence smearing out the cracks over structural body. For reinforced concrete members, without initial and dominant cracks, the smeared crack model represents the more suitable approach.

For the case of 2D or 3D stress states, in which compressive stress could exceed the compressive strength of concrete material, the crack model can be combined with plastic model to describe the crushing within the finite element. This combination model is based on the flow theory of plasticity, where nonlinear stress-strain states obey the condition of the yield criterion, the flow and hardening rules and the crushing condition. The yield criterion specifies the stress states where plastic flow is initiated. For the concrete slab of the composite girder in the current study, the transverse shear from shear stud connectors are taken into account and hence the 3D yield criterion must be employed. The Mohr-Coulomb and Drucker-Prager, for the frictional material such as concrete, soil, rock, etc, yield criteria are offered. In these materials, the initiation of yield also means the inelastic deformation or failure.

The yield condition of Mohr- Coulomb with pressure dependence behavior is represented via formulation of yield function (Eq.4.2-1) and Fig.4.2-1.

$$F = \frac{1}{2}(\sigma_1 - \sigma_3) + \frac{1}{2}(\sigma_1 + \sigma_3)\sin\phi - c\cos\phi \tag{4.2-1}$$

where c is the cohesion and ϕ is the angle of internal friction

$$c = \frac{\sigma_c(1-\sin\phi)}{2\cos\phi} \tag{4.2-2}$$

σ_c is the compressive strength of concrete

The Drucker-Prager yield criterion is approximate the Mohr-Coulomb yield criterion (shown in Fig.4.2-1). Study in (Gupta et al., 2006) reported that with investigating both Drucker-

Prager and Mohr-Coulomb yield criteria, the numerical model obtained the same ultimate strength; so current study only Mohr-Coulomb yield criterion is applied.

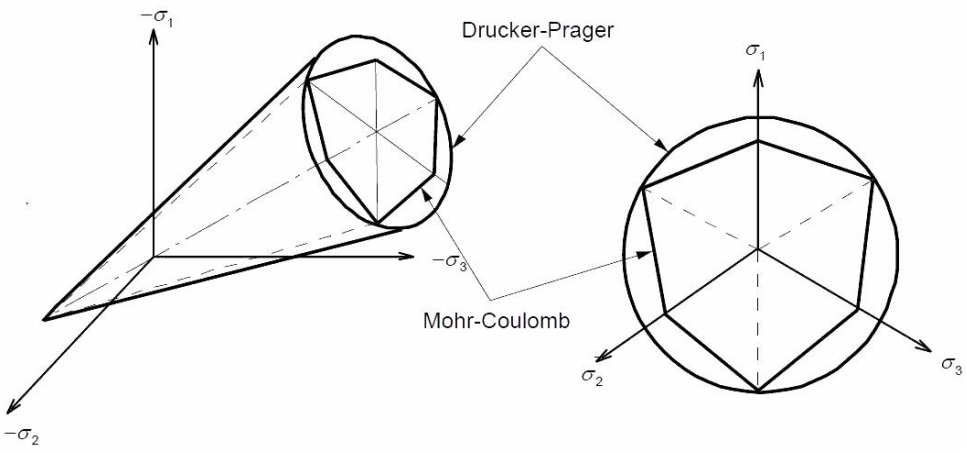

Fig. 4.2-1 Drucker-Prager and Mohr-Coulomb yield criterions

The current study doesn't consider the crushing of concrete. Concrete is assumed as isotropic material prior cracking, the maximum compressive strain = 0.003 is modeled material. The assumptions of linear-elastic, plastic hardening are employed for the material model. The uniaxial stress-strain relation for concrete material model in compression applies the equation proposed by Japanese Society of Civil Engineer (JSCE) and is presented in Eq.4.2-3 and Fig.4.2-2

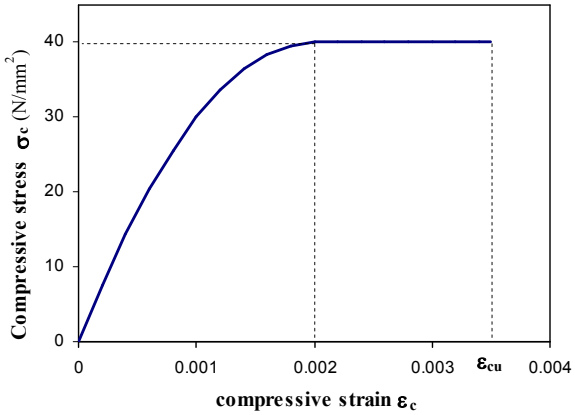

Fig. 4.2-2 Stress – strain relation for concrete material model

$$\sigma_c = \begin{cases} f_c \dfrac{\varepsilon_c}{0.002}\left(2.0 - \dfrac{\varepsilon_c}{0.002}\right) & (\varepsilon_c \le 0.002) \\ f_c & (0.002 < \varepsilon_c \le 0.0035) \end{cases} \qquad (4.2\text{-}3)$$

where, σ_c and ε_c stand for corresponding stress and strain of concrete, respectively. f_c=40MPa is characteristic compressive strength of the concrete material. The angle of internal friction ϕ is assigned = 20°.

Steel material model

For steel material, the assumptions of isotropic elasto-plastic hardening, Von Mises yield surface and strain hardening hypothesis are applied for steel material model. The uni-axial stress-strain relation of different steel grades is idealized from actual test as presented in Chapter 3. The idealized stress-strain relations of SM490Y and SBHS500 steel grades are presented in Fig.4.2-3 The inelastic characteristics of these steel grades are shown in Fig.4.2-3.

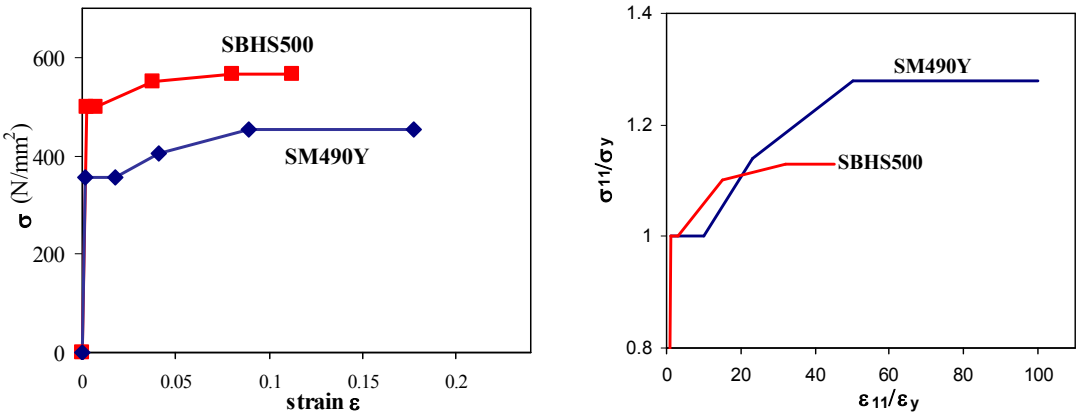

Fig. 4.2-3 Idealized stress – strain relations for steel material model

The simplified composite girder structure

The simplified composite girder structures in this study are assigned with fixed girder length = 9m, web depth = 3m and concrete slap thickness = 300cm as presented in Fig.4.2-4. The concrete slab thickness and web depth are assigned based on the dimensions of actual composite girder constructions. The girder length of 9m is designed with referring the distance between cross beams of 5-10 (m) for twin I-section composite girder. Following practical structural scale can avoid the size effect in concrete members. The current study analyses hundreds of composite girder models considering various values of concrete slab width b_c, upper and lower flange width buf and b_{lf}, respectively, upper and lower flange thickness t_{uf} and t_{lf}, respectively, and web thickness t_w with the aim to consider various levels compression web depth D_{cp} and D_c. The dimensions of investigated simulation girders in the current study are presented in Table 4.2-1, 4.2-2 and 4.2-3. The calculation of corresponding values D_{cp} and D_c, which associating to the compressive parameter α and α', respectively are presented in Appendix A3

For symmetrical condition, all nodes at symmetrical surface of the composite girder structure are assigned as simple support according X axis and free displacement according Y and Z axis as presented in Fig.4.2-5. Under a pure bending load acting at support as shown in Fig 4.2-5, on the symmetrical surface, there is a reaction of compression and bending moment at axis coincident with girder support. Because the girder support is assigned to displace on X axis, the reaction volume compression doesn't exist and only pure bending moment is produced in the composite girder structure.

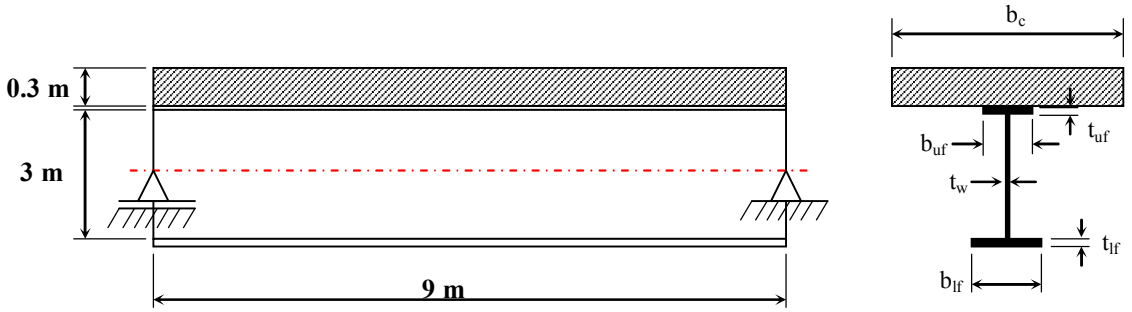

Fig. 4.2-4 Simplified composite girder structure and its dimensions

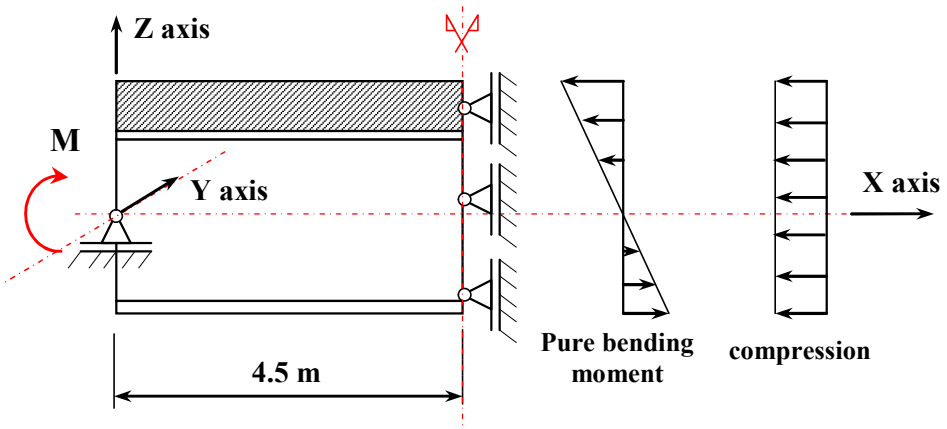

Fig. 4.2-5 Boundary condition for the simplified structure

The effect of local buckling in web plate on flexural capacity of composite girder is main issue in the current study; so displacement control method is applied to produce the pure bending moment in the girder. The application of displacement control method is presented in Fig.4.2-6.

All the nodes on the end surface of the girder are forced to displace on longitudinal X axis a sufficient small distance in each increment analysis but all these nodes are control to maintain on a flat surface, which can rotate around Y axis as illustrated in Fig.4.2-6. Against the displacement control, by stiffness of the girder, a reaction bending moment is produced in the

girder support. The reaction bending moment values and corresponding rotations in girder support at every analysis increment step are collected to identify the ultimate bending capacity of the girder.

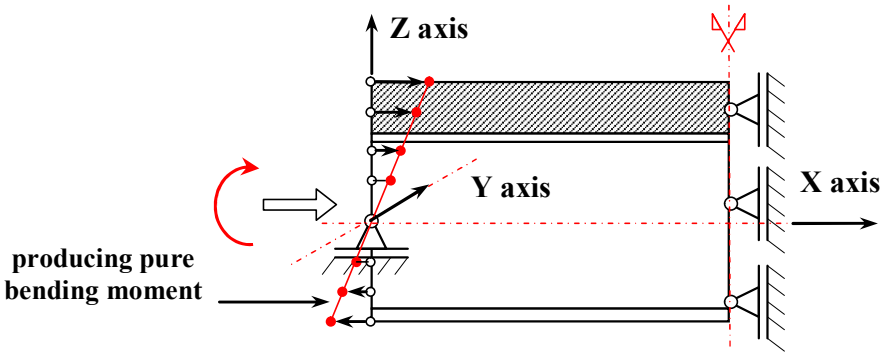

Fig. 4.2-6 Pure bending moment produced by displacement control method

The current study will investigate the simplified girders with dimensions presented in table

Table 4.2-1 Girders with compact composite SBHS500 homogeneous steel sections

Girder ID	b_w [mm]	t_w [mm]	b_{uf} [mm]	t_{uf} [mm]	b_{lf} [mm]	t_{lf} [mm]	t_c [mm]	b_c [mm]
PS2.8c	3000	15	460	65	1200	56	300	2800
PS2.9a	3000	15	460	45	1200	58	300	2900
PS2.9b	3000	15	330	100	1200	56	300	2900
PS1.8c	3000	19	520	60	800	60	300	1800
PS2.8a	3000	19	520	55	1200	60	300	2800
PS2.8a-2	3000	19	520	55	1200	65	300	2800
CS2.5a	3000	19	520	91	1200	60	300	2500
PS2.5a	3000	25	590	52	1200	60	300	2500
PS2.5a-2	3000	25	590	52	1200	65	300	2500
C1.2a	3000	25	590	52	800	46	300	1200

Table 4.2-2 Girders with noncompact and slender composite SBHS500 homogeneous steel sections

Girder ID	b_w [mm]	t_w [mm]	b_{uf} [mm]	t_{uf} [mm]	b_{lf} [mm]	t_{lf} [mm]	t_c [mm]	b_c [mm]
CS1.2h	3000	15	540	58	1200	35	300	1200
CS1.2h-2	3000	15	540	55	1200	35	300	1200
CS1.2h-3	3000	15	540	55	1200	38	300	1200
CS1.2h-4	3000	15	540	49	1200	35	300	1200
CS1.2h-5	3000	15	540	53	1200	35	300	1200
CS2.2a	3000	15	460	46	1200	55	300	2200
CS2.0e	3000	15	460	47	1200	51	300	2000

Girder ID	b_w	t_w	b_{uf}	t_{uf}	b_{lf}	t_{lf}	t_c	b_c
C1.5b	3000	19	520	36	800	52	300	1500
C1.5b-2	3000	19	520	36	800	50	300	1500
C1.5b-3	3000	19	520	40	800	50	300	1500
CS1.5c	3000	19	520	42	1200	40	300	1500
CS1.2d	3000	19	520	39	1200	36	300	1200
CS1.2d-2	3000	19	520	41	1200	36	300	1200
CS1.5	3000	25	590	42	1200	46	300	1500
CS1.5-2	3000	25	590	44	1200	46	300	1500
CS1.5-3	3000	25	590	43	1200	49	300	1500
CS1.6a	3000	25	590	47	1200	45	300	1600
CS1.6a-2	3000	25	590	50	1200	45	300	1600
CS1.6a-3	3000	25	590	45	1200	46	300	1600

Table 4.2-3 Girders with noncompact and slender composite SBHS500-SM490Y hybrid steel sections

Girder ID	b_w [mm]	t_w [mm]	b_{uf} [mm]	t_{uf} [mm]	b_{lf} [mm]	t_{lf} [mm]	t_c [mm]	b_c [mm]
PS2.8c1hy	3000	15	460	60	1200	56	300	2800
PS2.9a1hy	3000	15	460	65	1200	44	300	2900
PS2.9a2hy	3000	15	460	66	1200	77	300	2900
PS2.9b1hy	3000	15	330	50	1200	88	300	2900
CS2.5a1hy	3000	15	520	54	1200	74	300	2500
CS1.5c1hy	3000	19	520	51	800	100	300	1500
CS2.5a2hy	3000	19	520	75	1200	52	300	2500
PS2.8c2hy	3000	19	460	58	1200	90	300	2800
PS2.9a3hy	3000	19	460	64	1200	84	300	2900
PS2.9a4hy	3000	19	460	60	1200	73	300	2900
CS1.5c2hy	3000	25	520	54	800	100	300	1500
CS1.6a1hy	3000	25	590	50	1200	92	300	1600
CS2.5a3hy	3000	25	520	61	1200	62	300	2500
PS2.8c3hy	3000	25	460	60	1200	88	300	2800
PS2.9a5hy	3000	25	460	60	1200	80	300	2900

Meshing of composite girder model

The web and flange plates of the steel girder are meshed by four-node quadrilateral isoparametric curved thin shell element (Q20SH), from DIANA software library, with five

degrees of freedom (3 translations and 2 rotations) per node in order to simulate the local buckling deformations and the spread of plasticity effects.

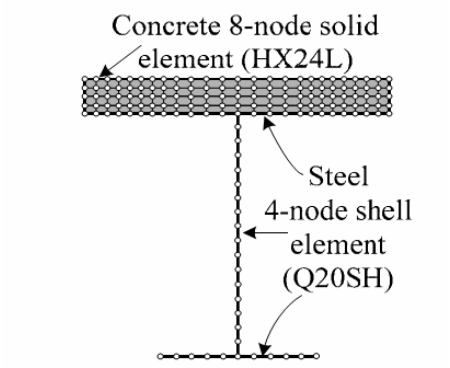

Fig. 4.2-7 Cross-section and type of elements

The concrete slab part is meshed by eight-node isoparametric solid element (HX24L), from DIANA software library, with 3 translations at each node with aim to simulate the plastic deformation, cracking in 3 orthogonal directions and crushing. Positive bending moment induces the concrete slab part of the composite girder only under compression. Besides, the flexural capacity of composite girder is just considered for maximum compressive strain of concrete = 0.0035, hence the modeling of reinforcement in concrete slab part can be neglected. The composite girder cross-section with meshing elements is presented in Fig.4.2-7

Initial geometrical imperfection

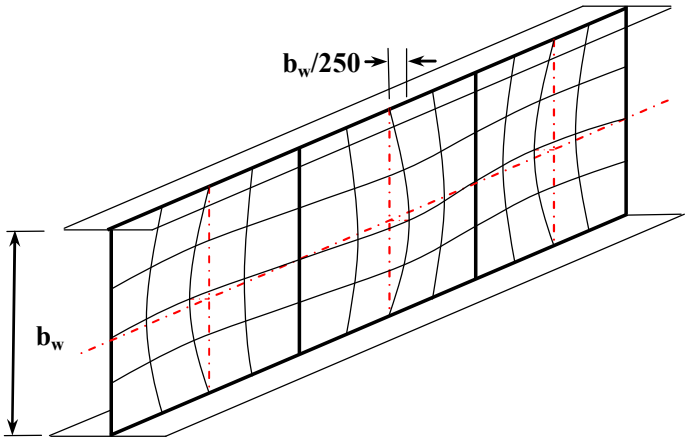

Fig. 4.2-8 Initial deflection for the web of the composite girder models

For non-linear analysis concerning the local buckling problem, it is necessary to describe the initial deflection on area, which is sensitive to the buckling. In the current study, the web plate is assigned with initial deflection level, which is presented by Eq.4.2-4 and Fig4.2-8.

$$\delta_y = \frac{b_w}{250}\sin\left(\frac{\pi}{b_w}z\right)\cos\left(\frac{\pi}{b_w}x\right) \tag{4.2-4}$$

where b_w is the web depth, x and z are global node coordinates of the web plate.

4.3. Proposal of hybrid factor

Derivation of hybrid factor

In this chapter, a hybrid factor for composite girders, which accounts for the effect of initial bending moment due to un-shored construction method, will be considered. In this construction method, first the initial bending moment M_1 due to the dead load at constriction stages is applied to steel sections alone, and then bending moment M_2 due to the live load is applied to composite sections, as shown in Fig.4.3-1. Since yielding is not allowed at the constriction stages in design practice, the web yielding due to the initial bending moment is not considered. The hybrid factor is developed for positive bending moment only, and for sections where the bottom web yields first.

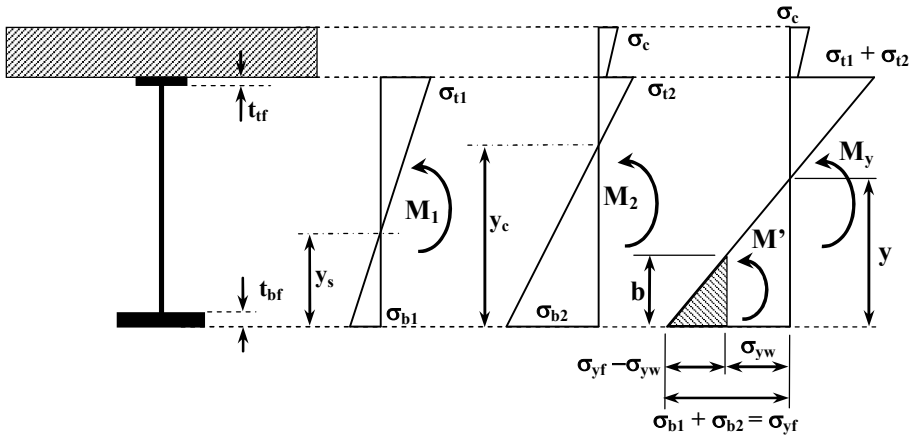

Fig. 4.3-1 Assumption on stress distributions for estimation of hybrid yield moment; (a) Initial bending moment on steel section alone, (b) Bending moment on composite section, (c) Superposed stress distribution

Furthermore, the following assumptions are made in the derivation of the hybrid factor:

1) Linear distribution of strain in a section,

2) Perfect elastic-plastic behavior of steel materials,
3) A flange thickness is negligible compared with a beam depth,
4) The position of an apparent neutral axis *y* shown in Fig.4.3-1 does not changed during yielding.

The yield moment of a composite hybrid section M_{yf} is estimated by subtracting the reduced contribution due to the prior yielding at web plate *M*' from the yield moment of the relevant composite homogeneous section M_y:

$$M_{yf} = M_y - M' = M_1 + M_2 - M' \tag{4.3-1}$$

where $M_y = M_1 + M_2$ is the yield moment of the homogeneous steel section.

The hybrid factor is defined as the ratio of M_{yf} to M_y, and expressed as

$$R_h = \frac{M_{yf}}{M_y} = \frac{M_1 + M_2 - M'}{M_y}$$

$$= \Phi S_{1.tf}\left(\frac{1}{S_{2.bf}} - \frac{1}{S_{1.bf}}\right) + 1 - \frac{M'}{\sigma_{yf} S_{2.bf}} \tag{4.3-2}$$

where $S_{1.tf}$, $S_{1.bf}$, and S_{2bf} are section modulus of steel section with respect to the top and bottom flanges, and that of composite section with respect to the bottom flange, respectively. σ_{yf} is the yield strength of flange plate. Φ represents the ratio of M_1 to the yield moment M_{ys} of homogeneous steel section only. M' is calculated from

$$M' = \frac{b^2 t_w (2\sigma_{yf} + \sigma_{yw})}{3}$$

$$= \frac{(\sigma_{yf} - \sigma_{yw})^2 y^2 t_w (2\sigma_{yf} + \sigma_{yw})}{3\sigma_{yf}^2} \tag{4.3-3}$$

$$= \frac{1}{3}(2+\alpha)(1-\alpha)^2 \left\{ \frac{h}{1 + \left[\Phi + \left(1 - \frac{\Phi y_s}{h - y_s}\right)\left(\frac{h}{y_c} - 1\right)\right]} \right\}^2 t_w \sigma_{yf}$$

where

$$y = \frac{\sigma_{yf}(t_{tf} + b_w + t_{bf})}{\sigma_{yf} + \sigma_{t1} + \sigma_{t2}} = \frac{h}{1 + \left[\Phi + \left(1 - \frac{\Phi y_s}{h - y_s}\right)\left(\frac{h}{y_c} - 1\right)\right]}$$

$$b = \frac{y(\sigma_{yf} - \sigma_{yw})}{\sigma_{yf}}$$

Hence R_h is yielded as presented in Eq.4.3-4

$$R_h = \Phi S_{1.tf}\left(\frac{1}{S_{2.bf}} - \frac{1}{S_{1.bf}}\right) + 1 - \frac{(2+\alpha)(1-\alpha)^2\left\{\frac{h}{1 + \left[\Phi + \left(1 - \frac{\Phi y_s}{h - y_s}\right)\left(\frac{h}{y_c} - 1\right)\right]}\right\}^2 t_w}{3S_{2.bf}} \quad (4.3\text{-}4)$$

The definitions of y, b, b_w, t_{tf}, and t_{bf} are shown in Fig.4.3-1.

Results and discussion

The yield moment M_y determined from FEM analysis is the reaction bending moment value at the model support when yielding strain starts attaining at either extreme steel section fibre of the girder model. The hybrid factor obtained from FEM results is the ratio of M_y and M_{yf} values (explanation of Eq.4.3-2) of composite hybrid steel girder and its corresponding composite homogeneous steel girder.

In this sub section, the proposal hybrid factors will be examined with those obtained from FEM analysis results. The composite girders with noncompact sections are employed for the comparison because M_y is important design quantity for noncompact composite sections. For the comparison, the proposal hybrid factors and the hybrid factors obtained from FEM analysis results and from the specification of AASHTO are plotted together with corresponding β values, which is explained in Eq.2.2-1. The β values corresponding to proposal hybrid factor are determined from elastic assumption and the values obtained from FEM analysis results are based on actual neutral axis when yielding strain start attaining at either flange of the numerical composite girder model. For a composite girder section, because of local buckling occurring in compression zone of the web plate, the β values based on elastic assumption and FEM analysis might be different.

The examination simulation models consider the practical range of β value, which resulted from elastic neutral axis and dimensions of composite section. In Fig.4.3-2, 4.3-3, 4.3-4 and 4.3-5 the lower bound of β value, which is about 0.45, represents the sections with web slenderness approaching the noncompact –slender limit. By referring to the design of some actual composite twin I-girder bridges built in France (Sétra, 2010), the practical range of β is from 0.65 to 1.0 when the initial bending moment is not considered and from 0.48 to 0.73 with considering pretty high level of initial bending moment $M_1 = 0.6\ M_{ys}$. Thus the range of β value considered in the current study covers the practical range. The composite girders with their dimensions considered in the current study are presented in following table

Table 4.3-1 Investigation girders for proposal hybrid factor

Girder ID	b_w [mm]	t_w [mm]	b_{uf} [mm]	t_{uf} [mm]	b_{lf} [mm]	t_{lf} [mm]	t_c [mm]	b_c [mm]
PS2.9a2hy	3000	15	460	66	1200	77	300	2900
PS2.8c1hy	3000	15	460	60	1200	56	300	2800
PS2.9a1hy	3000	15	460	65	1200	44	300	2900
CS2.5a1hy	3000	15	520	54	1200	74	300	2500
CS2.5a2hy	3000	19	520	75	1200	52	300	2500
PS2.9a3hy	3000	19	460	64	1200	84	300	2900
PS2.9a4hy	3000	19	460	60	1200	73	300	2900
CS2.5a3hy	3000	25	520	61	1200	62	300	2500
PS2.9a5hy	3000	25	460	60	1200	80	300	2900

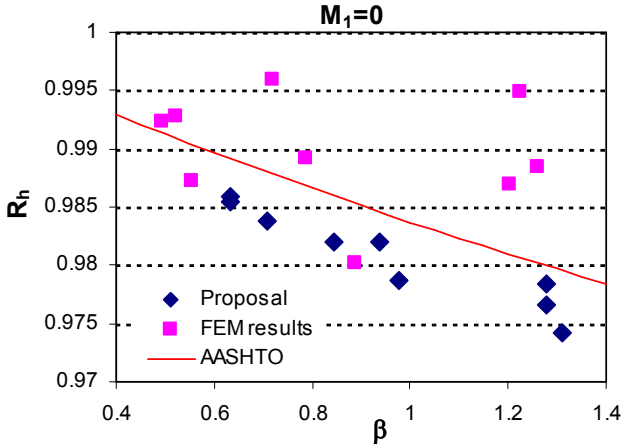

Fig. 4.3-2 Comparison of hybrid factors for the case without considering initial bending moment

The case in which initial bending moment is not considered is shown in Fig. 4.3-2, almost all proposal hybrid factors are lower than those obtained from FEM analysis results. The lower

bound of proposal and FEM analysis results are similar. The proposal hybrid factors are slightly lower than those of AASHTO specifications; the differences are about 0.5 %.

Fig. 4.3-3, 4.3-4 and 4.3-5 represent the results with considering initial bending moment. All the proposal hybrid factors are lower than those of AASHTO specification and FEM analysis results. For the case with initial bending moment M_1 = 0.2; 0.4 and 0.6 M_{ys} the differences between the proposal and AASHTO specification values are about 2%, 3% and 5%, respectively.

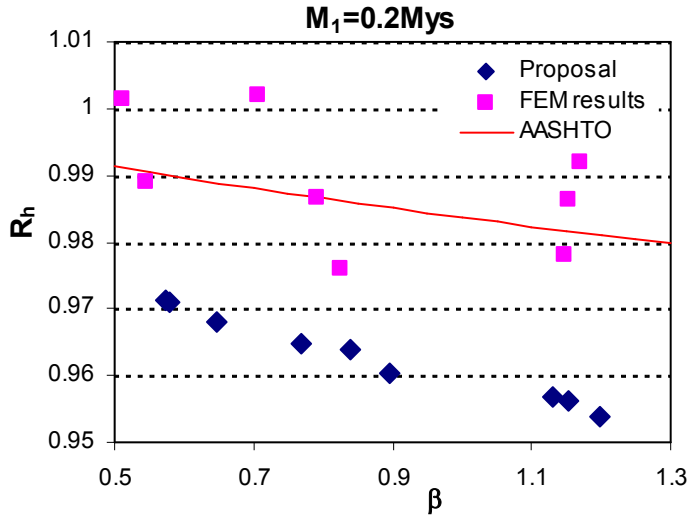

Fig. 4.3-3 Comparison of hybrid factors for the case with initial bending moment $M_1 = 0.2\ M_{ys}$

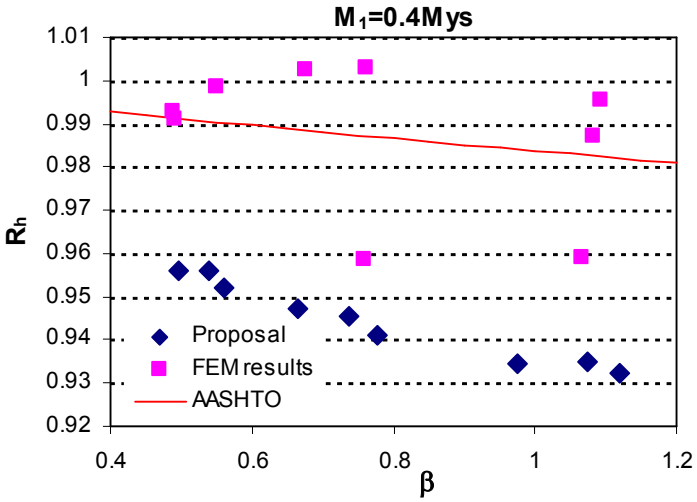

Fig. 4.3-4 Comparison of hybrid factors for the case with initial bending moment $M_1 = 0.4\ M_{ys}$

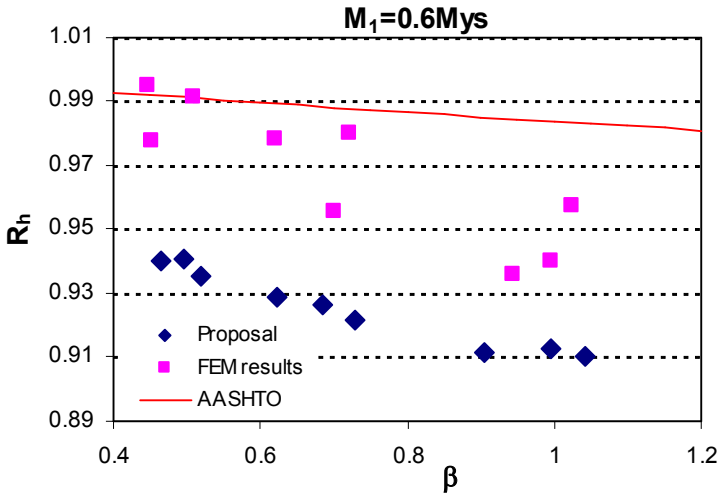

Fig. 4.3-5 Comparison of hybrid factors when with initial bending moment $M_1 = 0.6\ M_{ys}$

With high level of initial bending moment: M_1=0.6 M_{ys}, the results of which are shown in Fig.4.3-5, almost all hybrid factors obtained from FEM analysis results are lower than those of AASHTO specifications , which shows the un-conservativeness of AASHTO specifications for the case of applying high level of initial bending moment.

4.4. Web slenderness limits in design of composite girders

Composite girders with SBHS500 homogeneous sections

The following figures will present the FE analysis results of composite SBHS500 homogeneous steel sections along with the web slenderness limit of AASHTO, Eurocode and the previous results (Gupta et al., 2006), in which b_w/t_w and α stand for the width-thickness ratio and the parameter of the compression region of web plate, respectively.

In Fig.4.4-1, the black symbols stand for the numerical results judged as compact sections, while the red ones for noncompact sections. Gupta et al. (2000) reported that the initial bending moment affects insignificantly on compact-noncompact web slenderness limit of composite section classification so that in the current study, the investigation of this limit won't consider the existence of the initial bending moment. The SBHS500 homogeneous sections with the initial bending moment M_1=0 present significant greater web slenderness limit than those of AASHTO, Eurocode and the ones proposed in (Gupta et al., 2006). The inelastic behavior of SBHS500 steel seems to be the main reason. Owing to the higher yield strength, smaller yield plateau of SBHS500, it can sustain a greater local bucking resistance of the member in compressive zone of web plate than that of conventional steel. The compact-noncompact web slenderness limit of composite SBHS500 homogeneous steel sections is

about 24% greater than that of composite SM490Y homogeneous steel section and AASHTO specification, and about 50% greater than that of Eurocode specification

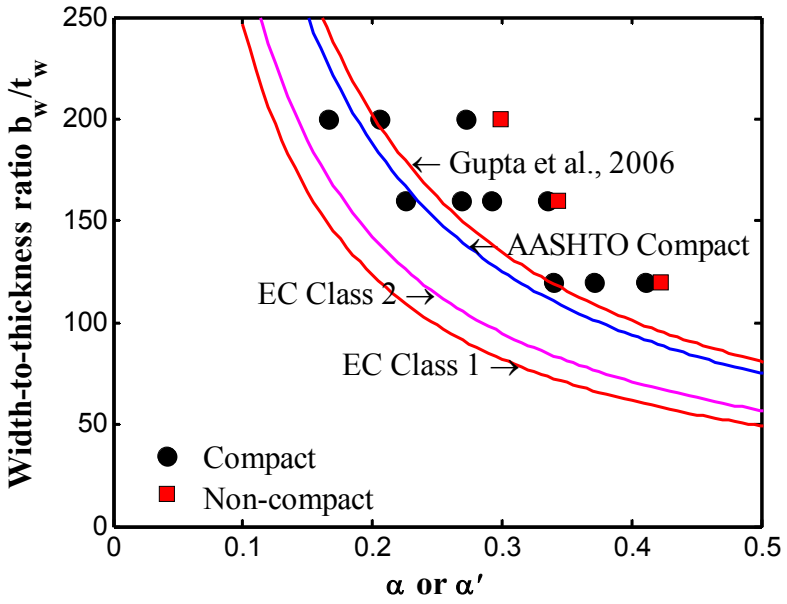

Fig. 4.4-1 Compact-noncompact limit of homogeneous SBHS500 steel section (M_1=0)

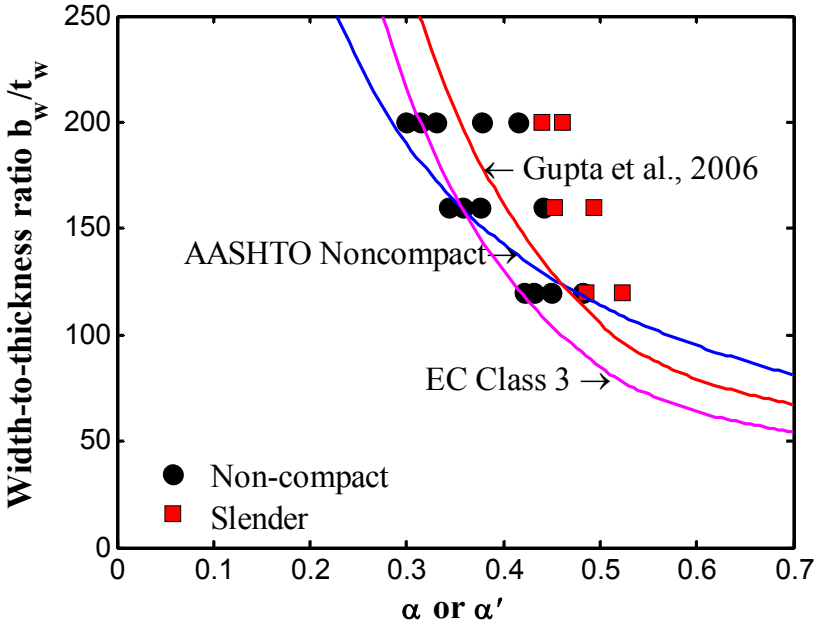

Fig. 4.4-2 Noncompact-slender limit of homogeneous SBHS500 steel sections (M_1=0)

The evaluation web slenderness limit which is based on normalized value M_u/M_y must consider the change of M_u and M_y values due to the influence of initial bending moment M_1 as well. Gupta et al. (2006), with considering SM490 steel and M_1= 0 – 0.4 M_{ys} reported the considerable effect of M_1 on the noncompact-slender limit. In this study the decrease of

ultimate bending moment M_u is explained due to the increase of compressive depth D_c which refers the local buckling behavior.

Fig. 4.4-2, 4.4-3, 4.4-4 and 4.4-5 present the numerical results for the web slenderness limit of noncompact-slender boundary for initial bending moments of M_1 =0, 0.2, 0.4, 0.6 M_{ys}, respectively. In these figures, the black symbols represent FE results classified as noncompact sections and the red ones represents slender sections. When initial bending moment is not considered, the noncompact-slender web slenderness limit of composite SBHS500 homogeneous steel sections is about 20% greater than that of composite SM490Y homogeneous steel section and about 50% greater than that that of AASHTO, Eurocode. The general tendency of noncompact-slender web-slenderness limit function to composite SBHS500 homogeneous steel section is steeper than that of SM490Y homogeneous steel section, AASHTO and Eurocode.

For $M_1 = 0.2\ M_{ys}$, no simulation girder appears as slender classification. The results of M_u and M_y in this case (referring appendix A3, table A3-2.2 and A3-2.2) show that the reduction of yield moment M_y values is more significantly than that of corresponding ultimate bending moment M_u. It is concluded that with this level of initial bending moment ($M_1 = 0.2\ M_{ys}$) the significant increase of web slenderness limit is represented compared to the case without considering the initial bending moment.

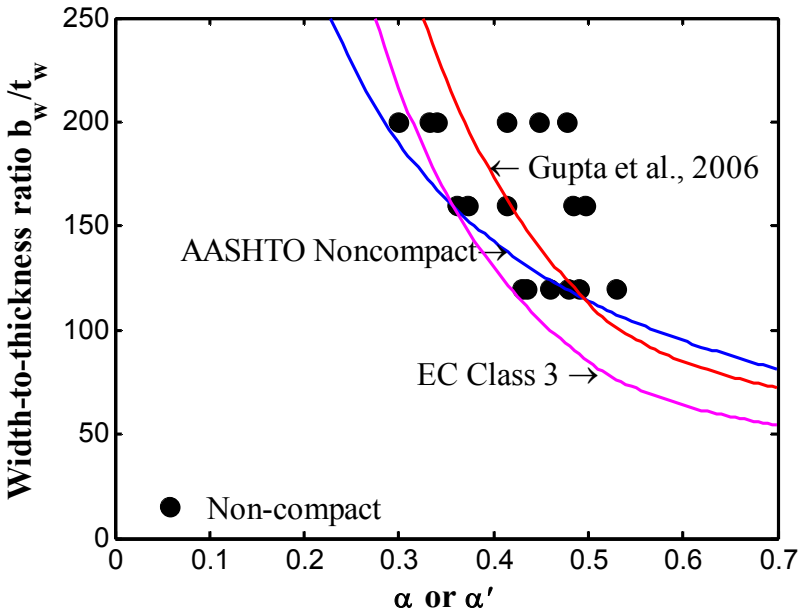

Fig. 4.4-3 Noncompact-slender limit of homogeneous SBHS500 steel sections (M_1=0.2M_{ys})

For M_1= 0.4 M_{ys} the analysis results represent that web slenderness limit of noncompact-slender to composite SBHS500 homogeneous steel sections remarkably decreases compared to that of case M_1= 0.2 M_{ys}. Under the increase of initial bending moment (from M_1=0.2M_{ys} to M_1=0.2M_{ys}) 2 simulation girders become slender classification instead of noncompact classification. The behavior of reducing web slenderness limit once increasing initial bending moment from M_1= 0.2 M_{ys} to M_1= 0.4 M_{ys} represent the opposite tendency reported in Gupta et al., (2006).

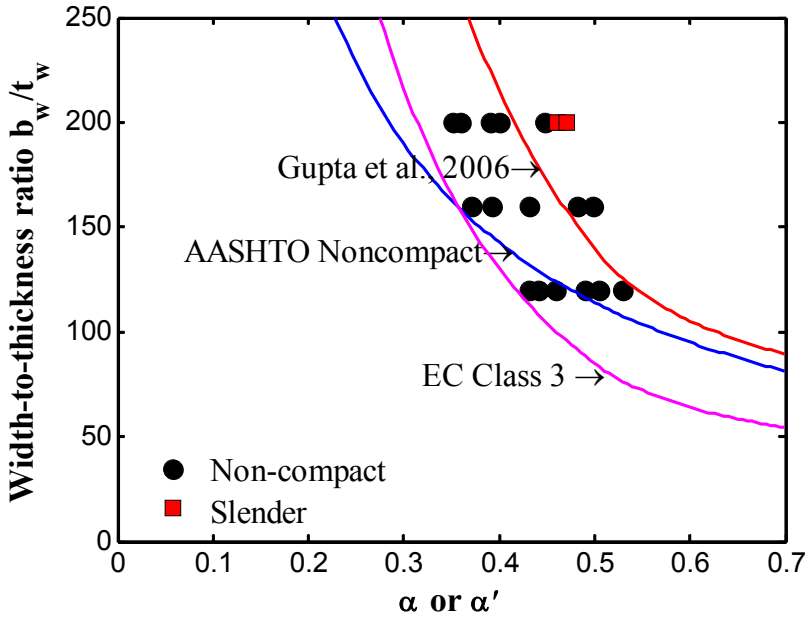

Fig. 4.4-4 Noncompact-slender limit of homogeneous SBHS500 steel sections (M_1=0.4M_{ys})

However, the web slenderness limit of noncompact-slender to composite SBHS500 homogeneous steel sections for M_1= 0.4 M_{ys} is still about 15 greater than that of composite SM490Y homogeneous steel sections. Compared to noncompact-slender web slenderness limits specified in AASHTO and Eurocode, the ones shown in analysis results of composite SBHS500 homogeneous steel sections with M_1= 0.4 M_{ys} is about 37 and 50 % respectively greater.

For M_1= 0.6 M_{ys} the analysis results (Fig.4.4-5) show the increase of web slenderness limit compared to that of the case M_1= 0.4 M_{ys} (about 10%). This limit increase represents the similar tendency as reported in Gupta et al., (2006). And the noncompact-slender web slenderness limit of composite SBHS500 homogeneous steel sections for M_1= 0.6 M_{ys} is pretty close to that of composite SM490Y homogeneous steel sections reported in Gupta et al.,2006.

The behavior of decreasing noncompact-slender web slenderness limit of composite SBHS500 homogeneous steel sections for M_1 increasing from 0.2 to 0.4 M_{ys}, opposite tendency as reported in Gupta et al. (2006), could be explained as following. For this level of initial bending moment M_1, and corresponding compressive depth D_c values of simulation girders considered in the current study, the ultimate bending moment M_u associates with local elastic-plastic buckling in compressive zone of web late. The difference of inelastic behavior would lead the better elastic-plastic buckling resistance of SBHS500 steel plates comparing to that of corresponding SM490Y steel plates. For $M_1 > 0.4M_{ys}$ and larger compressive depth D_c, the ultimate bending moment M_u might associate with the local elastic buckling behavior in compressive zone of web late. Hence, the noncompact-slender web slenderness limit of composite SBHS500 homogeneous steel sections is pretty similar to that of composite SM490Y homogeneous steel sections but still slightly greater.

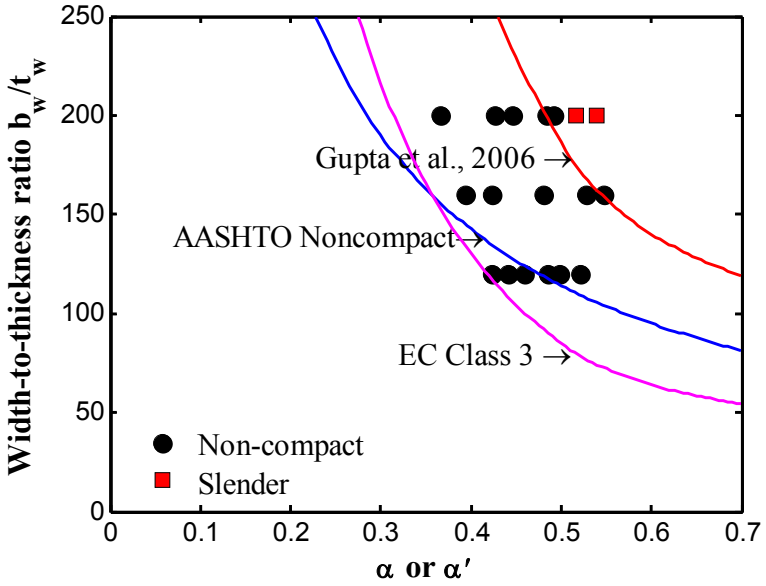

Fig. 4.4-5 Noncompact-slender limit of homogeneous SBHS500 steel sections (M_1=0.6M_{ys})

For actual design of composite girders, the α and α' values are commonly lower than 0.5. Within this range of α and α' values and for high level of initial bending moment with $M_1 \geq 0.2M_{ys}$, as shown in Fig.4.4-4 and 4.4-5, almost all composite SBHS500 homogeneous steel sections are classified as compact.

Composite girders with SBHS500-SM490Y hybrid steel sections

In this sub section, the yield moment M_{yf} of the composite SBHS500-SM490Y hybrid steel sections is defined by multiplying yield moment M_y of the corresponding homogeneous

section and relevant hybrid factor R_h which is defined in Section 4.3 - Proposal of hybrid factor.

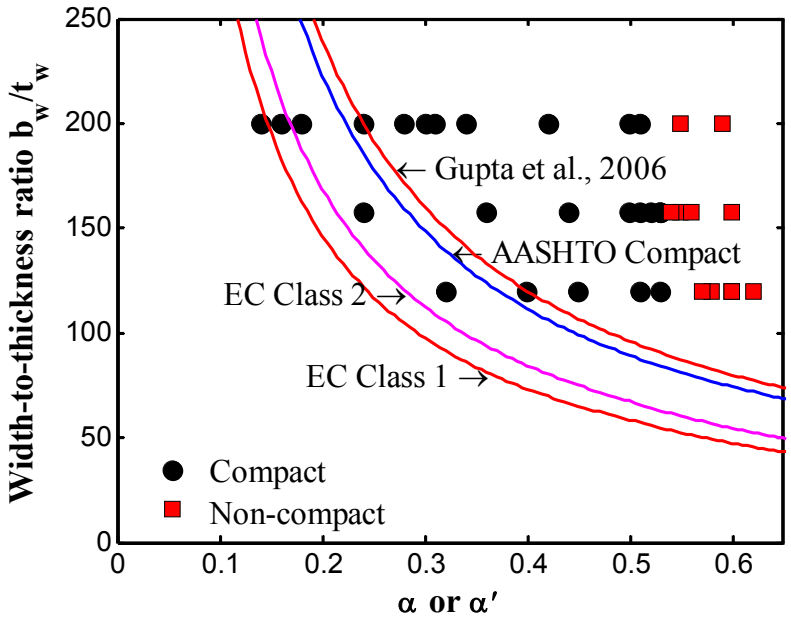

Fig. 4.4-6 Compact-noncompact slenderness limit of hybrid SBHS500-SM490Y steel section (M_1=0)

In Fig.4.4-6 the FE results for composite girders with SBHS500-SM490Y hybrid sections are plotted along with the equation of compact-noncompact slenderness limits of AASHTO and Eurocode. The FE results present the greater compact-noncompact slenderness limit than those of AASHTO and Eurocode. In addition, comparing Fig. 4.4-1 and 4.4-6, the web slenderness limit for hybrid sections is even greater than that of homogeneous SBHS500 steel sections. Besides, as shown in Fig. 4.4-1 and 4.4-6 as well, the general tendency of compact-noncompact web slenderness limit boundary of composite girder with SBHS500-SM490Y hybrid steel sections is steeper than that of the girders with SBHS500 homogeneous steel sections.

Fig. 4.4-7 shows the noncompact-slender limit without considering the initial bending moment. Comparing to the case of homogeneous sections in Fig. 4.4-3, the Fig.4.4-7 indicates that the web slenderness limit for the hybrid sections is shown almost vertically with unchanged $\alpha' \approx 0.375$. This tendency of the noncompact-slender web slenderness limit for composite SBHS500 –SM490Y hybrid steel sections is totally different compared to that of composite SBHS500 homogeneous steel sections, composite SM490Y homogeneous steel

sections (proposed in Gupta et al., 2006)) and corresponding equations specified in the current AASHTO and Eurocode.

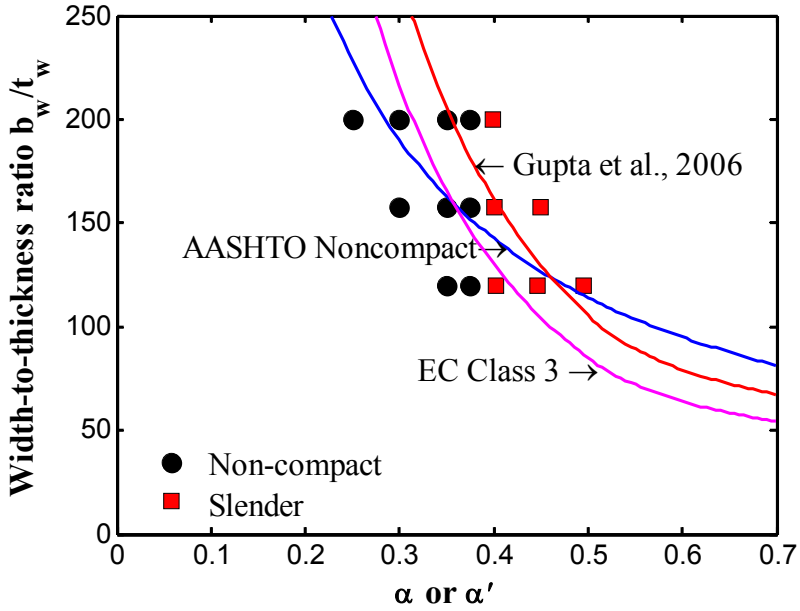

Fig. 4.4-7 Noncompact-slender limit of hybrid SBHS500-SM490Y steel section (M_1=0)

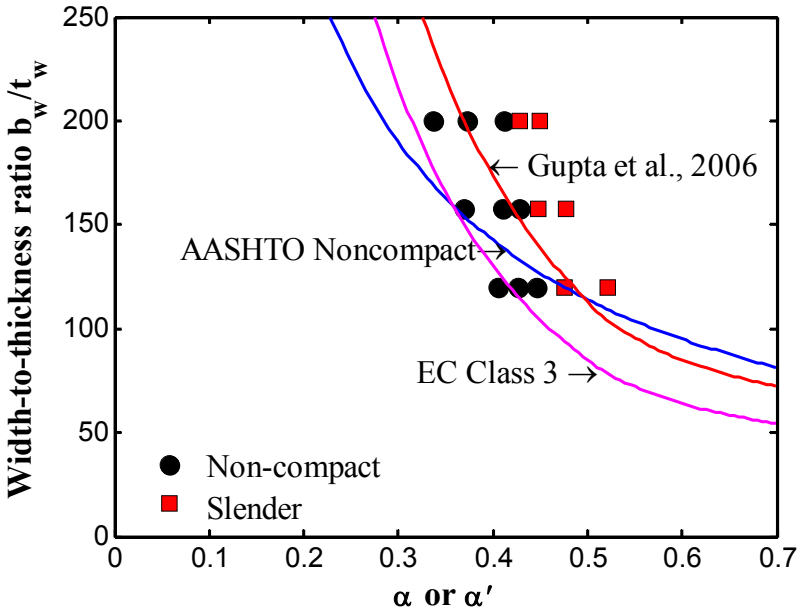

Fig. 4.4-8 Noncompact-slender limit of hybrid SBHS500-SM490Y steel section (M_1=0.2 M_{ys})

In the Fig.4.4-8, 4.4-9 and 4.4-10, results of investigated composite girders with the hybrid steel section with considering the effect of initial bending moment are plotted along with equations of noncompact-slender web slenerness limit specified by AASHTO and Eurocode and the ones proposed in Gupta *et al.* (2006). As shown in these figures the general slopes of

noncompact-slender limit curves for composite girders with hybrid steel sections without and with considering initial bending moment are steeper than those for the composite SBHS500 homogeneous steel sections, proposal of Gupta *et al.,* (2006), AASHTO and Eurocode. The noncompact-slender web slenderness limit for composite SBHS500-SM490Y hybrid steel sections is generally slightly lower than that for composite SBHS500 homogenous steel sections.

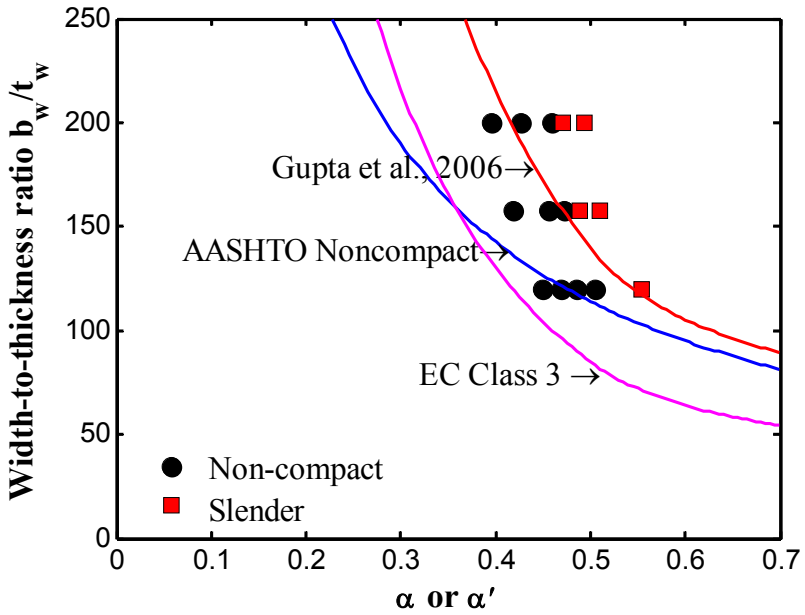

Fig. 4.4-9 Noncompact-slender limit of hybrid SBHS500-SM490Y steel section (M_1=0.4 M_{ys})

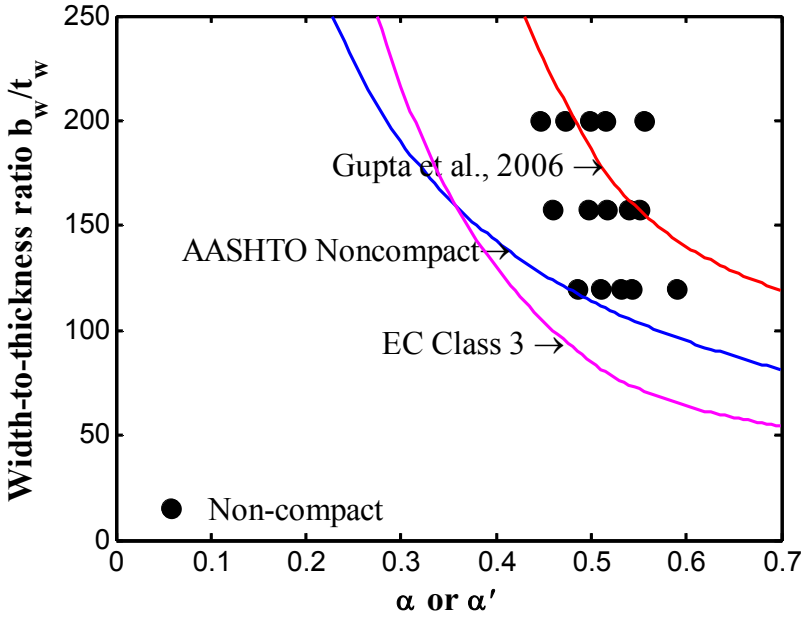

Fig. 4.4-10 Noncompact-slender limit of hybrid SBHS500-SM490Y steel section (M_1=0.6 M_{ys})

As reported in Gupta *et al.* (2006), the initial bending moment affects on noncompact-slender web slenderness limit of composite SBHS500-SM490Y hybrid steel sections as well. For M_I=0.2M_{ys}, the initial bending moment change one simulation girder from noncompact classification to slender classification for b_w/t_w = 200, and one from slender classification to noncompact classification for b_w/t_w = 120. This change could be explained that for the girder with relevant α value around noncompact-slender limit and b_w/t_w = 200, the decrease of ultimate bending M_u is significant if compared to the decrease of yield moment M_y of the girder section. The change tendency of 2 these quantities makes the normalization (M_u/ M_y) become lower than 1. For the girder with web slenderness b_w/t_w = 120, the opposite tendency is observed, which is the decrease of ultimate bending M_u is insignificant if compared to the decrease of yield moment M_y , then it makes the normalized quantity (M_u/ M_y) become greater than 1. For the change of section classification of 2 girders, the noncompact-slender web slenderness limit boundary of composite SBHS500-SM490Y hybrid steel sections is no longer vertical as seen in Fig.4.4-7 corresponding to M_I=0. However, the tendency of the limit boundary is still steeper than that of composite SBHS500 homogeneous steel sections, composite SM490Y homogeneous steel sections, and the limits specified by AASHTO and Eurocode.

In the case of initial bending moment level M_I= 0.2 M_{ys} with α' ≈ 0.429 and M_I=0.4M_{ys} with α' ≈ 0.472, the noncompact-slender limits of SBHS500-SM490Y hybrid sections are similar to proposal of Gupta et al., 2006 but lower than that of SBHS500 homogeneous section about 15%. For α' < 0.429 and 0.472 corresponding to the case M_I=0.2 and 0.4M_{ys} respectively, the noncompact-slender limits for the hybrid sections are similar to those for homogeneous sections. And for α' > 0.429 and 0.472, noncompact-slender limits for the hybrid sections are lower than those for homogeneous sections and about 10% lower than proposal of Gupta et al. (2006). The reduction of noncompact-slender limit for the hybrid sections compared to that of the homogeneous sections is due to the early yielding in flange vicinity zone of the web plates.

For M_I = 0.6M_{ys}, regarding the analysis results shown in Fig.4.4-10 no simulation girder appears as slender classification. With considering the effect of high level of initial bending moment (M_I = 0.6M_{ys}), all 5 girders become noncompact class instead of slender class. As explained above, the insignificant decrease of ultimate moment M_u compared to the decrease M_y might induce the normalized quantity (M_u/M_y) of these girders to become greater than 1.

In practice, hardly any composite girder is designed with compression parameter $\alpha'>0.45$. Besides, for initial bending moment $M_1 \geq 0.4M_{ys}$, all simulation girders in the current study are classified as noncompact and for $M_1=0.2M_{ys}$, almost all of simulation girders are classified as noncompact section. Thus, in practice almost all of composite girders, including hybrid steel girder, are designed with compact and noncompact classification for members under positive bending moment.

4.5. Conclusions

- Applying SBHS500 steel to both homogeneous and hybrid sections can extend significantly the web slenderness limits for section classification
- The compact-noncompact web slenderness limit boundary of composite SBHS500 homogeneous steel sections is about 70% greater than that of AASHTO about 50% and Eurocode. This behavior represents the better performance of SBHS500 steel on flexural resistance of composite SBHS500 homogeneous steel sections.
- Compared to noncompact-slender web slenderness limit of the composite SBHS500 homogeneous steel sections investigated with $M_1= 0.4M_{ys}$, the investigation of corresponding girder with $M_1= 0.2M_{ys}$ results in the higher noncompact-slender web slenderness limit. This behavior represents the opposite tendency reported in Gupta et al, 2006. The investigation of the composite SBHS500 homogeneous steel sections with $M_1= 0.2M_{ys}$ and shows $M_1= 0.4M_{ys}$ the moderately similar noncompact-slender web slenderness limit.
- For high level of the initial bending moment ($M_1= 0.6M_{ys}$), the noncompact-slender web slenderness limit increases compared to the case of $M_1= 0.4M_{ys}$, which presents the similar tendency as reported by Gupta et al.,2006 (composite SM490Y homogeneous steel section) and similar to the relevant equation of noncompact-slender web slenderness limit proposed in Gupta et al.,2006 but greater than that about 15%.
- For all levels of initial bending moment (M_1=0; 0.2; 0.4; and $0.6M_{ys}$) the noncompact-slender web slenderness limit of composite SBHS500 homogeneous steel sections is significantly greater than that of AASHTO and Eurocode specifications.
- Compared to the investigation of the composite SBHS500 homogeneous steel sections, the compact-noncompact web slenderness limit for composite SBHS500-SM490Y hybrid steel sections is greater but much steeper boundary slope.
- The noncompact-slender limit of composite girder with SBHS500-SM490Y hybrid girders considering initial bending moment is greater than that of AASHTO and Eurocode but still

about 15% lower than that of composite SBHS500 homogeneous steel sections. For $M_1=0.2M_{ys}$, the web slenderness limit of SBHS500-SM490Y hybrid sections is about 15% and 30% greater than that of AASHTO and Eurocode specifications, respectively. For M_1=0.4 M_{ys}, the noncompact-slender web slenderness limit of SBHS500-SM490Y hybrid sections is about 25 and 40 % greater than that of AASHTO and Eurocode specifications, respectively.

- For initial bending moment level $M_1=0.6M_{ys}$ in practical range of α' (<0.45), none of composite SBHS500-SM490Y hybrid steel sections is judged as slender classification.
- The general slope of limit boundary curve of noncompact-slender web slenderness limit regarding the composite girders with SBHS500-SM490Y hybrid steel sections is steeper than that of composite girders with SBHS500 homogeneous steel sections. Applying initial bending moment level M_1=0.2 and 0.4 M_{ys} the noncompact-slender web slenderness regarding the SBHS500-SM490Y steel hybrid sections limit is about 15% lower than that of the SBHS500 homogeneous steel sections.
- For composite girders with non-compact sections considering initial bending moment, the proposal hybrid factors are slightly lower than that which obtained from FEM analysis results and differences are about 5%
- With considering high level of initial bending moment the AASHTO specification of hybrid factors shows the un-conservativeness.

CHAPTER 5

CONCLUSIONS AND RECOMMENDATIONS

5.1. Conclusion remarks

In an effort to investigate the capacity of steel-concrete composite girders regarding un-shored construction method and accounting for SBHS steels, the current study gives conclusions on probabilistic information of the steel plate LBS, proposal of the standard LBS equation and partial safety factor, and web slenderness limit for section classification of composite girders.

Steel plate LBS and its probabilistic information

- The mean results obtained in current study are similar to the mean (M) curve proposed in Fukumoto and Itoh (1984), which was based on the experimental data. Compared to the experimental-based curve the mean results of current study are slightly greater within the range $0.65<R<0.85$ because of current study considers SBHS steel plates and normalized initial deflection levels $\overline{W}_0 \leq 1/150$.
- Compared to the standard deviation obtained from experimental results reported in Fukumoto and Itoh (1984), the corresponding results of the current study exhibits about half of that within a range of $0.6<R<1.2$ and clearer tendency.
- Regarding the LBS, the high strength steel plates represent better performance than normal steel plates.
- In the range of $0.4\leq R\leq 0.85$ the influence on the steel plate LBS of initial deflection is more sensitive than that of residual stress. However, in the range of $R>0.9$ the influence on the steel plate LBS of residual stress is more sensitive than that of initial deflection.
- For $0.8<R<1.04$ the influence of residual stress on the plate LBS regarding high strength steels is more sensitive than that regarding normal steels.
- For $0.55<R<0.85$ the influence of initial deflection on the plate LBS regarding normal steels is more sensitive than that regarding high strength steels.
- In the range of $0.4\leq R\leq 0.55$ under the effect of much smaller plastic strain range of high strength steels compared to normal steels, the influence of initial deflection on the plate LBS regarding high strength steels is more sensitive than that regarding normal steels. Considering high strength steels (SBHS500, SBHS700 and SM570) because of the different 1^{st} hardening strain slope, the influence of initial deflection on steel plate LBS regarding SM570 steel is the most sensitive followed by SBHS500 and SBHS700.

- The difference of normalized residual stress within the range $0.15 \leq \bar{\sigma}_r \leq 0.3$ does not induce the significant difference of steel plate LBS variance with respect to residual stress variable.
- The difference of normalized residual stress within the range $0.15 \leq \bar{\sigma}_r \leq 0.3$ does not induce the significant difference of steel plate LBS variances with respect to variable of residual stress.

Proposal of partial safety factor

- With assumption of normal distribution function applying to probabilistic distribution of steel plate LBS and the LBS mean values considered as standard strengths, the partial safety factors obtained are equal to 1.11, 1.13 and 1.16 corresponding to 5%, 3% and 1% fractile, respectively.
- Applying the obtained partial safety factors considering the mean results as characteristic design resistance, the obtained designed LBS values are lower than those specified by AASHTO in the range of $0.6<R<1.3$ and greater than those specified by JSHB in whole range of R.
- The tendency of designed LBS results plotted with respect to corresponding R value in the current study are much less steep compared to those specified by AASHTO and JSHB, which are based on result of elastic local buckling theory.

Web slenderness limit for section classification of composite girders

- Applying SBHS500 steel to both homogeneous and hybrid sections can extend significantly the web slenderness limits for section classification
- The compact-noncompact web slenderness limit boundary of composite SBHS500 homogeneous steel sections is about 70% greater than that of AASHTO about 50% and Eurocode. This behavior represents the better performance of SBHS500 steel on flexural resistance of composite SBHS500 homogeneous steel sections.
- Compared to noncompact-slender web slenderness limit of the composite SBHS500 homogeneous steel sections investigated with $M_1 = 0.4M_{ys}$, the investigation of corresponding girder with $M_1 = 0.2M_{ys}$ results in the higher noncompact-slender web slenderness limit. This behavior represents the opposite tendency reported in Gupta et al, 2006. The investigation of the composite SBHS500 homogeneous steel sections with $M_1 = 0.2M_{ys}$ and shows $M_1 = 0.4M_{ys}$ the moderately similar noncompact-slender web slenderness limit.

- For high level of the initial bending moment (M_1= 0.6M_{ys}), the noncompact-slender web slenderness limit increases compared to the case of M_1= 0.4M_{ys} , which presents the similar tendency as reported by Gupta et al.,2006 (composite SM490Y homogeneous steel section) and similar to the relevant equation of noncompact-slender web slenderness limit proposed in Gupta et al.,2006 but greater than that about 15%.
- For all levels of initial bending moment (M_1=0; 0.2; 0.4; and 0.6M_{ys}) the noncompact-slender web slenderness limit of composite SBHS500 homogeneous steel sections is significantly greater than that of AASHTO and Eurocode specifications.
- Compared to the investigation of the composite SBHS500 homogeneous steel sections, the compact-noncompact web slenderness limit for composite SBHS500-SM490Y hybrid steel sections is greater but much steeper boundary slope.
- The noncompact-slender limit of composite girder with SBHS500-SM490Y hybrid girders considering initial bending moment is greater than that of AASHTO and Eurocode but still about 15% lower than that of composite SBHS500 homogeneous steel sections. For M_1=*0.2*M_{ys}, the web slenderness limit of SBHS500-SM490Y hybrid sections is about 15% and 30% greater than that of AASHTO and Eurocode specifications, respectively. For M_1=0.4 M_{ys}, the noncompact-slender web slenderness limit of SBHS500-SM490Y hybrid sections is about 25 and 40 % greater than that of AASHTO and Eurocode specifications, respectively.
- For initial bending moment level M_1=0.6M_{ys} in practical range of α' (<0.45), none of composite SBHS500-SM490Y hybrid steel sections is judged as slender classification.
- The general slope of limit boundary curve of noncompact-slender web slenderness limit regarding the composite girders with SBHS500-SM490Y hybrid steel sections is steeper than that of composite girders with SBHS500 homogeneous steel sections. Applying initial bending moment level M_1=0.2 and 0.4 M_{ys} the noncompact-slender web slenderness regarding the SBHS500-SM490Y steel hybrid sections limit is about 15% lower than that of the SBHS500 homogeneous steel sections.
- For composite girders with non-compact sections considering initial bending moment, the proposal hybrid factors are slightly lower than that which obtained from FEM analysis results and differences are about 5%
- With considering high level of initial bending moment the AASHTO specification of hybrid factors shows the un-conservativeness.

5.2. Contributions of the current study

The current study contribute to code writers the statistical information of the steel plate LBS in which considering the new steel grades SBHS500 and SBHS700 as the bases to proposed the improved standard LBS design equation and partial safety factor covering prediction model and the initial imperfection (initial deflection and residual stress).

The results of the current study represent the better performance of SBHS steels on steel plate LBS than that of normal steels. In the practical range of $0.6<R<1.2$ LBS mean values regarding SBHS steels are greater than those regarding normal steels, and LBS standard deviations regarding SBHS steels are lower than those regarding normal steels. With the same level of normalized residual stress and initial deflection the normalized steel plate LBS regarding SBHS steels are greater than that regarding normal steels, especially in the range of $0.65<R<0.85$.

The Monte Carlo based method with the usage of the response surface can be applied to statistically investigate a number of engineering problems without consuming time for preparing input data and FE analysis processing.

The investigation of web slenderness limits for composite section classifications regarding composite girders which applying SBHS500 steel to both homogeneous and hybrid steel girders represents that in practice the web plate of steel girder can be designed with higher slenderness than requirements of current specifications as AASHTO and Eurocode.

The analysis data of the current study can contribute to code writer as the basic to propose the improved equation of web slenderness limits for section classification of composite girders in which considering the application of high strength steel grade SBHS500 to both homogeneous and hybrid steel girders and also the effect of initial bending moment. Besides, the improved design equation of hybrid factor which consider the effect of initial bending moment can be proposed based on the analysis data of the current study.

5.3. Recommendations for future research

Beside proposing a partial safety factor which taking into account the varied steel material properties as the format of value γ_m using in Eurocode, the influence of varied inelastic properties; such as yield strength, plastic range, 1st hardening strain slope; of steel material on the design steel plate LBS is necessary to be investigated. The current study found out that in

the range of 0.65<R<0.90 yield strength value has significant effect on normalized LBS of the steel plates. For R=0.7, $\overline{W}_0$ =1/400 and $\overline{\sigma}_r$ =0.23 the difference of $\overline{\sigma}_{cr}$ (SM400) and $\overline{\sigma}_{cr}$ (SBHS700) is about 6%. And in the range of R<0.5 the plastic strain and first strain hardening slope influence on the normalized local buckling strength of the steel plates as well.

The scatterness of normalized residual stress level need to be further investigated. Rasmussen and Hancock (1982) stated that the normalized residual stress level depends on the width-to-thickness parameter R value of the plate, decrease as the plate become more slender. Besides, some recent study (Uy B., 2001) reported that the average normalized compressive residual stress ($\overline{\sigma}_r$) of SBHS500 and SBHS700 is lower than 0.1 and maximum normalized tensile residual stress (σ_{rt}/σ_y, explained in Fig.3.4-4) is lower than 0.5. This degree of residual stress distribution is significantly lower than that of mean value of normalized residual stress which employed in the current study ($\overline{\sigma}_r$ =0.23). The low level of $\overline{\sigma}_r$ values would lead the significant increase of LBS values, especially in the range of R>1.

According to opinion of the dissertation's author, flexural resistance of composite SBHS500-SM490Y hybrid steel sections is necessary to further study, especially in investigating the web slenderness limits for section classification. The design flexural capacity equation of composite hybrid steel girders of noncompact and slender classes regarding improved web slenderness limits need to be proposed. For application of SBHS500 and SBHS700 steel to composite hybrid steel girder, the reasonable material strength of concrete slab needs to be investigated.

REFERENCES

American Association of State Highway and Transportation Officials. *AASHTO LRFD bridge design specification – Fourth edition*, 2007.

CEN, Eurocode3. *Design of Steel Structures, Part 1-5, plated structural elements*, 2004

CEN Eurocode4. *Design of Composite Steel and Concrete Structures, Part 2, General rules and rules for bridges*, 1994

Chatterjee, S., *The Design of Modern Steel Bridges*, Wiley-Blackwell, 2003

Collings, D. *Steel-Concrete Composite Bridges*, Thomas Telford, 2005

Committee on Steel Structures of Japanese Society of Civil Engineers Standard. *Specifications for Steel and Composite Structures*, (General Provision, Basic Planning, Design), 2007.

Dwight, J., B., Harrison, J. D. "Local buckling problems in steel columns." *Brit. Wldg Res. Assoc.*, November 1962.

Dwight, J, B., Chin, T. K. and Ractliffe, A. T. "Local buckling of thin-walled columns, effect of locked-in welding stress." *CIRIA, Res. Rep. No. 12 (Pt.1)*, May 1968

Dwight, J, B., Moxham, K, E. "Welded steel plates in compression." *The Structural Engineer*, Vol. 47, No. 2, pp. 49-66, 1969

Fukumoto, Y. and Itoh, Y. "Basic compressive strength of steel plates from test data*". Proc. of JSCE* No.334/I-1, 1984

Gaspar, B., Naess, A., Leira, B.J., Guedes Soares, C., "System reliability analysis of a stiffened panel under combined uniaxial compression and lateral pressure loads." *Structural Safety*, Vol.39, pp.30-43, 2012

Guan, X.L. and Melchers R.E. "Effect of response parameter variation on structural reliability estimates." *Structural Safety*, Vol.23, pp.429-444, 2001

Guedes Soares, G. and Kmiecik M. “Simulation of ultimate compressive strength of unstiffened rectangular plates.” *Marine Structures*, Vol 6, pp. 553-569, 1993

Gupta, V.K., Okui, Y., and Nagai, M. “Development of web Slenderness Limits for Composite I-Girders accounting for Initial Bending Moment”, *Doboku Gakkai Ronbunshuu A*, Vol.62, No.4, 854-864, 2006

Gupta, V.K., Okui, Y., Inaba N. and Nagai, M. “Effect of concrete crushing on flexural strength of steel-concrete composite girders.” *Journal of Japanese Society of Civil Engineers (A)*, Vol.63, No.3, pp.475-485, 2007.

Haldar, A. and Mahadevan, S. *Probability, Reliability, and Statistical Methods in Engineering Design*, *First edition*, 1999

International Standard ISO 2394. *General principles on reliability for structures, Third edition*, 1998

Japan Road Association. *Specifications for Highway Bridges – part II. Steel Bridges*, 1980

Japan Road Association. *Specifications for Highway Bridges – part II*. Steel Bridges, 1996

Japan Road Association. *Specifications for Highway Bridges – part II. Steel Bridges*, 2002

Japanese Industrial Standard. *JIS G 3140, Higher yield strength steel plates for bridges*, 2008

Kitada, T., Yamaguchi, T., Matsumura, M., Okada, J., Ono, K. and Ochi, N. “New technology of steel bridge in Japan.” *Journal of Constructional Steel Research*, Vol.58, pp. 21-70, 2002

Kiymaz, G. “Stability and Strength Criteria for High Performance Steel Plates under Edge Compression.” *Journal of Istanbul Kültür University*, Vol.3, pp.1-26, 2003.

Komatsu, S. and Nara, S. “Statistical study on steel plate members.” *Journal of Structural Engineering*, ASCE, Vol. 109, No. 4, 1983

Komatsu, S., Ushio, M. and Kitada, T. “An experimental study on residual stress and initial deformations of stiffened plates” *Proceedings of JSCE*, No. 265, 25–35, September 1977 [in Japanese].

Murakoshi, J., Yanatory, N., Arima, K., Shimizu, H., Komori, D., "Report on statistical data of steel members ans strength." *Technical Note of Public Work Research Institute*, No.4090, ISSN 0386-5878, 2008

Nagai M., Inaba N., Okui Y., Miyashita T. and Hirayama S. "Study on flexure and flexure/shear strength of composite I-girder" *Journal of Structural Engineering, JSCE*, Vo.55A, pp.115-123, 2009 (in Japanese)

Nippon Steel a: http://www.nsc.co.jp/en/product/use/bridge/adoption_case/Nagata.html

Nippon Steel b:
http://www.nsc.co.jp/en/product/use/bridge/adoption_case/Tokyo_Rinkai_Doro.html

Ohgaki, K., Yabe, J., Kawaguchi, Y., Ohta, Y., Kawashiri, K. and Nagai, M. "Experimental study on ultimate strength of plate girders with large aspect ratio and web width-to-thickness-ratio." *Proceedings of Eurosteel* '99, CTUT Prague, Vol.1, pp.141-144, 1999.

Okada, J. and Kato M. "Study on characteristics of bending resistance to composite I-girders using high strength steels allowing for yielding." *Journal of Japan Society of Civil Engineers, Ser. A*, Vol.1, No.65, pp.151-164, 2009.

Rasmussen, K. J. R. and Hancock, J. G. "Plate slenderness limits for high strength steel sections." *J. Construct. Steel Research*. Vol.23, pp. 73-96, 1992

Roik, E.h.K., Bergmann, R., Haensel, J. and Hanswille, G. *Beton-Kalender, Verbundkonstruktionen, Bemessung auf der Grundlage des Eurocode 4 Teil 1*, Ernst and Sohn, Berlin, Germany, 1993.

Sétra . Steel –concrete composite bridge - Sustainable design guide, www.setra.developpement-durable.gouv.fr/,2010.

Schilling, G. "Bending Behavior of Composite Hybrid Beams". *Journal of the Structural Division, ASCE*, 94, ST8, pp. 1945-11964, 1968

Sir Gilbert Roberts. *Forth Road Bridge, part 2 – Design*, Institute of Civil Engineers, 1967

Soares, G. C., and Kmiecik M., "Simulation of the Ultimate Compressive Strength of Unstiffened Rectangular Plates". *Marine Structures*, 6, pp. 553-569, 1993.

Subcommittee on Hybrid Beams and Girders (1968) "Design of Hybrid Steel Beams." *Journal of the Structural Division, ASCE*, 94, ST6, pp. 1397-1426.

Timoshenko, S. P. & Gere, J. M. *Theory of elastic stability*. New York, NY: McGraw-Hill, 1961

Tonegawa, T., Yamahuchi, T., Sugiura, K., and Watanabe, E. "Assessment on ultimate strength of composite hybrid steel box girder with thinner web panel by using FE analysis." *Journal of Japan Society of Civil Engineers, Ser. A*, Vol.62, No. 2, pp.300-311, 2006

Usami, T. and Fukumoto, Y. "Deformation analysis of locally buckled steel compression members." *Journal of Constructional Steel Research*, Vol.13, pp. 111-135, 1989

Usami, T. "Effective width of locally buckled plates in compression and bending." *Journal of Structural Engineering*, *ASCE*, Vol. 119, No. 5, pp. 1358-1373, 1993

Uy, B. "Strength of short concrete filled high strength steel box columns." *Journal of Constructional Steel Research,* vol. 57 (2), pp. 113-134, 2001.

APPENDIX 1

RESPONSE SURFACES

A1-1 . Case 1 – regarding all 6 steel grades for each R value

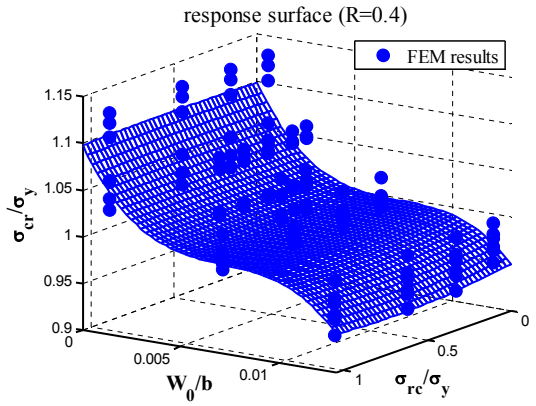

a

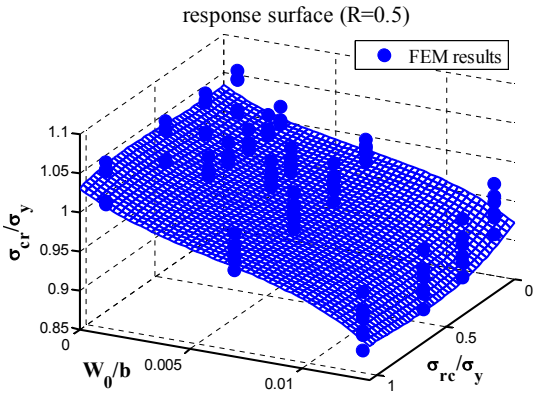

b

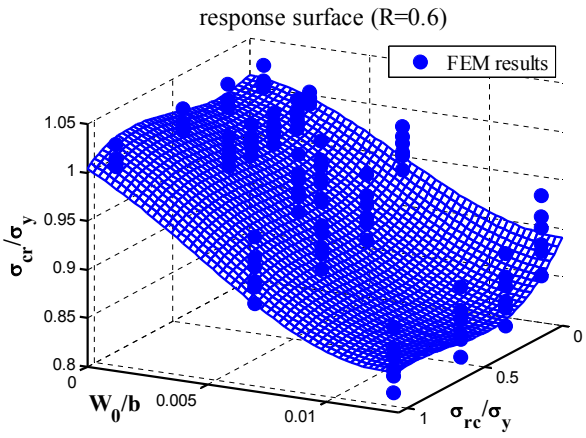

c

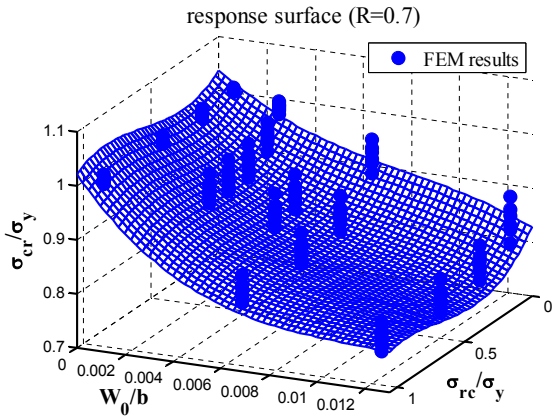

d

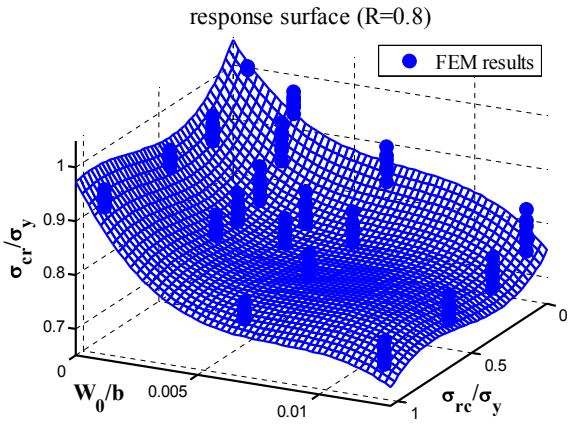

e

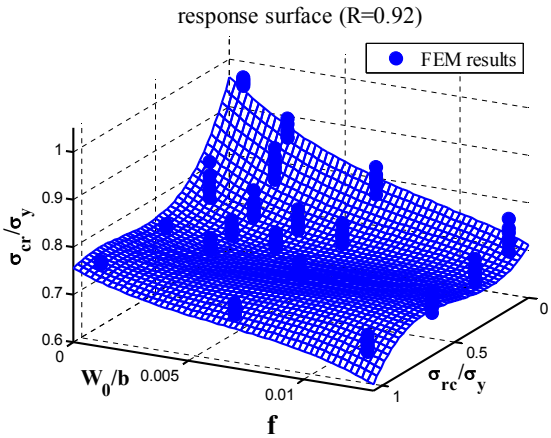

f

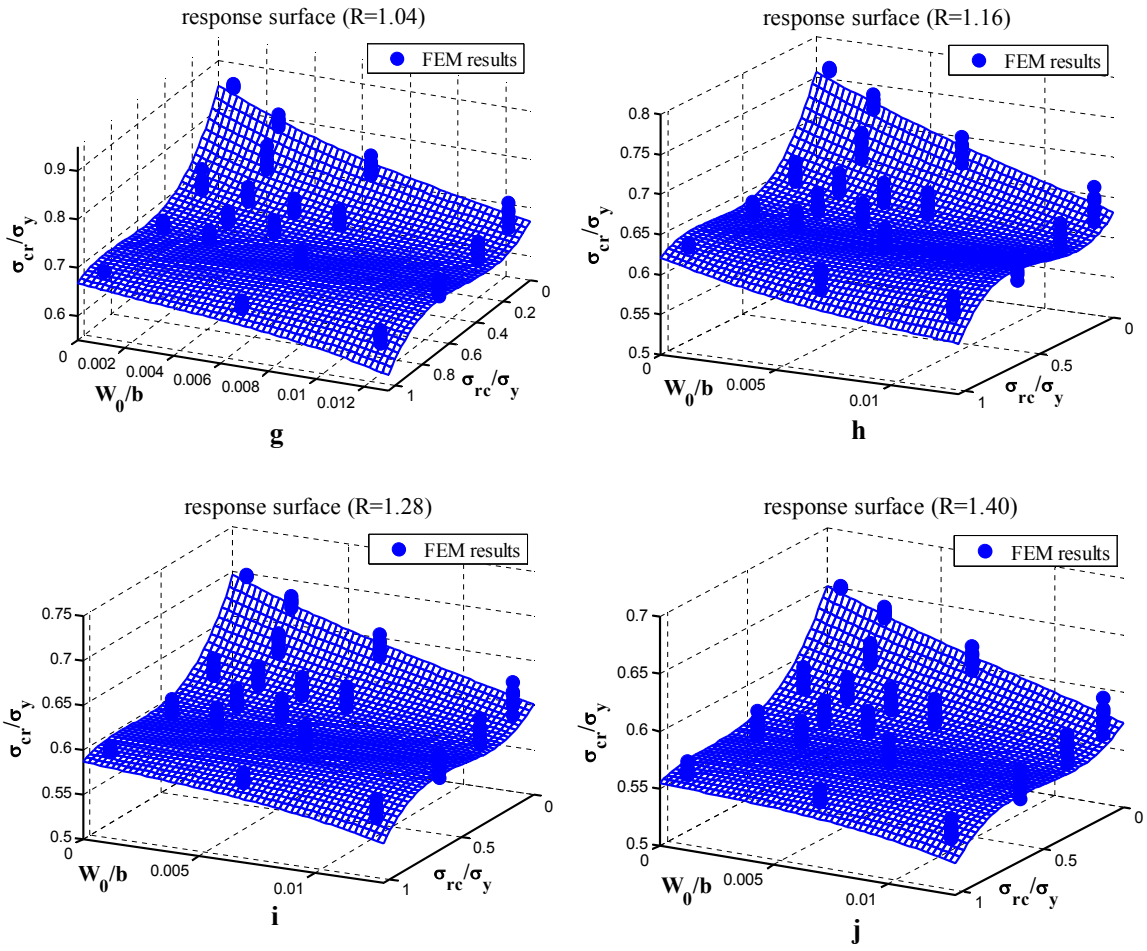

Fig. A 1-1.1 Response surface regarding 6 steel grades for each R value

A1-2 . Case 2 – regarding each among 6 steel grades for each R value

R=0.4

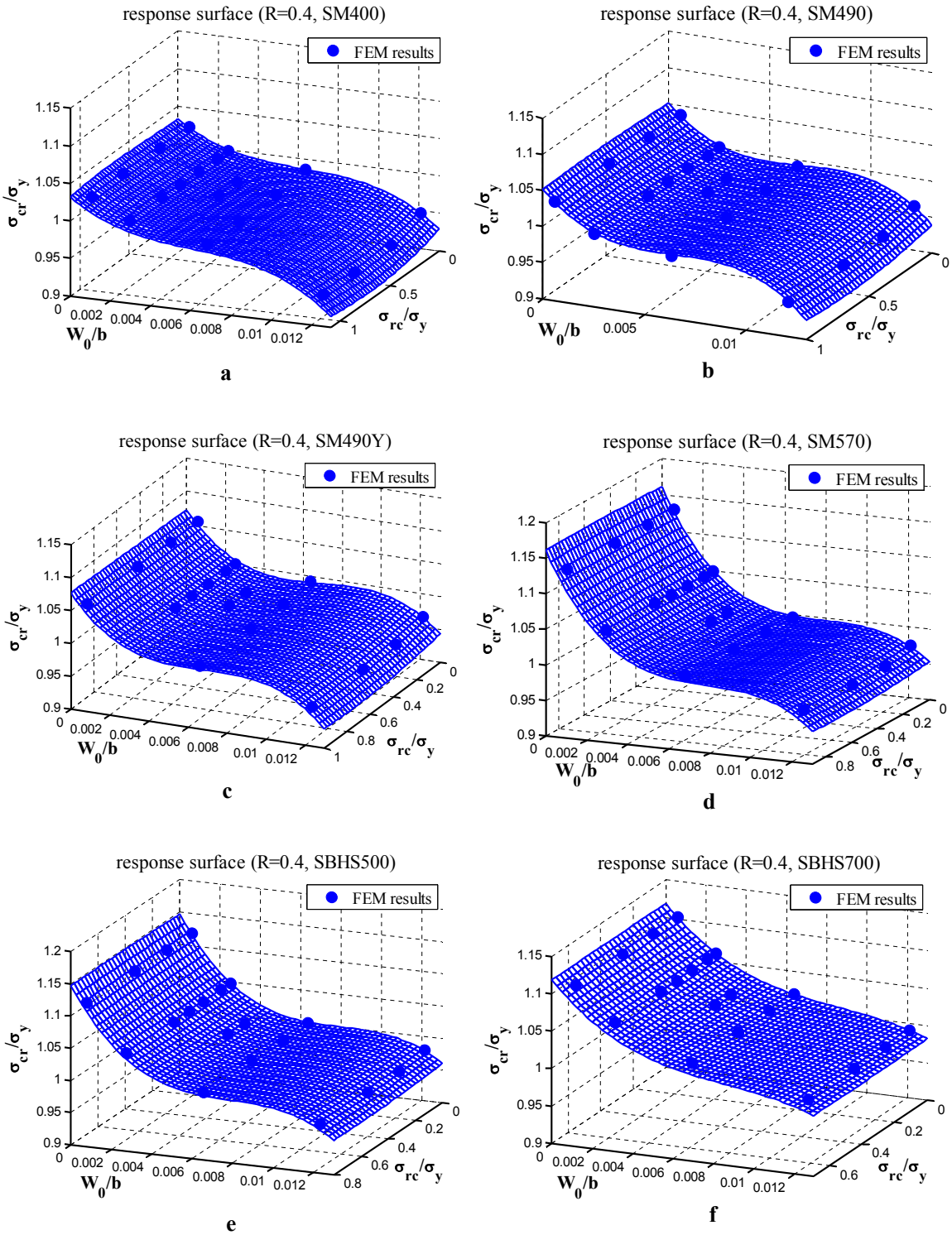

Fig. A 1-2.1 Response surface regarding each steel grade for R=0.4

R=0.5

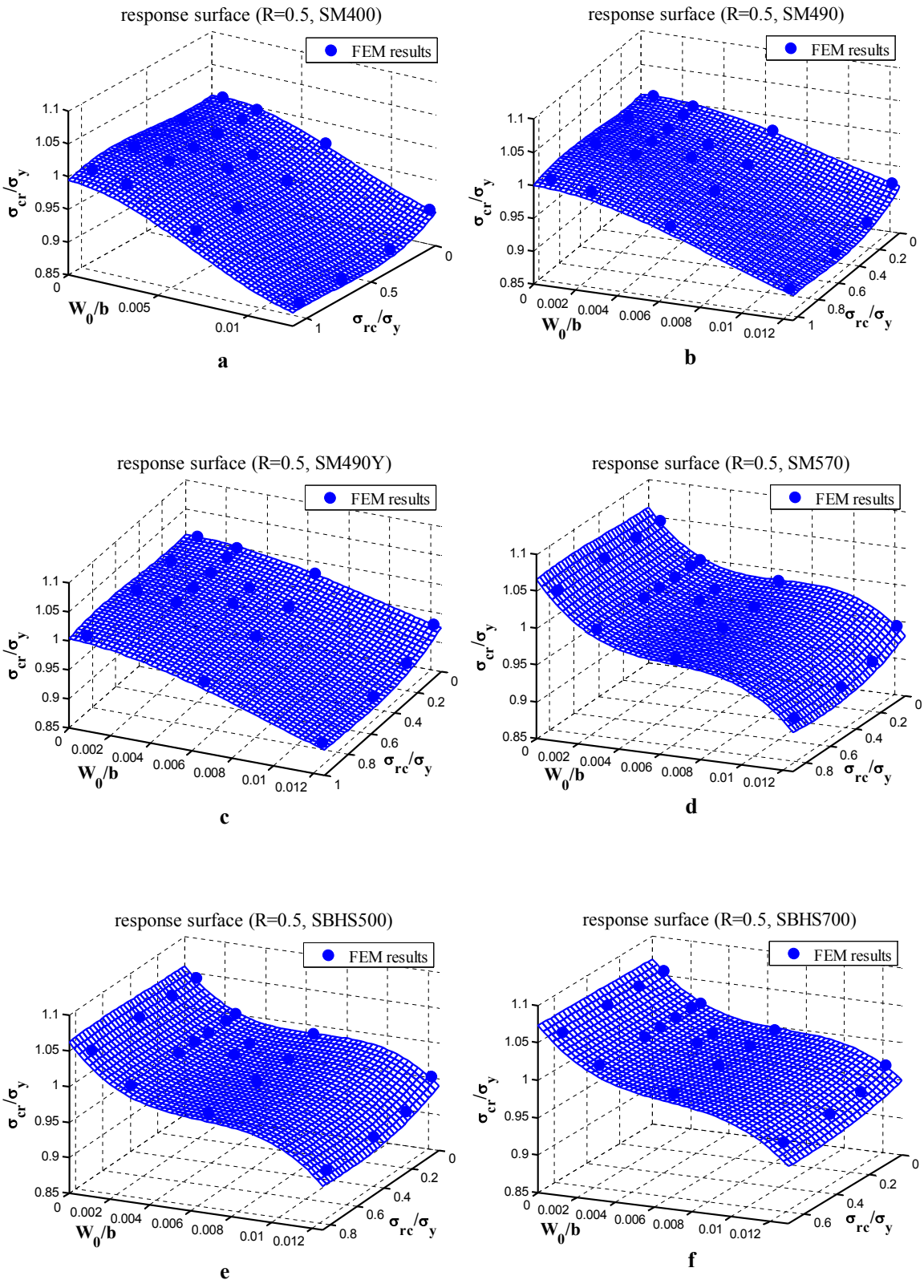

Fig. A 1-2.2 Response surface regarding each steel grade for R=0.5

R=0.6

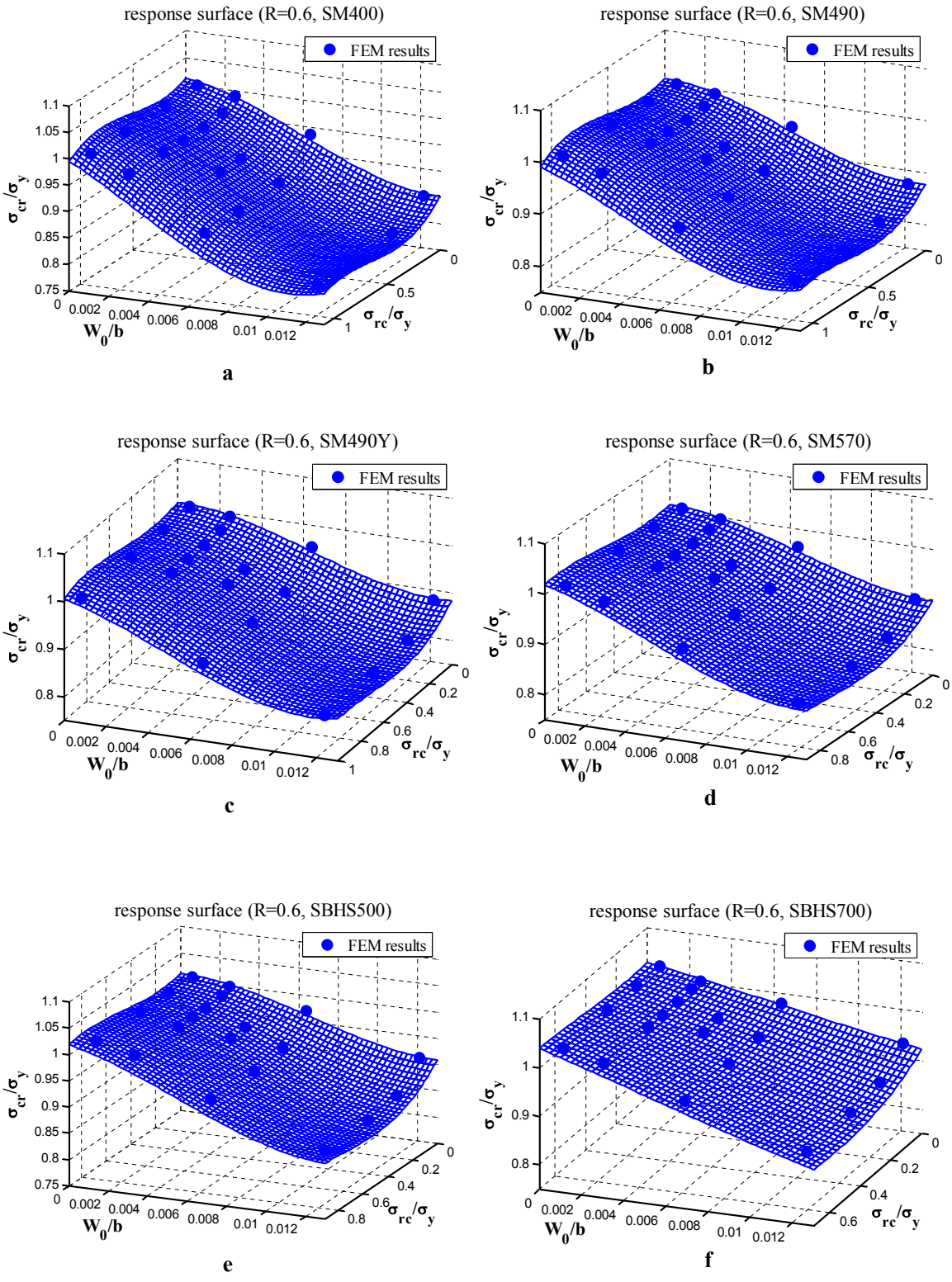

Fig. A 1-2.3 Response surface regarding each steel grade for R=0.6

R=0.7

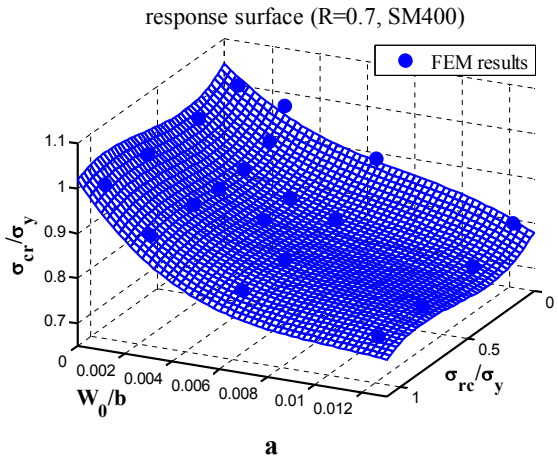
response surface (R=0.7, SM400)
FEM results
σcr/σy
W0/b
σrc/σy

a

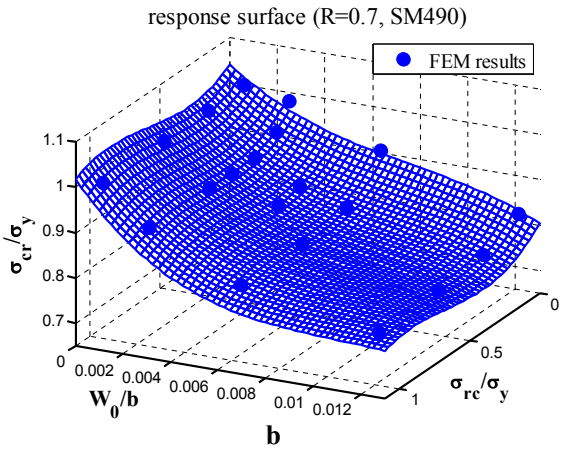
response surface (R=0.7, SM490)
FEM results
σcr/σy
W0/b
σrc/σy

b

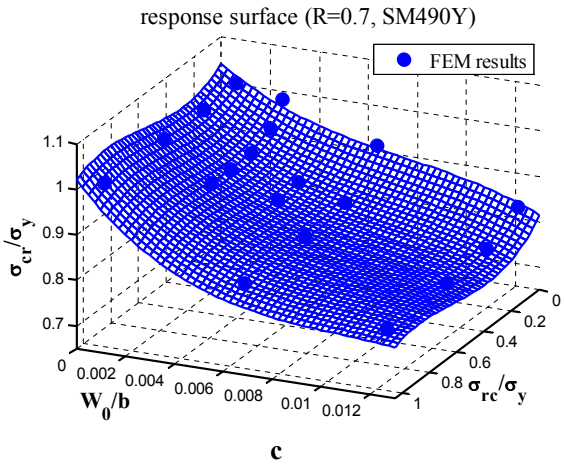
response surface (R=0.7, SM490Y)
FEM results
σcr/σy
W0/b
σrc/σy

c

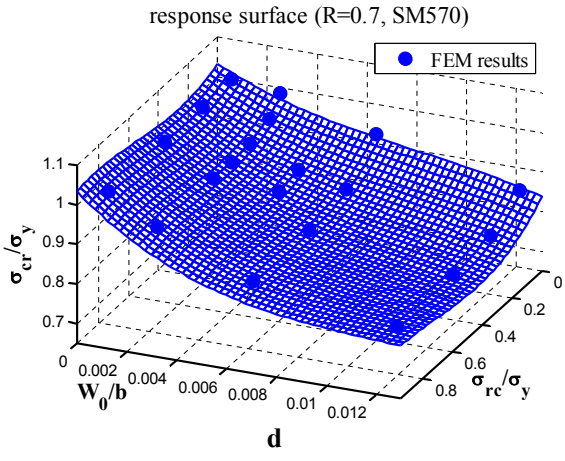
response surface (R=0.7, SM570)
FEM results
σcr/σy
W0/b
σrc/σy

d

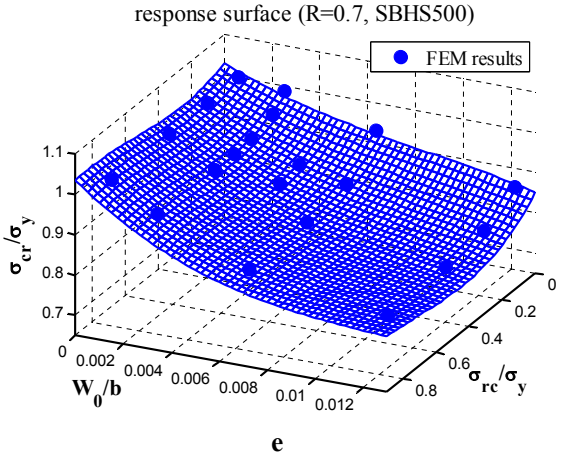
response surface (R=0.7, SBHS500)
FEM results
σcr/σy
W0/b
σrc/σy

e

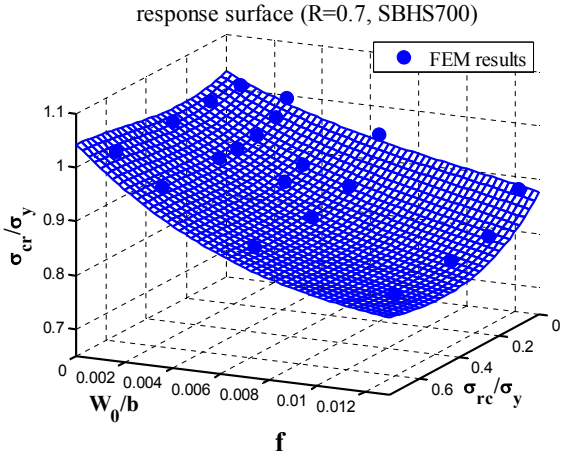
response surface (R=0.7, SBHS700)
FEM results
σcr/σy
W0/b
σrc/σy

f

Fig. A 1-2.4 Response surface regarding each steel grade for R=0.7

R=0.92

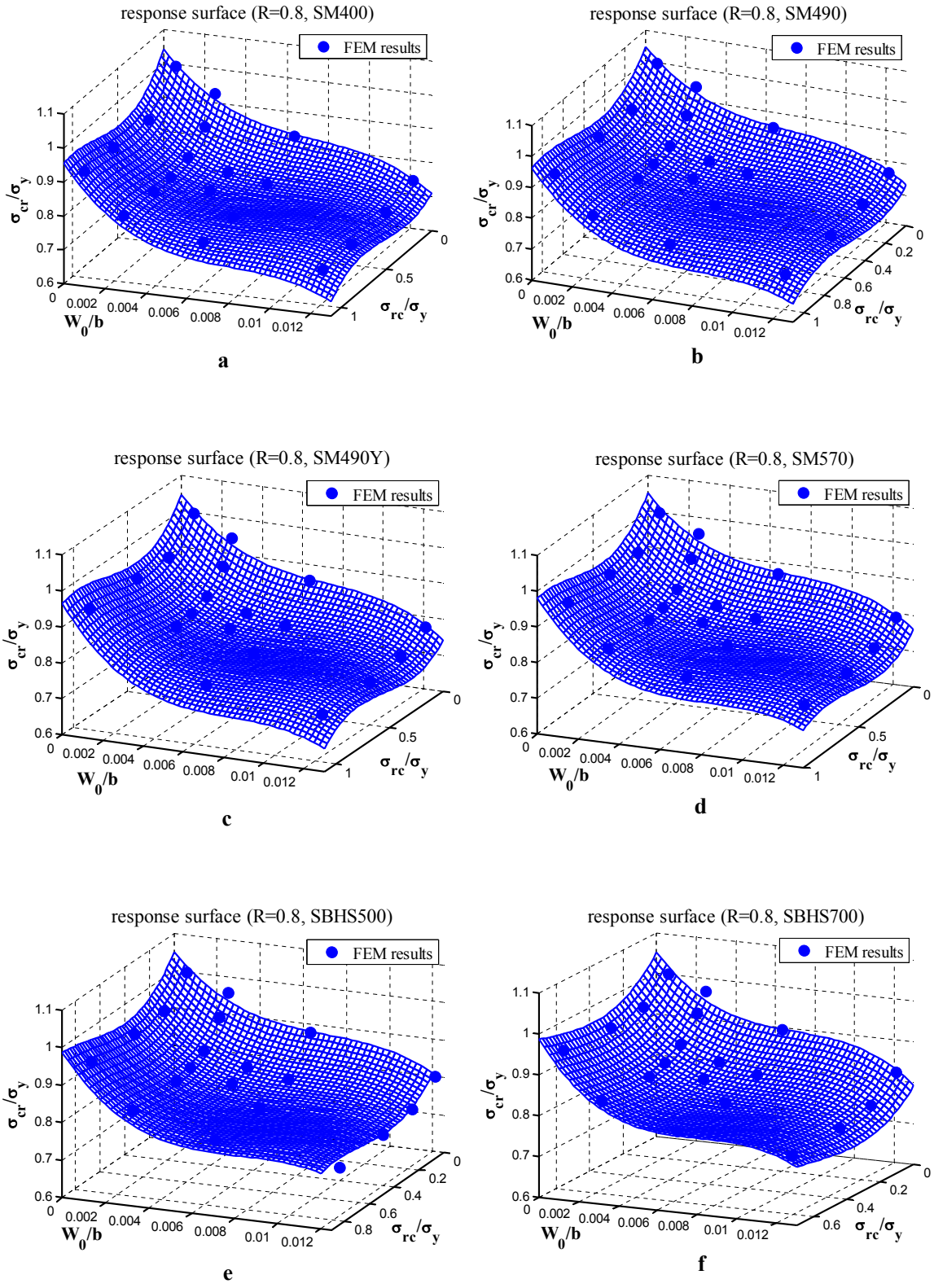

Fig. A 1-2.5 Response surface regarding each steel grade for R=0.8

R=0.92

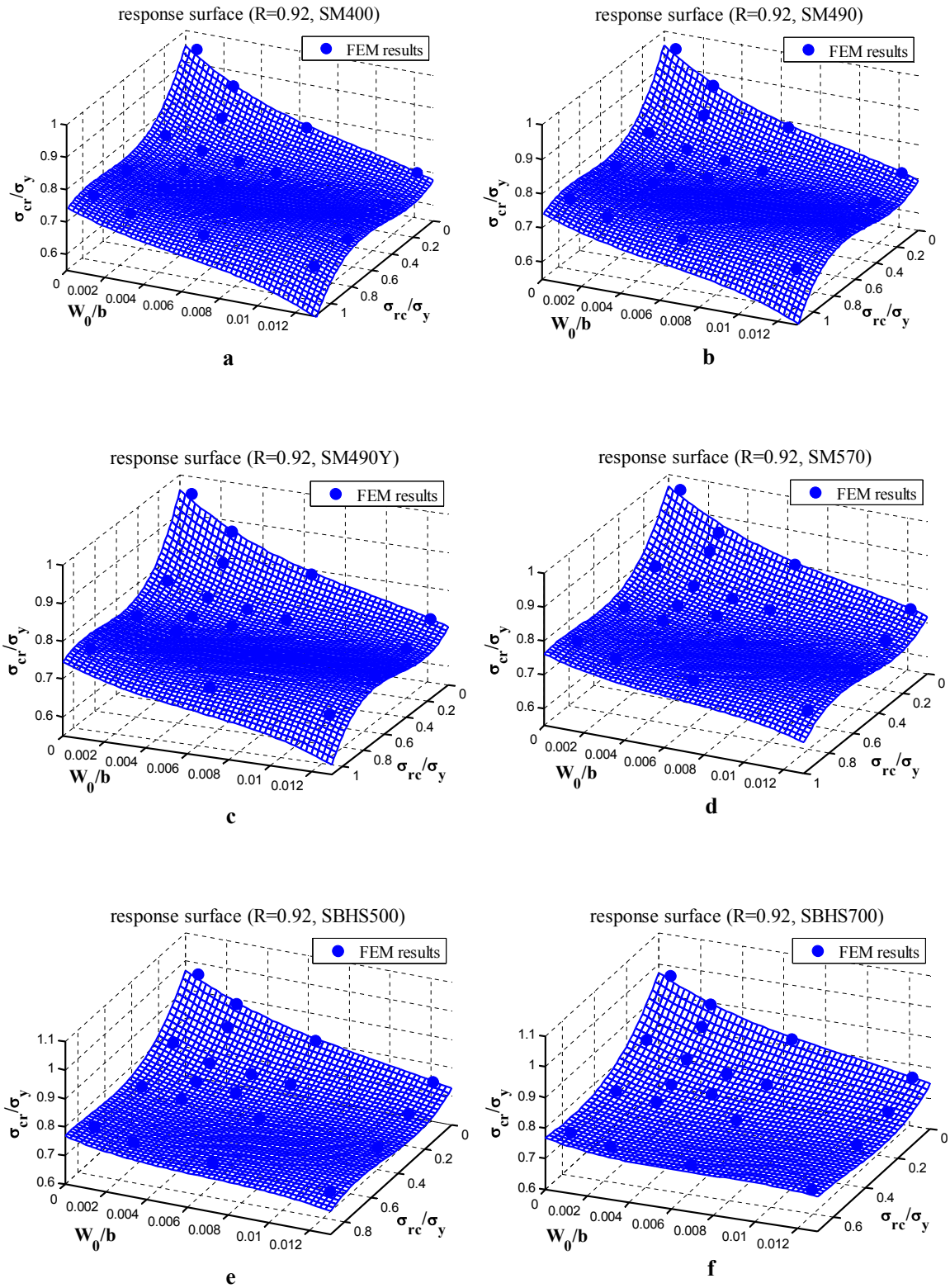

Fig. A 1-2.6 Response surface regarding each steel grade for R=0.92

R=1.04

response surface (R=1.04, SM400)

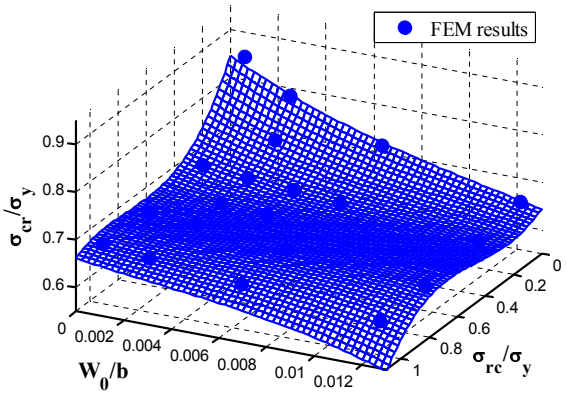

a

response surface (R=1.04, SM490)

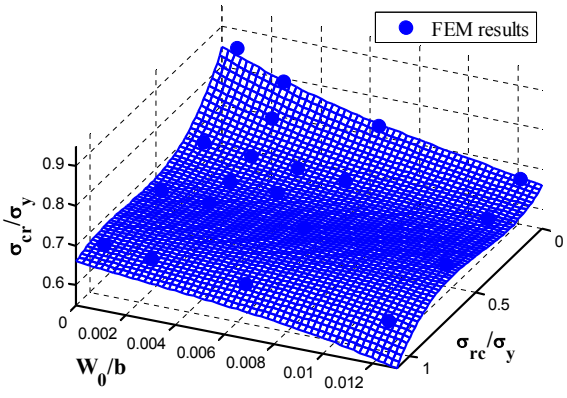

b

response surface (R=1.04, SM490Y)

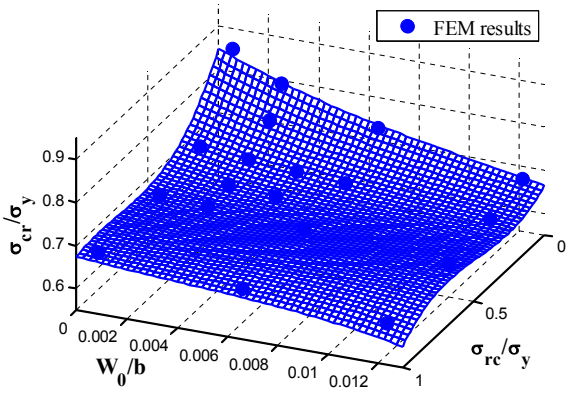

c

response surface (R=1.04, SM570)

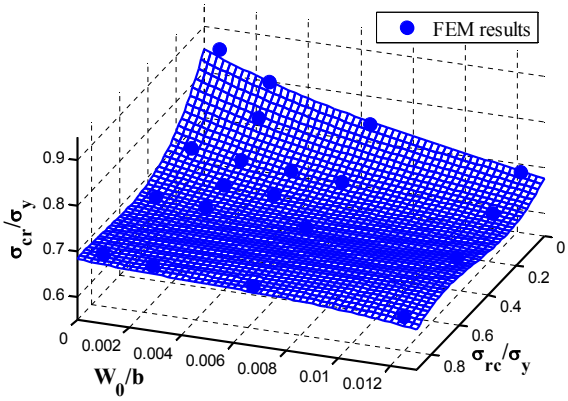

d

response surface (R=1.04, SBHS500)

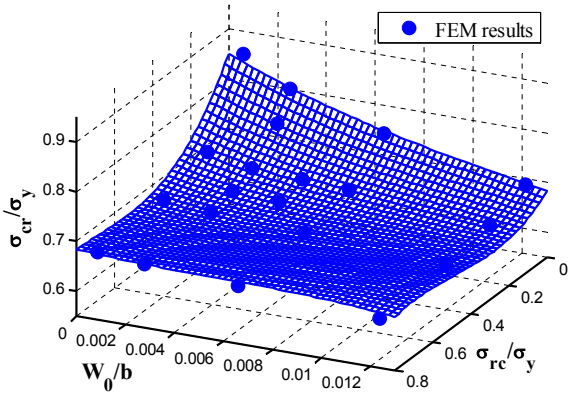

e

response surface (R=1.04, SBHS700)

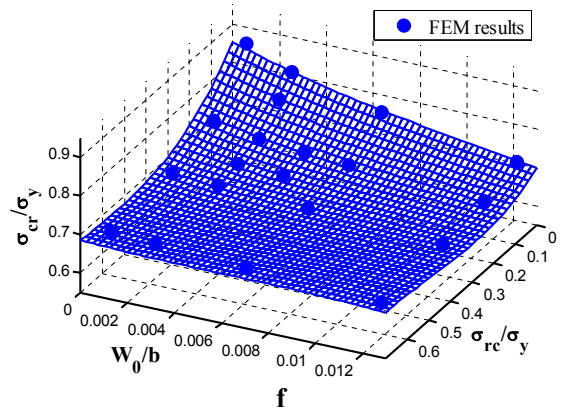

f

Fig. A 1-2.7 Response surface regarding each steel grade for R=1.04

R=1.16

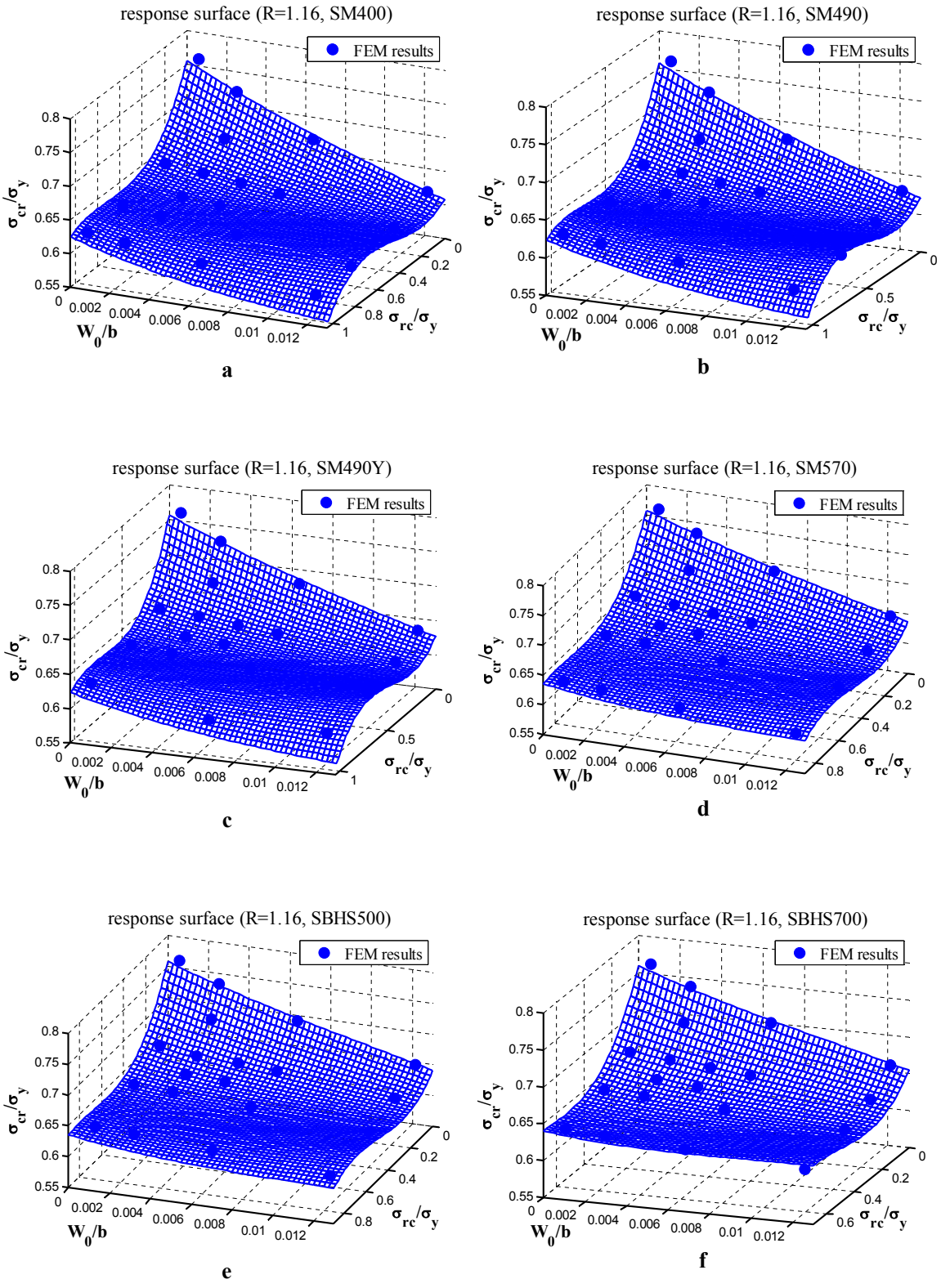

Fig. A 1-2.8 Response surface regarding each steel grade for R=1.16

R=1.28

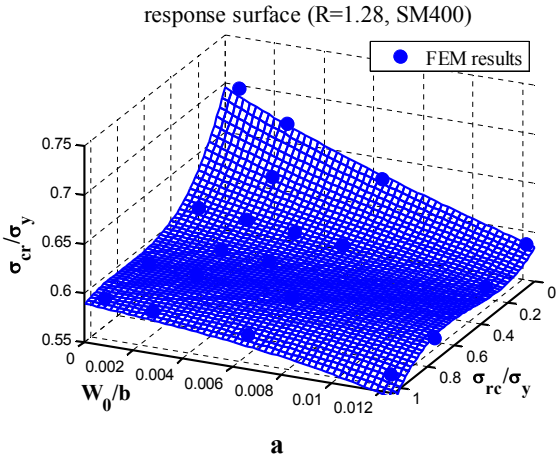

a

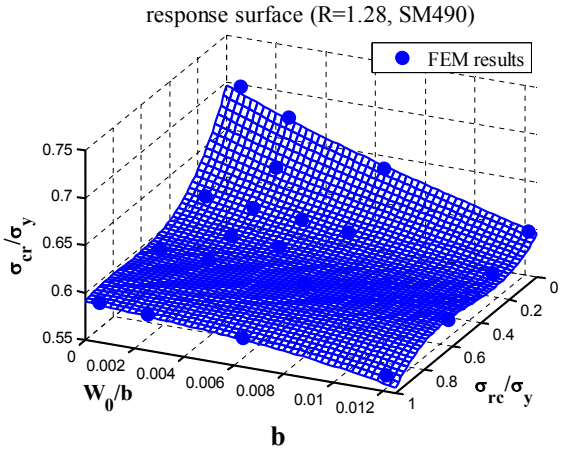

b

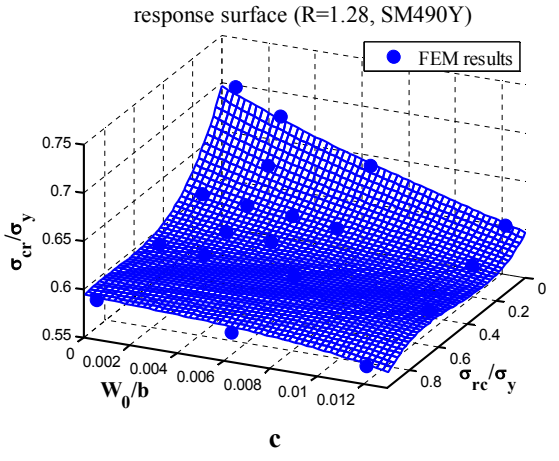

c

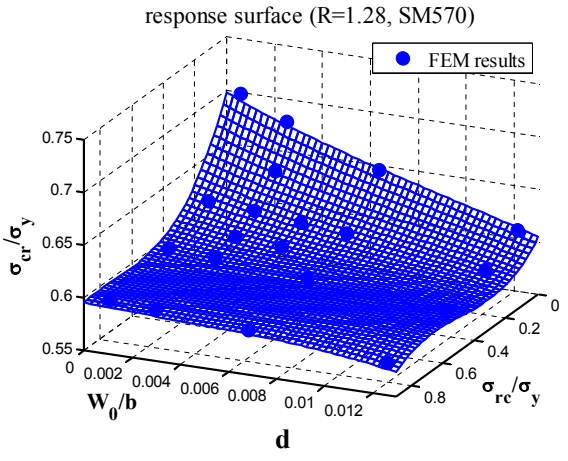

d

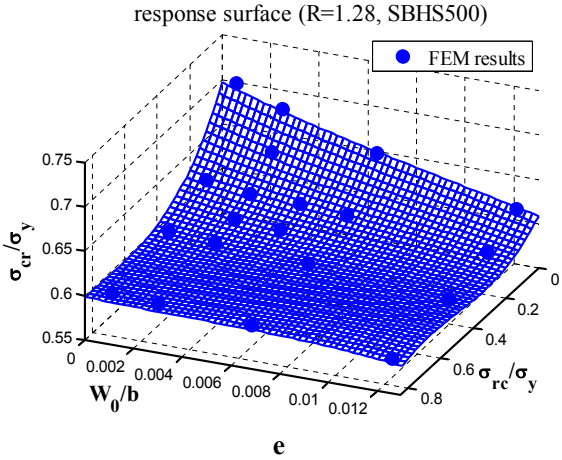

e

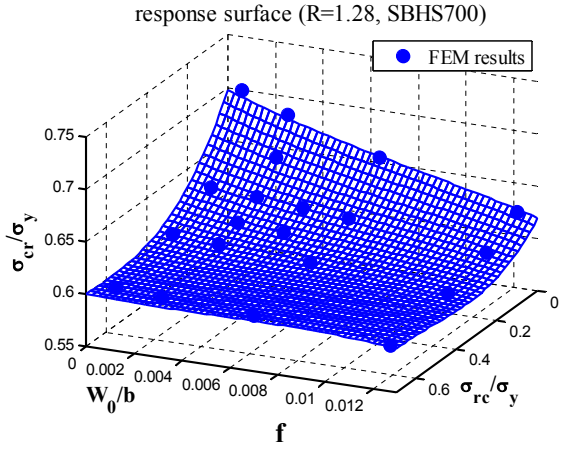

f

Fig. A 1-2.9 Response surface regarding each steel grade for R=1.28

R=1.40

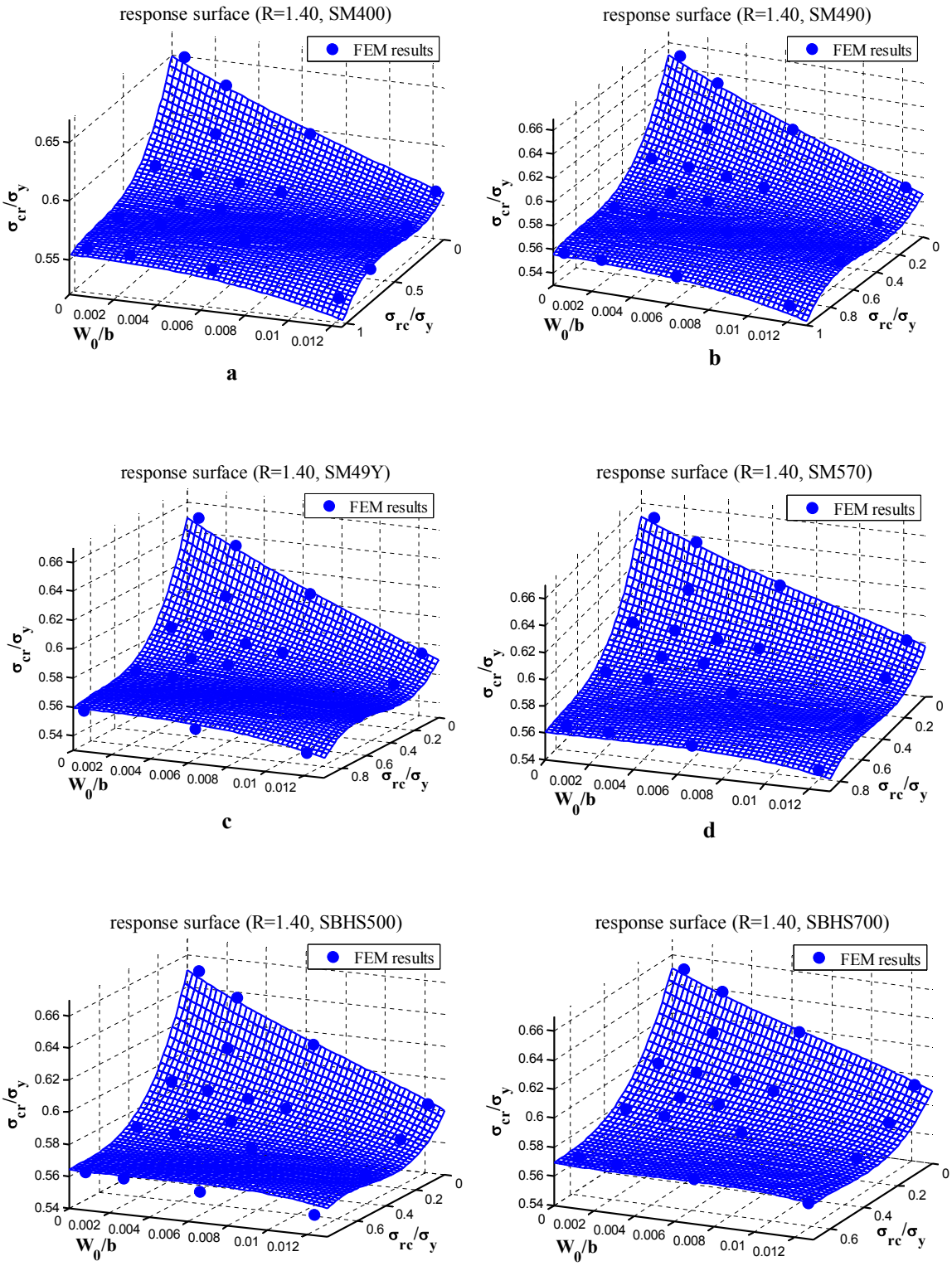

e **f**

Fig. A 1-2.10 Response surface regarding each steel grade for R=1.40

Table A2-1. Coefficients of 60 Response surfaces

R	Grade	p_{00}	p_{01}	p_{02}	p_{03}	p_{10}	p_{11}	p_{12}	p_{20}	p_{21}	p_{30}
0.4	SM400	1.03	-19.51	2911	-156100	0.0048	-3.98	-58.23	0.0075	3.39	-0.0117
	SM490	1.05	-23.94	3454	-170000	0.0008	-3.08	-68.82	0.0149	2.84	-0.0150
	SM490Y	1.07	-38.74	5856	-280000	0.0039	-2.25	-92.85	0.0037	2.10	-0.0027
	SM580	1.16	-61.41	7683	-322300	0.0112	-1.92	-86.11	-0.0235	2.85	0.0106
	SBHS500	1.15	-55.17	6915	-290600	0.0116	-1.82	-78.34	-0.0277	2.87	0.0149
	SBHS700	1.12	-30.32	3035	-116100	-0.0002	-0.56	-4.40	0.0007	0.76	-0.0013
0.5	SM400	1.00	3.72	-2047	89230	-0.0267	-10.52	121.90	0.0915	6.225	-0.0620
	SM490	1.00	1.61	-1268	48560	-0.02364	-9.47	-12.49	0.0938	6.833	-0.0686
	SM490Y	1.01	0.59	-971	33370	-0.02166	-9.37	-34.74	0.0963	7.252	-0.0759
	SM580	1.06	-31.15	4445	-220000	-0.002993	-9.57	-83.15	0.0616	8.961	-0.0651
	SBHS500	1.06	-29.84	4407	-220000	0.001552	-9.36	-134.80	0.0526	10.120	-0.0666
	SBHS700	1.07	-28.65	3914	-186300	0.007595	-5.30	-288.20	0.0131	10.070	-0.0426
0.6	SM400	1.01	-1.41	-2812	154900	-0.1019	-20.56	831.7	0.256	6.46	-0.147
	SM490	1.01	2.12	-3007	161200	-0.1022	-20.94	620.3	0.293	8.92	-0.184
	SM490Y	1.01	1.15	-2588	136300	-0.0982	-22.68	641.9	0.312	10.83	-0.215
	SM580	1.01	1.01	-2252	117500	-0.0956	-23.75	504.3	0.359	14.25	-0.283
	SBHS500	1.01	1.15	-2034	104200	-0.0892	-24.61	398.6	0.378	17.34	-0.328
	SBHS700	1.03	-6.75	-331	18900	-0.0508	-24.04	89.1	0.338	24.55	-0.392
0.7	SM400	1.03	-40.49	4383	-246800	-0.2436	-57.39	3751	0.648	21.20	-0.407
	SM490	1.04	-40.20	3815	-162600	-0.266	-25.26	1517	0.578	2.89	-0.317
	SM490Y	1.04	-37.91	3707	-163000	-0.2634	-29.39	1540	0.635	6.49	-0.381
	SM580	1.03	-29.13	2192	-85330	-0.2899	-34.4	1742	0.807	8.35	-0.550
	SBHS500	1.03	-24.99	1588	-56550	-0.2912	-39.08	1859	0.890	11.71	-0.660
	SBHS700	1.03	-17.93	645.1	-14670	-0.2872	-51.38	2099	1.175	24.95	-1.118
0.8	SM400	1.05	-77.08	10010	-469800	-0.517	9.601	985	0.747	-17.74	-0.317
	SM490	1.05	-73.09	9625	-453800	-0.549	2.271	1223	0.877	-14.66	-0.408
	SM490Y	1.05	-67.49	8520	-394700	-0.586	2.445	1255	0.987	-16.88	-0.474
	SM580	1.05	-65.63	8606	-407600	-0.624	-5.952	1782	1.197	-17.36	-0.663
	SBHS500	1.05	-62.26	8111	-384600	-0.641	-10.520	2059	1.296	-17.85	-0.757
	SBHS700	1.05	-55.92	7343	-352600	-0.665	-24.480	2861	1.586	-18.00	-1.095
0.92	SM400	0.954	-47.29	3908	-148500	-0.781	57.01	-1042	0.98	-32.03	-0.396
	SM490	0.959	-43.79	3609	-139000	-0.863	55.07	-874	1.18	-32.45	-0.518
	SM490Y	0.961	-41.60	3169	-115000	-0.926	59.33	-919	1.34	-37.39	-0.613
	SM580	0.965	-47.35	4617	-190300	-0.940	62.37	-1119	1.42	-42.06	-0.692
	SBHS500	0.974	-41.34	3259	-119300	-1.067	68.13	-1104	1.72	-50.32	-0.898
	SBHS700	0.985	-42.15	3514	-130800	-1.184	78.96	-1449	2.07	-65.85	-1.189
1.04	SM400	0.847	-28.96	1732	-55020	-0.658	48.57	-940	0.816	-26.64	-0.327
	SM490	0.848	-25.67	1477	-47990	-0.728	46.52	-790	1.003	-26.81	-0.445
	SM490Y	0.849	-24.15	1251	-36980	-0.779	48.56	-800	1.141	-29.77	-0.537
	SM580	0.853	-23.20	1225	-37270	-0.882	53.03	-847	1.468	-37.17	-0.795
	SBHS500	0.855	-22.65	1116	-30670	-0.927	56.26	-925	1.617	-41.65	-0.927
	SBHS700	0.863	-23.50	1403	-44090	-1.065	65.04	-1203	2.181	-55.19	-1.511
1.16	SM400	0.760	-18.89	948.1	-29970	-0.493	34.37	-571.5	0.599	-19.57	-0.236
	SM490	0.760	-16.13	746.0	-24260	-0.540	32.10	-450.1	0.732	-19.28	-0.322
	SM490Y	0.773	-28.33	4777.0	-402300	-0.685	56.69	-1966.0	1.081	-37.28	-0.542
	SM580	0.761	-13.53	486.5	-13490	-0.648	35.50	-445.4	1.077	-26.17	-0.588

1.28	SBHS500	0.761	-12.44	308.3	-4229	-0.683	37.14	-466.3	1.207	-29.27	-0.706
	SBHS700	0.763	-11.19	301.3	-5901	-0.796	40.41	-481.0	1.737	-39.01	-1.273
	SM400	0.697	-13.04	528.2	-16660	-0.377	25.78	-378.3	0.438	-14.92	-0.166
	SM490	0.697	-11.27	456.8	-16120	-0.410	23.80	-291.4	0.535	-14.48	-0.230
	SM490Y	0.697	-10.40	358.0	-11560	-0.435	24.36	-284.0	0.610	-15.75	-0.282
	SM580	0.698	-9.57	333.8	-11390	-0.485	25.58	-275.7	0.785	-19.09	-0.426
	SBHS500	0.698	-8.77	220.5	-5656	-0.508	26.44	-280.4	0.875	-21.12	-0.508
	SBHS700	0.698	-7.44	171.5	-4824	-0.586	27.96	-269.4	1.258	-27.62	-0.925
1.40	SM400	0.650	-9.55	290.4	-8504	-0.297	21.27	-314.8	0.317	-11.81	-0.112
	SM490	0.650	-8.05	230.0	-7936	-0.324	19.22	-223.9	0.397	-11.41	-0.164
	SM490Y	0.650	-7.53	195.4	-6643	-0.343	19.29	-211.3	0.458	-12.08	-0.208
	SM580	0.650	-7.02	210.7	-7960	-0.377	19.74	-196.0	0.584	-14.39	-0.312
	SBHS500	0.650	-6.43	133.3	-4034	-0.393	20.19	-192.6	0.650	-15.81	-0.375
	SBHS700	0.651	-5.64	142.3	-5409	-0.443	20.75	-170.3	0.906	-20.34	-0.655
R	**Grade**	p_{00}	p_{01}	p_{02}	p_{03}	p_{10}	p_{11}	p_{12}	p_{20}	p_{21}	p_{30}

APPENDIX 2

PROBABILISTIC INFORMATION OF LBS

A2-1 Case 1 – regarding all 6 steel grades for each R value

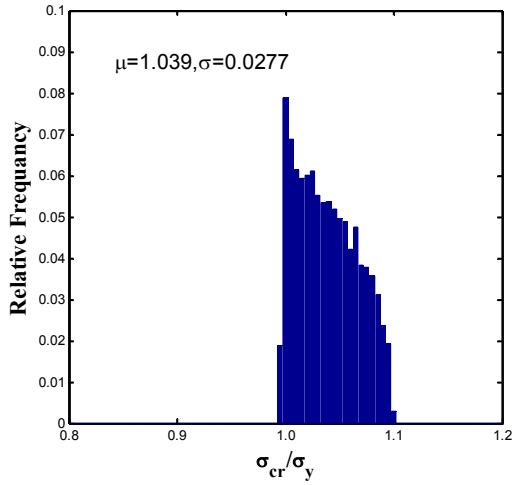

a. R=0.4

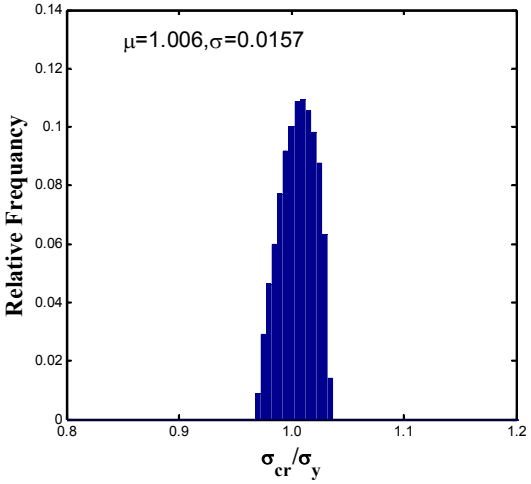

b. R=0.5

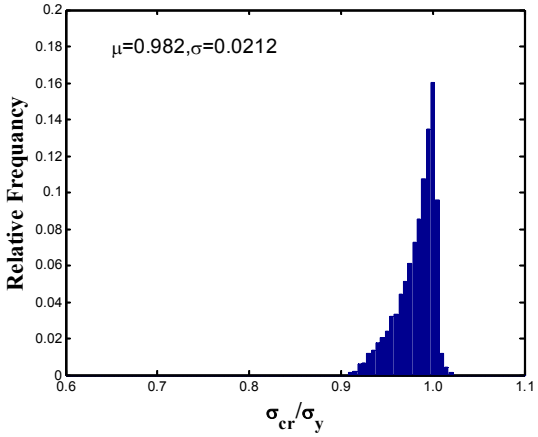

c. R=0.6

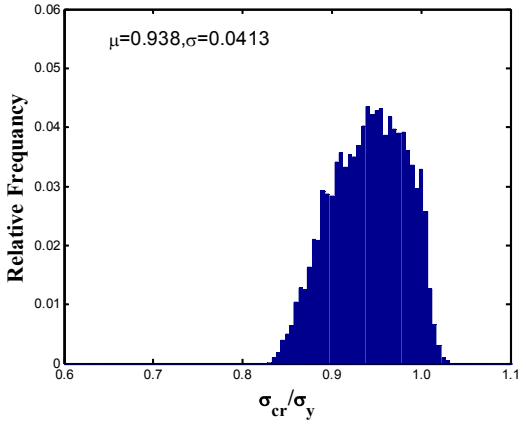

d. R=0.7

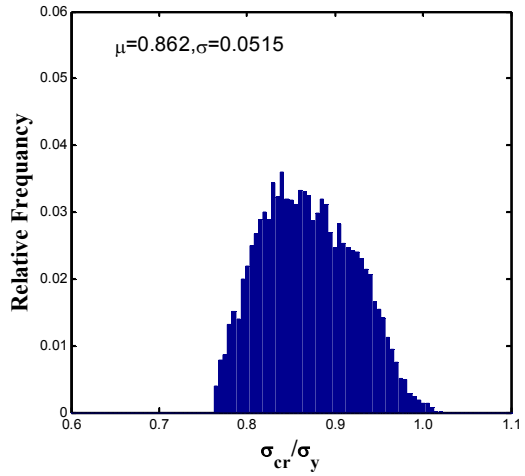

e. R=0.8

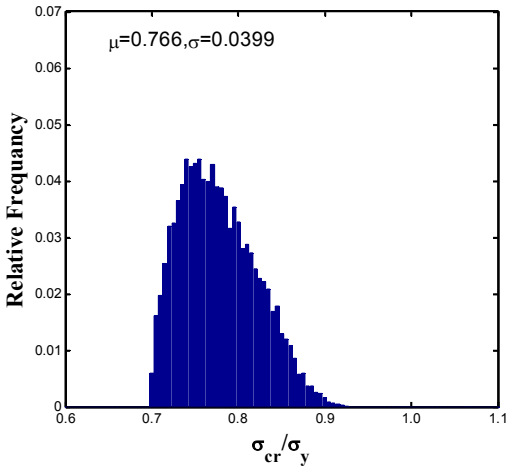

f. R=0.92

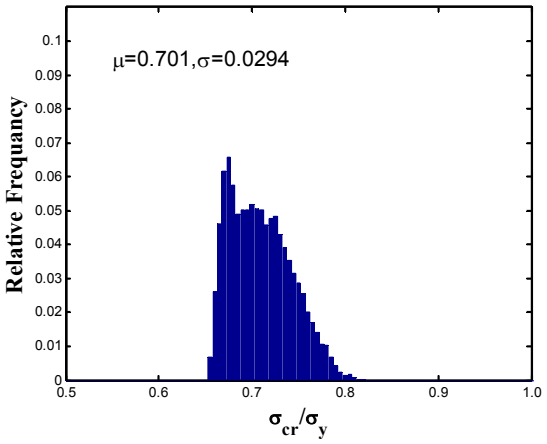

g. R=1.04

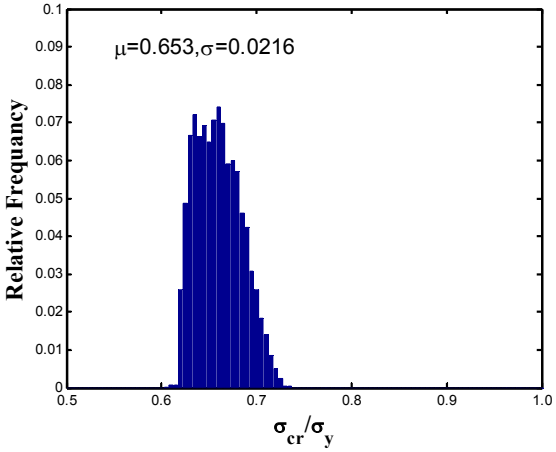

h. R=1.16

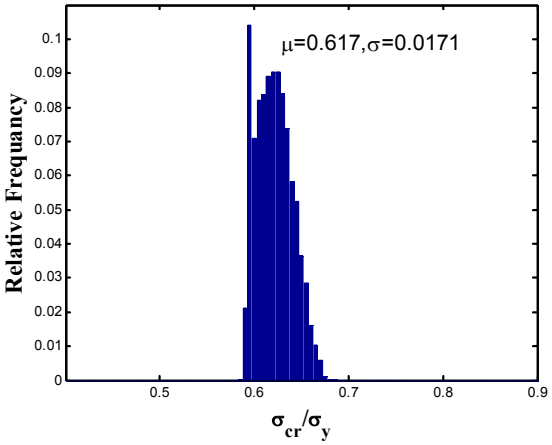

i. R=1.28

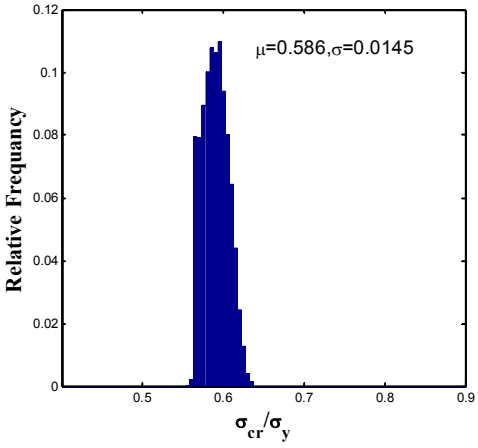

j. R= 1.40

Fig. A 2-1.1 Probabilistic distribution of LBS for R ranging from 0.4 to 1.4

A2-2 Case 2 – regarding each steel grade for each R value

R=0.4

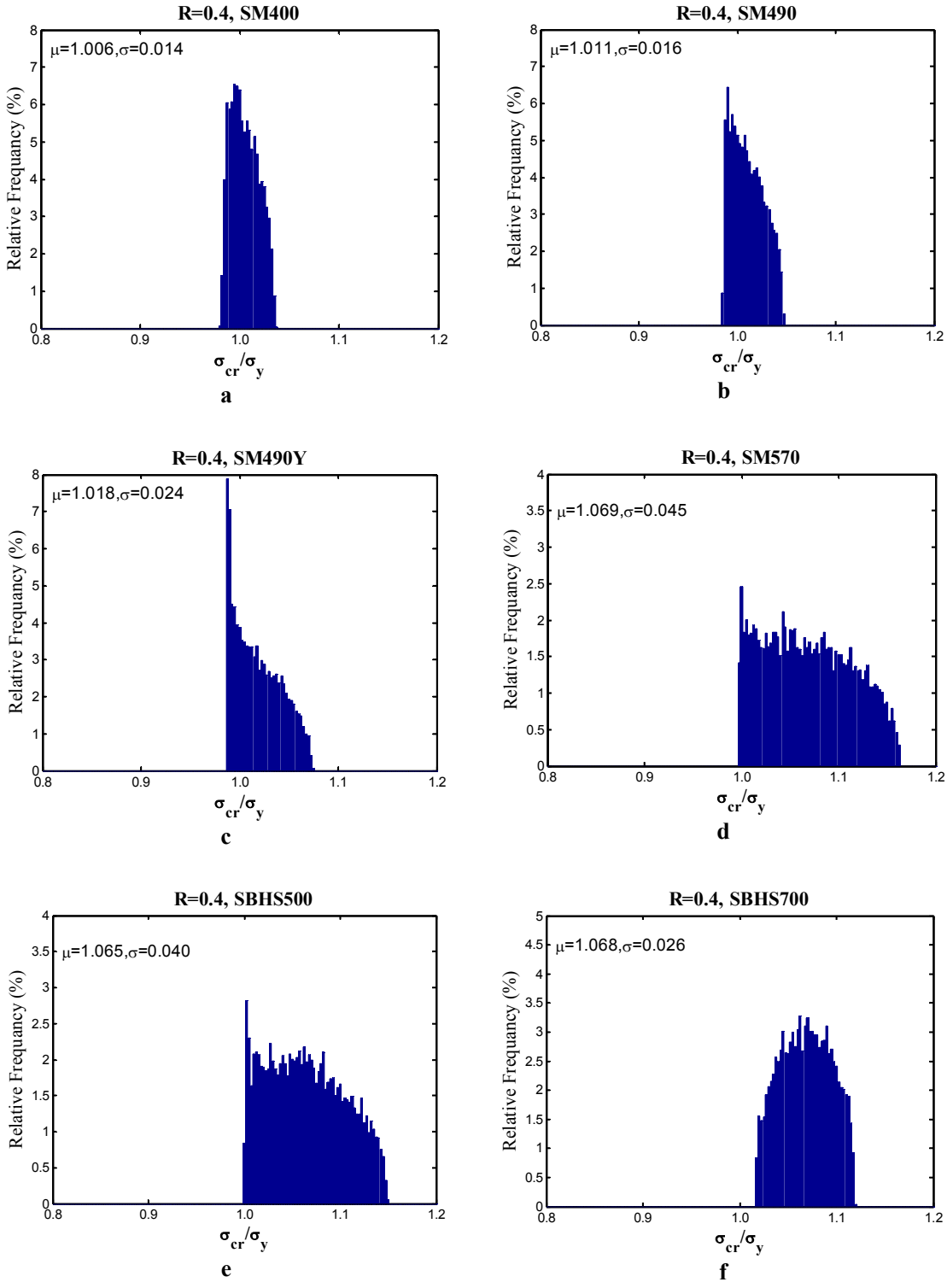

Fig. A 2-2.1 Probabilistic distribution of LBS for R =0.4

R=0.5

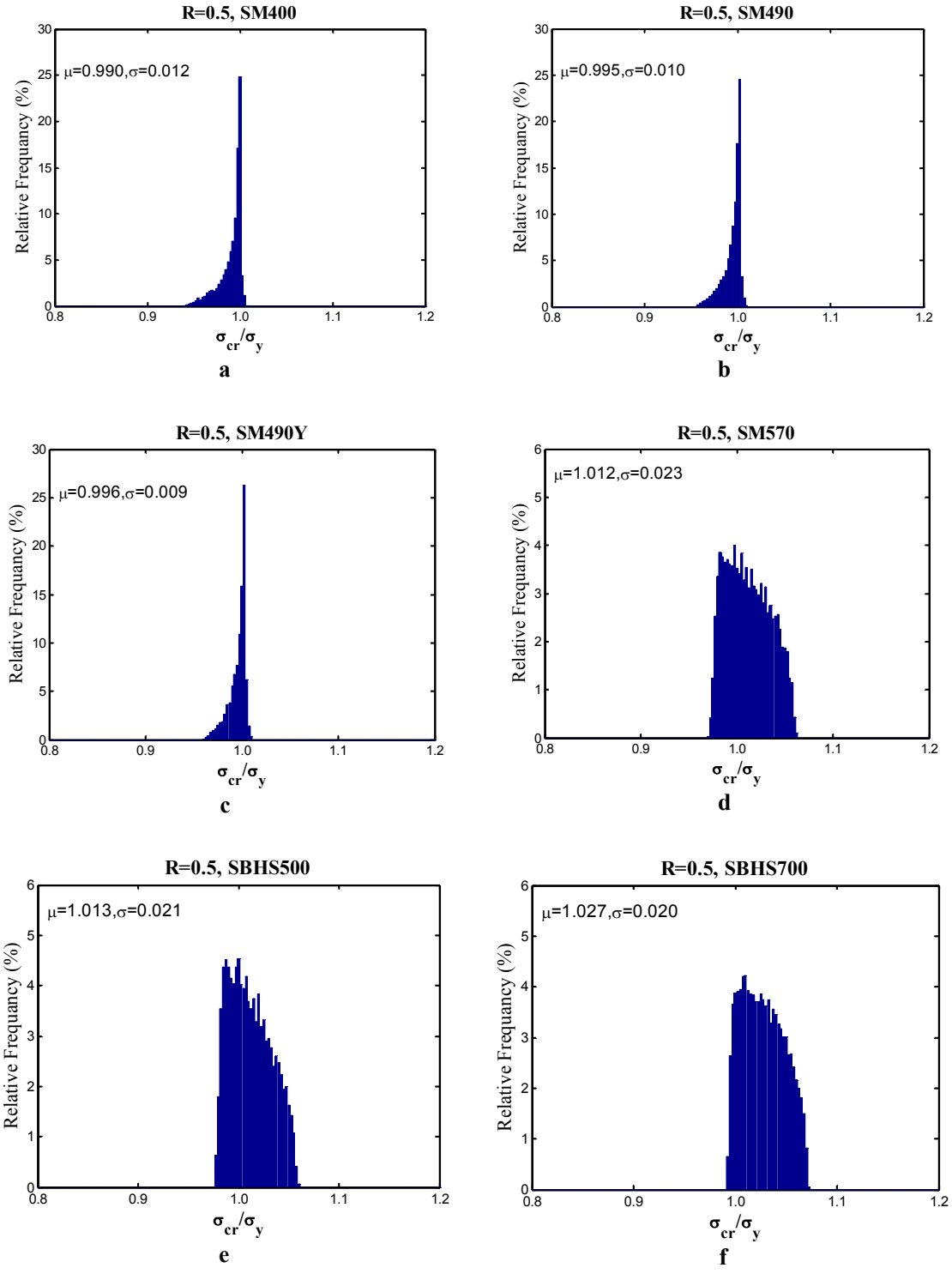

Fig. A 2-2.2 Probabilistic distribution of LBS for R =0.5

R=0.6

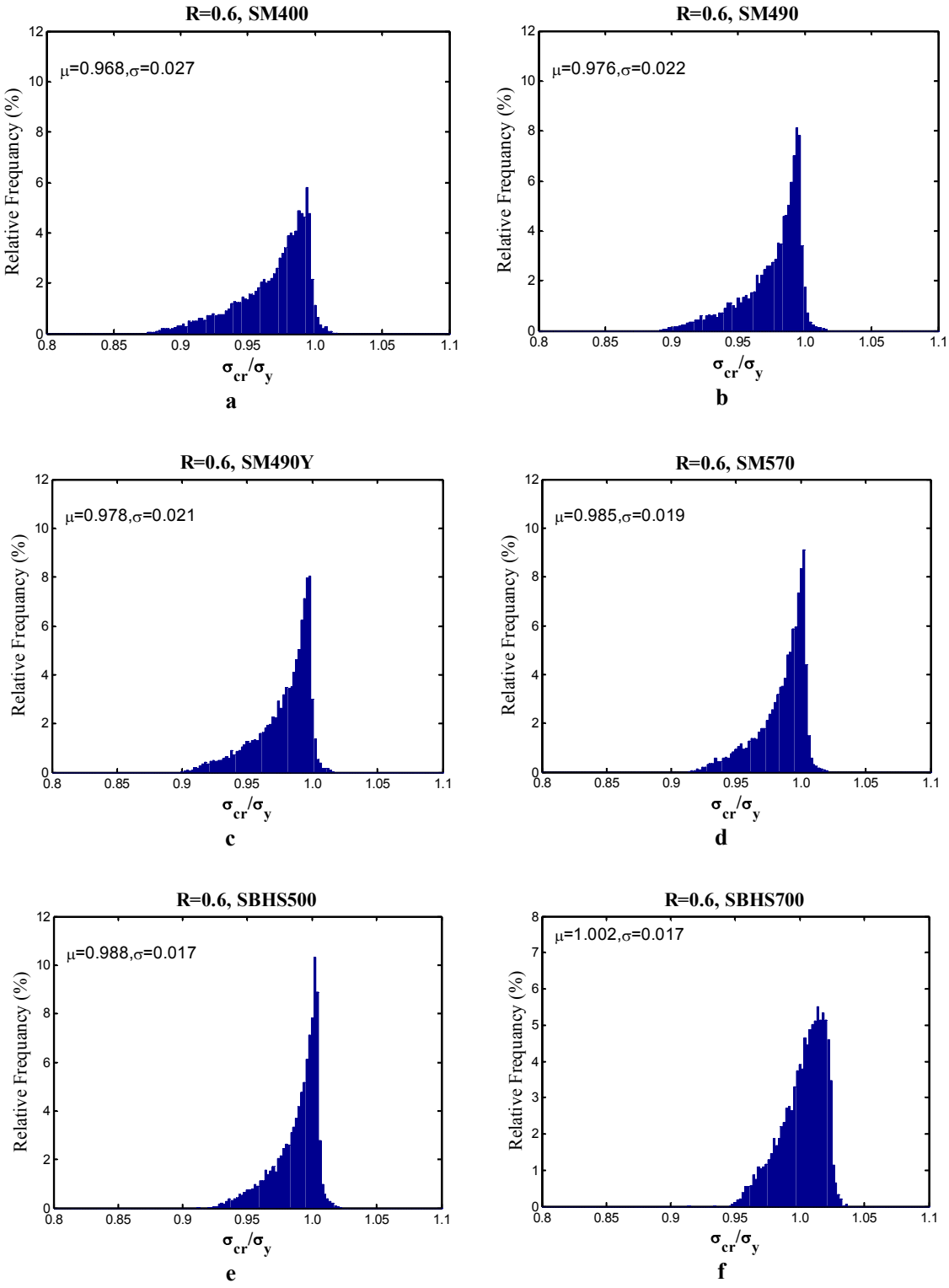

Fig. A 2-2.3 Probabilistic distribution of LBS for R =0.6

R=0.7

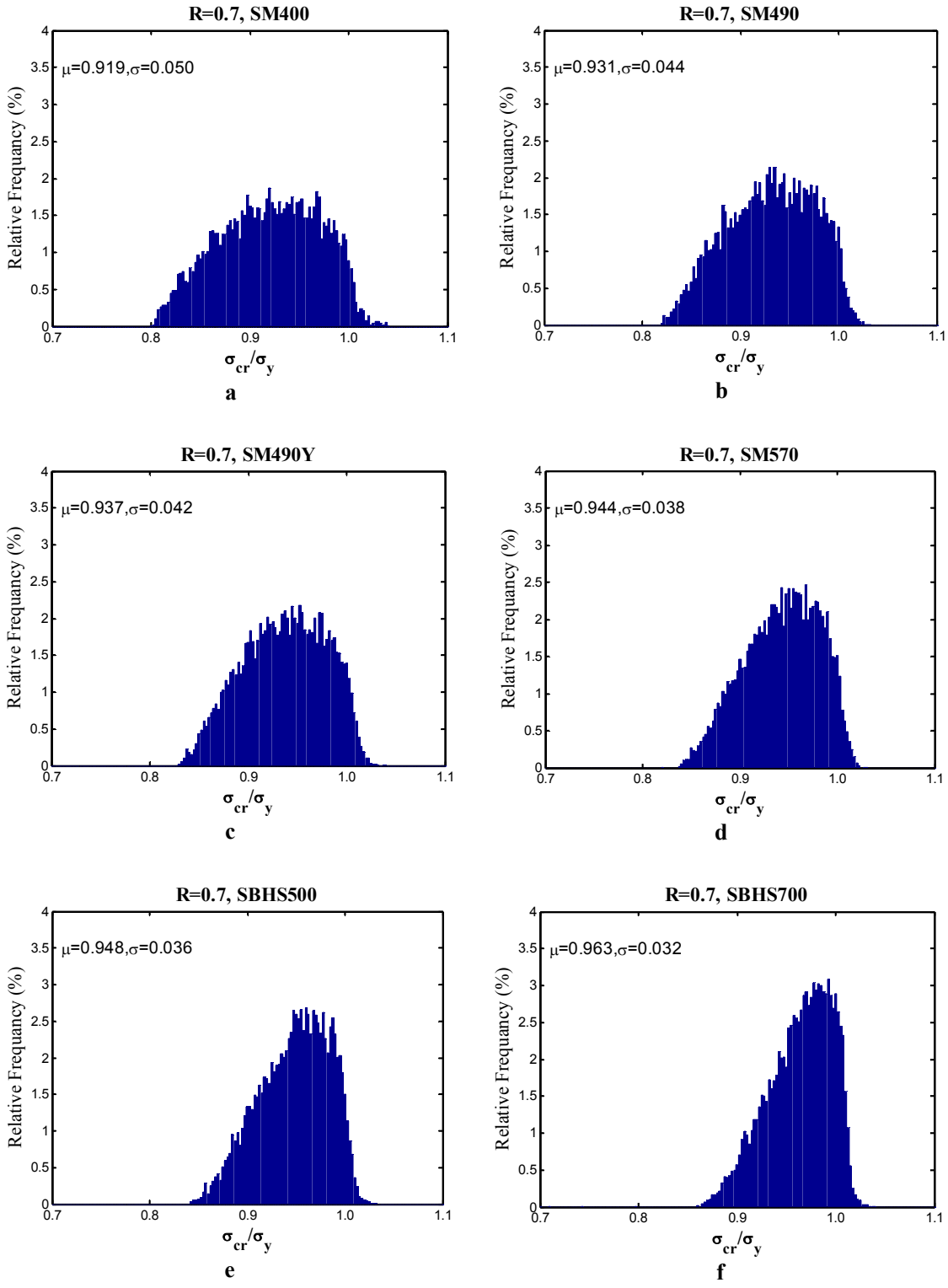

Fig. A 2-2.4 Probabilistic distribution of LBS for R =0.7

R=0.8

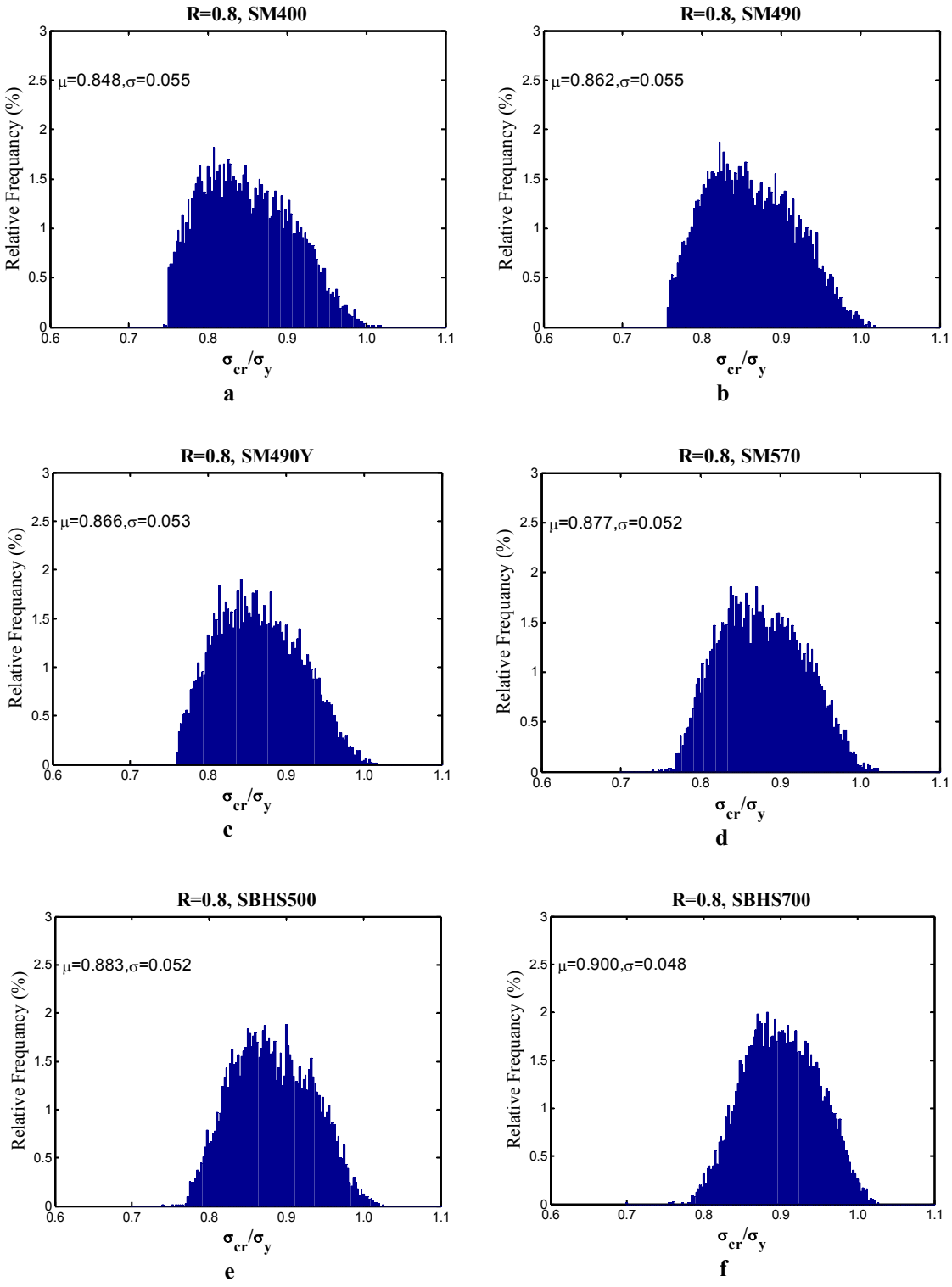

Fig. A 2-2.5 Probabilistic distribution of LBS for R =0.8

R=0.92

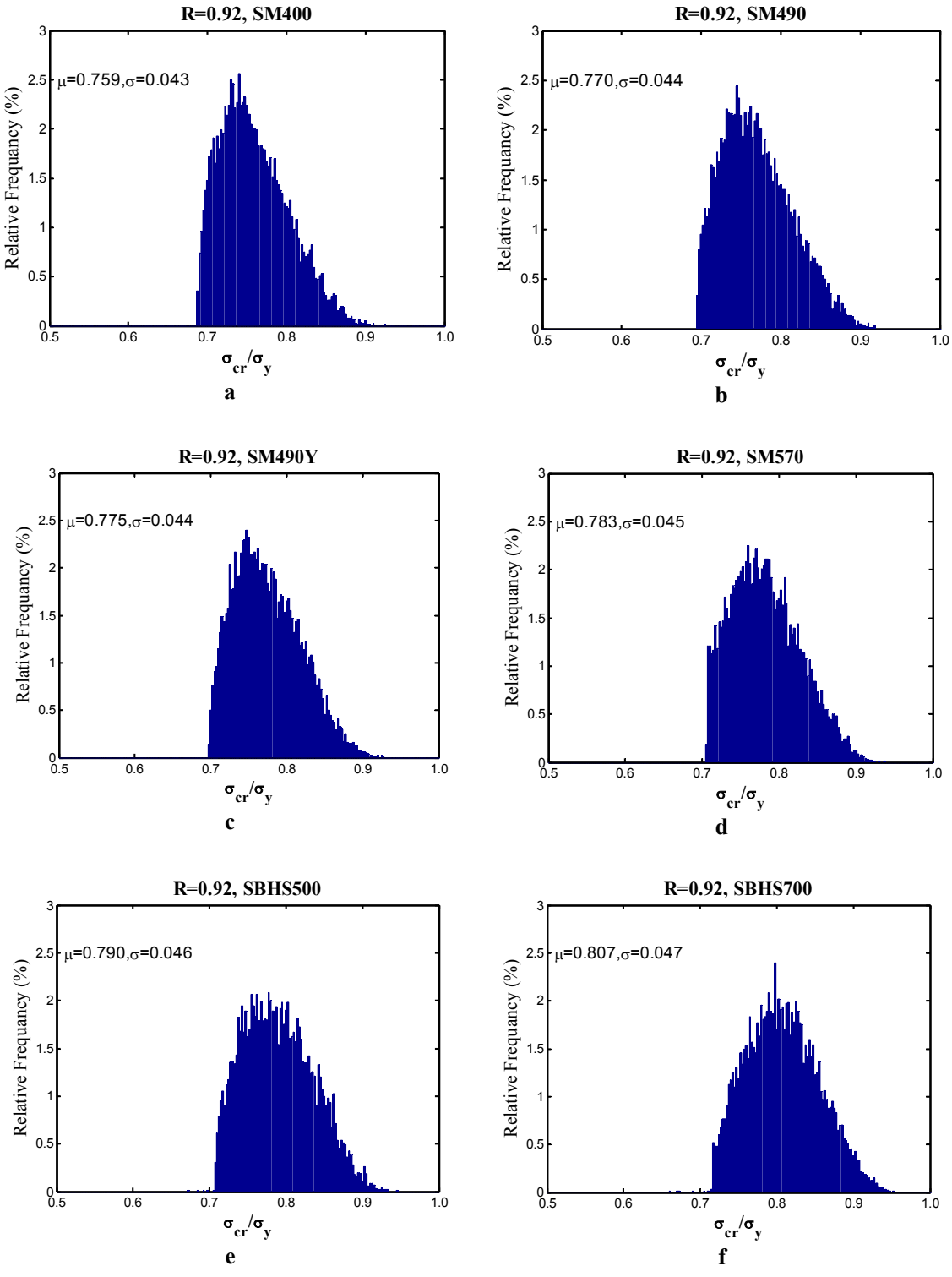

Fig. A 2-2.6 Probabilistic distribution of LBS for R =0.92

R=1.04

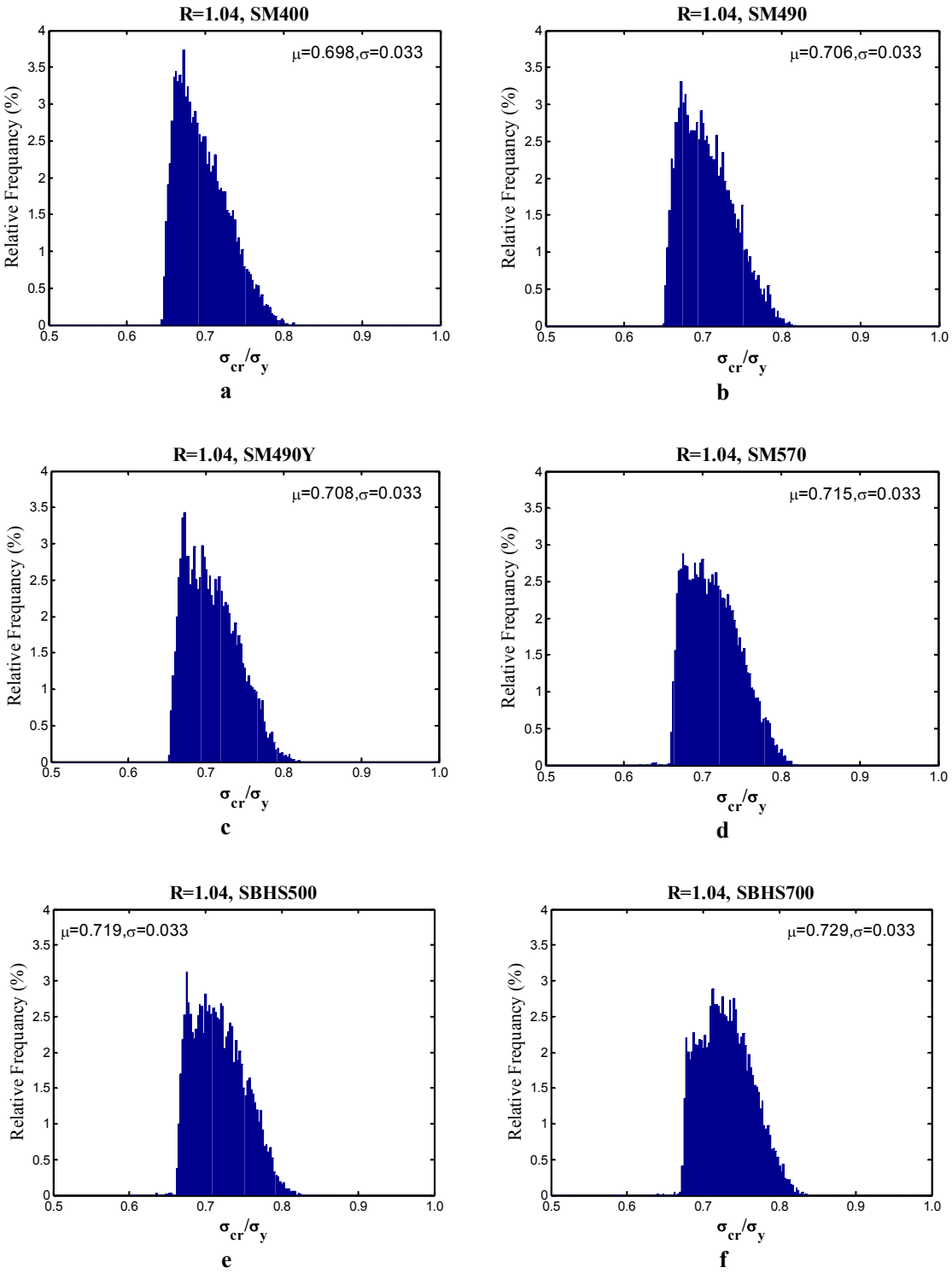

Fig. A 2-2.7 Probabilistic distribution of LBS for R =1.04

R=1.16

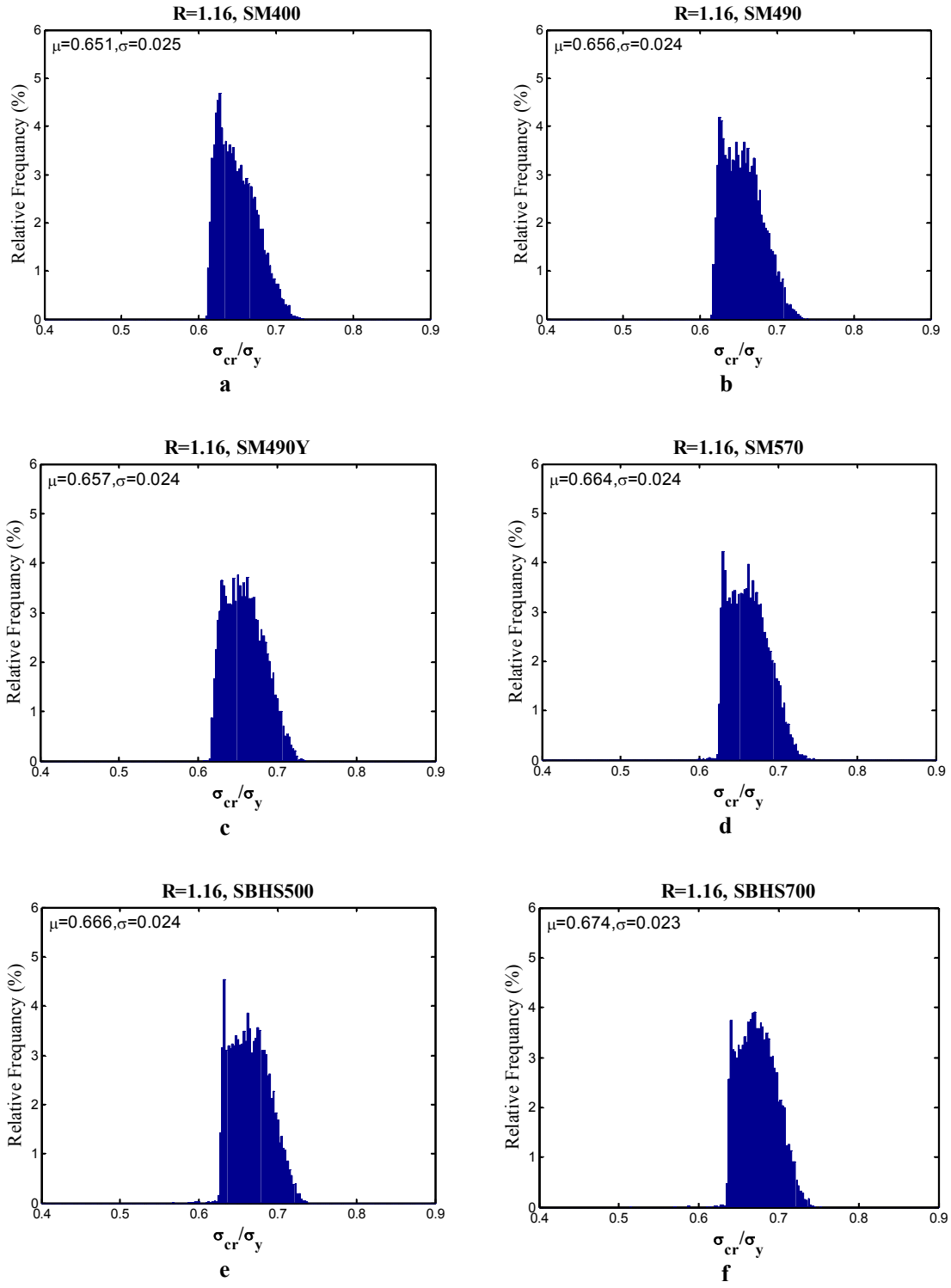

Fig. A 2-2.8 Probabilistic distribution of LBS for R =1.16

R=1.28

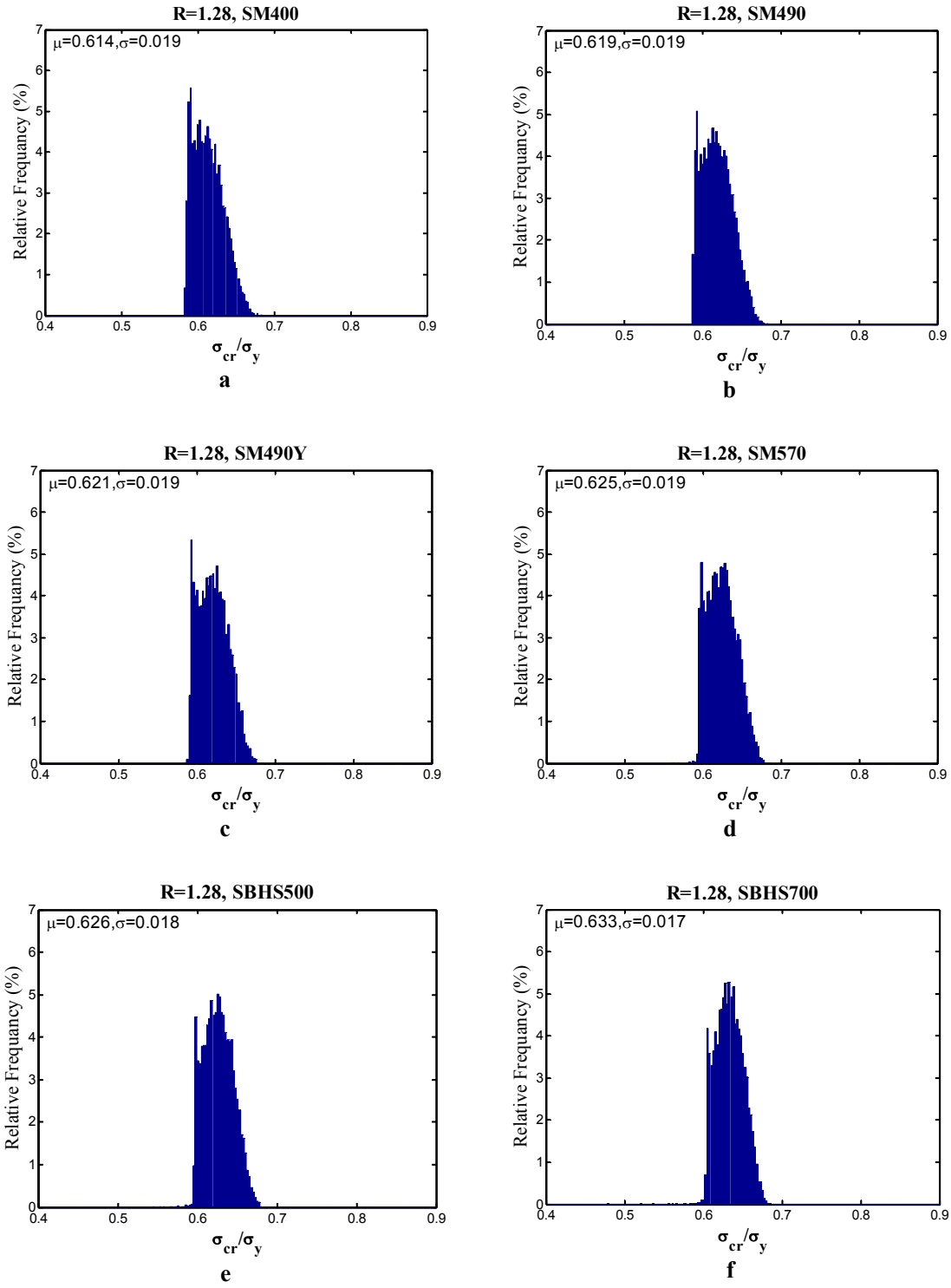

Fig. A 2-2.9 Probabilistic distribution of LBS for R =1.28

R=1.40

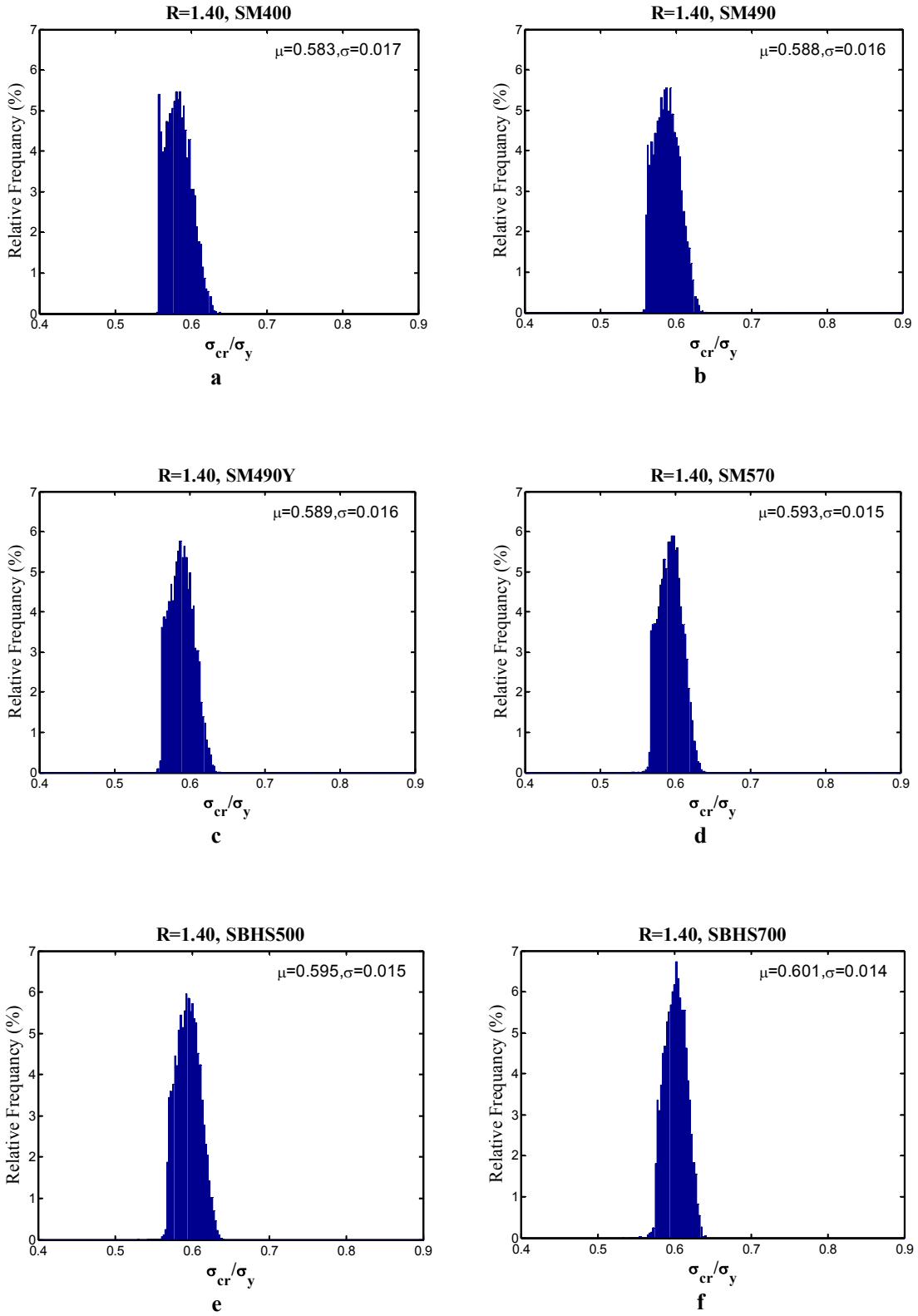

Fig. A 2-2.10 Probabilistic distribution of LBS for R =1.40

APPENDIX 3

PROPERTIES OF COMPOSITE SECTION

The calculation of yield moment, My and plastic moment, Mp for concrete - steel composite girders – homogeneous section was carried out in accordance with the AASHTO specifications. In all of the following figures, the positive (+) and negative (-) sign in stress diagrams represents the stress distribution of girders in tension and compression, respectively.

A3-1. Yield moment

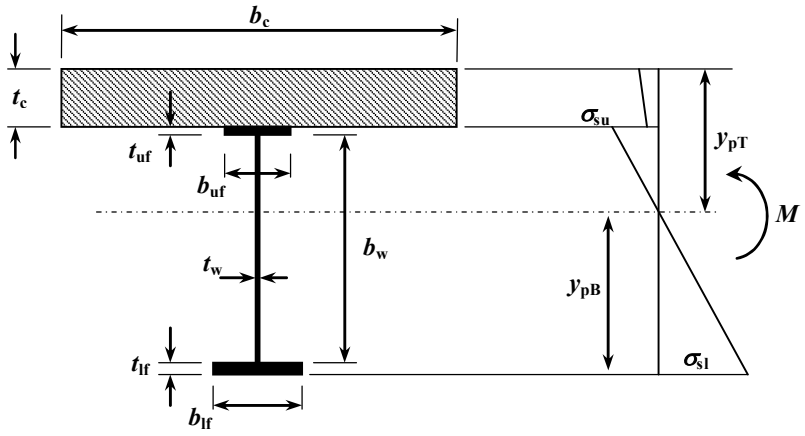

Fig. A 3-1.1 Composite section elastic stress distribution under positive bending

As mentioned in Chapter 4, yield moment *M*y is calculated with assumption of elastic stress distribution in the section once either of extreme steel section firber start yielding. In the Fig. A3-1.1 The depth of elastic neutral axis from bottom, y_{pB} for composite girders under positive bending (Fig.A3-1.1) is calculated as given below

$$y_{pB} = \frac{\sum A_i y_i}{A_{pc}} = \frac{\left(\frac{Ac}{n}\right) y_c + A_{uf} y_{uf} + A_w y_w + A_{lf} y_{lf}}{\left(\frac{Ac}{n}\right) + A_{uf} + A_w + A_{lf}} \qquad \text{(A3-1.1)}$$

where A_c, A_{uf}, A_w and A_{lf} are the areas and yc, y_{uf}, y_w and y_{lf} are the centroidal depth of each component from bottom of the steel girder and A_{pc} is the total area of composite girder.

ratio of the moduli of steel to concrete n: $n = \frac{E_s}{E_c}$

where E_s and E_c are the Young's modulus of steel and concrete, respectively.

The moment of inertia of composite girder, I_{pc} is

$$I_{pc} = \frac{b_c t_c^{\,3}}{12n} + \frac{b_{uf} t_{uf}^{\,3}}{12} + \frac{t_w b_w^{\,3}}{12} + \frac{b_{lf} t_{lf}^{\,3}}{12} + \frac{A_c}{n}\left(y_{pT} - \frac{t_c}{2}\right)^2 + A_{uf}\left(y_{pT} - t_c - \frac{t_{uf}}{2}\right)^2 + A_w\left(y_{pB} - t_{lf} - \frac{b_w}{2}\right)^2 + A_{lf}\left(y_{pB} - \frac{t_{lf}}{2}\right)^2 \quad \text{(A3-1.2)}$$

The section modulus, $S_{\min}$ is given by

$$S_{\min} = \frac{I_{pc}}{y_{p\max}(y_{pT}, y_{pB})} \quad \text{(A3-1.3)}$$

Hence, the moment of resistance of composite girder, My can be determined as following

$$M_y = f_y S_{\min}$$

where f_y is the yield stress of steel material.

Yield moment of a composite section accounting for initial bending moment

Calculation of initial bending moment M_1

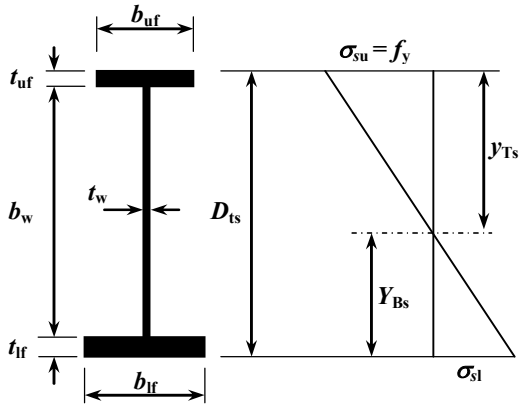

Fig. A 3-1.2 Steel section elastic stress distribution under positive bending

From Fig. the depth of the elastic neutral axis from bottom, y_{Bs} is calculated as

$$y_{BS} = \frac{\sum A_i y_i}{A_s} = \frac{A_{uf} y_{uf} + A_w y_w + A_{lf} y_{lf}}{A_{uf} + A_w + A_{lf}} \tag{A3-1.4}$$

where A_{uf}, A_w and A_{lf} stand for the areas and y_{uf}, y_w and y_{lf} are the centroidal depth of each member from bottom of the steel girder and A_s is the total area of steel girder.

The depth of neutral axis from top, y_{Ts} is

$$y_{TS} = D_{Ts} - y_{Bs} \tag{A3-1.5}$$

where D_{Ts} is the total depth of the steel section.

The moment of inertia of steel girder, I_s is given by

$$I_s = \frac{b_{uf} t_{uf}^{\ 3}}{12} + \frac{t_w b_w^{\ 3}}{12} + \frac{b_{lf} t_{lf}^{\ 3}}{12} + A_{uf}\left(y_{Ts} - \frac{t_{uf}}{2}\right)^2 + A_w\left(y_{Ts} - t_{uf} - \frac{b_w}{2}\right)^2 + A_{lf}\left(y_{Bs} - \frac{t_{lf}}{2}\right)^2 \tag{A3-1.6}$$

The section modulus of steel section, S_{Ts}

$$S_{Ts} = \frac{I_s}{y_{Ts}} \tag{A3-1.7}$$

The moment of resistance of steel girder, M_{ys} is given by

$$M_{ys} = f_y S_{Ts} \tag{A3-1.8}$$

Hence, the initial bending moment, M_1 applied only on the steel girder is taken as a percentage of M_{ys}.

$$M_1 = \phi M_{ys} \tag{A3-1.9}$$

The yield moment,My considering initial bending moment is defined once first yielding attaining at either flange of the steel section. Because the cross section behaves elastically until the first yielding, superposition of moments is valid. Hence, M_y is the sum of moment applied separately on the steel section (M_1) and the composite section (M_2). The section capacity is reached when the first element has reached its limiting stress.

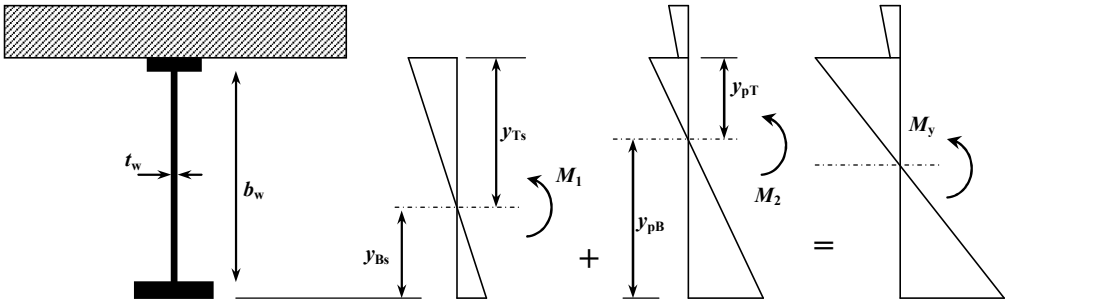

a. Stress state on steel section only

b. Stress state on composite section

c. superposition of 2 stress state M_1 and M_2

Fig. A 3-1.3 Flexural stresses at first yield

For composite sections the yield moment depends on the stress history (Fig. A.3) is determined from

$$\frac{M_1}{S_1} + \frac{M_2}{S_2} = f_y \tag{A3-1.9}$$

$$M_y = M_1 + M_2 \tag{A3-1.10}$$

where M_1 and S_1 are the initial bending moment and section modulus of steel section only. The additional moment requires yielding at either of the steel flanges is M_2. This moment is due to composite section modulus, S_2. The section modulus S_1 and S_2 are depended on the moment causing first yielding in either flange of the steel section. Therefore, moment M_2 can be solved from the eq.(A3-1.11) or .(A3-1.12)

$$M_2 = \left(f_y - \frac{M_1}{S_{Bs}} \right) S_{pB} \tag{A3-1.11}$$

$$M_2 = \left(f_y - \frac{M_1}{S_{Ts}} \right) S_{pT} \qquad \text{(A3-1.12)}$$

A3-2. Plastic neutral axis and plastic moment capacity of homogeneous and hybrid section

The general dimensions and plastic forces at ultimate limit state are represented as shown in Fig. A3-2.1. The idealized rectangular stress distribution has been adopted in calculation because it simplifies considerably flexural strength calculations. For the ultimate strength design calculations, it is assumed that the concrete slab is not reinforced in the longitudinal direction and there is full interaction between concrete slab and steel girder.

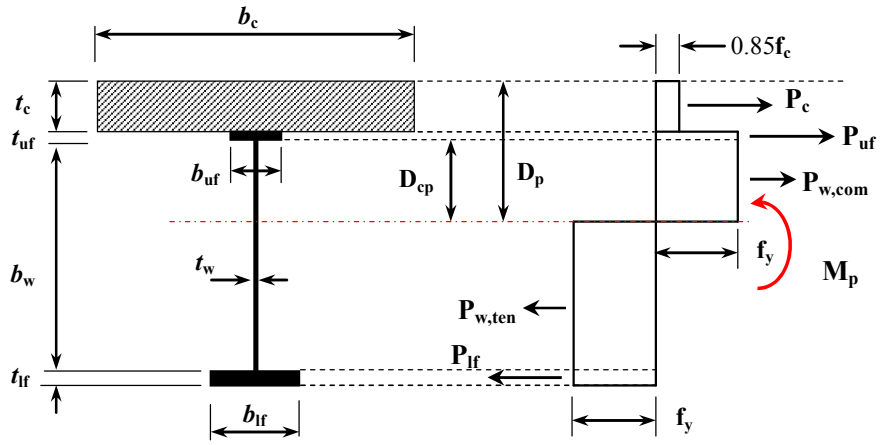

Fig. A 3-2.1 Stress block for a composite homogeneous steel section at the ultimate limit state

For plastic neutral axis lies in the web of the steel girder because

$$P_w + P_{lf} > P_c + P_{uf} \qquad \text{(A3-2.1)}$$

The plastic forces of different components of composite girders are calculated as follows:

The homogeneous steel section

a. Concrete slab: $P_c = 0.85 f_c b_c t_c$ (A3-2.2)

b. Compression flange: $P_{uf} = f_y b_{uf} t_{uf}$ (A3-2.3)

c. Web: $P_w = f_y b_w t_w$ (A3-2.4)

$$P_w = f_y D_{cp} t_w \quad \text{(A3-2.5)}$$

$$P_w = f_y (b_w - D_{cp}) t_w \quad \text{(A3-2.6)}$$

d. Tension flange: $P_{lf} = f_y b_{lf} t_{lf}$ (A3-2.7)

The hybrid steel section

a. Concrete slab: $P_c = 0.85 f_c b_c t_c$ (A3-2.8)

b. Compression flange: $P_{uf} = f_{yf} b_{uf} t_{uf}$ (A3-2.9)

c. Web: $P_w = f_{yw} b_w t_w$ (A3-2.10)

$$P_w = f_{yw} D_{cp} t_w \quad \text{(A3-2.11)}$$

$$P_w = f_{yw} (b_w - D_{cp}) t_w \quad \text{(A3-2.12)}$$

d. Tension flange: $P_{lf} = f_{yf} b_{lf} t_{lf}$ (A3-2.13)

where f_{yf} stands for yield strength of steel of girder flanges and f_{yw} stands for yield strength of steel of girder web.

Force equilibrium equation for assumed plastic stress distribution in the homogeneous composite sections

$$P_c + P_{uf} + P_{w,com} = P_{w,ten} + P_{lf} \quad \text{(A3-2.8)}$$

The distance from top of the web to the plastic neutral axis is given by

$$D_{cp} = \frac{P_{lf} - P_c \_ P_{uf}}{2 f_y t_w} + \frac{b_w}{2} \quad \text{(A3-2.9)}$$

where D_{cp} is the depth of the plastic neutral axis from the top of the web.

The nominal plastic moment capacity of the composite section, M_p is calculated next by taking moment of the compressive and tensile forces about plastic neutral axis

$$M_p = P_c\left(\frac{t_c}{2} + t_{uf} + D_{cp}\right) + P_{uf}\left(\frac{t_{uf}}{2} + D_{cp}\right) + P_{w,com}\frac{D_{cp}}{2} + P_{w,ten}\left(\frac{b_w - D_{cp}}{2}\right) + P_{lf}\left(\frac{t_{lf}}{2} + b_w - D_{cp}\right) \quad \text{(A3-2.10)}$$

Results

Table A 3-2.1 Results regarding girders with compact SBHS500 homogeneous steel section

Girder	α	M_y [N.mm]	M_p [N.mm]	M_u [N.mm]	M_u/M_y	M_u/M_p
PS2.8c	0.280	1.253.E+11	1.368E+11	1.425E+11	1.137	1.041
PS2.9a	0.386	1.282.E+11	1.351E+11	1.381E+11	1.077	1.022
PS2.9b	0.223	1.270.E+11	1.404E+11	1.464E+11	1.153	1.043
PS1.8c	0.325	9.810.E+10	1.107E+11	1.128E+11	1.150	1.019
PS2.8a	0.380	1.365.E+11	1.458E+11	1.485E+11	1.088	1.019
PS2.8a-2	0.432	1.453.E+11	1.513E+11	1.528E+11	1.051	1.010
CS2.5a	0.269	1.374.E+11	1.529E+11	1.582E+11	1.151	1.035
PS2.5a	0.435	1.418.E+11	1.495E+11	1.511E+11	1.065	1.010
PS2.5a-2	0.475	1.504.E+11	1.546E+11	1.551E+11	1.031	1.003
C1.2a	0.378	8.543.E+10	9.870E+10	9.870E+10	1.155	1.000

Table A 3-2.2 Results regarding girders with noncompact and slender SBHS500 homogeneous steel section for M_1=0

Girder	α'	M_y [N.mm]	M_p [N.mm]	M_u [N.mm]	M_u/M_y	M_u/M_p
CS1.2h	0.299	8.302.E+10	9.201.E+10	9.159E+10	1.103	0.995
CS1.2h-2	0.315	8.289.E+10	9.106.E+10	9.008E+10	1.087	0.989
CS1.2h-3	0.415	8.805.E+10	9.445.E+10	9.269E+10	1.053	0.981
CS1.2h-4	0.377	8.262.E+10	8.904.E+10	8.794E+10	1.064	0.988
CS1.2h-5	0.330	8.280.E+10	9.040.E+10	8.948E+10	1.081	0.990
CS2.2a	0.461	1.211.E+11	1.215.E+11	1.203E+11	0.994	0.990
CS2.0e	0.439	1.134.E+11	1.146.E+11	1.083E+11	0.955	0.945
C1.5b	0.359	8.658.E+10	9.273.E+10	9.165E+10	1.059	0.988
C1.5b-2	0.377	8.433.E+10	9.131.E+10	9.082E+10	1.077	0.995
C1.5b-3	0.343	8.453.E+10	9.269.E+10	9.268E+10	1.096	1.000
CS1.5c	0.442	9.628.E+10	1.002.E+11	9.812E+10	1.019	0.979
CS1.2d	0.493	8.771.E+10	9.023.E+10	8.616E+10	0.982	0.955
CS1.2d-2	0.453	8.783.E+10	9.103.E+10	8.729E+10	0.994	0.959
CS1.5	0.486	1.123.E+11	1.149.E+11	1.120E+11	0.997	0.975

CS1.5-2	0.482	1.125.E+11	1.158.E+11	1.132E+11	1.006	0.977
CS1.5-3	0.523	1.174.E+11	1.181.E+11	1.140E+11	0.971	0.965
CS1.6a	0.432	1.117.E+11	1.178.E+11	1.169E+11	1.047	0.992
CS1.6a-2	0.422	1.119.E+11	1.191.E+11	1.185E+11	1.059	0.995
CS1.6a-3	0.450	1.132.E+11	1.180.E+11	1.165E+11	1.029	0.988

Table A 3-2.3 Results regarding girders with noncompact and slender SBHS500 homogeneous steel section for M_l=0.2 M_{ys}

Girder	α'	M_y [N.mm]	M_p [N.mm]	M_u [N.mm]	M_u/M_y	M_u/M_p
CS1.2h	0.299	7.833.E+10	9.201.E+10	9.151E+10	1.168	0.995
CS1.2h-2	0.340	7.781.E+10	9.106.E+10	9.028E+10	1.160	0.991
CS1.2h-3	0.414	8.205.E+10	9.445.E+10	9.268E+10	1.130	0.981
CS1.2h-4	0.414	7.676.E+10	8.904.E+10	8.757E+10	1.141	0.983
CS1.2h-5	0.332	7.746.E+10	9.040.E+10	8.952E+10	1.156	0.990
CS2.2a	0.449	1.066.E+11	1.215.E+11	1.202E+11	1.127	0.990
CS2.0e	0.476	1.005.E+11	1.146.E+11	1.134E+11	1.128	0.989
C1.5b	0.361	7.866.E+10	9.273.E+10	9.220E+10	1.172	0.994
C1.5b-2	0.373	7.681.E+10	9.131.E+10	9.069E+10	1.181	0.993
C1.5b-3	0.345	7.749.E+10	9.269.E+10	9.271E+10	1.196	1.000
CS1.5c	0.414	8.736.E+10	1.002.E+11	9.885E+10	1.132	0.986
CS1.2d	0.496	7.997.E+10	9.023.E+10	8.606E+10	1.076	0.954
CS1.2d-2	0.483	8.033.E+10	9.103.E+10	8.720E+10	1.086	0.958
CS1.5	0.479	1.022.E+11	1.149.E+11	1.124E+11	1.099	0.978
CS1.5-2	0.490	1.027.E+11	1.158.E+11	1.132E+11	1.103	0.977
CS1.5-3	0.530	1.065.E+11	1.181.E+11	1.142E+11	1.072	0.967
CS1.6a	0.435	1.024.E+11	1.178.E+11	1.170E+11	1.143	0.993
CS1.6a-2	0.430	1.030.E+11	1.191.E+11	1.186E+11	1.151	0.995
CS1.6a-3	0.460	1.034.E+11	1.180.E+11	1.164E+11	1.126	0.987

Table A 3-2.4 Results regarding girders with noncompact and slender SBHS500 homogeneous steel section for M_l=0.4 M_{ys}

Girder	α'	M_y [N.mm]	M_p [N.mm]	M_u [N.mm]	M_u/M_y	M_u/M_p
CS1.2h	0.461	7.364.E+10	9.201.E+10	7.221E+10	0.981	0.785
CS1.2h-2	0.351	7.273.E+10	9.106.E+10	9.040E+10	1.243	0.993
CS1.2h-3	0.400	7.604.E+10	9.445.E+10	9.275E+10	1.220	0.982
CS1.2h-4	0.391	7.089.E+10	8.904.E+10	8.763E+10	1.236	0.984
CS1.2h-5	0.359	7.212.E+10	9.040.E+10	8.946E+10	1.240	0.990
CS2.2a	0.471	9.214.E+10	1.215.E+11	9.071E+10	0.984	0.747
CS2.0e	0.448	8.765.E+10	1.146.E+11	1.137E+11	1.297	0.992
C1.5b	0.392	7.073.E+10	9.273.E+10	9.185E+10	1.299	0.991
C1.5b-2	0.371	6.928.E+10	9.131.E+10	9.095E+10	1.313	0.996
C1.5b-3	0.431	7.045.E+10	9.269.E+10	9.272E+10	1.316	1.000

CS1.5c	0.498	7.844.E+10	1.002.E+11	9.840E+10	1.254	0.982
CS1.2d	0.482	7.223.E+10	9.023.E+10	8.633E+10	1.195	0.957
CS1.2d-2	0.505	7.283.E+10	9.103.E+10	8.739E+10	1.200	0.960
CS1.5	0.490	9.215.E+10	1.149.E+11	1.121E+11	1.217	0.976
CS1.5-2	0.530	9.283.E+10	1.158.E+11	1.134E+11	1.222	0.979
CS1.5-3	0.442	9.569.E+10	1.181.E+11	1.142E+11	1.193	0.967
CS1.6a	0.431	9.315.E+10	1.178.E+11	1.171E+11	1.257	0.994
CS1.6a-2	0.460	9.416.E+10	1.191.E+11	1.187E+11	1.261	0.996
CS1.6a-3	0.392	9.355.E+10	1.180.E+11	1.166E+11	1.246	0.989

Table A 3-2.5 Results regarding girders with noncompact and slender SBHS500 homogeneous steel section for M_l=0.6 M_{ys}

Girder	α'	M_y [N.mm]	M_p [N.mm]	M_u [N.mm]	M_u/M_y	M_u/M_p
CS1.2h	0.540	6.895.E+10	9.201.E+10	5.165E+10	0.749	0.561
CS1.2h-2	0.366	6.765.E+10	9.106.E+10	9.037E+10	1.336	0.992
CS1.2h-3	0.447	7.004.E+10	9.445.E+10	9.289E+10	1.326	0.984
CS1.2h-4	0.427	6.503.E+10	8.904.E+10	8.770E+10	1.349	0.985
CS1.2h-5	0.517	6.678.E+10	9.040.E+10	6.572E+10	0.984	0.727
CS2.2a	0.492	7.767.E+10	1.215.E+11	1.206E+11	1.553	0.993
CS2.0e	0.484	7.475.E+10	1.146.E+11	1.135E+11	1.518	0.990
C1.5b	0.424	6.280.E+10	9.273.E+10	9.173E+10	1.461	0.989
C1.5b-2	0.394	6.175.E+10	9.131.E+10	9.085E+10	1.471	0.995
C1.5b-3	0.480	6.341.E+10	9.269.E+10	9.272E+10	1.462	1.000
CS1.5c	0.548	6.952.E+10	1.002.E+11	9.832E+10	1.414	0.981
CS1.2d	0.528	6.449.E+10	9.023.E+10	8.621E+10	1.337	0.955
CS1.2d-2	0.424	6.532.E+10	9.103.E+10	8.715E+10	1.334	0.957
CS1.5	0.498	8.205.E+10	1.149.E+11	1.119E+11	1.364	0.974
CS1.5-2	0.485	8.300.E+10	1.158.E+11	1.132E+11	1.364	0.977
CS1.5-3	0.522	8.483.E+10	1.181.E+11	1.142E+11	1.346	0.967
CS1.6a	0.441	8.389.E+10	1.178.E+11	1.171E+11	1.396	0.994
CS1.6a-2	0.424	8.530.E+10	1.191.E+11	1.188E+11	1.393	0.997
CS1.6a-3	0.460	8.372.E+10	1.180.E+11	1.166E+11	1.393	0.989

Table A 3-2.6 Results of hybrid factor obtained from FEM analysis and proposal of the current study for M_1=0.0 M_{ys}

Girder ID	b_w/t_w	M_y [N.mm]	M_{yfFEM} [N.mm]	R_{hFEM}	β_{FEM}	$R_{hprop.}$	$\beta_{prop.}$
PS2.9a2hy	200	-1.54E+11	-1.53E+11	0.993	0.522	0.986	0.633
PS2.8c1hy	200	-1.21E+11	-1.19E+11	0.980	0.887	0.982	0.938
PS2.9a1hy	200	-1.01E+11	-9.96E+10	0.988	1.260	0.978	1.278
CS2.5a1hy	200	-1.43E+11	-1.42E+11	0.992	0.492	0.985	0.634
CS2.5a2hy	160	-1.17E+11	-1.50E+11	1.278	1.223	0.977	1.280
PS2.9a3hy	160	-1.64E+11	-1.62E+11	0.987	0.555	0.984	0.707
PS2.9a4hy	160	-1.51E+11	-1.50E+11	0.996	0.720	0.982	0.846
cs25a3	120	-1.38E+11	-1.36E+11	0.987	1.201	0.974	1.310
ps29a5	120	-1.66E+11	-1.64E+11	0.989	0.788	0.979	0.976

Table A 3-2.7 Results of hybrid factor obtained from FEM analysis and proposal of the current study for M_1=0.2 M_{ys}

Girder ID	b_w/t_w	M_y [N.mm]	M_{yfFEM} [N.mm]	R_{hFEM}	β_{FEM}	$R_{hprop.}$	$\beta_{prop.}$
PS2.9a2hy	200	-1.54E+11	-1.54E+11	1.001	0.510	1.001	0.573
PS2.8c1hy	200	-1.21E+11	-1.19E+11	0.976	0.826	0.976	0.840
PS2.9a1hy	200	-1.01E+11	-9.86E+10	0.978	1.146	0.978	1.132
CS2.5a1hy	200	-1.43E+11	-1.42E+11	0.993	0.492	0.993	0.580
CS2.5a2hy	160	-1.17E+11	-1.16E+11	0.986	1.154	0.986	1.153
PS2.9a3hy	160	-1.64E+11	-1.63E+11	0.989	0.544	0.989	0.646
PS2.9a4hy	160	-1.51E+11	-1.51E+11	1.002	0.707	1.002	0.768
cs25a3	120	-1.38E+11	-1.37E+11	0.992	1.170	0.992	1.197
ps29a5	120	-1.66E+11	-1.64E+11	0.987	0.790	0.987	0.895

Table A 3-2.8 Results of hybrid factor obtained from FEM analysis and proposal of the current study for M_1=0.4 M_{ys}

Girder ID	b_w/t_w	M_y [N.mm]	M_{yfFEM} [N.mm]	R_{hFEM}	β_{FEM}	$R_{hprop.}$	$\beta_{prop.}$
PS2.9a2hy	200	-1.54E+11	-1.53E+11	0.991	0.491	0.956	0.496
PS2.8c1hy	200	-1.21E+11	-1.16E+11	0.959	0.758	0.945	0.737
PS2.9a1hy	200	-1.01E+11	-9.67E+10	0.959	1.065	0.935	0.974
CS2.5a1hy	200	-1.43E+11	-1.42E+11	0.993	0.488	0.956	0.540
CS2.5a2hy	160	-1.17E+11	-1.16E+11	0.987	1.084	0.935	1.075
PS2.9a3hy	160	-1.64E+11	-1.64E+11	0.999	0.549	0.952	0.560
PS2.9a4hy	160	-1.51E+11	-1.51E+11	1.003	0.676	0.947	0.664
cs25a3	120	-1.38E+11	-1.37E+11	0.996	1.093	0.932	1.120
ps29a5	120	-1.66E+11	-1.66E+11	1.003	0.762	0.941	0.778

Table A 3-2.9 Results of hybrid factor obtained from FEM analysis and proposal of the current study for M_l=0.9 M_{ys}

Girder ID	b_w/t_w	M_y [N.mm]	M_{yfFEM} [N.mm]	$\mathbf{R_{h}}_{FEM}$	β_{FEM}	$\mathbf{R_{h}}_{prop.}$	$\beta_{prop.}$
PS2.9a2hy	200	-1.54E+11	-1.51E+11	0.978	0.453	0.940	0.464
PS2.8c1hy	200	-1.21E+11	-1.16E+11	0.956	0.701	0.926	0.685
PS2.9a1hy	200	-1.01E+11	-9.43E+10	0.936	0.942	0.912	0.905
CS2.5a1hy	200	-1.43E+11	-1.42E+11	0.995	0.446	0.941	0.495
CS2.5a2hy	160	-1.17E+11	-1.10E+11	0.940	0.995	0.913	0.994
PS2.9a3hy	160	-1.64E+11	-1.63E+11	0.991	0.509	0.935	0.520
PS2.9a4hy	160	-1.51E+11	-1.47E+11	0.978	0.620	0.929	0.623
cs25a3	120	-1.38E+11	-1.32E+11	0.957	1.023	0.910	1.043
ps29a5	120	-1.66E+11	-1.62E+11	0.980	0.721	0.921	0.728

Table A 3-2.10 Results regarding girders with noncompact and slender SBHS500-SM490Y hybrid steel section for M_l=0.0 M_{ys}

Girder	α'	R_h	M_y [N.mm]	M_u [N.mm]	$M_u/(M_y*R_h)$	Clas.
PS2.8c1hy	0.300	0.982	1.25E+11	1.28E+11	1.043	**Non-comp.**
PS2.9a1hy	0.250	0.978	1.04E+11	1.08E+11	1.059	**Non-comp.**
PS2.9a2hy	0.350	0.986	1.63E+11	1.66E+11	1.035	**Non-comp.**
PS2.9b1hy	0.399	0.987	1.82E+11	1.54E+11	0.861	**Slender**
CS2.5a1hy	0.375	0.985	1.56E+11	1.57E+11	1.018	**Non-comp.**
CS1.5c1hy	0.450	0.979	1.41E+11	1.06E+11	0.769	**Slender**
CS2.5a2hy	0.299	0.977	1.22E+11	1.32E+11	1.106	**Non-comp.**
PS2.8c2hy	0.400	0.985	1.89E+11	1.55E+11	0.832	**Slender**
PS2.9a3hy	0.375	0.984	1.80E+11	1.79E+11	1.014	**Non-comp.**
PS2.9a4hy	0.350	0.982	1.60E+11	1.60E+11	1.017	**Non-comp.**
CS1.5c2hy	0.450	0.974	1.46E+11	1.16E+11	0.811	**Slender**
CS1.6a1hy	0.499	0.980	1.89E+11	1.22E+11	0.658	**Slender**
CS2.5a3hy	0.350	0.974	1.46E+11	1.46E+11	1.030	**Non-comp.**
PS2.8c3hy	0.400	0.980	1.92E+11	1.64E+11	0.872	**Slender**
PS2.9a5hy	0.375	0.979	1.78E+11	1.67E+11	0.955	**Slender**

Table A 3-2.11 Results regarding girders with noncompact and slender SBHS500-SM490Y hybrid steel section for M_l=0.2 M_{ys}

Girder	α'	R_h	M_y [N.mm]	M_u [N.mm]	$M_u/(M_y*R_h)$	Clas.
PS2.8c1hy	0.373	0.964	1.22E+11	1.27E+11	1.075	**Non-comp.**
PS2.9a1hy	0.336	0.957	1.01E+11	1.06E+11	1.095	**Non-comp.**
PS2.9a2hy	0.412	0.971	1.60E+11	1.59E+11	1.019	**Non-comp.**
PS2.9b1hy	0.450	0.974	1.79E+11	1.41E+11	0.809	**Slender**
CS2.5a1hy	0.428	0.971	1.53E+11	1.42E+11	0.954	**Slender**
CS1.5c1hy	0.478	0.964	1.38E+11	1.07E+11	0.801	**Slender**
CS2.5a2hy	0.369	0.956	1.20E+11	1.25E+11	1.093	**Non-comp.**
PS2.8c2hy	0.448	0.970	1.86E+11	1.56E+11	0.866	**Slender**
PS2.9a3hy	0.429	0.968	1.76E+11	1.72E+11	1.006	**Non-comp.**
PS2.9a4hy	0.410	0.965	1.57E+11	1.57E+11	1.036	**Non-comp.**
CS1.5c2hy	0.476	0.957	1.43E+11	1.28E+11	0.932	**Slender**
CS1.6a1hy	0.521	0.967	1.71E+11	1.35E+11	0.818	**Slender**
CS2.5a3hy	0.406	0.954	1.42E+11	1.46E+11	1.076	**Non-comp.**
PS2.8c3hy	0.446	0.963	1.88E+11	1.86E+11	1.027	**Non-comp.**
PS2.9a5hy	0.427	0.960	1.74E+11	1.75E+11	1.045	**Non-comp.**

Table A 3-2.12 Results regarding girders with noncompact and slender SBHS500-SM490Y hybrid steel section for M_l=0.4 M_{ys}

Girder	α'	R_h	M_y [N.mm]	M_u [N.mm]	$M_u/(M_y*R_h)$	Clas.
PS2.8c1hy	0.427	0.945	1.20E+11	1.27E+11	1.118	**Non-comp.**
PS2.9a1hy	0.396	0.935	9.87E+10	1.17E+11	1.263	**Non-comp.**
PS2.9a2hy	0.459	0.956	1.58E+11	1.59E+11	1.054	**Non-comp.**
PS2.9b1hy	0.494	0.960	1.76E+11	1.42E+11	0.840	**Slender**
CS2.5a1hy	0.471	0.956	1.51E+11	1.43E+11	0.989	**Slender**
CS1.5c1hy	0.510	0.949	1.30E+11	1.08E+11	0.876	**Slender**
CS2.5a2hy	0.418	0.935	1.17E+11	1.39E+11	1.272	**Non-comp.**
PS2.8c2hy	0.488	0.954	1.83E+11	1.57E+11	0.900	**Slender**
PS2.9a3hy	0.472	0.952	1.73E+11	1.69E+11	1.028	**Non-comp.**
PS2.9a4hy	0.457	0.947	1.54E+11	1.57E+11	1.078	**Non-comp.**
CS1.5c2hy	0.505	0.940	1.37E+11	1.31E+11	1.018	**Non-comp.**
CS1.6a1hy	0.553	0.953	1.47E+11	1.25E+11	0.894	**Slender**
CS2.5a3hy	0.449	0.932	1.39E+11	1.47E+11	1.138	**Non-comp.**
PS2.8c3hy	0.485	0.945	1.84E+11	1.78E+11	1.023	**Non-comp.**
PS2.9a5hy	0.469	0.941	1.71E+11	1.67E+11	1.043	**Non-comp.**

Table A 3-2.13 Results regarding girders with noncompact and slender SBHS500-SM490Y hybrid steel section for M_l=0.6 M_{ys}

Girder	α'	R_h	M_y [N.mm]	M_u [N.mm]	$M_u/(M_y*R_h)$	Clas.
PS2.8c1hy	0.472	0.926	1.17E+11	1.18E+11	1.082	**Non-comp.**
PS2.9a1hy	0.447	0.912	9.61E+10	9.78E+10	1.116	**Non-comp.**
PS2.9a2hy	0.499	0.940	1.55E+11	1.59E+11	1.089	**Non-comp.**
PS2.9b1hy	0.556	0.946	1.37E+11	1.41E+11	1.090	**Non-comp.**
CS2.5a1hy	0.515	0.941	1.39E+11	1.41E+11	1.076	**Non-comp.**
CS1.5c1hy	0.550	0.932	1.07E+11	1.18E+11	1.173	**Non-comp.**
CS2.5a2hy	0.460	0.913	1.14E+11	1.07E+11	1.028	**Non-comp.**
PS2.8c2hy	0.540	0.938	1.52E+11	1.59E+11	1.115	**Non-comp.**
PS2.9a3hy	0.516	0.935	1.58E+11	1.51E+11	1.019	**Non-comp.**
PS2.9a4hy	0.496	0.929	1.50E+11	1.41E+11	1.008	**Non-comp.**
CS1.5c2hy	0.542	0.922	1.15E+11	1.06E+11	1.007	**Non-comp.**
CS1.6a1hy	0.590	0.938	1.22E+11	1.25E+11	1.085	**Non-comp.**
CS2.5a3hy	0.486	0.910	1.35E+11	1.56E+11	1.265	**Non-comp.**
PS2.8c3hy	0.531	0.927	1.57E+11	1.63E+11	1.118	**Non-comp.**
PS2.9a5hy	0.510	0.921	1.60E+11	1.56E+11	1.063	**Non-comp.**